UNIVERSITAT ROVIRA I VIRGILI
NANOMATERIALS IN CATALYSIS: STUDY OF MODEL REACTIONS.
Ricardo José Chimentao
ISBN: 978-84-690-7618-7 / DL: T.1326-2007

Department of Chemical Engineering

Universitat Rovira i Virgili

Spain

Nanomaterials in Catalysis

Study of Model Reactions

Thesis submitted by

RICARDO JOSÉ CHIMENTÃO

to obtain the degree of

Doctor from the Universitat Rovira i Virgili

Tarragona, March 2007

UNIVERSITAT ROVIRA I VIRGILI
NANOMATERIALS IN CATALYSIS: STUDY OF MODEL REACTIONS.
Ricardo José Chimentao
ISBN: 978-84-690-7618-7 / DL: T.1326-2007

Prof. Jesús Eduardo Sueiras Romero and Dr. Francesc Medina Cabello, professor and associate professor of the Department of Chemical Engineering at the Universitat Rovira i Virgili

Certify: That the doctoral thesis entitled “Nanomaterials in Catalysis: Study of Model Reactions” by RICARDO JOSÉ CHIMENTÃO to obtain the degree of doctor from the Universitat Rovira I Virgili has been carried out under our supervision in the Department of Chemical Engineering of the Universitat Rovira i Virgili.

Tarragona, April 2007

Prof. Jesús Eduardo Sueiras Romero

Dr. Francesc Medina Cabello

UNIVERSITAT ROVIRA I VIRGILI
NANOMATERIALS IN CATALYSIS: STUDY OF MODEL REACTIONS.
Ricardo José Chimentao
ISBN: 978-84-690-7618-7 / DL: T.1326-2007

Tribunal de la Tesis

Prof. Jose Luis Garcia Fierro
Instituto de Catalisis y Petroleoquimica, CSIC, Cantoblanco, España

Prof. Guido Busca
Universita` di Genova, Italia

Dr. Francisco López Bonillo
Universitat Rovira i Virgili, España

Dr. Jordi Llorca
Institut de Tècniques Energètiques. Universitat Politècnica de Catalunya, España

Dra. Sònia Abelló
Institut Catalá d' Investigació Química, España

Suplentes

Dr. Anton Dafinov
Universitat Rovira i Virgili, España

Dra. Yolanda Cesteros
Universitat Rovira i Virgili, España

UNIVERSITAT ROVIRA I VIRGILI
NANOMATERIALS IN CATALYSIS: STUDY OF MODEL REACTIONS.
Ricardo José Chimentao
ISBN: 978-84-690-7618-7 / DL: T.1326-2007

To my beloved parents

UNIVERSITAT ROVIRA I VIRGILI
NANOMATERIALS IN CATALYSIS: STUDY OF MODEL REACTIONS.
Ricardo José Chimentao
ISBN: 978-84-690-7618-7 / DL: T.1326-2007

Acknowledgements

I extend my sincere gratitude and appreciation to many people who made this doctoral thesis possible. Special thanks are due to my supervisor Dr. Francesc Medina to believe in me and for his attentive criticism which helped me to correct many ideas about catalysis and about myself. Thanks are also due to my lab mates: Dr. Anton Dafinov, Clara Cabús, Dra Ilham Kirm, Iuliana Cota, Noelia Barrabes and Dra. Sònia Abelló.

I am highly in indebted to Prof. Jose Luis Garcia Fierro for the excellent XPS analysis. I would also to thank Dr. Jordi Llorca for the HRTEM measurements. I wish to express my profound gratitude to Dr. Francesc Guirado for the skillfully helping with the XRD measurements.

I would like to thank Prof. Chuck Peden, Dr. Janos Szanyi and Dr. Jose Herrera for make possible my short research stay in USA in the Environmental Molecular Sciences Laboratory (EMSL) at the Pacific Northwest National Laboratory (PNNL) operated by the Battelle for the U. S. Department of energy (DOE). Thanks also to the workers of the Guest House for providing a private, comfortable, and affordable room within easy walking distance of most PNNL research facilities.

I would also like to thank the Universitat Rovira i Virgili for the scholarship and the financial support of the projects REN 2002-04464-CO2-01 and PETRI 95-0801.OP.

I wish to express my special thanks to my family for their cooperation, support and encouragement during the time of my research.

UNIVESITAT ROVIRA I VIRGILI
NANOMATERIALS IN CATALYSIS: STUDY OF MODEL REACTIONS.
Ricardo José Chimentón
ISBN: 978-84-690-7618-7 / DL: T.1326-2007

Preface

The generation of catalysts consisting of small metallic particles dispersed over a support has a long history in catalysis as a means of maximizing the available metallic surface area and assessing whether such particles have properties which differ from those of the bulk metal. It is accepted that for metallic catalysts, control at the atomic level is needed to design active sites because the chemical and catalytic properties of atoms at terraces, corners, and edges of a metal crystallite are different, and can be different from atoms at the metal-support interface. The location of the metal cluster on the support may be also important if its properties are affected by its proximity to the support defects. These problems become even more acute if one has to consider multimetallic rather than monometallic systems. The application of highly sensitive techniques like high resolution electron microscopy and XPS to highly dispersed metal catalysts lead to a better understanding of structural and electronic properties of supported small particles and allowed the determination of the bulk and surface composition of bimetallic clusters. Bimetallic catalysts have played an important role in heterogeneous catalysis. They have been extensively for fundamental investigations and have had a major technological impact, especially in the petroleum industry. A complicating feature in catalytic studies on metal alloys is the possibility of a difference between surface and bulk compositions.

The focus of this dissertation is the synthesis and characterization of noble metal and metal oxide nanoparticles and their chemistry including catalytic properties. The subject in this work can be divided at least into two parts. The Part I is treated by the *Chapter I.1* dealing with the structural physical and electronic properties of transition metal nanoparticles. The surface and relevant bulk properties are also discussed which may be helpful to understand the content in the Part II (*Chapters II.1-II.6*). Some portions of the text occur in multiple places in different chapters to help readers understand without needing to shuffle through the entire document. The essentials of characterization techniques are covered in the chapters on instrumentation, characterization sections and spectra interpretation. Whenever appropriate, relationships among various topics are indicated.

In general terms, the scope of *Nanomaterials in Catalysis: Study of Model Reactions*, is

UNIVESITAT ROVIRA I VIRGILI
NANOMATERIALS IN CATALYSIS: STUDY OF MODEL REACTIONS.
Ricardo José Chimentón
ISBN: 978-84-690-7618-7 / DL: T.1326-2007

limited to topics which are, to some extent at least, relevant to industrial processes. The whole of heterogeneous catalysis fall within its scope, nevertheless the field of catalysis is so wide and detailed, and its ramifications are so numerous, that the production of the entire subject is well beyond the capability of any single author. Ancillary subjects such as surface science, materials properties and other fields of catalysis are given adequate treatment but not to extent to obscuring the central theme. *Nanomaterials in Catalysis: Study of Model Reactions* concentrates in the catalytic study of the metal nanoparticles in model reactions covered in the *Chapters II.1-II.6.* It is not expedient to impose a preconceived ordered structure. Instead each chapter is dealt when is most appropriate to do so. It will be sufficient if the entire subject in this work has been properly covered in the following chapters:

Chapter I.1. Because of the multidisciplinary nature of the nanomaterials, it would be difficult to cover all areas of interest. Accordingly, the shape, the size, and composition of the nanocrystals would play an important role in modulating its properties. These materials show very interesting properties that have been attributed to the high volume fraction of interfacial structures that are different from the crystalline structures of the core. Various synthesis methods or techniques can be grouped into two categories: thermodynamic equilibrium approach and kinetic approach. Here the synthesis of nanoparticles through thermodynamically approach was based on the formation of monosized metallic silver by a combination of a low concentration of solute and polymeric monolayer adhered onto the growth surfaces. For the kinetic approach we synthesized metal nanoparticles by kinetically confining the reaction in a restrict space.

Chapters II.1 and II.2. This chapter is an attempt to study the silver nanoparticles in the styrene epoxidation. Amongst the metal supports catalysts, silver occupies a unique position. Ethylene epoxidation has been produced almost exclusively by partial oxidation of ethylene over a silver catalyst. The study of the silver-oxygen system is complicated by the fact that oxygen is often present in multiple states including atomic, molecular, and subsurface states. The key role of oxygen adsorption on silver has been realized since the early studies, and several publications deal with the number and nature of

UNIVESITAT ROVIRA I VIRGILI
NANOMATERIALS IN CATALYSIS: STUDY OF MODEL REACTIONS.
Ricardo José Chimentón
ISBN: 978-84-690-7618-7 / DL: T.1326-2007

adsorbed oxygen species, under reaction conditions, and their role in the epoxidation and combustion routes.

Chapter II.3. Propylene oxide (PO) is one of the important bulk chemicals, which is used for producing polyurethane and polyols. Gold supported on TiO_2 catalysts were reported for the first time by Haruta and co-workers as selective catalyst for direct epoxidation of propene. Recently Lambert et al. also showed that copper catalysts also show promise for the epoxidation of propene. Here we present the study of the Au-Cu alloy nanoparticles in the propene epoxidation. The incorporation of copper seems to affect the gold dispersion giving longer distance of the perimeter interface which is probably indispensable for the epoxidation of propylene.

Chapter II.4. The target of this chapter was to investigate phase development in the V_2O_5 catalyst system consisting of TiO_2 (anatase) and MCM-41 supports. Among these metal oxides, vanadium oxide catalysts have attracted much attention due to their unique catalytic properties and commercial applicability for various chemical processes. Here it is described the effect of alkaline metal (Na) promotion on V_2O_5/TiO_2 and V_2O_5/MCM-41 in the selective oxidation of ethanol to acetaldehyde. We have observed that depending of the supported used the vanadia become an effective catalyst for selective oxidation of alcohols. The incorporation of alkaline ions such as Na result an increase of the catalytic activity and selectivity to acetaldehyde.

Chapter II.5. It is well know that clay minerals undergo spontaneous exfoliation in water. This chapter reports evidences on platelet defects induced by the use of ultrasounds or high mechanical stirring during reconstruction of hydrotalcites in water. Exfoliation is regarded as an effective way of maximizing the accessibility and utility of the LDH host layers as well as introducing physicochemical properties effects. Here, the catalytic properties of the activated hydrotalcites have been investigated in the base-catalyzed epoxidation of styrene.

Chapter II.6. Skeletal of hydrocarbons, skeletal isomerization and hydrogenolysis, occur

UNIVESITAT ROVIRA I VIRGILI
NANOMATERIALS IN CATALYSIS: STUDY OF MODEL REACTIONS.
Ricardo José Chimentón
ISBN: 978-84-690-7618-7 / DL: T.1326-2007

over a number of metallic catalysts. These reactions provide very good examples of the way in which reaction selectivity is related to catalyst structure. From works, realized by Dr. G. Maire and Dr. F. G. Garin, which has involved the use of both dispersed metal catalysts and single crystal catalysts, together with carbon isotopic tracer studies, some of the main mechanistic features of these processes are now reasonable well understood and this is the subject of this chapter. Here we describe the study of the hydrogenolysis of methylcyclopentane over Ir-Au/γ-Al_2O_3. Methylcyclopentane (MCP) is a recognized probe molecule in the investigation of the structure sensitivity of several hydrocarbon conversions catalyzed usually by noble metal-based catalysts. The Ib metals can be considered as almost inactive in these reactions as compared with the group VIII metals. We reported some phenomena in which in our opinion indicate the Au metal plays a strong role in the adsorptive and catalytic properties of Ir even in bimetallic systems of immiscible components such as the case of Ir-Au metal system.

UNIVESITAT ROVIRA I VIRGILI
NANOMATERIALS IN CATALYSIS: STUDY OF MODEL REACTIONS.
Ricardo José Chimentón
ISBN: 978-84-690-7618-7 / DL: T.1326-2007

Abstract

Metal nanoparticles catalysts considered in this work included systems consisting essentially of a single metal component (Ag) and bimetallic system. Bimetallic systems of miscible (Au-Cu and Au-Ag) and immiscible components (Ir-Au) have been investigated. The study of these materials with chemical probes including chemisorption and selected catalytic reaction, in conjunction with physical and chemical methods such as electron microscopy, X-ray diffraction (XRD), temperature programmed reduction (TPR), UV-vis, photoelectron spectroscopy (XPS) has been performed to contribute the knowledge of their structures. The fact that surface composition can differ substantially from bulk composition was also studied. High resolution electron microscopy (HRTEM) provided independent evidence of the highly dispersed nature of the metal clusters. Concepts concerning the effect of additives on the structure and physicochemical and catalytic properties of oxide catalysts in selective oxidation reactions were considered.

This work was also carried out in an attempt to study the different oxygen species formed on silver. Of particular interest is to understand the role and nature of the elusive subsurface O species in the function of silver as an oxidant catalyst. The effect of additives on acid-base and redox properties and on their bearing on catalytic performance was discussed, with particular emphasis on alkaline metal additives such as cesium and sodium. The phenomena occurring in monophasic and supported mixed oxide containing the additives, including modification of structure, segregation, defect formation and spill-over of the reactants was also described.

The nature of the surface of the bimetallic systems was the question of interest. Will the individual clusters be monometallic or will they contain atoms of both metals and therefore be bimetallic? It is interesting to consider how the state of dispersion the metal catalysts affects the relationship between chemisorption capacity or catalytic activity and catalyst composition. The bimetallic clusters discussed thus far have been combination of a Group VIII and a Group IB metal. In spite of the great importance in petrochemistry, skeletal hydrocarbon reactions, such as hydrogenolysis of methylcyclopentane, offers an interesting fingerprint of the dependence of specific rate on catalyst structure. The first reported case of a reaction with large dependence on catalyst structure was performed for neopentane on platinum. This result led Boudart to classify reactions on metals as: (i)

UNIVESITAT ROVIRA I VIRGILI
NANOMATERIALS IN CATALYSIS: STUDY OF MODEL REACTIONS.
Ricardo José Chimentón
ISBN: 978-84-690-7618-7 / DL: T.1326-2007

"facile" or "structure-insensitive" reactions, for which the specific rate does not depend upon the size of the metal particle, and (ii) "demanding" or "structure sensitive" reactions, for which the specific rate is highly dependent on the metal dispersion. The rate per surface metal atom is the fundamental interest. Thus, the metal dispersion is extremely important parameter to be determined. An experimental scheme based on selective H_2 chemisorption was developed to investigate the surface composition of bimetallic system. With this capability, the activity of such a catalyst was referred to the amount of metal in the surface rather than to the metal content of the catalyst as a whole.

The interaction between catalytically active metal oxide particles and oxide carriers greatly influences their structure and size. Vanadia catalysts constitute also a relevant example of the influence of this interaction. Accordingly, it was decided to study the effect of the support (TiO_2 and MCM-41) with the aim of understanding the interrelations on the catalytic properties of V_2O_5 as a way to improve its performance for the selective oxidation of ethanol.

Finally, the catalytic role of the different basic sites in hydrotalcite interlayer was envisaged through the study of the styrene epoxidation in liquid phase. Hydrotalcite-like compounds are not only interesting for their industrial applications, but are also beautiful examples of the scientific preparation of catalysts. All the stages of the preparation of a catalyst based on hydrotalcite-like precursor need precise chemical foundations in order to avoid inhomogeneties and/or chemical segregations, which would be detrimental to the properties of the final compounds. Layered double hydroxides (LDHs), also known as hydrotalcites or anionic clays, are a class of ionic lamellar compounds made of positive-charged hydroxide layers with charge balancing anions and water molecules sandwiched between layers. Exfoliated Mg-Al layered double hydroxide in water was investigated in the styrene epoxidation. The change in the basic properties during the rehydration process of the calcined samples as well the influence on catalytic activity was studied. Hydrotalcites are very attractive for this type of oxidation reaction because their ability to give Lewis type acid-base bifunctional catalysts or basic catalysts with Brönsted type sites, proceeding from the mixed oxide and the meixnerite-like structures, respectively.

UNIVESITAT ROVIRA I VIRGILI
NANOMATERIALS IN CATALYSIS: STUDY OF MODEL REACTIONS.
Ricardo José Chimentón
ISBN: 978-84-690-7618-7 / DL: T.1326-2007

Resumen

En este trabajo se han sintetizado y estudiado diferentes catalizadores a base de nanopartículas metálicas con diferentes tamaños y morfologías. Se han estudiado tanto sistemas monometálicos como bimetálicos con componentes de diferentes miscibilidad (por ejemplo sistemas Au-Cu y Au-Ag de total miscibilidad, así como Ir-Au de prácticamente total inmiscibilidad) con la finalidad de estudiar el cambio que producen tanto en el tamaño como en la morfología de las nanopartículas obtenidas.

Los nanomateriales obtenidos han sido estudiados mediante el empleo de diferentes técnicas de caracterización como pueden ser, fisisorción, quimisorción microscopia electrónica (SEM-TEM), difracción de rayos X (XRD), reducción a temperatura programada (TPR), espectroscopia ultravioleta-visible (UV-vis), espectroscopia fotoelectrónica (XPS), etc., así como mediante diferentes ensayos catalíticos modelo con la finalidad de correlacionar las propiedades físico-químicas de dichos materiales con los métodos de síntesis de éstos.

Se ha hecho especial énfasis en el estudio de las diferentes especies de oxígeno que presentan estos nanomateriales en superficie, así como su correlación con la actividad catalítica que presentan en diferentes reacciones de oxidación selectiva de olefinas. Por otra parte, la modificación de las propiedades ácido-base de dichos materiales y su carácter redox cuando se adiciona metales alcalinos del tipo sodio y cesio, también ha sido exhaustivamente estudiado.

La formación de sistemas bimetálicos y su homogeneidad, así como el efecto de dispersión y el cambio en sus propiedades físico-químicas que hace un metal sobre el otro, ha sido también objeto de estudio en este trabajo. Este hecho se ha puesto en evidencia en el estudio de reacciones de hidrogenolisis del metilciclopentano que permite una buena comprensión de la actividad catalítica, así como de la dependencia de la estructura en la actividad catalítica previamente ya descrita por Boudart.

La interacción entre las especies metálicas cataliticamente activas y los soportes empleados también pueden ejercer una notable influencia en la estructura y tamaño de la especie activa, y por consiguiente en el comportamiento catalítico. En este contexto, se han estudiado la interacción de óxido de vanadio en diferentes soportes como TiO_2 y MCM-4, para comprender el comportamiento catalítico del V_2O_5 en otra reacción test como es la de

UNIVESITAT ROVIRA I VIRGILI
NANOMATERIALS IN CATALYSIS: STUDY OF MODEL REACTIONS.
Ricardo José Chimentón
ISBN: 978-84-690-7618-7 / DL: T.1326-2007

oxidación selectiva del etanol.

Finalmente, el papel del los diferentes sitios básicos de materiales tipo hidrotalcita, el estudio de la exfoliación de dichos materiales y el cambio en sus propiedades básicas después de diferentes protocolos de rehidratación han sido estudiados en otra reacción test como es la reacción de epoxidación del estireno en fase liquida.

UNIVESITAT ROVIRA I VIRGILI
NANOMATERIALS IN CATALYSIS: STUDY OF MODEL REACTIONS.
Ricardo José Chimentón
ISBN: 978-84-690-7618-7 / DL: T.1326-2007

Table of Contents

UNIVESITAT ROVIRA I VIRGILI
NANOMATERIALS IN CATALYSIS: STUDY OF MODEL REACTIONS.
Ricardo José Chimentón
ISBN: 978-84-690-7618-7 / DL: T.1326-2007

Part II - Nanomaterials: Study of model reactions

UNIVESITAT ROVIRA I VIRGILI
NANOMATERIALS IN CATALYSIS: STUDY OF MODEL REACTIONS.
Ricardo José Chimentón
ISBN: 978-84-690-7618-7 / DL: T.1326-2007

Chapter II.4 Oxidation of Ethanol to Acetaldehyde over Na-promoted vanadium oxide catalysts

Chapter II.5 Effect of a sonicated reconstruction on the accessibility of active sites in hydrotalcite-like compounds

Chapter II.6 Metal catalyzed skeletal rearrangement of hydrocarbons

UNIVESITAT ROVIRA I VIRGILI
NANOMATERIALS IN CATALYSIS: STUDY OF MODEL REACTIONS.
Ricardo José Chimentón
ISBN: 978-84-690-7618-7 / DL: T.1326-2007

UNIVESITAT ROVIRA I VIRGILI
NANOMATERIALS IN CATALYSIS: STUDY OF MODEL REACTIONS.
Ricardo José Chimentón
ISBN: 978-84-690-7618-7 / DL: T.1326-2007

List of Figures

UNIVESITAT ROVIRA I VIRGILI
NANOMATERIALS IN CATALYSIS: STUDY OF MODEL REACTIONS.
Ricardo José Chimentón
ISBN: 978-84-690-7618-7 / DL: T.1326-2007

UNIVESITAT ROVIRA I VIRGILI
NANOMATERIALS IN CATALYSIS: STUDY OF MODEL REACTIONS.
Ricardo José Chimentón
ISBN: 978-84-690-7618-7 / DL: T.1326-2007

UNIVESITAT ROVIRA I VIRGILI
NANOMATERIALS IN CATALYSIS: STUDY OF MODEL REACTIONS.
Ricardo José Chimentón
ISBN: 978-84-690-7618-7 / DL: T.1326-2007

UNIVESITAT ROVIRA I VIRGILI
NANOMATERIALS IN CATALYSIS: STUDY OF MODEL REACTIONS.
Ricardo José Chimentón
ISBN: 978-84-690-7618-7 / DL: T.1326-2007

UNIVESITAT ROVIRA I VIRGILI
NANOMATERIALS IN CATALYSIS: STUDY OF MODEL REACTIONS.
Ricardo José Chimentón
ISBN: 978-84-690-7618-7 / DL: T.1326-2007

UNIVESITAT ROVIRA I VIRGILI
NANOMATERIALS IN CATALYSIS: STUDY OF MODEL REACTIONS.
Ricardo José Chimentón
ISBN: 978-84-690-7618-7 / DL: T.1326-2007

UNIVESITAT ROVIRA I VIRGILI
NANOMATERIALS IN CATALYSIS: STUDY OF MODEL REACTIONS.
Ricardo José Chimentón
ISBN: 978-84-690-7618-7 / DL: T.1326-2007

UNIVESITAT ROVIRA I VIRGILI
NANOMATERIALS IN CATALYSIS: STUDY OF MODEL REACTIONS.
Ricardo José Chimentón
ISBN: 978-84-690-7618-7 / DL: T.1326-2007

UNIVESITAT ROVIRA I VIRGILI
NANOMATERIALS IN CATALYSIS: STUDY OF MODEL REACTIONS.
Ricardo José Chimentón
ISBN: 978-84-690-7618-7 / DL: T.1326-2007

List of Tables

UNIVESITAT ROVIRA I VIRGILI
NANOMATERIALS IN CATALYSIS: STUDY OF MODEL REACTIONS.
Ricardo José Chimentón
ISBN: 978-84-690-7618-7 / DL: T.1326-2007

UNIVERSITAT ROVIRA I VIRGILI
NANOMATERIALS IN CATALYSIS: STUDY OF MODEL REACTIONS.
Ricardo José Chimentao
ISBN: 978-84-690-7618-7 / DL: T.1326-2007

Part I

Nanomaterials: synthesis & characterization

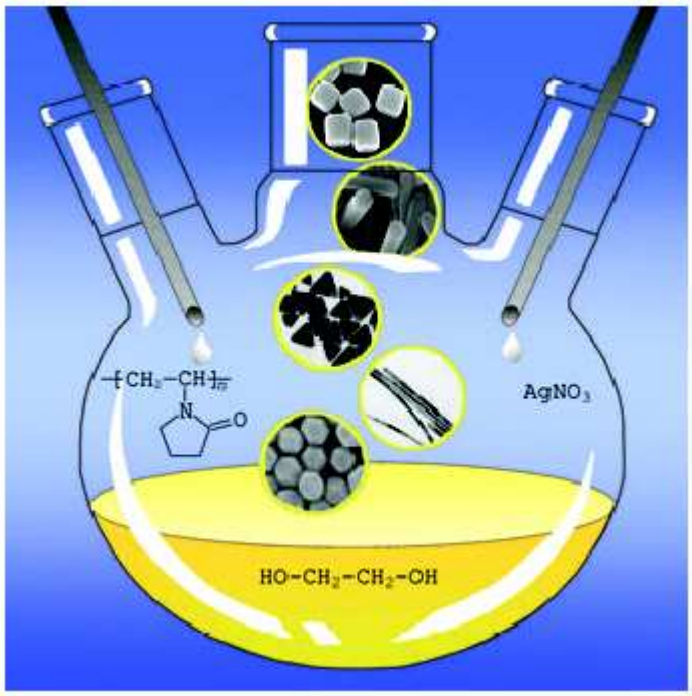

UNIVERSITAT ROVIRA I VIRGILI
NANOMATERIALS IN CATALYSIS: STUDY OF MODEL REACTIONS.
Ricardo José Chimentao
ISBN: 978-84-690-7618-7 / DL: T.1326-2007

Chapter I.1

Synthesis and characterization of metal nanoparticles

UNIVERSITAT ROVIRA I VIRGILI
NANOMATERIALS IN CATALYSIS: STUDY OF MODEL REACTIONS.
Ricardo José Chimentao
ISBN: 978-84-690-7618-7 / DL: T.1326-2007

I.1 Initial Considerations

This chapter focuses on the synthesis and fabrication of nanostructures and nanomaterials, but also includes properties of nanomaterials, particularly inorganic nanomaterials. Both bulk and surface characterization techniques find applications in the study of nanomaterials.

However, bulk methods are used to characterize the collective information of nanomaterials such as XRD and gas sorption isotherms. They do not provide information of individual nanoparticles. Surface characterization methods such as XPS offer the possibility to study individual nanostructures. Bulk and surface characterization techniques are complementary in the study of nanomaterials.

I.2 Literature Review

I.2.1 Introductory comments

Materials in nanometer scale are of great interest due to their unique optical, electrical, and magnetic properties. Many heterogeneous catalysts utilize nanoparticles.

Nanoparticles of metal and oxides have been developed and used as catalysts for hydrocarbon conversion, partial oxidation and combustion reactions since 1920's; as such they represent the oldest commercial application of nanotechnology [1]. These properties are strongly dependent on the size and the shape of the particles and therefore it is very important to be able to finely control the morphology of the nanomaterials [2, 3]. Besides, nanoparticles have a large fraction of

UNIVERSITAT ROVIRA I VIRGILI
NANOMATERIALS IN CATALYSIS: STUDY OF MODEL REACTIONS.
Ricardo José Chimentao
ISBN: 978-84-690-7618-7 / DL: T.1326-2007

surface atoms per unit of volume [4].

Current research has been focused on one-dimensional nanoparticles such as nanorods and nanowires since the morphological anisotropy results in very complex physical properties and self assembly behaviors compared to those bulk materials [5].

All solids may be divided into crystalline and amorphous substances. The former are characterized by an ordered periodic arrangement of the structural elements in space, whereas in the case of the latter the structural elements do not form an ordered structure. Irrespectively, however, of whether the structure as a whole is ordered or not, the nearest surrounding of each atom is usually ordered and its form may be explained on the basis of the type of chemical bonds linking the given atom with its nearest neighbors, which may be considered as ligands, forming a coordination polyhedra.

In general, geometrical shape is determined by the composition and properties of the synthesized material. For most metal transition nanoparticles, distinct structures can occur that are not characteristic of the bulk crystal structure [6].

These structures are: cubooctahedron, icosahedron and decahedron as depicted in Figure I.2.1. Surface atoms differ from atoms in the bulk because they have an incomplete set of neighbors. For a spherical single-crystalline particle, its surface must contain high-index crystallography planes, which possibly result in a higher surface energy. Facets tend to form on the particle surface to increase the portion of the low-index planes.

UNIVERSITAT ROVIRA I VIRGILI
NANOMATERIALS IN CATALYSIS: STUDY OF MODEL REACTIONS.
Ricardo José Chimentao
ISBN: 978-84-690-7618-7 / DL: T.1326-2007

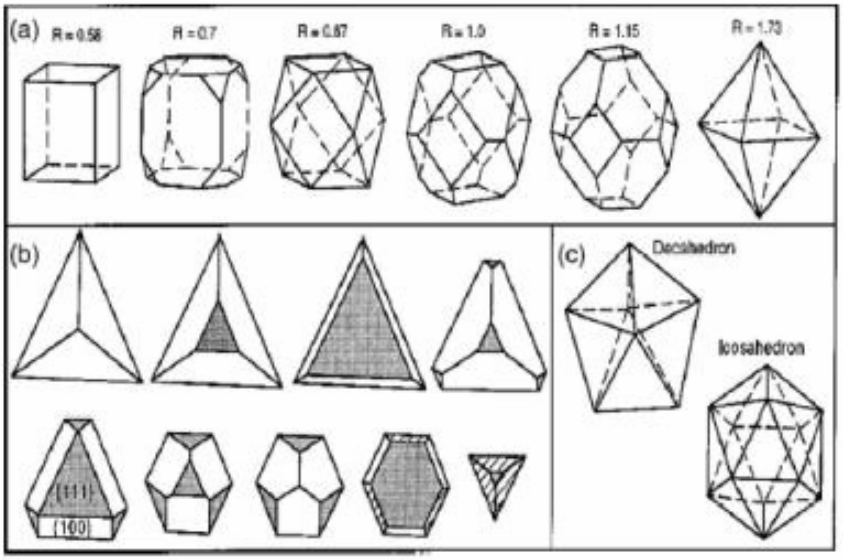

Figure I.2.1 (a) Geometrical shapes of cubooctahedral nanocrystals as a function of ratio, *R*, of the growth rate along the <100> to that of the <111>. Evolution in shapes of a series of (111) based nanoparticles as the ratio of {111} to [100} increases. The beginning particle is bounded by three {100} facets and a (111) base, while the final one is a {111} bounded tetrahedron. (c) Geometrical shapes of multiply twinned decahedral and icosahedral particles [6].

When solid particles are very small the decrease in bond length between the surface atoms and interior atoms becomes significant and the lattice constants of the entire solid particles show an appreciable reduction [7]. Therefore, for particles smaller than 10-20 nm, the surface is a polyhedra. The extra energy possessed by the surface atoms is described as surface energy, surface free energy or surface tension. Surface energy, γ, by definition, is the energy required to create a unit area of "new" surface ($\gamma = (\partial G/\partial A)_{ni,T,P}$) , where *A*, is the surface area. Surface energies associated with different crystallographic planes are

UNIVERSITAT ROVIRA I VIRGILI
NANOMATERIALS IN CATALYSIS: STUDY OF MODEL REACTIONS.
Ricardo José Chimentao
ISBN: 978-84-690-7618-7 / DL: T.1326-2007

usually different and a general sequence may hold, $\gamma_{\{111\}} < \gamma_{\{100\}} < \gamma_{\{110\}}$. Figure I.1.2a shows a group of cubooctahedral shapes as a function of the ratio, *R*, of the growth rate in the <100> to that the <111>. The longest direction in a cube is the <111> diagonal, and the longest direction in the cucooctahedron (*R*= 0.87) is the <110> direction. The particles with 0.87< R< 1.73 have the {100} and {111} facets, which are named truncated octahedral (TO). The other group of particles has a fixed (111) base with exposed {111} and {100} facets (Figure I.1.2b). It is obvious that, for a given particle geometry, as the particle size increases the fraction of atoms which exist in the surface will decrease, and the fraction of surface atoms which exist in very low coordination number (corner and edge atoms) will decrease. The ratio of surface atoms to bulk depends on the particle size. The particle size below which departure from bulk properties can be expected is very small, and appears to be around 2 nm [8]. A metal particle containing 400 atoms would be about 2 nm in size, and one would thus expect electrons properties to change below this size. Metallic clusters containing less than 10-20 atoms have electronic properties which differ substantially from bulk metal values. Atoms in position of low co-ordination have different electronic properties, and hence may show different chemical bonding properties to atoms in low index planes. Due to the high surface energy of the small metal particles all factor influencing it such as adsorption, alloying or the support may change the structure of the dispersed metal. Relevance of these phenomena to catalysis is obvious in view the fact that the behavior of the metal in the catalytic reaction strongly depends on the arrangement of the metal atoms on the surface. In summary, as the size of a metal particle is decreased, a number of things happen: (i) obviously the fraction of

UNIVERSITAT ROVIRA I VIRGILI
NANOMATERIALS IN CATALYSIS: STUDY OF MODEL REACTIONS.
Ricardo José Chimentao
ISBN: 978-84-690-7618-7 / DL: T.1326-2007

surface atoms increase, and because these vibrate more freely the melting temperature falls and surface atom mobility rises. (ii) Because the overlap of electron orbitals decreases as the average number of bonds between atoms becomes less, the structure is weakened, and surface atoms in particular start to behave more as individuals than as members of the club. (iii) At the same time, a greater fraction of the atoms comes into contact with the support, and the length of the periphery per unit of mass of metals rises.

Metal particles have been synthesized by using various methods such as templating [9, 10], photochemistry [11], seeding [12, 13], and electrochemistry [14, 15]. Reduction of the metal complexes in diluted solutions is the general method in the synthesis of metal nanoparticles. Various synthesis methods or techniques can be grouped into two categories: thermodynamic equilibrium approach and kinetic approach. In the thermodynamic approach, synthesis process consists of (i) generation of supersaturation, (ii) nucleation, and (iii) subsequent growth. In the kinetic approach, formation of nanoparticles is achieved by either limiting the amount of precursors available for the growth such as used in molecular beam epitaxy, or confining the growth in a limited space such as aerosol synthesis or micelle synthesis. In this work, the attention will be focused on both synthesis approaches. A broad more general review of new nanoscience and nanotechnology methods has been given by Tolles [16].

Here the synthesis of nanoparticles through thermodynamically approach was based on the formation of monosized metallic silver by a combination of a low concentration of solute and polymeric monolayer adhered onto the growth surfaces. Silver nanowires have been synthesized via polyol process [17]. Controlling the size, shape and

UNIVERSITAT ROVIRA I VIRGILI
NANOMATERIALS IN CATALYSIS: STUDY OF MODEL REACTIONS.
Ricardo José Chimentao
ISBN: 978-84-690-7618-7 / DL: T.1326-2007

structure of metal nanoparticles is technically important because of strong correlation between these parameters and catalytic properties. The formation of monosized metallic nanoparticles can be achieved in most cases by a combination of a low concentration of solute and the use of polymeric stabilizers such as polyvinyl-pyrrolidone (PVP). Ethylene glycol has been widely used in this synthesis process due to its strong reducing power and relatively high boiling point. The growth of the Ag particles is generated by the reduction of $AgNO_3$ with ethylene glycol whereas the anisotropy growth is controlled by the presence of stabilizers such as PVP. The presence of the polymer in the solution of colloids is believed to have two functions. First, it stops the growth of the particles at a small size distribution. Second it prevents individual colloidal particles from coalescing with each other [19]. It is generally accepted that the coordination reagent kinetically controls the growth rates of various faces of a metal through selective adsorption and desorption on these surfaces. There seems to be selectivity between the metal surfaces and the functional groups of the coordination reagent. The *fcc* nanocrystals normally have {111} twins. The *fc* tends to nucleate and grow into twinned and multiply twinned particles (MTP) with their surfaces bounded by the lowest energy {111} facets [20]. Twinning is the result of two subgrains sharing a commom crystallographyic plane. In this case, the structure of one subgrain is the mirror refletion of the other by the twin plane. The two most examples of MTP are decahedron and icosahedron. As demonstrated by Wang [21], the shape of an *fcc* crystal is mainly determined by the ratio (*R*) between the growth rates in the (100) direction to that of (111). Octahedra and tetrahedral bounded by the most stable {111} planes will be formed when $R = 1.73$. Perfect cubes bounded by the less stable

UNIVERSITAT ROVIRA I VIRGILI
NANOMATERIALS IN CATALYSIS: STUDY OF MODEL REACTIONS.
Ricardo José Chimentao
ISBN: 978-84-690-7618-7 / DL: T.1326-2007

{100} planes will result if *R* is reduced to 0.58. Figure I.2.2 shows a schematic illustration of the mechanism that previous studies proposed [22] to account for the evolution of silver into 1D nanostructure.

Two components are critical for this growth mechanism: the MTP has 5- fold symmetry, which its surface bounded by ten {111} facets. In terms of surface energy minimization, it is favorable to form such twinned nanostructure once the particle size has reached a critical size [23]. A set of five twin boundaries are required to generate the decahedral particle because it is impossible to fill the space of an-object of 5-fold symmetry with only a single crystalline lattice. Pentagonal arrangement in MTPs is quite well known and five-fold symmetry nanoparticles have provoked much attention during the last 50 years. Indeed, multi-twinned nanoparticles of transition metals with *fcc* lattice [24] have been reported. Five-fold twinning is not only found in synthetic materials, but also in structures with natural origin [25].

For the kinetic approach we synthesized gold nanoparticles by kinetically confining the reaction in a restrict space. This method is exemplified by the synthesis of nanoparticles inside micells or in microemulsion. In micelle synthesis, reactions precede among the reactants that are available only inside and the particle stops growing when the reactants are consumed. When the surfactant or block polymers typically consisting of two parts, one hydrophilic and another hydrophobic, are dissolved in a solvent they preferentially self assembly at hydrocarbon/aqueous solution in such way to form micelles. The dynamic exchange of reactants such as metallic salts and reducing agents between droplets via the continuous oil phase is strongly depressed due to restricted solubility of inorganic salts in the oil phase.

UNIVERSITAT ROVIRA I VIRGILI
NANOMATERIALS IN CATALYSIS: STUDY OF MODEL REACTIONS.
Ricardo José Chimentao
ISBN: 978-84-690-7618-7 / DL: T.1326-2007

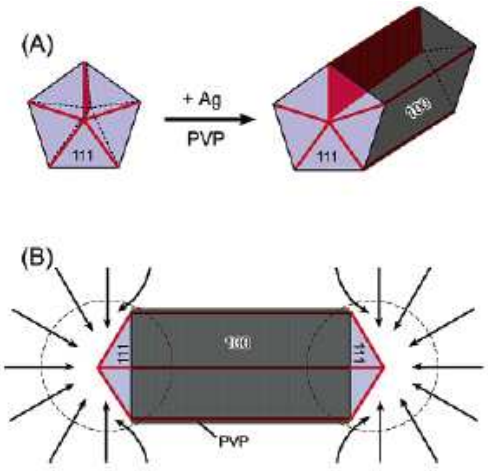

Figure I.2.2 Schematic representation illustrating the diffusion of silver atoms toward the two ends of a nanorod, with the side surfaces completely passivated by PVP. This drawing shows a projection perpendicular to one of the five side facets of a nanorod, and the arrows represent the diffusion flux of silver atoms [22].

This is the reason of the attractive interactions (percolation) between droplets play a dominant role in particle nucleation and growth in the water/oil microemulsion reaction medium. For example, a bimolecular reaction between two hydrophilic reactants metallic salt (A≡ MCl_2) and inorganic reducing agent (B≡ $NaBH_4$) forms a product C (≡ M, a metal particle) with all reacting species confined within the dispersed aqueous phase of a water/oil microemulsion system (Figure I.2.3). The surfactant-stabilized water pools provide a microenvironmental for the preparation of a nanoparticle by exchanging their contents via the fusion-redispersion process and preventing the excess aggregation of particles. As a result, the particles obtained in such a medium are generally very fine and monodisperse. Many kinds of nanoparticles have been prepared in water/oil microemulsions, including metals [27],

UNIVERSITAT ROVIRA I VIRGILI
NANOMATERIALS IN CATALYSIS: STUDY OF MODEL REACTIONS.
Ricardo José Chimentao
ISBN: 978-84-690-7618-7 / DL: T.1326-2007

metal oxides and hydroxides [28].

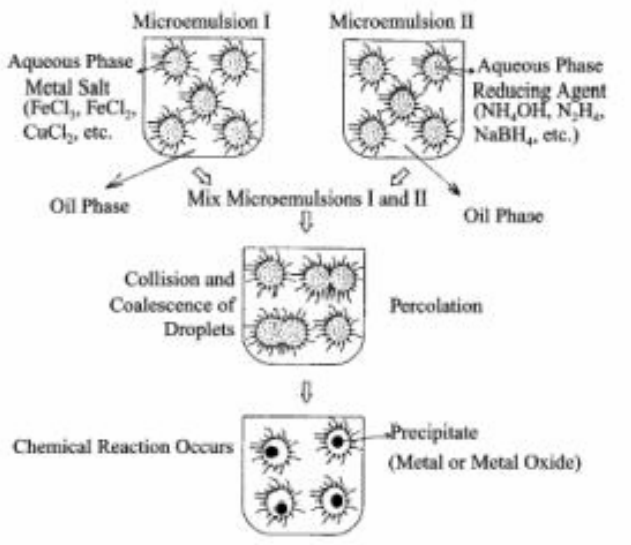

Figure I.2.3 Proposed percolation mechanism [26].

Here in this work the preparation of Au-Ag bimetallic nanoparticles in water/hexadecylamine/toluene by coreduction of chloroauric and silver nitrate with sodium borohydride ($NaBH_4$) at 25 ˚C is reported. The size, structure, optical properties, and composition distribution of the resultant nanoparticles were characterized by transmission electron microscopy (TEM), X-ray diffraction (XRD), UV-vis and X-ray photoelectron spectroscopy (XPS). Also the formation process for the alloying is discussed.

I.2.2 Characterization and properties of the nanoparticles

The discussion in this chapter is focused mainly on the fundamentals and basic principles of the characterization methods. Technical details,

UNIVERSITAT ROVIRA I VIRGILI
NANOMATERIALS IN CATALYSIS: STUDY OF MODEL REACTIONS.
Ricardo José Chimentao
ISBN: 978-84-690-7618-7 / DL: T.1326-2007

operation procedures and instrumentations are not the subjects of discussion here. The intention of this chapter is to provide readers with the basic information on the fundamentals that the characterization methods are based on. For technique details are recommended to relevant literature [29, 30].

I.2.2.1 Structural Characterization

I.2.2.1.1 X-ray diffraction (XRD)

X-ray diffraction is a very important technique that has long been used to address all issues related to the crystal structure of solids, including lattice constants and geometry, identification of unknown materials, orientation of single crystals, preferred orientation of polycrystals, defects, stress, etc [31]. X-ray diffraction line broadening is widely used for measuring metal particle size and particle size distributions. The simplest method to evaluate XRD profiles is the application of the Scherrer equation to obtain average crystallite sizes [29]. The limits of the technique are generally stated to lie between 3 nm and 50 nm, however with careful experimentation it is possible to study metal particles < 2 nm. For smaller particles the application of X-ray diffraction becomes very difficult, as it does for supported metal catalysts of any kind having such high dispersions. The lines in the diffraction patterns are then extremely broad and weak, becoming indistinguishable from the background. In XRD, a collimated beam of X-rays, with a wavelength typically ranging from 0.7 to 2 Å, is incident on a specimen and is diffracted by the crystalline phases in the specimen according Bragg's law:

UNIVERSITAT ROVIRA I VIRGILI
NANOMATERIALS IN CATALYSIS: STUDY OF MODEL REACTIONS.
Ricardo José Chimentao
ISBN: 978-84-690-7618-7 / DL: T.1326-2007

$$\lambda = 2d \sin\theta \qquad \text{(I.1)}$$

where d is the spacing between atomic planes in the crystalline phase and λ is the X-ray wavelength. Thus d is easily measured if λ and θ are known. XRD it's a powerful method for bulk structure determination and estimation of lattice constant by one of the standard methods [32] serves to identify the diffracting phase. The intensity of the diffracted X-rays is measured as a function of the diffraction angle 2θ and the specimen's orientation. This diffraction pattern is useful to identify the specimen's crystalline phases and to measure its structural properties. XRD is nondestructive technique. For more details the readers are highly recommended to an excellent book by Cullity and Stock [29]. Diffraction peak positions are accurately measured with XRD, which makes it best method for characterizing homogeneous and inhomogeneous strains [35]. Homogeneous or uniform elastic strain shifts the diffraction peak positions. From the shift in peak positions, one can calculate the change in d-spacing, which is a result of the change of lattice constants under a strain. Inhomogeneous strains vary from crystallite to crystallite and this causes a broadening of the diffraction peaks that increase with $\sin\theta$. Peak broadening is also caused by the finite size of crystallites, but here the broadening is independent of $\sin\theta$. If there is no inhomogeneous strain, the crystallite size, D, can be estimated from the peak width with Scherrer's formula:

$$D = K\lambda / B\cos\theta_B \qquad \text{(I.2)}$$

where λ is the X-ray wavelength, B is the full width of height

ISBN: 978-84-690-7618-7 / DL: T.1326-2007

maximum (FWHM) of a diffraction peak, θ_B is the diffraction angle, and K is the Scherrer's constant of the order of unity for usual crystal. However one should be alerted to the fact that nanoparticles often form twinned structures, therefore, Scherrer's formula may produce results different from the true particle sizes.

From the XRD analysis it is also possible to generate a particle size distribution by analysis of the peak profile, and its most elaborate form consideration is given to the concentration of defects, which manifest themselves as local deviations of the lattice constant, and to lattice strain. The theoretical base is provided by the Warren-Averbach procedure [34] which has been applied for to a number of systems.

The technique is also useful to study alloy formation in bi- and multimetallic catalysts from the position and shape of diffraction peaks. However, similar limitations apply as discussed in the use of XRD line broadening for crystallite size determinations. In addition the appearance of a symmetric diffraction peak at a position expected from the alloy composition by Vergard's law does not guarantee a uniform particle composition. The metal dispersion of the alloy is equal to the overall if and only if surface composition is equal to the bulk composition. From the shift in peak positions, one can calculate the change in *d*-spacing, which is the result the change in the lattice constants under a strain. However, the surface composition of alloy particles can vary significantly from that of the bulk. In most cases, the surface of an alloy is enriched with one of its components. The driving force for this process is the minimization of the total free energy of the system. Thus, the surface of the alloy may be enriched with the components with the lower surface free energy. Usually another parameter that may affect the surface composition is selective

ISBN: 978-84-690-7618-7 / DL: T.1326-2007

chemisorption of a gas on the components of the alloy. The component that interacts more strongly with the ambient gas enriches the surface. Discrepancies between theoretical predictions and experimental results as well as between experimental results of different investigators can be caused by factors such as temperature, particle size, and support material, in the case of supported alloy particles it would be expected that equilibrium surface composition depends on size and morphology of alloy crystals. Therefore different carries and different metal contents may lead to different results. Furthermore, the regular solution model assumes ideal entropy of mixing and statistical distribution of atoms over lattice points. Deviations from such distributions can occur due to electronic or geometric factors, present at the surface of alloy particles.

I.2.2.1.2 Microscopy

In catalysis, the main interest of the microscopy lies in the possibility of studying the surface topography and morphology of particles. Transmission electron microscopy (TEM) and scanning electron microscopy (SEM) are indeed outstanding tools in textural analysis of solids. The information given by these techniques is generally very useful for the critical discussion of the data coming from adsorption isotherms and XRD analysis.

I.2.2.1.2.1 Scanning electron microscopy (SEM)

In a typical SEM, a source of electrons is focused into a beam, with a very fine size of 5 nm and having energy ranging from a few hundred

UNIVERSITAT ROVIRA I VIRGILI
NANOMATERIALS IN CATALYSIS: STUDY OF MODEL REACTIONS.
Ricardo José Chimentao
ISBN: 978-84-690-7618-7 / DL: T.1326-2007

eV to 50 keV, that is rastered over the surface of the specimen by deflection coils. As the electrons strike and penetrate the surface, a number of interactions occur that result in the emission of electrons and photons from the sample, and SEM images are produced by collecting the emitted electrons on a cathode ray tube (CRT). Various SEM techniques are differentiated on the basis of what is subsequently detected and imaged, and the principle images produced in SEM are of three types: secondary electron images, backscattered electron images and elemental X-ray maps. When a high energy primary electron interacts with an atom, it undergoes either inelastic scattering with atomic electrons or elastic scattering with the atomic nucleous. In an inelastic collision with an atom, the primary electron transfers part of its energy to the other electrons. When the energy transferred is large enough, the other electron will emit from the sample. If the electron emitted has energy less than 50 eV, its referred to as a secondary electron [35]. Backscattered electrons are the high energy electrons that are elastically scattered and essentially possess the same energy as the incident or primary electrons. The probability of backscattering increases with the atomic number of the sample material. Although backscattering images cannot be used for elemental identification, useful contrast can develop between regions of the specimen that differ widely in atomic number, Z. An additional electron interaction in the SEM is that the primary electron collides with and ejects a core electron from an atom in the sample. The excited atom will decay to its ground state by emitting either a characteristic X-ray photon or an Auger electron, of which have been used for chemical characterization and will be discussed later in this chapter. Combining with chemical analytical capabilities, SEM not only provides the image of the

morphology and microstructures of bulk and nanostructure materials and devices, but can also provide detailed information of chemical composition and distribution. The theoretical limit to an instrument's resolving power is determined by the wavelengths of the electron beam used and the numerical aperture of the system. The resolving power, R, of an instrument is defined as:

$$R=\lambda/2NA \qquad (I.3)$$

Where λ is the wavelength of electrons used and NA is the numerical aperture, which is engraved on each objective and condenser lens system, and a measure of the electron gathering ability of the objective, or the electron providing ability of the condenser.

I.2.2.1.3 Transmission electron microscopy (TEM)

TEM is likely to be very powerful for revealing the atom distributions on nanocrystal surfaces. Today's TEM is a versatile tool that provides not only atomic-resolution lattice images but also chemical information at a spatial resolution of 1 nm or better, allowing direct identification the chemistry of a single nanocrystal [36, 37]. With a finely focused electron probe, the structural characteristics of a single nanoparticle can be fully characterized. TEM is unique for characterization the in situ structural evolution of nanocrystals resulting from annealing. TEM has played a major role in characterizing the shape-controlled nanocrystals.
In TEM, electrons are accelerated to 100 keV or higher (up to 1 MeV), projected onto him specimen (less than 200 nm) by means of the condenser lens system, and penetrate the sample thickness either

ISBN: 978-84-690-7618-7 / DL: T.1326-2007

undeflected or deflected. The greatest advantages that TEM offers are the high magnification from 50 to 10^6 and its ability to provide both image and diffraction information from a single sample.

A modern TEM is composed of an illumination system, a specimen stage, an objective lens system, the magnification system, the data recording system, and the chemical analysis system. The electrical gun is the heart of the illumination system, which typically uses LaB_6 thermoionic emission source or a field emission source.

Finally the chemical analysis system is the energy- dispersive X- ray spectroscopy (EDS) and electron loss spectroscopy (EELS), both can be used complementary to quantify the chemical composition of the specimen. EDS relies on the counting of X-rays emitted from the beam illuminated specimen region as a function of photon energy and it is probably the most precise microanalysis technique in TEM. EELS analyses the intensity distribution of the transmitted electrons as function of their energy loss. It provides not only the chemical information on the specimen but also its electronic structure. Selected area diffraction (SAD) offers a unique capability to determine the crystal structural of individual nanomaterials, such as nanocrsytals and nanorods, and the crystal structures of different parts of a sample. In SAD, the condenser lens is defocused to produce parallel illumination at the specimen and a selected area aperture is used to limit the diffracting volume. SAD patterns are often used to determine the Bravais lattices and lattice parameters of crystalline materials by the same procedure used by XRD [29]. Although TEM has no inherent ability to distinguish atomic species, electron is exceedingly sensitive the target element and various spectroscopy and developed for the chemical composition analysis.

UNIVERSITAT ROVIRA I VIRGILI
NANOMATERIALS IN CATALYSIS: STUDY OF MODEL REACTIONS.
Ricardo José Chimentao
ISBN: 978-84-690-7618-7 / DL: T.1326-2007

I.2.2.1.3 Gas adsorption

Physical and chemical adsorption isotherm is a powerful technique in determining the surface area and characteristic sizes of the particles and porous structures regardless of their chemical composition and crystal structures.

I.2.2.1.3.1 Physical adsorption

When a gas comes in contact with a solid surface, under suitable temperature and pressure, gas molecules will adsorb onto the surface so as to reduce the imbalanced attractive force on surface atoms, and thus reduce the surface energy. Adsorption may be either physical or chemical in nature [38]. The forces responsible for the physisorption depend on the molecule in question and on the chemical nature of the surface, but they are of the some kind as those that hold molecules together in liquids, and are collectively described as Van der Waals forces, comprising dipole-dipole interactions, induced dipole charges, London forces due to mutually-induced fluctuating dipoles and nuclear quadrupole forces. In 1940, Brunauer et al. [39] proposed to classify the physical adsorption isotherms in five different groups numbered from *I* to *V*. This is well known classification relates the shape of the isotherms to both the mean pore size of the adsorbent and the intensity of adsorbate-adsorbent interaction [40]. The five types of adsorption isotherm are schematically represented in Figure I.2.4. It is generally admitted that:

UNIVERSITAT ROVIRA I VIRGILI
NANOMATERIALS IN CATALYSIS: STUDY OF MODEL REACTIONS.
Ricardo José Chimentao
ISBN: 978-84-690-7618-7 / DL: T.1326-2007

- *isotherms of type I* are characteristic of microporous adsorbents
- *isotherms of types II and III* are observed for macroporous adsorbent. Type *II* isotherms frequently occur. On the contrary type *III* isotherms are rather unusual and correspond to very weak adsorbate-adsorbent interaction
- *isotherms of types IV and V* are obtained for mesoporous adsorbents. Type *IV* isotherms are widespread whereas type *V* isotherms (which correspond to very weak adsobate-adsorbent interactions) are seldom encountered.

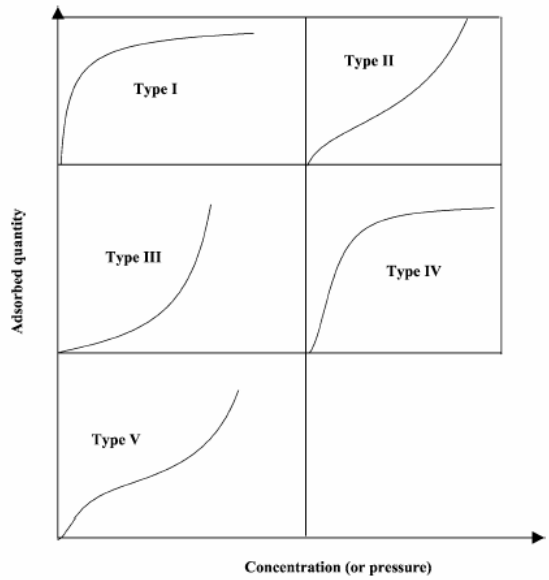

Figure I.2.4 The five types of adsorption isotherms [41].

In everyday practice, the shape of the isotherm usually gives a rather good idea of the mean size of the pores present in the solid. Sometimes, however, an isotherm cannot be related to one definite group of this classification because different types of pores are present in the

UNIVERSITAT ROVIRA I VIRGILI
NANOMATERIALS IN CATALYSIS: STUDY OF MODEL REACTIONS.
Ricardo José Chimentao
ISBN: 978-84-690-7618-7 / DL: T.1326-2007

adsorbent. These “mixed” isotherms are also indicative of the general porosity of the solid. Another easy way to get information on the porous texture of the adsorbent is to look the shape of the hysteresis loop. The presence of an hysteresis loop into five main groups have been proposed by Boer [41]. Each group is related to the general shape of the pores present in the solid, as illustrated in Figure I.2.5.

- *Type A hyteresis* is associated with “cylinder shaped” pores of rather constant cross section
- *Type B hyteresis* points to the presence of slit-shaped pores
- *Type C and D hyteresis* derive from the type *A* and *B* respectively and formed the non parallel plates (type *D*). These two types of hysteresis loops are rather unusual
- *Type E hyteresis* very frequently occurs. It corresponds to “ink-bottle”pores, spherical cavities or voids between close-packed spherical-like particles.

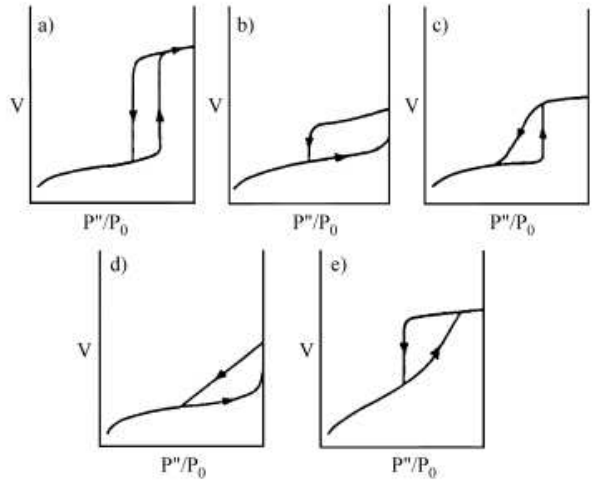

Figure I.2.5 The five types of hysteresis loops [41].

UNIVERSITAT ROVIRA I VIRGILI
NANOMATERIALS IN CATALYSIS: STUDY OF MODEL REACTIONS.
Ricardo José Chimentao
ISBN: 978-84-690-7618-7 / DL: T.1326-2007

This classification is widely used [42] even if in practice the hysteresis loop shape appears rather different from the ideal curves presented in Figure I.2.5. The mean reason for these differences is the existence of real solids of a more and less broad pore size distribution whereas the models used are based on ideal solids where all pores have the same size. In general the broader pore size distribution, the wider the hysteresis loop. Furthermore, "mixed" hysteresis loop may often observed if different pore shapes are present in the same solid. Since the publication, in 1938, by Brunauer, Emmett and Teller [43] of their famous model for physical adsorption of vapors on solid, the BET theory and its use as a toll for determination of specific surface area of solids have formed the subject of many papers, reviews and books. [44,45]. The limitations and the range of applicability of the BET-model have been critically discussed by several authors. It is highly recommended for the readers the book of Gregg and Sing [40] and the review paper of Nicolaon [46]. The BET equation is more conveniently written in the following form:

$$x/V_a(1-x)=1/V_mc + (c-1)/V_mc \qquad (I.4)$$

where V_a is the adsorbed volume of the adsorbate per unit mass of adsorbent, V_m is the volume of adsorbate just sufficient to cover the surface developed by unit of mass of adsorvent, x is the relative pressure P/P_0, c is a constant varying with the adsorbent-adsorbate interactions. The V_m value is directly proportional to the specific surface area of the adsorbent, because V_m is, by definition, the amount of adsorbate just sufficient to cover with a complete monolayer the whole surface developed by the unit mass of adsorbent. The specific

UNIVERSITAT ROVIRA I VIRGILI
NANOMATERIALS IN CATALYSIS: STUDY OF MODEL REACTIONS.
Ricardo José Chimentao
ISBN: 978-84-690-7618-7 / DL: T.1326-2007

surface area of the solid is thus equal to the area occupied by one adsorbate molecule multiplied by the number of adsorbate molecules contained is $V_{m,}$ so that

$$s=a_m.\ v_m.N_a/\ V_m \qquad (I.5)$$

where s is the specific surface area, v_m is the monolayer capacity of unit mass of solid, N_A is the Avogadro constant, V_m is the molar volume of adsorbate and a_m is the part of surface occupied by one molecule of adsorbate in a closed layer. In the case of nitrogen adsorption at liquid nitrogen temperature (77 K) the most widely admitted [47] and used value of the area occupied by a nitrogen molecule is: $a_m(N_2)=16.2 \times 10^{-20}$ m^2.

In this conditions, if N_A and V_m are taken respectively equal to $6.025x10^{23}$ $mole^{-1}$ and $22.414x10^{-3}$ $m^3.mole^{-1}$, the specific surface area of the solid (expressed in m^2/kg of solid) is given by $s_{BET} =4.37x10^6\ v_m$, v_m being the monolayer capacity expressed in m^3 STP of N_2/kg of solid. If other adsorbates than N_2 are used, it is rarely possily to assign a fixed value to the molecular surface area am of a given adsoptive. In general a range of value is given for each adsorptive [42] but, from their comprehensive review of the literature, McClellan and Harnsberger [43] recommended the following values of am expressed in 10^{-20} m^2:

Ar *at 77 K: 13.8*

Kr *at 77 K: 20.2*

nC_4H_{10} *at 273 K: 44.4*

C_6H_6 *at 293 K: 43.0*

However great caution should be exercise while using these values because the molecular surface area of an adsorbate depends somewhat

UNIVERSITAT ROVIRA I VIRGILI
NANOMATERIALS IN CATALYSIS: STUDY OF MODEL REACTIONS.
Ricardo José Chimentao
ISBN: 978-84-690-7618-7 / DL: T.1326-2007

on the nature of the adsorbent. In practice, the use of nitrogen as adsorbate in textural studies Is thus generally more reliable and technically simpler than the utilization of other adsorbates.

I.2.2.1.3.2 Chemical adsorption

Selective chemisorption has been used extensively since the early sixties to measure the number of surface metal atoms, and to obtain metal surface areas and average metal particle sizes. A selected gas is chemisorbed under conditions which permit the formation of a monolayer on the metal without any significant contribution of the support. Metallic catalysts exist in the form of bulk metal (powder, wire) or in a dispersed state on a nonmetallic porous support (alumina, silica, alumina-silica, zeolites, titania, magnesia, carbon, etc). Whereas the multilayer physisorption of N_2 and Kr is used to determine the total surface area of the solid, selective chemisorption with formation of a monolayer has been used systematically the surface area of the metals. What is measured is the total number of accessible surface atoms, which not necessarily equal to the number of catalytic sites in a given reaction [49]. The dispersion *D* of the metal ($D \leq 1$) is defined as the ratio of the number of surface metal atoms to the total number of metal atoms in the sample [50]. Dispersion is also expressed as percentage. According to IUPAC rules, the expression "*percentage exposed*" should be preferred over the word dispersion. The most common adsorptives used in the selective chemisorption are H_2, CO, O_2, N_2O and C_6H_6 [51]. Since percentage exposed, particle size and surface area are related, it is recommended, whenever possible, to check the results of the selective chemisorption by means physical techniques: X-ray

UNIVERSITAT ROVIRA I VIRGILI
NANOMATERIALS IN CATALYSIS: STUDY OF MODEL REACTIONS.
Ricardo José Chimentao
ISBN: 978-84-690-7618-7 / DL: T.1326-2007

diffraction and electron microscopy [52]. Unfortunately, these physical tools fail when the metallic clusters are very small. Also the averages are different: number average (electron microscopy), surface average (chemisorption), volume average (X-ray diffraction). Besides, if a particle is polycrystalline, the size determined by the X-ray diffraction will be smaller than a given electron microscopy. From the view point of catalysis, the percentage exposed is the most direct and pertinent measurement. If part of the metal surface is poisoned, the percentage exposed may correlate directly the catalytic activity [53, 54], although particle size translated into dispersion would not be a useful quantity. In typical hydrogen adsorption experiment the metallic catalyst is first contacted with flowing hydrogen in the adsorption cell at appropriate temperature to ensure thorough reduction. The cell is then evacuated and cooled to room temperature for the determination of total adsorption [50]. When this isotherm is completed, the weakly adsorbed hydrogen is removed from the sample by evacuating the adsorption cell at room temperature for 10 minutes to a pressure approximately 10^{-6} torr. A second isotherm is then run at room temperature. This isotherm constitutes the weakly adsorbed hydrogen. The difference between the total adsorption and the weakly adsorbed hydrogen is strongly chemisorbed hydrogen. From the volume of the total hydrogen adsorption and the irreversible adsorption one can determine the dispersion, *D*. For further details on supported metals catalysts, the reader should consult the Anderson's book (1975) [55].

UNIVERSITAT ROVIRA I VIRGILI
NANOMATERIALS IN CATALYSIS: STUDY OF MODEL REACTIONS.
Ricardo José Chimentao
ISBN: 978-84-690-7618-7 / DL: T.1326-2007

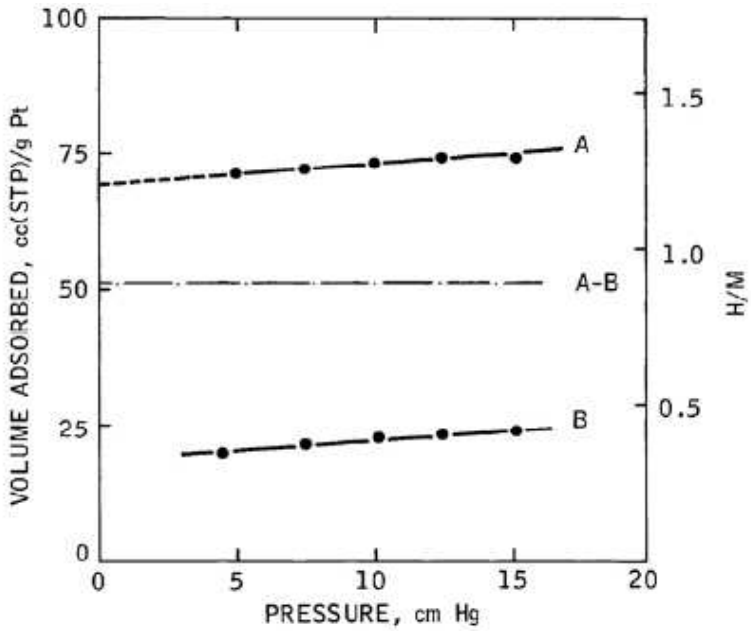

Figure I.2.6. Typical hydrogen chemisorption at room temperature on a platinum-on-alumina catalyst containing 1 wt.% platinum. The quantity H/M is the ratio of the number of hydrogen atoms adsorbed to the number of platinum atoms in the catalyst [56].

In hydrogen chemisorption on the Group VIII metals, it is generally accepted that the hydrogen molecule dissociates, so that hydrogen atoms are adsorbed on the surface. Typical data on the chemisorption of hydrogen on room temperature on a platinum on alumina catalyst are show in Figure I.2.6. Isotherm A represents the total chemisorption, and isotherm B represents the weakly chemisorbed fraction, since it is removed by simple evacuation at room temperature. Isotherm B includes adsorption on the alumina carrier. The difference isotherm, labeled A-B, is obtained by subtracting isotherm B from A and is independent of pressure over the range of pressures used in obtaining the isotherm. It represents the strongly chemisorbed fraction, that is, the

UNIVERSITAT ROVIRA I VIRGILI
NANOMATERIALS IN CATALYSIS: STUDY OF MODEL REACTIONS.
Ricardo José Chimentao
ISBN: 978-84-690-7618-7 / DL: T.1326-2007

amount that cannot be removed by evacuation at room temperature. The quantity *H/M* in the right-hand ordinate of Figure I.2.6 represents the ratio of the number *H* of hydrogen atoms adsorbed to the number *M* of platinum atoms in the catalyst. If we assume a stoichiometry of one hydrogen atom per surface platinum atom in the case of strongly chemisorbed fraction, the value of H/M determined from the difference isotherm A-B corresponds to the ratio of surface platinum atoms to total platinum atoms in the catalyst. This ratio is about 0.9 for the catalyst in Figure I.2.6. If a comparison with results from physical techniques is wanted, or just out of habit of dealing with particle size, a handy conversion between dispersion *D* and particle size *d*, in nm, is given by: $D \approx 0.9/d$ or more simply $D = 1/d$, (d in nm). More rigorous determination of the particle size should take into account the shape of the particle. In this case the average particle size *d* is obtained by means of: $d = f\ V_{sp}/S_M$, where S_M is the specific surface area of the metal obtained from the selective chemisorption data by assuming an average number density, V_{sp} is the specific volume of the metal and f is the shape factor of small particles of metal on supports. The values of *f* collected in Table I.2.1 are between 1 and 6. In the absence of any other information, the value $f = 6$ is not unreasonable [49].

Table I.2.1 Relation between shape and size

Shape of Particle	Dimension	Factor
Cube	*Edge*	*5 or 6*
Sphere	*Diameter*	*6*
Cylinder	*Diameter*	*4*
Plate	*Thickness*	*1 or 2*

UNIVERSITAT ROVIRA I VIRGILI
NANOMATERIALS IN CATALYSIS: STUDY OF MODEL REACTIONS.
Ricardo José Chimentao
ISBN: 978-84-690-7618-7 / DL: T.1326-2007

I.2.2.1 Chemical Characterization

I.2.2.2 – X-ray photoelectron spectroscopy (XPS)

XPS is also known as electron spectroscopy for chemical analysis (ESCA). Semi-quantitative technique for determining composition based on the photoelectric effect. In ESCA measurements, electrons are emitted from a substance as a result of irradiation by X-rays [57]. Since an ESCA analysis is carried out in ultrahigh vacuum, most ESCA spectrometers are equipped with "in situ" high pressure treatment chambers, where the catalyst activation treatment can be reproduced and the sample transferred into the analysis chamber without exposure to air. Like other characterization methods XPS suffers from a series limitations like overlap, sample degradation in the beam, insensitivity to subtle changes in chemical environment and difficulties in acquisition of quantitative results. The main components of a XPS instrument are the X-ray source, the electron energy analyzes, the electron detector and an efficient pumping system for the high vacuum required. The laboratory conventional source of the X-ray tube where X-rays are generated by electron bombardment of magnesium or aluminum from which $K_{\alpha 1,2}$ radiation is produced. Table I.2.2 lists X-ray lines energies and line widths for various characteristic lines from some materials. The yttrium and zirconium Mζ lines are narrow and have been used successfully in special applications, but their energies are too much low for general application. The only other lines that fit the requirements are the K_{α} lines of magnesium, aluminum and silicon. Although silicon has also been used for special applications, it is not a metal, so that the heat transfer characteristics are poor and it is difficult

UNIVERSITAT ROVIRA I VIRGILI
NANOMATERIALS IN CATALYSIS: STUDY OF MODEL REACTIONS.
Ricardo José Chimentao
ISBN: 978-84-690-7618-7 / DL: T.1326-2007

to apply to an anode surface.

Table I.2.2 Some X-ray lines of use in photoelectron spectroscopy

Line	Be K	Y Mζ	Zr Mζ	Nb Mζ	Mo Mζ	Ru Mζ	Rh Mζ	C K	Ti Ll	Ti La	O K	Cr La
Energy (eV)	108.9	132.3	151.4	171.4	192.3	236.9	260.1	278	395.3	452.2	524.9	572.8
Width (eV)	5.0	0.47	0.77	1.21	1.53	2.49	4.0	6	3	3	4	3

Line	Ne Kα	Ni Lα	Cu Lα	Zn Lα	Na Kα	Mg Kα	Al Kα	Zr Lα	Ti Kα	Cr Kα	Cu Kα
Energy (eV)	849	851.5	929.7	1011.7	1041.0	1253.6	1486.6	2042	4510	5417	8048
Width (eV)	0.3	2.5	3.8	2.0	0.42	0.7	0.85	1.7	2.0	2.1	2.6

It can be seen that there are indeed very few materials whose characteristic X-ray lines have sufficient small widths. Thus one is left with the magnesium and aluminum K_α lines, and in fact it is these two that are used so universally in XPS. XPS is based on the photoelectric effect arising when high energy photon (usually in keV range) hit a material with the consequent emission of electron (photoelectrons). The photoelectron kinetic energy, E_{KE}, is given by the Eisntein's law

$$E_{KE}=h\nu - E_B - e\phi \qquad \text{(I.6)}$$

where the energy of the ejected electron, E_E, is determined by both the energy of the incident photon, $h\nu$, and the bound electron state, E_B (Figure I.2.7). In order for an electron to be emitted from an atom by an incident X-ray photon, the energy of the X-ray photon must be at least as high as the binding energy of the electron within the atom. The energy the X-ray photon in excess of the binding energy is imparted to the emitted in the form of kinetic energy.

UNIVERSITAT ROVIRA I VIRGILI
NANOMATERIALS IN CATALYSIS: STUDY OF MODEL REACTIONS.
Ricardo José Chimentao
ISBN: 978-84-690-7618-7 / DL: T.1326-2007

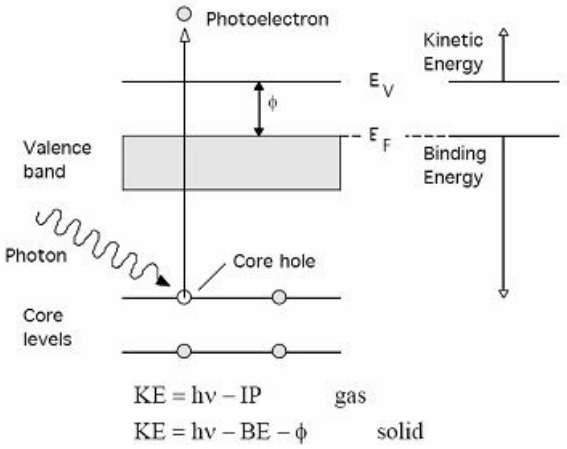

Figure I.2.7 XPS process.

Mainly because of inelastic scattering the information depth is in the range of 2-5 nm and varies the take-off in XPS, relatively low-energy X-rays used to eject the electrons from an atom via the photoelectronic effect [58]. Since the excitation process in XPS involves core electrons, the technique is element specific, and the elements can be identified according to their binding energy (BE). The exact biding energy values reflect the chemical environment (oxidation state, ligands) of atoms, which makes a powerful tool to monitor chemical changes during various treatment procedures in catalyst preparation. Since an atom possesses electrons with various binding energies corresponding to the different electron energy levels, irradiation by X-ray photons of a particular energy will result in the emission of electrons with a definite set of kinetic energies corresponding to lines in ESCA spectrum. Readers interested in more detailed descriptions should consult previous works [59,60]. A feature of particular interest in ESCA is its structure sensitivity. The surface sensitivity of XPS analysis is due to the limited escape depth of the emitted electrons used for analysis.

UNIVERSITAT ROVIRA I VIRGILI
NANOMATERIALS IN CATALYSIS: STUDY OF MODEL REACTIONS.
Ricardo José Chimentao
ISBN: 978-84-690-7618-7 / DL: T.1326-2007

Electrons emitted by atoms in subsurface layers of a material are subject to inelastic scattering process. Theses processes decrease the probability that the electrons will emerge from the material with the expected kinetic energy [61]. The deeper atoms are located in the material, the lower this probability becomes. For atoms at a given depth, the probability of an electron escaping from a material with its kinetic energy unchanged depends on the magnitude of the kinetic energy. The XPS signal decreases exponentially with the distance of the examined atoms from the surface and it is expected that the values obtained mainly refer to the composition of the topmost surface layers off the material. If λ is the inelastic mean free path (IMPF) of the emerging electron than 95 per cent of the signal intensity is derived from a distance 3λ within the solid (Figure I.2.8). However the vertical depth sampled is clearly given by $d = 3\lambda \sin \alpha$ and this is a maximum when $\alpha = 90°$. The major requirement for surface sensitivity enhancement is that the surface is flat. Surface roughness leads to an averaging of electron exit angles and also to shadowing effects (both of the incident X-rays and emerging electrons) such that in most cases the surface enhancement effect cannot be observed.

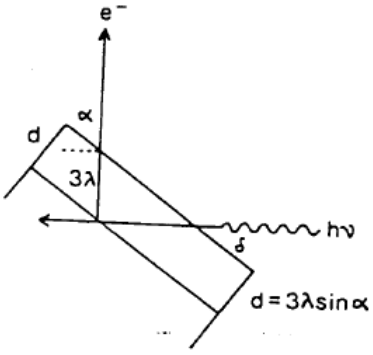

Figure I.2.8 Surface sensitivity enhancement by variation of the electron take-off angle.

UNIVERSITAT ROVIRA I VIRGILI
NANOMATERIALS IN CATALYSIS: STUDY OF MODEL REACTIONS.
Ricardo José Chimentao
ISBN: 978-84-690-7618-7 / DL: T.1326-2007

It should be noted that surface segregation extends beyond the outermost atomic layer, especially in solid solutions, so that compositional variations include several layers underneath. Detailed experimental determination of the segregated multilayer is not an easy task. Conventional surface analysis techniques, such as Auger electron spectroscopy (AES) or X-ray photoelectron spectroscopy (XPS), often used in segregation studies, are not strictly surface specific, and the detected signal intensity is a superposition originating from a number of atomic layers, yielding some average composition throughout the characteristic probing depth.

I.2.2.2.3 Temperature programmed reduction (TPR)

The chemistry involved in the reduction process depends on the type of the precursor. If it is an oxide or hydroxide, or other precursor subjected to calcination, the product of reduction by hydrogen is simply water, but reduction of a chloride will form hydrogen chloride which may not immediately vacate the surface. It is worth noting too that the water formed by reduction of an oxide may hydrate the surface of the support, or just become physically adsorbed on it: the successful application of the hydrogen-oxygen titration for measuring metal dispersion hinges on this. Reduction of nitrates without calcination can also lead to some complex chemistry, since the first reduced metal can catalyze reactions of the gases liberated. It is often desirable to know the precise conditions under which a precursor will become reduced to an active form, and whether the reduction takes place in one stage or more than one. In the letter case one would infer the existence of two or

UNIVERSITAT ROVIRA I VIRGILI
NANOMATERIALS IN CATALYSIS: STUDY OF MODEL REACTIONS.
Ricardo José Chimentao
ISBN: 978-84-690-7618-7 / DL: T.1326-2007

more different species of different reducibility. A widely-used technique for studying these questions is *temperature- programmed reduction* (TPR) [62, 63].

The principle of the method is as follows. A diluted mixture of hydrogen in an inert gas (nitrogen, or preferably argon) flows through one arm of the thermal conductivity cell and then over the sample; water or other condensable products are held back in a trap, and the gas proceeds through the second arm of the thermal conductivity cell (TCD) and thence via a flow-meter to exhaust. Consumption of hydrogen due to reduction of the sample is revealed by detector wires differing in temperature: they form two arms of a Wheatstone bridge and the out-of-balance signal is captured by a microprocessor. Signal calibration is achieved by injecting a know volume of pure hydrogen. For most purposes of the profile is characterized by the T_{max} values and by the integrated volume of hydrogen consumed. The increase in the T_{max} value qualitatively reflects a decrease on the overall reducibility of the sample. Extensive use has also been made of TPR in seeking evidence for the formation of alloys in bimetallic catalysts [64, 65]. The logic employed is simple but fallible. One presumes that if one observes two peaks, each of which is clearly associated with the reduction of one of the components, then there has been the creation of two separate metallic phases and no alloy formation has occurred [62]. Per contra if one sees only a single peak when reducing a bicomponent precursor, it is supposed that the more easily reduced species has catalyzed the reduction of the less easily reduced, perhaps by the intervention of hydrogen spillover, and that there is then every chance of an alloy having been formed Unfortunately, these assumptions are not necessarily truth. There is good evidence however that the

UNIVERSITAT ROVIRA I VIRGILI
NANOMATERIALS IN CATALYSIS: STUDY OF MODEL REACTIONS.
Ricardo José Chimentao
ISBN: 978-84-690-7618-7 / DL: T.1326-2007

occurrence of a single peak, in reducing mixed copper and ruthenium oxides on silica, does not signify to alloy formation, as only separate metal particles result: this is probably due to very effective and rapid hydrogen spillover giving action at a distance [66]. For the technique details, it is highly recommend for the readers the epic study realized by Monti and Baker [67].

I.2.2.4 UV-visible-DRS spectroscopy

Based on the position of the absorption edges, a relative comparison can be made between the energies of the support species. The absorption bands reflect a ligand to metal charge transfer band (LCT) transition [68, 69]. A general power law form has been suggested by Davis and Mott [70] which relates the absorption coefficient with the photon energy. The order of the power function is determined by the type of transition involved. Diffuse reflectance has been analyzed using Kubleka-Munk treatments [71, 72]. The diffuse reflectance for infinitely thick samples ($R\infty$) is given by the reflectance of a sample of finite thickness (R_{sample}) divided by the reflectance of highly reflective standards ($R_{reference}$), such as MgO:

$$R_\infty = R_{sample} / R_{reference} \qquad (I.7)$$

The Kubleka Munk function, $F(R\infty)$

$$F(R_\infty) = (1- R_\infty)^2/2\, R_\infty = K/S \qquad (I.8)$$

Represents the ratio of absorption (K) and scattering (S) coefficients. Scattering coefficients depend weakly on photon energy, but absorption

cross sections increase abruptly as electronic transitions become possible with increasing incident photon energy. Thus, $F(R_\infty)$ provides a measure of absorbance throughout the experimental spectral energy [72]. Barton et al. have recommended using the square root of the Kubelka- Munk function multiplied by the photon energy. By plotting this new function versus the photon energy, the position of the absorption edge can then be determined by extrapoling the linear part of the rinsing curve to zero [73] the values thus obtained carry the information about the average domain size of the oxide nanoparticles since, as for the case of a particle in a box, the band gap energy decreases as the domain sizes increases [74].

I.2.2.3 References

[1] G. A. Somorjai, Y. G. Borodko, *Catal. Lett.* **76** (2001) 1.

[2] J. A. Creighton and D. G. Eadon, *J. Chem. Soc. Faraday Trans.* **87** (1991) 3881.

[3] Y. Cao, R Jin and C. A. Mirkin, *J. Am. Chem. Soc.* **123** (2001) 7961.

[4] C. Nutzenadel, A. Zutell, D. Chartouni, G. Shimid and L.Schalapbach, *Eur. Phys J. D8*, **245** (2000).

[5] A. N. Goldstein, C. M. Echer and A. P. Alivisatos, *Science* **256** (1992) 1425.

[6] S. C. Tjong, H. Chen, *Mater. Science Eng.* **R 45** (2004) 1.

[7] A. N. Goldstein, C. M. Echer, A. P. Alivisatos, *Science* **256** (1992) 1425.

[8] J. R. Anderson, *Sci. Prog. Oxf.* **69** (1985) 461.

[9] M. R. Bohmer, L. G. J. Fokkink, C. Schonenberger and B. M. I.

Van Der Zande, *J. Phys. Chem. B* **101** (1997) 852.

[10] S. R. Nicewarner, R. G. Freeman, B. D. Reiss, L. HE, D. J. Pena, I. D. Walton, R. Cromer, C. D. Keating and M. J. Natan, *Science* **294** (2001) 137.

[11] K. Esumi, K. Matsuhisa and K. Torigoe, *Langmui*r **11** (1995) 3285.

[12] C. J. Murphy and N. R. Jana, *Adv Mater*. **14** (2002) 80.

[13] Y. G. Sun and Y. N. Xia, *Adv Mater*. **14** (2002) 833.

[14] Y. Y. Yu, S. S. Chang, C. L. Lee and C. R. C. Wang, *J. Phys. Chem. B* **101** (1997) 6661.

[15] S. S. CHang, C. W. Shih, C. D. Chen, W. C. Lai and C. R. C. Wang, *Langmuir* **15** (1999) 701.

[16] W. M. Tolles, *Nanotechnology, molecular designed materials*, ACS, Symposion series 622, ACS, Washington, DC, 1996, p.2.

[17] Y. Sun and Y. Xia, *Science* **298 (**2002) 2176.

[18] Z. L. Wang, M. B. Mohamed, S. Link, and M. A. El-Sayed, *Surf. Sci* **440** (1999) L809.

[19] T. S. Ahamadi, Z. L. Wang, T. C. Green, A. Henglein, M. A. El-Sayed, *Science* **272** (1996) 1924.

[20] J. G. Allpress, J. V. Sanders, *Surf. Sci.* **7** (1967) 1.

[21] Z. L. Wang, *J. Phys. Chem. B* **104** (2000) 1153.

[22] Y. Sun, B. Mayers, T. Herricks, Y. Xia, *Nano Lett.* **3** (2003) 955.

[23] L. D. Marks, *Rep. Prog. Phys.* **57** (1994) 603.

[24] K. Heinemann, M.J. Yacatan, C.Y. Yang, H. Poppa, *J. Cryst. Growth*, **47** (1979) 177.

[25] S. Ino, S. Ogawa, *J. Phys. Soc. Jpn.*, **22** (1967) 1365.

[26] I. Capek, *Adv. Colloid Interface Science* **110** (2004) 49.

UNIVERSITAT ROVIRA I VIRGILI
NANOMATERIALS IN CATALYSIS: STUDY OF MODEL REACTIONS.
Ricardo José Chimentao
ISBN: 978-84-690-7618-7 / DL: T.1326-2007

[27] M. Boutonnet, J. Kizling, P. Stenius, G. Maire, *Colloids Surf.* **5** (1982) 209.

[28] C. L. Chang, H. S. Fogler, *Langmuir* **13** (1997) 3295.

[29] B. D. Cullity and S.R. Stock, *Elements of X-ray Diffraction*, 3rd edition, Prentice Hall, Upper Saddle River, NJ, 2001.

[30] L. H. Schwartz, J. B. Cohen, *Diffration from Materials*, Springer-Verlag, Berlim, 1987.

[31] G. M. Clark, *The structures of non-molecular solids*. London: Applied Science Publ. Ltd. 1972.

[32] G. B. Carpenter, *Principles of crystal structure determination*, Benjamin, New York, 1969.

[33] A. Segmuller, M. Murakami, *Analytical Techniques for thin films*, eds. K. N. Tu, R. Rosenberg, Academic Press, San Diego, CA, p.143, 1988.

[34] B. E. Warren, B. L. Averbach, *J. Appl Phys* **21** (1950) 595.

[35] J. Goldstein, D. E. Newbury, D. C. Joy, C. E. Lyman, P. Echlin, E. Lifshin, L.C. Sawyer, J.R. Michael, *Scanning Electron Microscopy and X-ray Microanalysis*, Hardcover 2003.

[36] P. Becker, *J. Colloid. Interface Sci.* **19** (1964) 468.

[37] E. J. Chatfield, *J. Sci. Instrum.* **44** (1967) 615.

[38] D. M Young, A. D. Crowell, *Physical Adsorption of Gases*, Butterworths, London, 1962.

[39] S. Brunauer, L. S. Deming, W. S. Deming. E. Teller, *J. Amer. Chem. Soc.* **62** (1940) 1723.

[40] S. J. Gregg, K. S. W. Sing, *Adsorption, Surface Area and Porosity*. London: Academic Pres 1967.

[41] J. H. de Boer, The shapes of capillaries. *The structure and properties of Porous Materials*. Everett, D. H. and Stone, F. S.

(eds). London: Butterworths 1958, pp. 68-94.

[42] B. C. Lippens, *Structure and Texture of Aluminas*. Thesis Delft 1961.

[43] S. Brunauer, P. H. Emmett, E. Teller, *J. Amer. Chem. Soc.* **60** (1938) 309.

[44] S. Brunauer, The adsorption of gases and vapours. Princeton: University Press 1943.

[45] J. E. Germain, *Catalyse hétérogène*. Paris: Monographie Dunod 1959.

[46] G. A. Nicolaon, *Bull. Soc. Chim. Fr.* 1969, 91.

[47] J. M. Thomas, W. J. Thomas, *Introduction to the Principles of Heterogeneous Catalysis*. London: Academic Press 1967.

[48] A. L. McCellan, H. F. Harnsberger, *J. Colloid. Interface Sci.* **23** (1967) 577.

[49] M. Boudart, G. D. Mariadassou, *Kinetics of Heterogeneous Catalytic Reactions*, Princenton University Press, 1984.

[50] M. Boudart, *Adv. Catal.* **20** (1969) 153.

[51] J. J. F. Scholten, J. A. Konvalinka, *Trans. Faraday Soc.* **65** (1969) 2465.

[50] L. Spenadel, M. Boudart, *J. Phys. Chem.* **64** (1960) 204.

[51] G. Leclercq and M. Boudart, J. Catal. **71** (1981) 127.

[54] H. Sinfelt, Y. L. Lam, J. A. Cusumano and A. E. Barnett, *J. Catal.* **42** (1976) 227.

[55] J. R. Anderson, *Structure of Metallic Catalysts*. New York: Academic Press.

[56] G. H. Via, J. H. Sinfelt, F. W. Hall, *J. Catal.* **17** (1970) 190.

[57] D. Briggs, M. P. Seah, *Practical surface analysis: by Auger and X-ray photoelectron spectroscopy*, John Wiley & Sons, New

UNIVERSITAT ROVIRA I VIRGILI
NANOMATERIALS IN CATALYSIS: STUDY OF MODEL REACTIONS.
Ricardo José Chimentao
ISBN: 978-84-690-7618-7 / DL: T.1326-2007

York 1987.

[58] J. W. Niemantsverdriet, *Spectroscopy in catalysis, VCH, Weineim*, 1993.

[59] J. H. Sinfelt, *Science* **195** (1977) 641.

[60] C. R. Helms, J. H. Sinflet, *Surface. Sci.* **72** (1978) 229.

[61] T. A. Carlson, *Photoelectron and auger spectroscopy*, Plenum Press, New York, 1975.

[62] J. W. Jenkins, B. P. McNicol, S. D. Robertson, *Chem. Technol.* 7 (1977) 316.

[63] A. Jones, B. D. McNicol, *Temperature-programmed reduction for solid materials characterization*, Dekker, New York, 1986.

[64] C. G. Bond, P. B. Wells *Appl. Catal.* **18** (1985) 225.

[65] L. van Tiep, M. B. Tardy, G. Bugli, G. D. Mariadassou, M. Che, G. C. Bond, *J. Catal.* **99** (1986) 449.

[66] C. G. Bond, X. Yide, *J. Mol. Catal.* **25** (1984) 141.

[67] D. A. M. Monti, A. Baiker, *J. Catal.* **83** (1987) 522.

[68] H. SO, M. T. Pope, *Inorg. Chem.* **11** (1972) 1441.

[69] M. L. Good, *Spectrochim. Acta A* **29** (1973) 707., M. Iwamoto, H. Furukawa, K. Matsukami, T. Takenaka, S. Kagawa, *J. Am. Chem. Soc.* **105** (1983) 3719.

[70] X. Gao, I. E. Wachs, *J. Phys. Chem. B* **104** (2000) 1261.

[71] P. Kubelka, F. Z. Munk, *Tech. Phys.* **12** (1931) 593.,

[72] G. Kortüm, *Reflectance spectroscopy*, Springger Verlag: Berlim 1969., W. N. Deglass, G. L. Haller, P. L. Gauss, *Basic Inorganic Chemistry*, 3rd ed.; Wiley: New York, 1995.

[73] D. G. Barton, M. Shtein, R. D. Wilson, S. L. Soled, E. Iglesia, *J. Phys Chem. B* **103** (1999) 630.

[74] R. S. Weber, *J. Catal.* **151** (1995) 470.

UNIVERSITAT ROVIRA I VIRGILI
NANOMATERIALS IN CATALYSIS: STUDY OF MODEL REACTIONS.
Ricardo José Chimentao
ISBN: 978-84-690-7618-7 / DL: T.1326-2007

I.3 Kinetically confined synthesis of nanoparticles

I.3.1 Abstract

We have studied the preparation of silver gold alloy nanoparticles based on the phase transfer of metal precursors from aqueous phase to organic solution by a fatty amine at room temperature. Silver-gold nanoparticles were synthesized with different molar ratios (2:1, 1:1, 1:2). UV-visible absorption spectra suggested the formation of alloy phases. The elemental Ag:Au ratios in the bimetallic nanoparticles determined by energy dispersive X-ray analysis (EDX) were consistent with the Ag-Au molar ratios used in the feeding solution. Transmission electron microscopy (TEM) revealed the formation of a uniform size distribution of Ag-Au nanoparticles (around 5 nm). X-ray photoelectron spectroscopy (XPS) showed that the composition in the outer part of the Au: Ag nanoparticles was similar to that obtained by EDX analysis, which indicates the formation of homogeneous silver-gold nanoparticles. Silver-gold alloy nanoparticles in a gram scale were obtained with this method.

Keywords: alloy, silver, gold, phase transfer, TEM, XPS, EDX,UV-vis.

UNIVERSITAT ROVIRA I VIRGILI
NANOMATERIALS IN CATALYSIS: STUDY OF MODEL REACTIONS.
Ricardo José Chimentao
ISBN: 978-84-690-7618-7 / DL: T.1326-2007

I.3.2 Introduction

Metal nanoparticles are currently a very active area of research thanks to their potential applications in areas such as electronics and catalysis [1]. Metal nanoparticles have significantly different properties from those of bulk metals [2]. The unique chemical and physical properties of nanoparticles are determined by the large proportion of atoms in surface positions and by the shape control of the crystallographic planes on the particle surface [3]. Bimetallic nanoparticles are particularly attractive thanks to the improved catalytic properties and the change in the surface plasmon band energy relative to the separate metals [4]. Many alternative routes to obtaining nanometer-sized particles of metals have been developed. These include templating [5], photochemistry [6], microemulsion [7] and organic encapsulation [8]. Recent publications have reported the formation of homogeneous Ag:Au alloy nanoparticles in a milligram scale [9-14]. However, these techniques do not avoid the precipitation of AgCl during the synthesis of Ag-Au nanoparticles, in a gram scale, when $HAuCl_4$ and $AgNO_3$ are used as metal precursors. A different gold salt or an adjustment in the solution concentrations is therefore required [10,15]. The Ag-Au system is a good choice because Ag and Au have face-centered cubic structures with similar parameters that lead to the formation of random solution alloys at all concentrations [16,17]. On the other hand, Ag and Au monometallic nanoparticles have a different plasmon absorption in the visible region and the absorption spectra of Ag:Au alloy exhibit only one surface plasmon band, which is related to the alloy composition. Moreover, the high f density states at E_F of gold are very susceptible to modification upon alloy formation [18].

UNIVERSITAT ROVIRA I VIRGILI
NANOMATERIALS IN CATALYSIS: STUDY OF MODEL REACTIONS.
Ricardo José Chimentao
ISBN: 978-84-690-7618-7 / DL: T.1326-2007

In this study we report a method for obtaining homogeneous Ag-Au nanoparticles in gram scale, using $HAuCl_4$ and $AgNO_3$ salts as precursors. This method is based on extracting the metal ions from the aqueous phase to an organic phase by a fatty amine such as hexadecylamine. Different organic solutions containing silver or gold metal ions protected by the amine were prepared separately. The resultant solutions were then mixed in appropriate amounts to obtain different Ag-Au molar ratios and finally reduced with sodium borohydride.

I.3.3 Experimental

Amine-capped silver-gold nanoparticles were synthesized in a toluene/water system at room temperature. All chemicals were used without further purification. The synthesis of the organic phase containing the metal ions was carried out as follows. The organic solutions containing the silver or gold metal ions were prepared separately. Two aqueous solutions of 3.4 g (0.01 mol) of $HAuCl_4$ (Aldrich, 99%) or 1.69 g (0.01 mol) of $AgNO_3$ in 350 ml of deionized water were prepared. Next, a toluene solution (350 ml) containing 7.23 g (0.03 mol) of hexadecylamine ($C_{16}H_{33}NH_2$) was added to the Au or Ag aqueous solutions under vigorous stirring. For the gold solution, an immediate two-layer separation was produced, with an orange-red organic phase on the top and an orange tinted aqueous phase on the bottom. The resulting solution was stirred for 48 h protected from the light and the $AuCl_4^-$ ions were allowed to diffuse gradually into the organic phase by complexing them with the amine. At the end of the process, a deep yellow toluene phase containing the $AuCl_4^-$ ions was in equilibrium with a colorless aqueous phase. Finally, the organic phase

UNIVERSITAT ROVIRA I VIRGILI
NANOMATERIALS IN CATALYSIS: STUDY OF MODEL REACTIONS.
Ricardo José Chimentao
ISBN: 978-84-690-7618-7 / DL: T.1326-2007

containing the gold ions was removed from the aqueous phase. The same approach was adopted to prepare the organic silver solution. The transfer of the metal ions to the organic phase arises from the coupling of the metal ions with the amine initially present in the organic phase [19]. Subsequently the organic solutions were washed several times with distilled water for further characterization. The metal ions concentration of each resulting toluene solution was measured by inductively coupled plasma atomic emission spectrometry (ICP AES). This showed that practically all the gold or silver ions were in the organic phase (Ag and Au nanoparticles yield at about 90% and 98%, respectively). The resulting organic phases containing silver or gold ions were then mixed in appropriate amounts to obtain solutions with Ag:Au molar ratios of (2:1, 1:1, 1:2) and then stirred for 1 hour protected from the light. A fresh aqueous solution of $NaBH_4$ (0.01M) was then added drop by drop under stirring for 30 minutes. Note that these final solutions containing silver-gold nanoparticles were free from flocculation or aggregation for several months. The obtained silver-gold nanoparticles in toluene were characterized by UV-vis spectroscopy, X-ray diffraction (XRD), transmission electron microscopy (TEM), selected area electron diffraction (SAED), energy dispersive X-ray (EDX) analysis and X- ray photoelectron spectroscopy (XPS). UV-vis spectra of the silver-gold solution were carried out at ambient temperature using a HP 8542 spectrophotometer by scanning wavelengths between 300 and 820 nm. X-ray diffraction (XRD) measurements were made using a Siemens D5000 diffractometer (Bragg-Bentano parafocusing geometry and vertical θ-θ goniometer) fitted with a grazing incident (ω: 0.52^0) attachment for thin film analysis and scintillation counter as a detector. The nanoparticles

UNIVERSITAT ROVIRA I VIRGILI
NANOMATERIALS IN CATALYSIS: STUDY OF MODEL REACTIONS.
Ricardo José Chimentao
ISBN: 978-84-690-7618-7 / DL: T.1326-2007

were dispersed on Si (510) sample holder. The angular 2θ diffraction range was between 30^0 to 60^0. The data were collected with an angular step of 0.03^0 at 12 s per step and sample rotation. $Cu_{K\alpha}$ radiation was obtained from a copper X-ray tube operated at 40 kV and 30 mA. Transmission electron microscopy (TEM) was used to analyze the size and electron density of the alloy nanoparticles. A drop of silver-gold nanoparticle solution prepared in toluene was placed on a Formvar-covered copper grid and allowed to evaporate in air at room temperature before the analysis. Structural information was obtained using selected area electron diffraction (SAED) patterns. The EDX analysis was carried out on a Noaran Model Voyager 1000 system. The XPS spectra were acquired in a VG Escalab 200R electron spectrometer equipped with a hemispherical electron analyzer, operating in a constant pass energy mode, and a non-monochromatic Mg-Kα (hv = 1253.6 eV, 1 eV = 1.603×10^{-19} J). X-ray source operated at 10 mA and 1.2 kV. The angle of the incident photon beam was 45^o with respect to the normal of the sample. The background pressure in the analysis chamber was kept below 7×10^{-9} mbar during data acquisition. The binding energy (BE C1s = 284.9 eV) of adventitious C_1 was used as reference. A Shirley background subtraction was applied and Gaussian-Lorentzian product functions were used to approximate the line shapes of the fitting components.

I.3.4 Results and Discussion

Figure I.3.1 shows the UV-visible spectra of the nanoparticle samples, with different Ag: Au molar ratios, protected with hexadecylamine in toluene solution. The absorption peaks around 390 and 520 nm are the

UNIVERSITAT ROVIRA I VIRGILI
NANOMATERIALS IN CATALYSIS: STUDY OF MODEL REACTIONS.
Ricardo José Chimentao
ISBN: 978-84-690-7618-7 / DL: T.1326-2007

plasmon bands due to pure Ag and Au nanoparticles, respectively. The UV-vis spectra for the bimetallic systems showed a blue shift of the absorption peak as the Ag:Au molar ratio changed from 2:1 to 1:2. The color of the silver-gold nanoparticle solutions was also strongly dependent on the Ag:Au molar ratio, as we can see in the inset in Figure I.3.1.

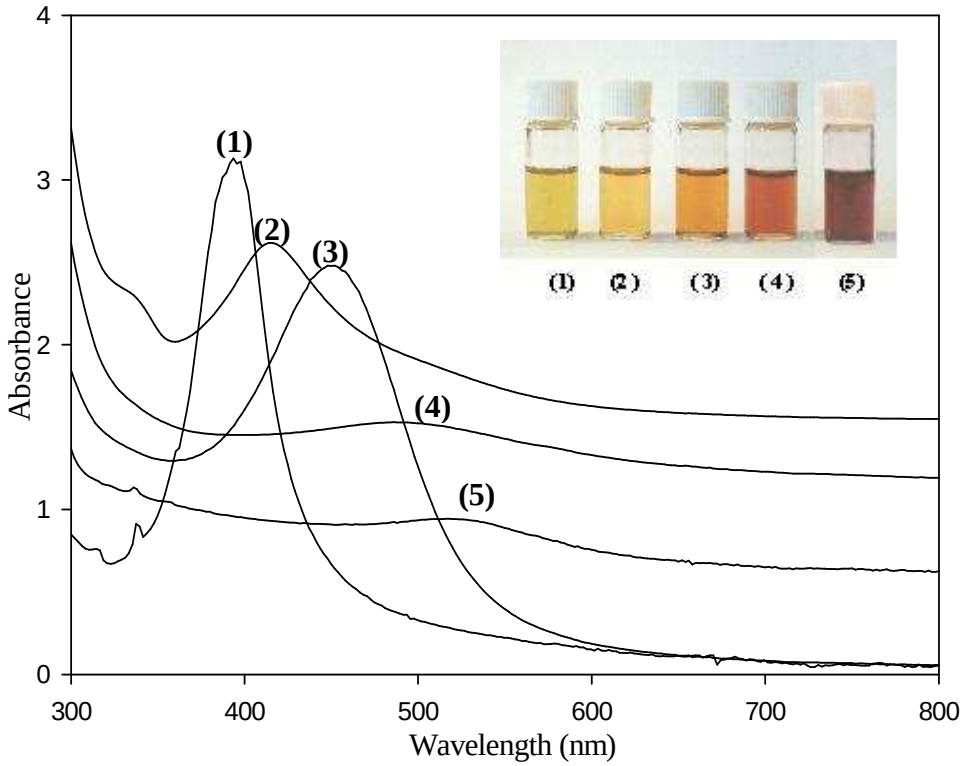

Figure I.3.1 UV-vis absorption spectra of toluene solutions of Ag:Au nanoparticles with Ag:Au molar ratios of 1:0 (1), 2:1 (2), 1:1 (3), 1:2 (4) and 0:1 (5). Inset: Pictures of the sample bottles containing solutions 1-5 showing the change in the color from light yellow to red wide as the gold content increase.

Figure I.3.2 shows the position of the maximum absorption band with respect to the Ag: Au molar ratio in the alloy nanoparticle. This

UNIVERSITAT ROVIRA I VIRGILI
NANOMATERIALS IN CATALYSIS: STUDY OF MODEL REACTIONS.
Ricardo José Chimentao
ISBN: 978-84-690-7618-7 / DL: T.1326-2007

increases linearly when the Au content increases. The wavelengths corresponding to the maximum absorbance (λ_{max}) for the different nanoparticle samples are also shown in Table I.3.1.

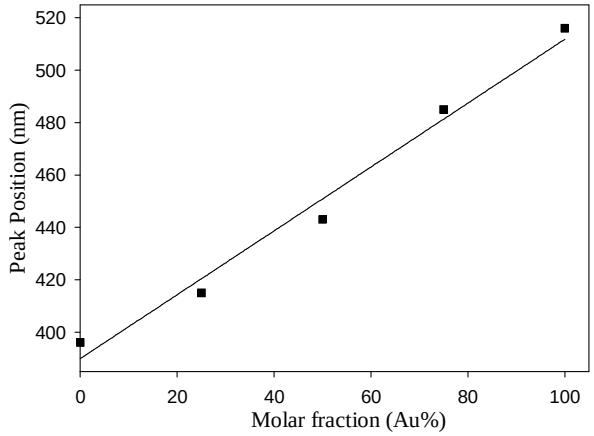

Figure I.3.2. Wavelength of the maximum absorbance for Ag:Au nanoparticles with respect to molar fractions of Au atom.

The pure Ag solution was light yellow. As the Au/Ag molar ratio increased, the color of the solution changed to red wine. Evidence that our particles were alloy rather than core-shell system is the fact that the UV-visible spectrum of the solution only showed one absorption band. Non-alloy Au-Ag nanoparticles usually exhibit two different plasmon bands whose relative intensities depend on the thickness of the shell [10,13]. The notable change in the absorption spectra can be primarily attributed to a change in the dielectric function when different metal atoms are mixed. Silver displays approximately free electron behavior in the visible range, which gives rise to a sharp absorption band. Other metals, including Au, have less free-electrons, which gives rise to a broad absorption band [20]. Figure I.3.3 shows the XRD pattern for the

UNIVERSITAT ROVIRA I VIRGILI
NANOMATERIALS IN CATALYSIS: STUDY OF MODEL REACTIONS.
Ricardo José Chimentao
ISBN: 978-84-690-7618-7 / DL: T.1326-2007

sample prepared with an Ag:Au molar ratio of 1:1. For this sample, only the lattice plane (111) was detected. It was difficult to judge whether the bimetallic nanoparticles were formed from the analysis of the XRD, since both Ag and Au crystallize in the face-centered cubic (fcc) structure form and have comparable atomic size and electronegativity.

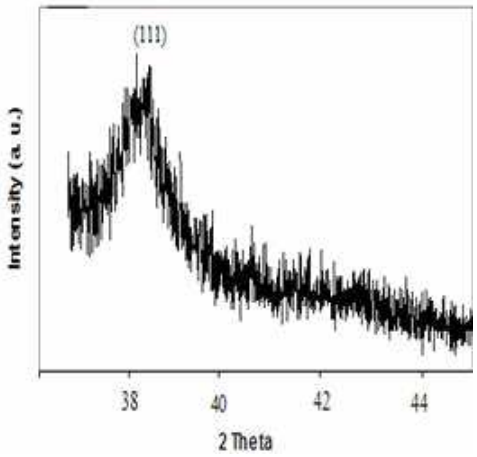

Figure I.3.3 XRD pattern of the silver-gold nanoparticles with Ag: Au molar ratio of 1:1.

Also, as observed by TEM (Figure I.3.4), the size of the nanoparticles formed was around 5 nm. The distribution of Ag and Au across the surface of an individual particle was further examined by EDX analysis to obtain direct evidence of the formation of Ag:Au alloy nanoparticles. This analysis (Table I.3.1) showed that the average composition of the nanoparticles was in agreement with those of the feeding solution. Figure I.3.4 (a-c) shows the images obtained by TEM for the monometallic samples and the bimetallic sample with an Ag:Au molar ratio of 1:1. The TEM analysis for the bimetallic sample (Figure I.3.4b) showed a uniform size distribution with an average diameter of 5.2 nm, while the size of the monometallic nanoparticles of Ag and Au were

UNIVERSITAT ROVIRA I VIRGILI
NANOMATERIALS IN CATALYSIS: STUDY OF MODEL REACTIONS.
Ricardo José Chimentao
ISBN: 978-84-690-7618-7 / DL: T.1326-2007

apparently more varied. Figure I.3.4 also shows that the bimetallic nanoparticles were smaller than the monometallic samples, probably because the nuclei for the bimetallic system may contain both Au and Ag and there may be fewer Ag and Au because of the different interactions between Au and Au, Ag and Ag and Au and Ag.

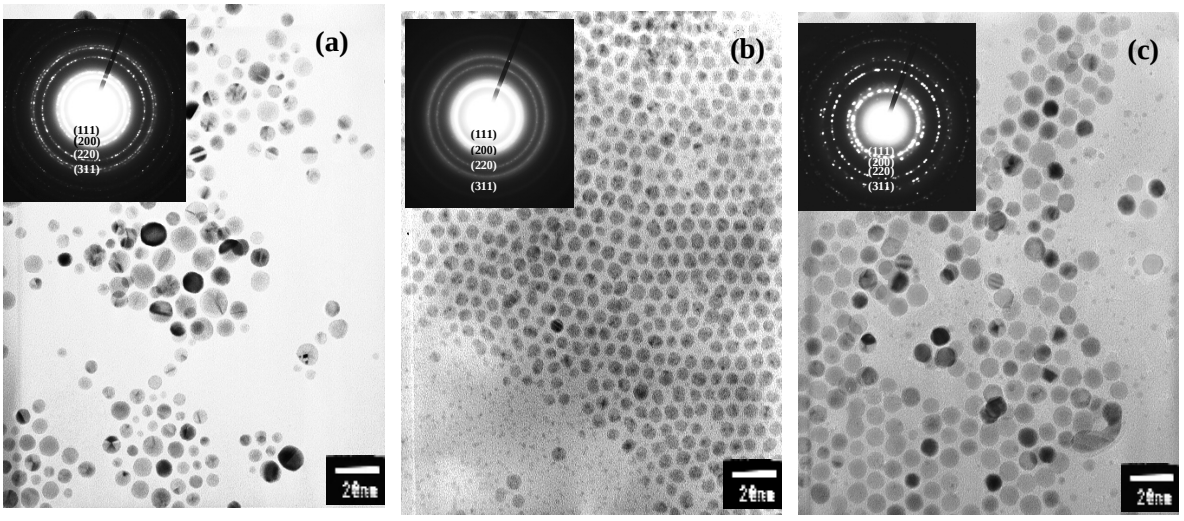

Figure I.3.4. Transmission electron micrographs of Ag:Au nanoparticles : (a) monometallic Au nanoparticles, (b) Ag:Au alloy nanoparticle (Ag:Au ratio molar 1:1), (c) monometalic Ag nanoparticles. Inset: Corresponding electron diffraction patterns (SAED) of the Ag:Au nanoparticles .

The electron diffraction patterns in the inset of the Figure 4 leads to identification of face-centered cubic (fcc) structure of Au and Ag. The lattice parameters of the silver and gold nanoparticles were 4.0772 and 4.0709 Å, respectively, which are ~ 0.2% smaller than the report data (a = 4.0862 Å for Ag and a = 4.0786 for Au from Joint Committee on Powder Diffraction Standards files 04-0783 and 04-0784, respectively). The lattice constants calculated for the Ag-Au alloy nanoparticles (Ag:Au molar ratio of 1:1) was 4.0737 Å. A similar contraction of the

UNIVERSITAT ROVIRA I VIRGILI
NANOMATERIALS IN CATALYSIS: STUDY OF MODEL REACTIONS.
Ricardo José Chimentao
ISBN: 978-84-690-7618-7 / DL: T.1326-2007

atomic separation of the nanoparticles, originating from the size effect has also been reported in other nanostructure systems [21]. The chemical composition of the near surface layer of the nanoparticles was evaluated by X-ray photoelectron spectroscopy (XPS). The corresponding XPS core-level spectra of the Au-4f and Ag-3d region acquired for the nanoparticles samples are shown in Figure I.3.5 and Table I.3.1.

Table I.3.1 Results of UV-vis, EDX and XPS of Ag:Au nanoparticles.

Feeding solution Mole ratio Ag:Au	UV-vis	EDX	XPS		
	λ_{max} (nm)	(Ag:Au)[a]	Binding energy (ev)[b]		(Ag:Au)[a]
			Au $4f_{7/2}$	Ag $3d_{5/2}$	
1:0	396		-	367.9	
2: 1	415	66.4/33.6	83.3	367.6 (63)	66.7/33.3
				368.7 (37)	
1: 1	443	52.6/47.4	83.2 (65)	366.9 (67)	53.7/46.3
			84.4 (35)	368.2 (33)	
1: 2	485	34.7/65.3	83.0 (34)	367.4 (80)	35.5/64.5
			84.4 (66)	368.6 (20)	
0: 1	516		84.0	-	

[a] Elemental ratio. [b] The values of binding energy were determined with respect to C_{1S} peak; the parentheses represent the percentage of the peaks.

For the pure gold nanoparticles sample (Ag:Au atomic ratio of 0:1), the Au 4f spectra, characterized by the spin-orbit splitting (Au $4f_{7/2}$ and Au $4f_{5/2}$ components), shows values of 84.0 eV and 87.7 eV, respectively. Both peaks originating from the Au indicate that these binding energies are consistent with the Au^0 oxidation state. The Au $4f_{7/2}$ binding energy obtained from the nanoparticle samples containing silver (alloy samples) was in the 83.3 to 84.4 eV range (Figure I.3.5 and Table I.3.1). There is no evidence that the Au was bonded to oxygen because

UNIVERSITAT ROVIRA I VIRGILI
NANOMATERIALS IN CATALYSIS: STUDY OF MODEL REACTIONS.
Ricardo José Chimentao
ISBN: 978-84-690-7618-7 / DL: T.1326-2007

the oxide shows binding energies around 85.8 and 89.5 eV for Au $4f_{7/2}$ and Au $4f_{5/2}$, respectively.[22-25] Table 1 shows the values of the binding energies of core-levels and surface atomic ratios of the samples. The most intense Au $4f_{7/2}$ emission showed two components, the percentages of which are summarized in Table I.3.1 (see also deconvoluted peaks in Figure I.3.5). As the silver content in the bimetallic nanoparticle increased, the binding energy of the Au $4f_{7/2}$ shifted towards lower binding energies with respect to the monometallic gold sample. According to Pauling´s eletronegativity table, the electronegativity of Au is higher than Ag. We should therefore expect some electron transfer from silver to gold atoms by shifting the Au core levels towards lower binding energies [26]. The shift of the Au $4f_{7/2}$ to the lower energies observed for our samples containing alloy nanoparticles (see Figure I.3.5 and Table I.3.1) is consistent with this general rule. On the other hand, the binding energies Ag $3d_{5/2}$ for the pure silver sample were around 367.9 eV, which corresponds to metallic silver [27]. Figure I.3.5 shows a series of Ag 3d core level spectra obtained for the samples with different Ag:Au molar ratios. As the Au content in the bimetallic samples increased, the binding energy (BE) of the Ag $3d_{5/2}$ shifted to lower energy values than those of the monometallic silver sample.The higher electron affinity of gold with respect to that of silver led to an electron transfer from the Ag to Au, thus decreasing the electron density of the Ag atoms. Usually, higher BE values are observed when the metal is oxidized. The positive BE shifts increase as the oxidation state increases. So, upon oxidation, the observed core-level binding energies for most transition metals shift towards higher binding energies [28]. However, silver is one of the few examples of a lowered binding energy in the

UNIVERSITAT ROVIRA I VIRGILI
NANOMATERIALS IN CATALYSIS: STUDY OF MODEL REACTIONS.
Ricardo José Chimentao
ISBN: 978-84-690-7618-7 / DL: T.1326-2007

oxidized state [29]. The surface composition of the samples was analyzed by XPS. From the intensities of the XPS peaks, we obtained the elemental ratios of Ag:Au on the surface of the bimetallic nanoparticles (see Table 1). The composition in the outer part of the particle detected by XPS was roughly equal to that of the feeding solution and similar to that obtained by EDX, which indicates good homogeneity of the alloy nanoparticle samples. In summary, we have described a phase-transfer system method for preparing Ag-Au with a homoge neous structure in gram scale. The amine tends to form micelle, which includes an insoluble core and a soluble shell [30]. Coupling silver with the amine has an important role as a stabilizer, because the addition of silver into gold could otherwise lead to the AgCl precipitate [31]. The polar part of the amine can bind metal ions of the precursors into the core of the micelle by transferring it from the aqueous phase to the organic phase. When the organic phases (containing separated silver and gold ions) were mixed, the micelles probably collided into each other and interchanging the metal ions [32,33]. The percolation between the micelles probably played a strong role in the formation of the bimetallic nanoparticles [34]. These collisions originate nanodroplets and confining the ions of both metals so, after reduction with sodium borohydride, homogeneous silver-gold alloy nanoparticles can be obtained. In most cases, the surface of a bimetallic system is enriched with one of its components. This is usually the component with the greatest ionization potential [35]. In the case of Ag-Au system, the ionization potential of the Ag atom (7.576 eV) is known to be lower than that of the Au atom (9.223 eV) The reduction of the Au ions would therefore proceed more easily than that of the Ag ions and the Au core structure should be formed sooner than

UNIVERSITAT ROVIRA I VIRGILI
NANOMATERIALS IN CATALYSIS: STUDY OF MODEL REACTIONS.
Ricardo José Chimentao
ISBN: 978-84-690-7618-7 / DL: T.1326-2007

the Ag core structure. However, use of a powerful reducing agent such

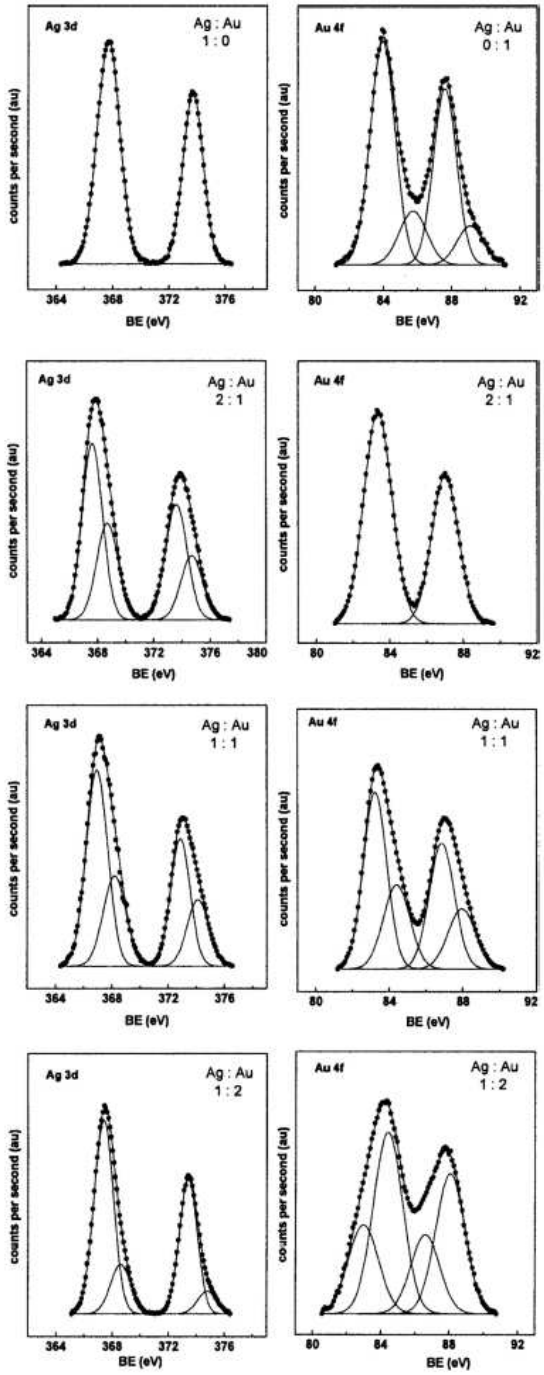

Figure I.3.5 Surface chemical analysis by X-ray photoelectron spectroscopy (XPS) of the Au-4f and Ag-3d for Ag:Au nanoparticles

with different Ag:Au molar ratios of : 1:0 , 2:1, 1:1, 1:2 and 0:1.

as $NaBH_4$ or the presence of the amine favors the formation of homogeneous structures of silver-gold nanoparticles [36,37]. The UV-vis, XPS and EDX results provide strong evidence that a homogeneous alloy nanostructure was obtained with the proposed synthesis method.

I.3.5 Conclusion

We have studied the formation of silver-gold alloy nanoparticles by phase transfer of metal precursors from aqueous phase into non-polar organic phase by fatty amine. Silver-gold nanoparticles were synthesized with different molar ratios (2:1, 1:1, 1:2). Structural and chemical analyses of Ag:Au alloy nanoparticles were performed by means UV-vis spectroscopy, TEM, XRD, EDX and XPS techniques. Our results suggest the formation of homogeneous silver-gold alloy nanoparticles with uniform size distribution (around 5 nm). This phase transfer method is also useful for obtaining silver-gold alloy nanoparticles in gram scale.

Acknowledgemments

This work was supported by the Ministerio de Ciencia y Tecnologia (Spain) under Projects REN2002-04464-CO2-01 and PETRI 95-0801.OP. Thanks are also due to Destilaciones Bordas S.A.

I.3.6 References

[1] Y. Sun, Y Xia, *J. Am. Chem. Soc.* **126** (2004)3892.

[2] R. Subramanian, PE. Denney, J. Singh and M. Otooni, *J. Mater. Sci*. **33** (1998) 3471**.**

[3] Z. L. Wang, *J. Phys. Chem. B.* **104** (2000)1153.

[4] S. T He, S. S. Xie, J. N.Yao and H. J.Gao, S. Pang, *J.* A*ppl*. *Phys*. *Lett*. **81** (2002)150.

[5] S. R. N. Pena, R. G. Freeman, B. D. Reiss, L. He, D. J. Pena, I. D. Walton, R. Cromer, C. D. Keating and M. J. Natan, *Science* **294** (2001) 137.

[6] K. Esumi, K. Matsuhisa and K. Torigoe, *Langmuir* **11** (1995) 3285.

[7] M. P. Pilene, *Crys. Res. Technol*. **33** (1998)1155.

[8] M. P. Pileni, J. Tanori, A. Filankembo, *Colloid Surf A* **123** (1997) 561.

[9] N. R. Jana, L. Gearheart and C. J.Murphy, *J. Phys. Chem. B.* **105** (2001) 4065.

[10] M. P. Mallin, C. J. Murphy, *Nano Lett*. **2** (2002) 1235.

[11] N. Aihara, K. Torigoe, K. Esumi, *Langmuir* **14** (1998) 4945.

[12] N. Sandhyarani, T. Pradeep *Chem*. *Mater*. **12** (2000) 1755.

[13] M. Moskovits, I. S. Sloufová, B. Vicková, *J. Chem*. *Phys*. **116** (2002) 10435.

[14] S. Devarajan, B. Vimalan, S. Sampath, *J. Colloid Interface Sci*. **278** (2004) 126.

[15] M. Yamamoto, M. Nakamoto, *Chem*. *Lett*. **33** (2004) 1340.

[16] B. D. Cullity, S. R. Stock. *Elements of X-Ray Diffraction*. (Prentice-Hall, Upper Saddle River, N.J., ed. 3, 2001), pp. 402-404.

[17] D. I. Kondarides, X. E. Verykios, *J. Catal*. **363** (1996)158.

[18] I. Capek, *Adv Colloid Interface Sci*. **110** (2004) 49.

[19] G. Suyal, *Thin Solid Films* **426** (2003) 53.

[20] H. C. Boyen, G. Kästle, F. Weigl, B. Kslowski, C. Dietrich, P. Ziemann, J. P. Spatz, S. Riethmüller, C. Hartmann, M. Möller,

UNIVERSITAT ROVIRA I VIRGILI
NANOMATERIALS IN CATALYSIS: STUDY OF MODEL REACTIONS.
Ricardo José Chimentao
ISBN: 978-84-690-7618-7 / DL: T.1326-2007

G. Schimid, M. G. Garnier, P. Oelhafen, *Science* **297** (2002) 1533.

[21] C. L. Cleveland1, U. Landman, T. G. Schaaff, M. N. Shafigullin, P. W. Stephens, R. L. Whetten, *Phys. Rev. Lett.* **79** (1997) 1873.

[22] D. Briggs and M.P. Seah: Practical Surface Analysis. Auger and X-ray Photoelectron Spectroscopy. (John Wiley and Sons, Chichester, 1990) pp .

[23] A. Q. Wang, J. H. Liu, S. D. Lin, T. S. Lin, C. Y. *J. Catal.* **233** (2005) 186.

[24] J. J. Pireau, M. Liehr, P. A. Thirty, J. P. Delrue, R. Caudano, *Surf. Sci*. **141** (1984) 221.

[25] B. Koslowski, H. G. Boyen, C. Wilderotter, G. Kästle, P. Ziemann, R. Wahrenberg, P. Oelhafen, *Surf. Sci*. **475** (2001) 1.

[26] L. Pauling: *The nature of the Chemical Bond* (Cornell University Press, New York, 1960**)** p.93.

[27] X. Bao, M. Muhler, Th. Schedel-Niedrig, R. Schlöl, *Phys. Rev. B.* **54,** *2249* (1996).

[28] K, Wandelt, *Surf. Sci. Rep*. **2** (1982) 1.

[29] L. H. Tjeng, M. B. Meinders, J. Van, E. J. Ghijsen, G. A. Sawatzky, R. L. Johnson, *Phys. Rev. B.* **41** (1990) 3190.

[30] J. Tanori, M. P. Pileni. *Langmuir* **13** (1997) 639.

[31] A. Manna, T. Imae, M. Iida, N. Hisamatsu, *Langmuir* **17** (2001) 6000.

[32] J. Tanori, M. P. Pileni, *Adv. Mater*. **7** (1995) 862.

[33] M. L. Wu, B. Lai, *Colloids Surf. A.* **244** (2004) 149.

[34] K. Torigoe, Y. Kakajima, K. Esumi, *J. Phys. Chem*. **97** (1993)8304.

[35] N. Toshima, M. Harada, Y. Yamazaki, K. Asakura, *J. Phys. Chem.* **96** (1992) 9927**.**

I.4 One-dimensional nanostructures: nanowires/rods and nanocubes

I.4.1 Introduction

One dimensional nanostructures have been called by a variety of names including: whiskers, fibers or fibrils, nanowires and nanorods [1]. In many cases, nanotubules and nanocables are also considered one-dimensional structures. Many techniques have been developed in the synthesis and formation of one-dimensional nanostructured materials, though same techniques have been explored extensively, while others have attracted far less

attention. These techniques can be grouped into four categories: *(i)* Spontaneous growth [3]; *(ii)* template based system [4, 5]; *(iii)* electrospinning [6-8] and *(iv)* litography [9, 10]. Here, we will focus on the template based system such as polyol process for the synthesis of silver nanostructures. Previous work [11] has demonstrated an effective approach based on the polyol process for the large scale synthesis of silver or gold nanostructures with controllable shape. Ethylene glycol has been widely used in this synthesis process due to its strong reducing power and relatively high boiling point [12]. The formation of monosized metallic nanoparticles is achieved in most cases by a combination of a low concentration of solute and polymeric monolayer adhered onto the growth surfaces. The growth of the Ag particles is generated by the reduction of $AgNO_3$ with ethylene glycol whereas the anisotropy growth is controlled by the presence of

UNIVERSITAT ROVIRA I VIRGILI
NANOMATERIALS IN CATALYSIS: STUDY OF MODEL REACTIONS.
Ricardo José Chimentao
ISBN: 978-84-690-7618-7 / DL: T.1326-2007

stabilizers such as poly(vinylpyrrolidone) (PVP). For the formation of nanowires/rods, nanocubes and nanopolyhedra, anisotropic growth is required; i. e. the crystal grows along a certain orientation faster than others. Uniformly sized nanowires, i. e. the same diameter along the longitudinal direction of a given nanowire, can be obtained when crystal growth proceeds along one direction, whereas no growth along other directions.

The polyol process involve the reduction of a precursor (such as silver nitrate for silver) by ethlylene glycol at elevated temperatures in the presence of the poly(vinylpirrolidone) (PVP). A number of metallic powders of easily reducible metals have been successfully synthesized by the polyol process [13, 14] and recent patent extend extends its use to the preparation of refractory metals and metal alloy powders [15]. The main feature of the reaction mechanism of the polyol process is that metal particles are formed by nucleation and growth from the solution [16]. Because the resulting metal suspension is an almost homodisperse system, nucleation and growth are completely separated stages in the particle formation. In particular, the metal is provided slowly in solution by the progressive reduction of the dissolved species. The silver atoms concentration increases and raises the saturation concentration where the nucleation occurs. Many nuclei are produced in a short time; they growth rapidly, and the metal concentration is lowered to a point below the nucleation concentration, but high enough to allow particle growth to occur at rate that just consumes all the metal generated. Therefore, the final metal particles are formed by nuclei that appear spontaneously at about the same time and have grown during the same time; consequently the particles should be very homogeneous in size. However, because of the relatively high temperature used in the

UNIVERSITAT ROVIRA I VIRGILI
NANOMATERIALS IN CATALYSIS: STUDY OF MODEL REACTIONS.
Ricardo José Chimentao
ISBN: 978-84-690-7618-7 / DL: T.1326-2007

synthetic process, wide Brownian motions characterize the particles and the atoms on their surface have an elevated mobility. As a result, the probability of particle collision, adhesion, and subsequent coalescence by sintering is enhanced. Consequently, sometimes the silver powders obtained by reduction of silver nitrate in ethylene glycol in the polyol process can show a wide range of shapes arising from the sintering of the quasispherical particles [17]. The Figure I.4.1 shows a schematic of the nucleation and growth process of the silver nanoparticles in the polyol process and the plot of surface plasmon wavelength versus reaction time versus from UV-vis absorption spectroscopy studies realized by A. Tao et al.

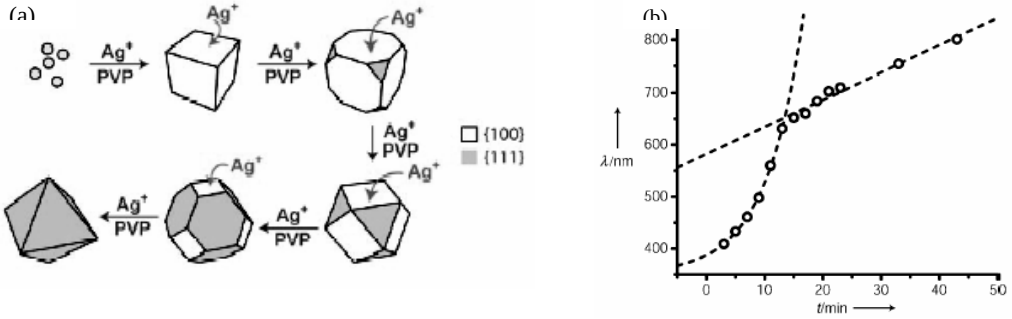

Figure I.4.1 (a) Scheme of the nucleation of the silver nanoparticles in the polyol process. (b) Plot of surface plasmon wavelength versus reaction time versus from UV-vis absorption spectroscopy [18].

The Figure I.4.1 shows the schematic of the nucleation and growth process, in which silver silver continuously deposits onto the {100} to eventually result in a completely {111}-bound octahedron. The graph indicates that the shape evolution may occur in two steps: fast nucleation, which occurs at a linear rate. Initially small silver particles

UNIVERSITAT ROVIRA I VIRGILI
NANOMATERIALS IN CATALYSIS: STUDY OF MODEL REACTIONS.
Ricardo José Chimentao
ISBN: 978-84-690-7618-7 / DL: T.1326-2007

nucleate and develod into nanocubes bound by {100} planes, which are thought to be selectively stabilized by adsorbed PVP. As the reaction is continued, silver deposits selectively onto the {110} nanocrystal facets rather than growing in layer-by layer fashion. The {111} capped corners of the nanocube are stabilized during this growth period in which the nanocrystal evolves from a {100}-bound cube to a {111}-bound octahedron. The stability of both {100} and {111} planes in the presence of PVP indicates that the shape control may not be explicitly dictated by the capping polymer. Rather, preferential crystal growth seems to result from a kinetically limited equilibrium influenced heavily by reaction parameters such as, temperature, reactant concentration, and reactant molar ratios. Another particle commonly observed is wires with pentagonal cross-sections. It has been proposed that they evolved from a multi-twinned decahedral nanoparticles growing in the {110} direction with the capping agent directing the structure by stabilizing more effectively the new formed {100} facets than the {111} facets; thus they may be considered as decahedra that have elongated parallel to the twin planes. In the case of PVP, its anisotropic binding specificity has been attributed to the difference in surface atom density between the {100} and {111} silver planes, 1.20×10^{19} *vs* 1.38×10^{19} atoms m^{-2}, respectively [19]. However, the preferential interaction between the capping agent and different metal surfaces can not fully explain the physical mechanism that allows the formation of such a structure and allows it to be energetically stable. A decahedron can be considered as a junction of five tetrahedra and, in that case, each vertex is the point where a fast-growing concave type face grew out, leaving five edges and two axis points as slow-growing convex faces. Thus, on the basis of that explanation, typically a fivefold

UNIVERSITAT ROVIRA I VIRGILI
NANOMATERIALS IN CATALYSIS: STUDY OF MODEL REACTIONS.
Ricardo José Chimentao
ISBN: 978-84-690-7618-7 / DL: T.1326-2007

particle must grow into decahedron and then be arrested in growth.

I.4.2 Experimental

I.4.2.1 Preparation of the silver nanoparticles

Silver nanowires catalysts were prepared by polyol process. In a typical synthesis of silver nanoparticles, 30 ml ethylene glycol solution of $AgNO_3$ (0.25 M, Aldrich) and 30 ml ethylene glycol (EG) solution of polyvinyl-pyrrolidone (PVP) (0.375 M in repeating unit weight-average molecular weight ≈ 40,000, Aldrich) were simultaneously added in 50 ml ethylene glycol at 433 K under vigorous magnetic stirring. The reaction mixture was then refluxed for 45 min at this temperature. The obtained nanoparticles were diluted with acetone and separated from ethylene glycol (EG) by centrifugation at 4000 rpm for 20 min. The silver nanocubes was synthesized with $AgNO_3$/PVP molar ratio of 3. Silver nanopolyhedra were also obtained when the silver nanocubes were maintained for longer period of time in the reaction mixture.

I.4.2.2 Catalyst Characterization

I.4.2.2.1 X-ray diffraction (XRD)

XRD measurements were made using a Siemens D5000 diffractometer (Bragg-Bentano parafocusing geometry and vertical θ-θ goniometer) fitted with a curved graphite diffracted-beam monochromator, incident and diffracted beam Soller slits, a 0.06º receiving slit and scintillation counter as detector. The angular 2θ diffraction range was between 30^0 and 90^0. The data were collected with an angular step of 0.05º at 3s per step and sample rotation. $Cu_{K\alpha}$ radiation was obtained from copper X-ray tube operated at 40 kV and 30 mA.

I.4.2.2.2 Scanning electron microscopy (SEM)

UNIVERSITAT ROVIRA I VIRGILI
NANOMATERIALS IN CATALYSIS: STUDY OF MODEL REACTIONS.
Ricardo José Chimentao
ISBN: 978-84-690-7618-7 / DL: T.1326-2007

*T*he morphologies of the catalysts were observed by SEM with a JEOL JSM-35C microscope operated at an acceleration voltage of 15 kV. A small portion of each sample powder was coated on a metallic disk holder and covered with a thin gold layer before the SEM analysis.

I.4.2.2.3 Transmission electron microscopy (TEM)

Transmission electron micrographs were taken of the samples using a JEOL-2010 electronic microscope operating at an accelerating voltage of 200 kV. Samples for TEM were prepared by depositing the sample on the copper grid and then the solvent was allowed to evaporate under vacuum before analysis.

I.4.2.2.4 UV-vis spectroscopy (UV-vis)

UV-vis spectra of the silver-gold solution were carried out at ambient temperature using a HP 8542 spectrophotometer by scanning wavelengths between 300 and 820 nm.

I.4.2.2.5 X-ray photoelectron spectroscopy (XPS)

The XPS spectra were acquired in a VG Escalab 200R electron spectrometer equipped with a hemispherical electron analyzer, operating in a constant pass energy mode, and a non-monochromatic Mg-Kα (hv = 1253.6 eV, 1 eV = 1.603×10^{-19} J). X-ray source operated at 10 mA and 12 kV. The background pressure in the analysis chamber was kept below 7×10^{-9} mbar during data acquisition. The binding energy (BE C1s = 284.9 eV) of adventitious C_1 was used as reference. A Shirley background subtraction was applied and Gaussian-Lorentzian product functions were used to approximate the line shapes of the fitting components.

UNIVERSITAT ROVIRA I VIRGILI
NANOMATERIALS IN CATALYSIS: STUDY OF MODEL REACTIONS.
Ricardo José Chimentao
ISBN: 978-84-690-7618-7 / DL: T.1326-2007

I.4.3 Results and Discussion

At elevate temperatures, ethylene glycol can reduce Ag^+ ions into Ag atoms, and thereby induce the nucleation and growth of silver nanostructures in the solution phase. On the basis of the reaction of silver nitrate and PVP in EG at 433 K, once the solutions of $AgNO_3$ and PVP had been introduced to the reaction system, a bright yellow color gradually appeared indicating the formation of silver nanoparticles through the reduction of $AgNO_3$ with ethylene glycol [20]. During polyol process, the mixture solution changed from clear to a yellowish color, red brown and finally to gray. The growth of silver nanowires was monitored by sampling aliquots from the refluxing solution at different periods of time and analyzed by TEM. Figure I.4.2 indicates the evolution of the morphologies of the silver nanoparticles as the reaction mixture was kept in reflux. The initial particles (yellow solution), had sizes at around 8-50 nm (Figure I.4.2). As the reaction proceeded the silver particles contact each other to form a chain like network (Figure 1b-c) and some larger nanoparticles (brown red solution) started to appear.

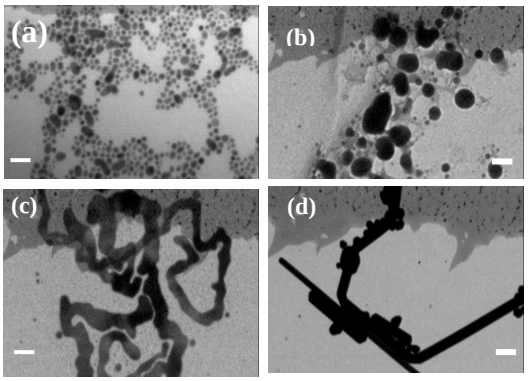

Figure 1.4.2 Growth of silver nanowires monitored by TEM (a-d). Scale bar of 100 nm.

UNIVERSITAT ROVIRA I VIRGILI
NANOMATERIALS IN CATALYSIS: STUDY OF MODEL REACTIONS.
Ricardo José Chimentao
ISBN: 978-84-690-7618-7 / DL: T.1326-2007

The growth of silver nanowires was also monitored by ultraviolet visible spectroscopy (UV-vis). Figure I.4.3a,b shows UV-vis spectra as well as the resultant colors of the samples during the synthesis of silver nanoparticles by polyol process. The growth of silver nanowires was monitored by sampling aliquots from the refluxing solution at different periods of time and analyzing these samples by ultraviolet visible spectroscopy (UV-vis). The spectrum of the solution at 15 min (yellow solution) shows a small plasmon band close to 410 nm, which represents the formation of silver nanoparticles by the reduction of Ag^{+} ions [21]. The appearance of the plasmon band is caused by 4d → 5s, p interband transitions [22]. The intensity of this band progressively increased during polyol process. Besides, the absorption band of the silver nanoparticles is shifted to larger wavelengths with the refluxing time. The nanoparticles obtained at 40 min (gray solution) displayed a broad peak at around 430 nm. The gray solution is formed by predominantly silver nanowires particles.

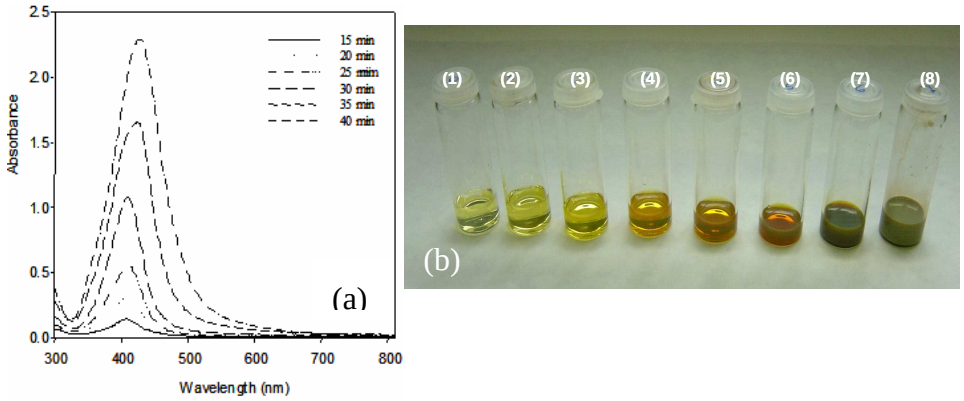

Figure I.4.3 UV-vis spectra during the formation of silver nanowires (a). Picture of the samples (1-8) taken from reaction mixture during different periods of time in the polyol process (b).

UNIVERSITAT ROVIRA I VIRGILI
NANOMATERIALS IN CATALYSIS: STUDY OF MODEL REACTIONS.
Ricardo José Chimentao
ISBN: 978-84-690-7618-7 / DL: T.1326-2007

The selected-area diffraction pattern (SAED) taken from these Ag nanoparticles exhibited Debye-Scherrer rings (Figure I.4.4b) which are assigned to (111), (200) and (220) reflections of the face centered cubic structure (fcc) of silver. The surface analysis of these silver nanoparticles was evaluated by X-ray photoelectron spectroscopy (XPS). The corresponding XPS core-level spectra of the Ag-3*d* region acquired for these silver nanoparticles sample is depicted in Figure I.4.4a. The Ag-3*d* spectra, characterized by the spin-orbit splitting (Ag $3d_{5/2}$ and Ag $3d_{3/2}$ components), shows values off 367.97 and 374.18 eV, respectively. Both peaks indicate that these binding energies are consistent with Ag^0 oxidation state [23, 24].

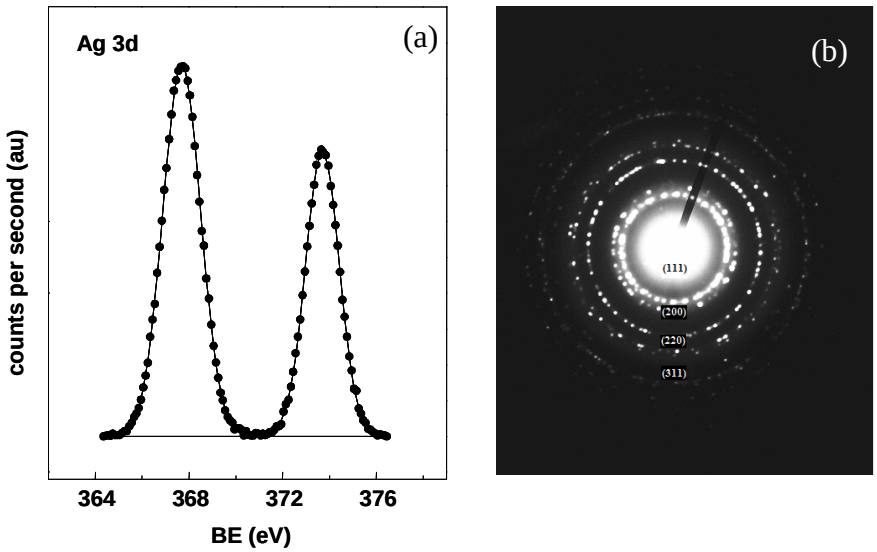

Figure I.4.4 (a) Corresponding XPS analysis of the silver nanoparticles taken in the first 10 minutes of the polyol process. (b) The selected-area diffraction pattern (SAED) taken from these Ag nanoparticles.

The silver nanoparticles were diluted in acetone separated from the ethylene glycol and PVP by centrifugation. It was found that the

UNIVERSITAT ROVIRA I VIRGILI
NANOMATERIALS IN CATALYSIS: STUDY OF MODEL REACTIONS.
Ricardo José Chimentao
ISBN: 978-84-690-7618-7 / DL: T.1326-2007

morphology of the silver particles was significantly influenced by the $AgNO_3$/PVP molar ratio, temperature and the time on reflux. Figure I.4.5(a–c) shows the silver nanoparticles obtained from the polyol process supported on α-Al_2O_3. The diameters of the silver nanoparticles were reasonably uniform with an average value of 150 nm. When the $AgNO_3$/PVP molar ratio was 1.5 the product was dominated by silver nanowires. SEM image of the as-synthesized silver nanowires supported on α-Al_2O_3 (11% $Ag^{(NW)}$/ α-Al_2O_3) is depicted in Figure I.4.5a. The inset of the Figure 1.4.5a shows that the cross section of the silver nanowires clearly has a pentagonal shape which is in agreement with previous results [25]. When this molar ratio increased from 1.5 to 3 truncated silver nanocubes where generated as shown in Figure I.4.5b. Silver nanopolyhedra were also obtained when the silver nanocubes were maintained for longer period of time in the reaction mixture. Figure I.4.5c shows the SEM image of the silver nanopolyhedra catalyst (11% $Ag^{(NP)}$/α-Al_2O_3).

X-ray diffraction (XRD) taken from these silver nanoparticles (Figure I.4.5d) revealed the presence of pure silver showing three diffraction peaks which are assigned to (111), (200) and (220) reflections of the face centered cubic structure (fcc) of silver (JCPDS file 04-0783). Figure I.4.5d (a, b and c) shows the XRD patterns from silver nanocubes, nanopolyhedra and nanowires, respectively. As shown in Figure I.4.5, the XRD pattern showed sharp reflections corresponding to the face-centered cubic (*fcc*) structure of metallic silver.

UNIVERSITAT ROVIRA I VIRGILI
NANOMATERIALS IN CATALYSIS: STUDY OF MODEL REACTIONS.
Ricardo José Chimentao
ISBN: 978-84-690-7618-7 / DL: T.1326-2007

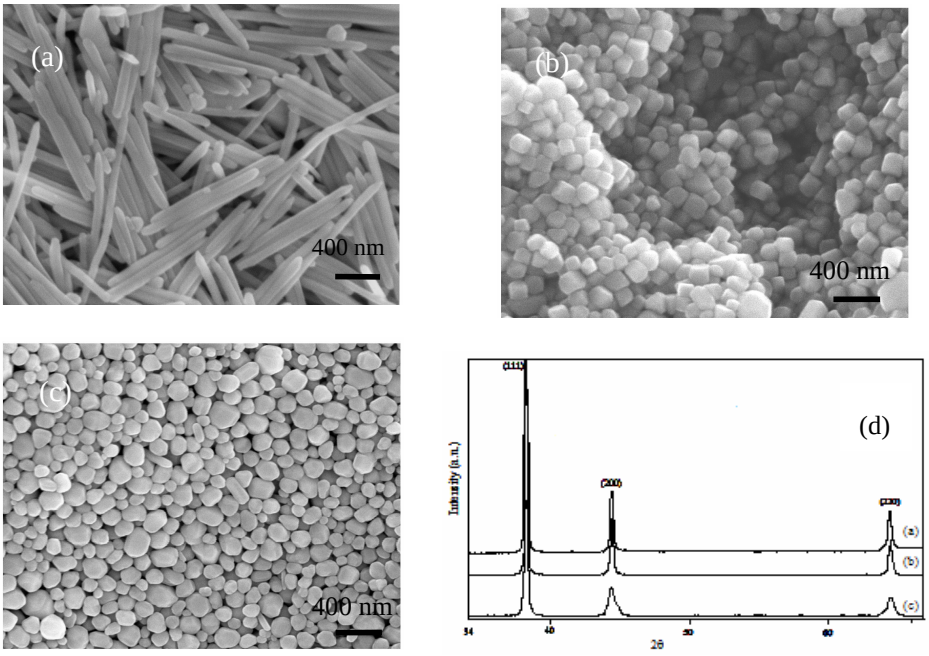

Figure 1.4.5 SEM image of the as-prepared by polyol process of the silver nanoparticles catalyst supported on α-Al_2O_3 (a) silver nanowires, (b) silver nanocubes, (c) silver nanopolyhedra and (d) Corresponding XRD patterns of the as synthesized Ag nanostructures by polyol process, (a) nanocubes (b) nanopolyhedra and (c) Ag nanowires.

The (111) reflection was intensified considerably indicating that the surface of silver nanoparticles is oriented in this plane. The presence of possible impurities such as Ag_2O and $AgNO_3$, was not detected. The lattice constants calculated by XRD for the nanowires was 4.0839, which is very close to the report data (a = 4.0862 Å, Joint Committee on Powder Diffraction Standards file 04-0783). The ratio of intensity between (111) and (200) peaks for nanowires was 4.5, that is higher than for the standard file (JCPDS) (4.5 versus 2.5). This indicates that nanowires show preferred orientation in (111) facets. Therefore it is

UNIVERSITAT ROVIRA I VIRGILI
NANOMATERIALS IN CATALYSIS: STUDY OF MODEL REACTIONS.
Ricardo José Chimentao
ISBN: 978-84-690-7618-7 / DL: T.1326-2007

highly possible the preferential adsorption of the cape agent (PVP) on the (111) plane of the Ag crystals. On the basis of energetic considerations, the optima particle shape for the *fcc* metal is a truncated octahedron with regular hexagonal faces. It has been proposed that the different interaction between PVP and various crystalline facets leads to anisotropic growth of Ag nuclei and further to the formation of different shaped Ag nanostructures [26]. In general, silver single crystal has a face-centered cubic (fcc) structure, therefore the pentagonal shape of the cross-sections observed for our silver nanowires indicates the multiple twinned structure. It becomes clear that these silver nanostructures tend to grow as bicrystals twinned along the (111) planes, showing (111) crystal faces at their surface [27].

I.4.4 Conclusion

Different shapes of Ag nanoparticles have been prepared by polyol process using PVP as a structure-directing agent. The morphologies of the silver nanoparticles prepared by the polyol process were found to depend heavily on the experimental conditions such as temperature and the molar ratio between PVP and $AgNO_3$.Three silver nanoparticles were obtained: silver nanowires, nanocubes and nanopolyhedra. We obtained silver nanowires when the molar ratio of PVP and $AgNO_3$ was 1.5. When the molar ratio was increased from 1.5 to 3, truncated nanocubes were the major product. Silver nanopolyhedra were also obtained when the silver nanocubes were maintained for longer period of time in the reaction mixture. The XRD of the nanowires, nanocubes and nanopolyhedra synthesised using the polyol process suggested that silver existed purely in the face-centered cubic structure. This indicates that nanowires show preferred orientation in (111) facets. The cross

section of the silver nanowires in the SEM image clearly shows a pentagonal shape.

AcknowledgementsThis work was supported by the Ministerio de Ciencia y Tecnologia (Spain) under Projects REN2002-04464-CO2-01 and PETRI 95-0801.OP.

I.4.5 References

[1] Y. Xia, P. Yang, Y. Sun, Y. Wu, B. Mayers, B. Gates, Y. Yin, F. Kim, H. Yan, *Adv. Mater.* **15** (2003) 353.

[2] G. Schimid, *Chem. Rev.* **92** (1992) 1709.

[3] A. Henglein, *Chem.Rev.* **89** (1989) 1861.

[4] M. R. Bomer, L. G. Fokkin, C. Schonenberger, B. M I. van der Zande, *Phys. Chem. B* **101** (1997) 852.

[5] S. R. Nicewarner, R. G. Freeman, D. B. Reiss, L. He, D. J. Pena, I. D. Walton, R. Cromer, C. D. Keating, M. J. Natan, *Science* **294** (2001) 137.

[6] M. R. Bohmer, L. G. J. Fokkink, C. Schonenberger, B. M. I. Van Der Zande, *J. Phys. Chem. B* **101** (1997) 852.

[7] S. R. Nicewarner, R. G. Freeman, B. D. Reiss, L. HE, D. J. Pena, I. D. Walton, R. Cromer, C. D. Keating, M. J. Natan, *Science* **294** (2001) 137.

[8] K. Esumi, K. Matsuhisa, K. Torigoe, *Languimui*r **11** (1995) 3285.

[9] C. J. Murphy, N. R. Jana, *Adv Mater*. **14** (2002) 80.

[10] Y. Sun, Y. Xia, *Adv Mater*. **14** (2002) 833.

[11] Y. Sun, B. Gates, B. Mayers, Y Xia, *Nano Lett.* **2** (2002) 165.

[12] Y. Sun and Y. Xia, *Science* **298 (**2002) 2176.

[13] F. Fievet, J. P. Lagier, M. Fliglarz, *MRS Bull.* **14** (1989) 29.

[14] F. Fievet, J. P. Lagier, B. Blin, B. Beaudoin, m. Fliglarz, *Solid State Ionics* **32** (1989) 198.

[15] US Patent 5 922 409, July 13, 1999.

[16] V. K. LaMer, R. H. Dinegar, *J. Amer. Chem. Soc.* **72** (1950) 4847.

[17] G. Carotenuto, *Appl. Organ. Chem.* **15** (2001) 344.

[18] A. Tao, P. Sinsermsuksakul, P. Yang, *Angew. Chem.* **118** (2006) 4713.

[19] B. Wiley, Y. Sun, B. Mayers, Y. Xia, *Chem. -Eur. J.*, **11** (2005) 454.

[20] Y. Sun, Y. Xia, *Adv. Mater.* **15** (2003) 695.

[21] H. J. Han and S. M. Koo, *J. Sol-Gel Sci. Tech.* **26 (**2003) 467.

[22] D. Meisel, *J. Phys. Chem. B* **102** (1998) 8364.

[23] J. H. Scofield, *J. electr. Rel. Phen.* **8** (1976) 129.

[24] XPS International fundamental XPS data tables, www. xpsdata.com.

[25] C. J. Murphy, N. R. Jana, *Adv. Mater.* **14** (2002) 80.

[26] A. W. Vere, Crystal Growth: *Principles and Progress*. Plenum, New York, 1987.

[27] B. D. Cullity, S. R. Stock, Elements of X-Ray Diffraction (Prentice-Hall, Upper Saddle River, N.J., ed. 3, 2001).

UNIVERSITAT ROVIRA I VIRGILI
NANOMATERIALS IN CATALYSIS: STUDY OF MODEL REACTIONS.
Ricardo José Chimentao
ISBN: 978-84-690-7618-7 / DL: T.1326-2007

Part II

Nanomaterials: Study of model reactions

UNIVERSITAT ROVIRA I VIRGILI
NANOMATERIALS IN CATALYSIS: STUDY OF MODEL REACTIONS.
Ricardo José Chimentao
ISBN: 978-84-690-7618-7 / DL: T.1326-2007

II. Introduction

II.1 Introductory Comments

Heterogeneous catalytic process may be divided into to large groups: redox reactions and acid-base reactions [1-4]. The first group comprises all those reactions in which the catalyst effects the homolytic bond rupture in the reactant molecules with the appearance of unpaired electrons, and formation of homolytic bounds with the catalyst with the participation of catalyst electrons. The important step of such reactions is thus the exchange of single electrons between the catalyst and the reactants, and therefore such catalytic properties are shown by solids which have the ability to accept and donate electrons. These are transition metals and their compounds, in which the cation can easily change its valence state. As this property is also responsible for the nonstoichiometry, catalysts for redox processes are found among nonstoichiometric transition metal compounds, the most important being oxides and sulfides.

The second group includes reactions in which the reactants form with the catalyst heterolytic bonds by using the free electron pair of the catalyst or reactants, or the free electron formed in the course of reaction by heterolytic rupture of bonds in the reactant molecules. Examples for catalysts for such reactions are simple oxide of main group elements or their complex acids and salts showing acid-base properties of both Brönsted or Lewis types. For the first group we focus the attention in the study of the selective oxidation of styrene, propene and ethanol in gas phase. The second group represented here was the epoxidation of styrene in liquid phase over exfoliated Mg-Al layered doubled hydroxides (LDHs) or hydrotalcites.

UNIVERSITAT ROVIRA I VIRGILI
NANOMATERIALS IN CATALYSIS: STUDY OF MODEL REACTIONS.
Ricardo José Chimentao
ISBN: 978-84-690-7618-7 / DL: T.1326-2007

II.1.1 General Introduction

II.1.1.1 Selective oxidation of olefins on metals

The heterogeneous selective oxidation of olefins on silver is an exceedingly important industrial catalytic reaction, and as such has received long and extensive study [5-7]. One particularly interesting is its uniqueness: not only silver a uniquely effective catalyst for heterogeneous epoxidation but also ethylene is the only hydrocarbon which may be epoxidized with high selectivity in practical conditions. Actually silver catalysts are used in industry to produce several tons of ethylene oxide yearly [8, 9]. The catalyst is usually promoted by alkali metals. Recent experimental studies show that, except for ethylene, only a few olefins such as styrene, 3,3-dimethylbutene, norbonene, and butadiene may epoxidized over silver with high selectivity. In contrast, other olefins such as propylene, butanes, and pentenes are epoxidized over silver but with extremely low selectivity [10-13]. The origin of this unique catalytic activity of silver has not yet been clarified. There are many reasons that silver is a unique catalyst for ethylene epoxidation [14]. First of all the catalyst must not decompose adsorbed ethylene and/or ethylene oxide by CH activation like VIII metals [15]. Secondly, ethylene is π- bonded to silver and the double bound is therefore readily accessible for reaction. On other metals such as Pt, Ni, CO, W and Ru ethylene adsorbs in the di-σ configuration [16]. Copper has the many features as silver however the presence of oxygen atmosphere a stable surface oxide is formed which poisons the catalyst. The catalyst also needs to form a special kind of oxygen that reacts with double bound without breaking the single bonds. Finally and

UNIVERSITAT ROVIRA I VIRGILI
NANOMATERIALS IN CATALYSIS: STUDY OF MODEL REACTIONS.
Ricardo José Chimentao
ISBN: 978-84-690-7618-7 / DL: T.1326-2007

maybe the most important reason for the uniqueness of silver is the favorable branching ratio of the oxymetallacycle. One the main questions about the mechanism of ethylene oxidation is the roles of adsorbed oxygen. Many scientists believe that the interaction between oxygen and silver plays an essential role in understanding ethylene epoxidation and a great research has been devoted to the silver-oxygen system [17, 18]. Lambert and co-workers [19, 20] and Carter and Goddard [21] suggested that two different atomic oxygen species were active in epoxidation (electrophilic) and combustion (nucleophilic), respectively. Nucleophilic oxygen exists on clean silver, while electrophilic oxygen is created in the presence of subsurface oxygen. X-ray photoelectron spectroscopy studies have shown that the two different bulk species O_β and O_γ differentiate themselves electronically [22]. The mechanism leading to the formation of these species is poorly understood. The subsurface specie, O_β, is formed when dissociatively adsorbed, atomic surface oxygen diffuses in to bulk. A second specie, O_γ, is formed at higher temperature (T> 873 K) via the segregation of O_β to the surface as depicted in Figure II.1.

Of particular interest is to understand the role and the nature of the elusive subsurface O species in the function of silver as an oxidation catalyst. Subsurface is thought to play a crucial role in the epoxidation of ethylene (i.e., formation of ethylene oxide, alternatively known as epoxide), which takes place under atmospheric pressure and temperatures of 500-600 K. For oxygen occupation in the subsurface region there are two possible sites: (i) octahedral site which has six nearest neighbor Ag atoms, three above and three below, and (ii) the tetrahedral site, which has four nearest neighbor Ag atoms [23]. A silver subsurface is therefore, formed as a result of incorporation of

UNIVERSITAT ROVIRA I VIRGILI
NANOMATERIALS IN CATALYSIS: STUDY OF MODEL REACTIONS.
Ricardo José Chimentao
ISBN: 978-84-690-7618-7 / DL: T.1326-2007

oxygen into the silver bulk.

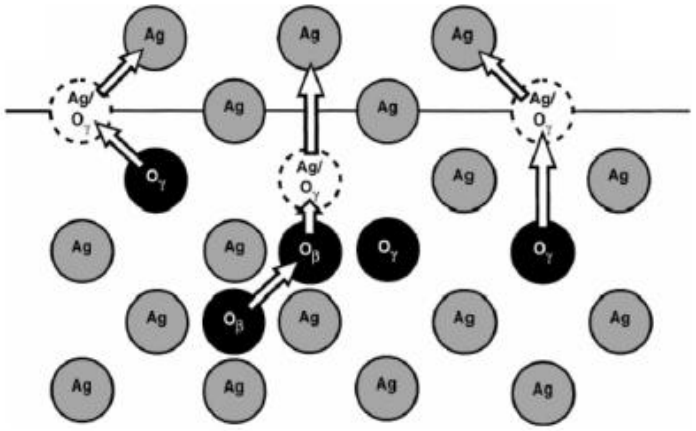

Figure II.1 Scheme of the interstitialcy bulk oxygen diffusion mechanism (vacancy diffusion) [22].

Experimental evidence indicates that the (111) orientation is an important crystal face for real silver catalysts since at high temperatures, facets with this face result presumably due to the fact that it has the lowest surface energy [24]. At high temperatures, the silver surface reconstructs to mainly form (111) surfaces. The catalyst eventually attains an equilibrium equimolar counter diffusion during which oxygen is adsorbed, dissolves in the bulk via interstitialcy diffusion mechanism by which O substitutes for Ag and eventually segregates back to the surface where it may desorb or react. It has been suggested that the actual catalytic reaction can only occur, in that moment when O_γ has segregates to the uppermost layer of the silver catalyst at which may react with the organic reactant present in the gas phase [25] and if the O_β specie does not participate in the epoxidation directly at least serve as like an oxygen reservoir that supplies oxygen

UNIVERSITAT ROVIRA I VIRGILI
NANOMATERIALS IN CATALYSIS: STUDY OF MODEL REACTIONS.
Ricardo José Chimentao
ISBN: 978-84-690-7618-7 / DL: T.1326-2007

for the reaction playing a key role for the epoxidation.

It is also known for long [26, 27] that this reaction is sensitive to particle size and more selective on larger particles, therefore on dense crystal planes. In these regards, the piece of work presented in the *Chapter II.1 and 2* will study the epoxidation in gas phase over the silver nanoparticles synthesize by the polyol process already mentioned in *Chapter I.1*. These silver nanoparticles were supported on α-Al_2O_3 in the styrene epoxidation. Styrene has no allylic hydrogens and is expected too behave as ethylene in epoxidation. The effect of an alkaline metal promotion, such as cesium, on the silver nanoparticles catalysts was also investigated.

Efforts to directly epoxidize other olefins, such as propene, to their corresponding epoxides using molecular oxygen in a commercially-viable process are necessary. The lower selectivity obtained for propene epoxidation instead of for ethylene has been attributed to a greater reactivity of the allylic hydrogen in propene compared to that of the vinyl hydrogen in ethylene [28]. However, Haruta and coworkers have reported that a feed stream consisting of C_3H_6, O_2 and H_2, can be selectively epoxidized to form propene oxide using highly dispersed gold supported on TiO_2 [29]. It seems that the size of the gold particle plays an important role in the selective oxidation reaction of propene in gas phase. An alternative oxidizing agent for the epoxidation of propene is nitrous oxide (N_2O). This oxidant has received much attention for many different oxidation reactions especially after the discovery that selective oxidation of benzene to phenol by nitrous oxide could be performed over Fe-ZSM-5 zeolite [30]. Nitrous oxide has certain properties which generate a mild electrophilic peroxide-like oxygen species but a nucleophilic one as well. Energetically, the

UNIVERSITAT ROVIRA I VIRGILI
NANOMATERIALS IN CATALYSIS: STUDY OF MODEL REACTIONS.
Ricardo José Chimentao
ISBN: 978-84-690-7618-7 / DL: T.1326-2007

release of an oxygen atom from N_2O is more favorable than from oxygen molecule [31]. However, the catalyst for the epoxidation of propene must adsorb and activate the N_2O molecule without decomposing it. A major disadvantage for an oxidation process using nitrous oxide for a bulk chemical such as propene oxide, however, is that nitrous oxide is not commercially available in large quantities. Virtually all nitrous oxide currently produced as a byproduct of the adipic acid production using the nitric oxide production of cyclohexanol [32]. Recently Lambert and co-workers [33] have shown that copper is also effective for propene epoxidation. The active phase appears to be highly dispersed form of metallic copper and the performance of these materials is comparable to that reported by Haruta et al. [29] in their first paper on propene epoxidation catalyzed by Au/TiO_2. It is reported that when allylic hydrogen atoms exist in the alkene molecules, epoxidation can still occur on Cu(111) surfaces. Thus, Cu based catalysts may be promising for propylene epoxidation. In this account, here we reported the study of the Au-Cu bimetallic system supported on TiO_2 in the propene epoxidation by nitrous oxide. The *Chapter II.3* intends to give an insight to the nature and distribution of these surface sites as well as the segregation of each element is strongly dependent of temperature. This fact is relevant for catalytic activity of nanoparticles in which alloying of elements provided an increase of chemical activity of the system.

II.1.1.2 Partial oxidation of ethanol on VO_x catalyst

Oxidative dehydrogenation (ODH) of alcohols into various aldehydes

or ketones is also of practical interest [34]. The industrially most important oxidation of an alcohol is the oxidative dehydrogenation of methanol to formaldehyde [35]. Here the study was devoted to the investigation of the partial oxidation of ethanol to acetaldehyde over highly dispersed VO_x catalysts. The present work is an attempt to demonstrate on the basis of the open literature data how alkaline additives, such as sodium, may affect the structure and properties of the oxide system. Metal oxides with the metal in oxidation state five or six have shown the highest activity of these kinds of transformations. This characteristically high oxidation state seems to be linked with the formation of redox and or Brønsted acid sites [36, 37]. Among these metal oxides, vanadium oxide catalysts have attrached much attention due to their unique catalytic properties and commercial applicability for various chemical processes. Hundreds of reports have appeared in the literature concerning the characterization of oxide-supported vanadia species, with the works of Wachs and coworkers, and Iglesia and coworkers being of particular relevance [38-40]. MCM-41 and TiO_2 was employed as supports. Indeed, silica is regarded as an inappropriate support for vanadia because the interaction of vanadium oxide with this particular support oxide surface is extremely weak. In fact, vanadium oxide (V) supported on titanium (IV) oxide (anatase) is one of the best catalytic system for these reactions [41]. The effect of the Na promotion over vanadium catalysts was accessed. This additive may affect the acid-base properties by changing the electron density around metal and oxide ions. This piece of work, presented in *Chapter II.3*, was realized in closed collaboration with the researchers at the Environmental Molecular Science Laboratory (EMSL) at the Pacific Northwest National Laboratory (PNNL). Extensive use was

UNIVERSITAT ROVIRA I VIRGILI
NANOMATERIALS IN CATALYSIS: STUDY OF MODEL REACTIONS.
Ricardo José Chimentao
ISBN: 978-84-690-7618-7 / DL: T.1326-2007

made of the user facilities at EMSL and at the Institute for Interfacial Catalysis. We extend our sincere gratitude and appreciation to the researchers from the PNNL who made possible the realization of this experimental work.

II.1.1.3 Epoxidation of styrene on Mg-Al hydrotalcite in the liquid phase

The increasing environmental pressure on industry to replace traditional homogenous catalysts by friendly technologies represents one of the most relevant driving forces for the development of heterogeneous catalysts. However, understanding the performance of basic sites in these heterogeneous systems actually deals with the systematic design of strategies that evidence clear structure-activity relationships at an atomic level. This is the case of activated hydrotalcites, which have been largely studied in the last years in the search of strategies for resolving their unparalleled activity, particularly their reconstructed mixed oxides. Hydrotalcites are layered double hydroxides with the general formula $[M^{2+}_{1-x}M^{3+}_{x}(OH)_2][X^{m-}]_{x/m}\cdot nH_2O$, consisting of brucite-type octahedral layers, in which M^{3+} cations partially substitute for M^{2+} cations. The net positive charge resulting from this substitution is compensated by anions (typically carbonate), located together with water molecules in the interlayer space [42]. This materials is often inactive and has to be activated by thermal decomposition to obtain a high-surface area and well-dispersed Mg(Al)O mixed oxide. In the presence of water and appropriate anions, the oxide mixture can be reconstructed back to the original hydrotalcite structure. This property, known as memory effect, provides an effective

UNIVERSITAT ROVIRA I VIRGILI
NANOMATERIALS IN CATALYSIS: STUDY OF MODEL REACTIONS.
Ricardo José Chimentao
ISBN: 978-84-690-7618-7 / DL: T.1326-2007

synthetic pathway for the insertion of organic and inorganic anions into the hydrotalcite. A particular example is meixnerite, which contains OH^- groups in the interlayer space after contacting the mixed oxide with decarbonated water or in a flow of gas saturated with water [43,44]. This material leads to outstanding activities for base-catalyzed reactions, requiring the presence of Brønsted-sites [45-47]. However, many applications are largely restricted due to the inaccessibility to the inner surfaces of the OH^- hosted between layers [48]. The original hypothesis by Roelofs et al. [49] claimed that the active sites are likely situated at the edges of the nanoplatelets, which represent a minor part of the Brønsted-sites in the hydrotalcite. This information has been so far obtained indirectly, by correlating ex situ characterization of the catalysts with specific trends in catalytic performance. Consequently, several studies have been carried out to maximize the number of edge sites, hereby inducing a more irregular morphology of the platelets [50,51]. This was achieved by preparation of small hydrotalcite nanoplatelets (≈ 20 nm) supported on carbon nanofibers [52] or by the use of ultrasounds during reconstruction [50], leading to an impressive enhancement of the catalytic activity in the aldol condensation reaction of citral and acetone. Particularly for base-catalyzed reactions, clear insights about the surface features differing in their catalytic activity have not been found yet. The most effective solution to maximize the utility of the platelets would be the delamination of the hydrotalcite into single layers. Roeffaers et al. [53] were able to map the spatial distribution of catalytic activity over an entire hydrotalcite crystal (crystal faces, edges and defects), by means of a wide field microscope.

UNIVERSITAT ROVIRA I VIRGILI
NANOMATERIALS IN CATALYSIS: STUDY OF MODEL REACTIONS.
Ricardo José Chimentao
ISBN: 978-84-690-7618-7 / DL: T.1326-2007

II.1.1.4 Metal catalyzed skeletal rearrangement of hydrocarbons

The skeletal reactions of hydrocarbon on metal represent an important class of reactions on heterogeneous catalysis both from a theoretical and an industrial point of view, in spite of some uncertainty concerning to the role of the metal and its dispersion on the support [54, 55]. It is fact - well established but not well understood- that various metals differ very much as catalysts in hydrocarbon reactions. In recent years numerous studies have been concerned with the selectivity of the platinum metals in catalytic hydrocarbon skeletal reactions [56-58]. Methylcyclopentane (MCP) is a recognized probe molecule in the investigation of the structure sensitivity of several hydrocarbon conversions catalyzed usually by noble metal-based catalysts [59-63]. For the readers it is highly recommended the classical work by Gault et al. [57] in which the arrangement of methylcyclopentane (MCP) and isomerization of hexane isomers on alumina supported platinum catalysts by ^{13}C tracer technique was investigated. They showed the identity of the product distributions from these two reactions, the almost complete absence of 2, 3-dimethylbutane and the formation of methylcyclopentane during isomerization. These results strongly suggested that a common intermediate with five membered ring structure is responsible for this reactions. The Figure II.2 summarizes the relationships between isomerization, hydrogenolysis and dehydrocyclization.

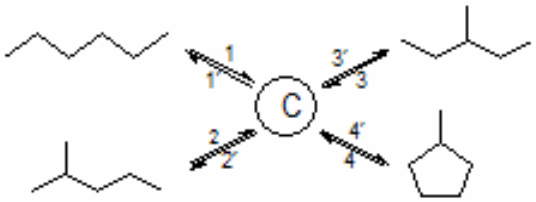

Figure II.2 Cyclic mechanism [64].

UNIVERSITAT ROVIRA I VIRGILI
NANOMATERIALS IN CATALYSIS: STUDY OF MODEL REACTIONS.
Ricardo José Chimentao
ISBN: 978-84-690-7618-7 / DL: T.1326-2007

Isomerization of n-hexane for instance is represented by the consecutive elementary steps 1-3' or 1-2', its dedydrocyclization by the reactions 1-4'; hydrogenolysis of methylcyclopentane by any of the steps 4-1', 4-2', and 4-3'. The Gault's laboratory in 1957 found that the distribution of the reaction products changed substantially with changing the percentage of the platinum on the carrier. An almost selective rupture CH-CH_2 bonds was found on the more concentrated catalysts (more than 2% of Pt), while on the less loaded ones (less than 1% of Pt) the rupture probabilities of the five C-C bonds of the ring were approximately equal as depicted in Figure II.34.

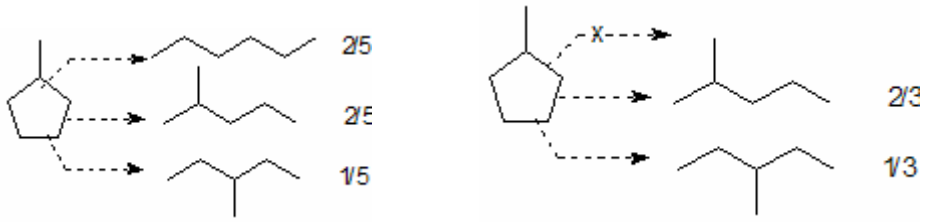

Figure II.3 (a) Non-selective hydrogenolysis on high dispersed catalysts and (b) Selective hydrogenolysis on low dispersed catalysts.

The catalysts for skeletal reactions of hydrocarbon are bifunctional. Some of the important reforming reactions are multistep processes in which certain steps occur on platinum sites and other steps on acid sites. The surface of the alumina in the reforming catalysts exhibits acid properties, largely due to the presence of chloride ions (Cl^-) on the surface. The chloride ions interact with hydroxyl (OH) groups to enhance the protonic acidity arising therefrom. The hydrogen partial pressure represents a substantial fraction of total pressure throughout the reaction zone. When the hydrogen partial pressure is too slow, the rate of formation of residues on the catalyst deactivates

UNIVERSITAT ROVIRA I VIRGILI
NANOMATERIALS IN CATALYSIS: STUDY OF MODEL REACTIONS.
Ricardo José Chimentao
ISBN: 978-84-690-7618-7 / DL: T.1326-2007

catastrophically. But if it is high enough can suppress extreme types of surface dehydrogenation processes that produce carbonaceous residues on the catalyst and deactivate the sample [65].

Scientists have been interested in bimetallic system as catalysts for many years. For longer beginning shortly after World War II, much attention was devoted to the use of metal alloys as catalysts to probe the relationship between the catalytic activity of a metal and its electronic structure [66, 67]. One type of alloy which was investigated extensively consisted of Group VIII and Group IB metal. In terms of energy band theory of electrons in metals, transitions metals such as those Group VIII possess *d*-bands whose those states are not completely occupied by electrons. By contrast, the d-bands of non-transition metals such as those of Group IB are completely filled. The IB metals can be considered as almost inactive in these reactions as compared with the Group VIII metals. When a Group VIII metal is alloying with an IB metal, one effect is always present: active atoms are diluted in a matrix which itself is much less active with respect to hydrocarbon reactions. As a rule the surface concentration of a Group VIII metal is considerably lower than in the bulk average concentration [68, 69]. By all that, the formation of big ensembles of active atoms is suppressed. However, this is not the only way the components is alloys influence each other. First it is possible, at least in principle, that the neighborhood of group VIII atoms ay cause the the IB atoms to became active, for example by supplying H_2 (by a spill-over effect) or other species formed on the group VIII atom sites. Second, the properties of individual group VIII may change when they dispersed in a matrix of IB (or another metal). Of course, the extent of such changes depends on the alloy components in consideration. These changes will be stronger

UNIVERSITAT ROVIRA I VIRGILI
NANOMATERIALS IN CATALYSIS: STUDY OF MODEL REACTIONS.
Ricardo José Chimentao
ISBN: 978-84-690-7618-7 / DL: T.1326-2007

with exotermically formed Pt-Cu which may form ordered structures and will be less pronounced with Pt-Au pr Pt-Ag systems with limited solubility. The bimetallic systems of interest are not limited to combinations of metallic elements that are highly miscible in bulk. For example, the ruthenium-copper system [70], in which the two components are virtually completely immiscible in the bulk, exhibits selectivity inhibition of hydrogenolysis similar to that observed with the nickel-copper system. The latter, of course, is well known as a system in which the two components form complete series of solid solution. Since the ability to form bulk alloys was not necessary condition for a system of interest as a catalyst, here in the present work it was decided to prove in the hydrogenolysis of methylcyclopentane the combination of two metals with very limit miscibility such as the Ir-Au system. Much of the focus of the *Chapter II.5* was concerned in the investigation directed toward the validation and elucidation of this bimetallic system in the methylcyclopentane hydrogenolysis.

II.3 References

[1] S. Z. Rogiński, *Problemy Kinet. Katal*, **8** (1955) 110.

[2] G. K. Boreskov, *Proc. 3rd Intern. Congr. Catalysis*, Amsterdam 1964, Amsterdam: North-Holland Publ. 1965 vol. 1 p. 163.

[3] J. H. Sinfelt, *Adv.. Catal.* **23** (1973) 91.

[4] B. G. Świerkosz, *Topics in Catal.* **11/12** (2000) 23.

[5] R. A. van Santen, H. P. C. Kuipers, *Adv. Catal.* **35** (1987) 265.

[6] W. M. H. Sachtler, C. Backx, R. A. van Santen, *Cat. Rev. Sci. Eng.* **23** (1981) 127.

[7] H. H. Voge, C. R. Adams, *Adv. Catal.* **17** (1967) 151.

[8] X. E. Verykios, F. P. Stein, R. W. Coughlin, *Catal. Rev. Sci.*

UNIVERSITAT ROVIRA I VIRGILI
NANOMATERIALS IN CATALYSIS: STUDY OF MODEL REACTIONS.
Ricardo José Chimentao
ISBN: 978-84-690-7618-7 / DL: T.1326-2007

Eng. **22** (1980) 197.

[9] K.A. Jørgensen, *Chem. Rev.* **89** (1989) 431.

[10] H. Nakatsuji, Z. M. Hu, H. Nakai, *Int. J. Quantum Chem.* **65** (1997) 839.

[11] J. W. Medlin, J. R. Monnier, M. A. Barteau, *J. Catal.* **204** (2001) 71.

[12] J. R. Monnier, J. W. Medlin, M. A. Barteau, *J. Catal.* **204** (2001) 71.

[13] S. Hawker, C. Mukoid, J. P. S. Badyal, R. M. Lambert, *Surf. Sci.* **219** (1989) L616.

[14] C. Stegelmann, N. C. Schiødt, C. T. Campbell, P. Stolze, *J. Catal.* **221** (2004) 630.

[15] C. T. Campbell, M. T. Paffett, *Surf. Sci.* **177** (1986) 417.

[16] R. I. Masel, *Principles of adsorption and reaction on solid surfaces*, Wiley 1996.

[17] R. A. van Santen, H. P. C. E. Kuipers, *Adv. Catal.* **35** (1987) 265.

[18] B. S. Bal'zhinimaev, *Kinet. Catal.* **40** (1999) 795.

[19] R. B. Grant, R. M. Lambert, *J. Catal.* **92** (1985) 364.

[20] R. A. van Santen, H. P. C. E. Kuipers, *Adv. Catal.* **35** (1987) 265.

[21] E. A. Carter W. A. Goodard III, *Surf. Sci.* **209** (1989) 243.

[22] X. Bao, M. Muhler, T. S. Weinberg, E. Kitzelmann, R. Schlögl, *Phys. Rev. B* **54** (1996) 2249.

[23] X. Bao, M. Muhler, B. Pettinger, R. Schögl, G. Ertl, *Catal. Lett.* **22** (1993) 215.].

[24] X. Bao, G. Lehmpfuhl, G. Weinberg, R. Schögl, G. Ertl, *J. Chem. Soc. Faraday Trans.* **88** (1992) 865.

UNIVERSITAT ROVIRA I VIRGILI
NANOMATERIALS IN CATALYSIS: STUDY OF MODEL REACTIONS.
Ricardo José Chimentao
ISBN: 978-84-690-7618-7 / DL: T.1326-2007

[25] X. Bao, M. Muhler, T. S. Niedrig, R. Schlögl, *Phys. Rev. B* **54** (1996) 2249.]

[26] Wu and Harriot, *J. Catal.* **39** (1975) 395-402,

[27] Jarjoui, Moraweck, Gravelle, Teichener, *J. Cim. Phys. Phys. Chim. Biol.* **75** (1978) 1060.

[28] M. A. Barteau, R. J. Madix, J. Am. Chem Soc. **105** (1983) 344.

[29] T. Hayashi, K. Tanaka, M. Haruta, J. Catal. **178** (1998) 566.

[30] V. N. Parmon, G. I. Panov, A. Uriarte, A. S. Noskov, Catal. Today 100

[31] G. Ramis, G. Busca, F. Bregani, Gazz. Chim. Ital. **122** (1992) 79.

[32] V. Duma, D. Hönicke, J. Catal. 191 (2000) 93.

[33] O. P. H. Vaughan, G. Kyriakou, N.Macleod, M. Tikhov, R. M. Lambert, *J. Catal.* **236** (2005) 401.

[34] R. W. Clayton, S. V. Norval, *Specialist periodical reports: catalysis*. Chem. Soc. London vol. 3 (1980) 70.

[35] C. N. Satterfield, *Heterogeneous Catalysis*, 2nd edition, McGraw-Hill, 1991.

[36] G. T. Went, S. T. Oyama, A. T. Bell, *J. Phys. Chem.* **94** (1990) 4240.

[37] L. R. Le Coustumer, B. Taouk, M. Le Meur, E. Payen, M. Guelton, J. Grimblot, *J. Phys Chem.* **92** (1988) 1230.

[38] I. E. Wachs, L. E. Briand, J. M. Jehng, L. Burcham, X. Gao, *Catal. Today* **57** (2000) 323.

[39] N. Y. Topsøe, H. Topsøe J. A. Dumesic, *J. Catal.* **151** (1995) 226.

[40] L. J. Burcham, I. E. Wachs, *Catal Today* **49** (1999) 467.

[41] J. J. Jimenez, J. M. Robles, E. R. Castellón, A. J. López, M. L.

UNIVERSITAT ROVIRA I VIRGILI
NANOMATERIALS IN CATALYSIS: STUDY OF MODEL REACTIONS.
Ricardo José Chimentao
ISBN: 978-84-690-7618-7 / DL: T.1326-2007

Granados, S. del Val, I. M. Cabrera, J. L. G. Fierro, *Catal. Today* **99** (2005) 179.

[42] F. Cavani, F. Trifirò, A. Vaccari, *Catal. Today* **11** (1991) 173.

[43] S. Abelló, F. Medina, D. Tichit, J. Pérez-Ramírez, J.C. Groen, J.E. Sueiras, P. Salagre, Y. Cesteros, *Chem. Eur. J.* **11** (2005) 728.

[44] D. Tichit, B. Coq, CATTECH 7 (2003) 206.

[45] K.K. Rao, M. Gravelle, J. Sanchez Valente, F. Figueras, J. Catal. 173 (1998) 115.

[46] Y. Ono, J. Catal. **216** (2003) 406.

[47] M.L. Kantam, B.M. Choudary, C.V. Reddy, K.K. Rao, F. Figueras, Chem. Commun. 9 (1998) 1033.

[48] M. Adachi-Pagano, C. Forano, J.-P. Besse, *Chem. Commun*. (2000) 91.

[49] J.C.A.A. Roelofs, A.J. van Dillen, K.P. de Jong, *Catal. Today* **60** (2000) 297.

[50] S. Abelló, F. Medina, D. Tichit, J. Pérez-Ramírez, Y. Cesteros, P. Salagre, J.E. Sueiras, *Chem. Commun.* (2005) 1453.

[51] F. Winter, X. Xia, B.P.C. Hereijgers, J.H. Bitter, A.J.van Dillen, M. Muhler, K.P.de Jong, *J. Phys. Chem. B* **110** (2006) 9211.

[52] F. Winter, A.J. van Dillen, K.P. de Jong, *Chem. Commun*. (2005) 3977.

[53] M.B.J. Roeffaers, B.F. Sels, H. Uji-i, F.C. De Schryver, P.A. Jacobs, D.E. De Vos, J. Hofkens, *Nature* **439** (2006) 572.

[54] F. G. Ciapetta, *Ind. Eng. Chem.* **45** (1953) 162.

[55] G. A. Mills, H. Heinemann, T. H. Milliken, A. G. Oblad, *Ind. Eng. Chem.* **45** (1953) 134.

[56] G. Maire, G. Plouidy, J. C. Prudhome, F. G. Gault, *J. Catal.* **4**

(1965) 556.

[57] Y. Barron, G. Maire, J. M. Muller, F. G. Gault, *J. Catal.* **5** (1966) 428.

[58] F. G. Gault, *Advances in catalysis and related subjects*, vol. 30, 1, Academic Press, New York/London, 1981.

[59] M. Boudart, Adv. Catal. **20** (1969) 153.

[60] G. Leclercq, L. Leclercq and R. Maurel, J Catal **50** (1977) 87.

[61] J. M. Dartigues, A. Chambellan, F. G. Gault, J. Am. Chem. Soc. 98 (1976) 856.

[62] J. H. Sinfelt, Bimetallic catalysts: Discoveries, concepts and Applications; John Wiley & Sons, New York, 1983.

[63] Z. Paál and P. Tétényi, Nature **267** (1977) 234.

[64] Y. Barron, D. Cornet, G. Maire, F. G. Gault, *J. Catal.* **2** (1963) 152.

[65] J. H. Sinfelt, *Catalytic reforming of hydrocarbons*, J. R. Anderson, M. Boudart (eds.), Catalysis Science and Technology, vol. 1, Springer, Berlin, 1981, p. 257.

[66] G. M. Schawb, *Disc. Faraday Soc.* **8** (1950).

[67] R. J. Best, W. W. Russell, *J. Amer. Chem. Soc.* **76** (1954) 838.

[68] V. Ponec, *Electronic structure and reactivity of metal surfaces*, ed. E. G. Derouane & A. A. Lucas, Plenum Press, New York, 1976, p. 537.

[69] V. Ponec, *Progress in surface and membrane science*, vol. 13, ed. Danielli & D. A. Cadenhead.

[70] J. H. Sinfelt, *J. Catal.* **29** (1973) 308.

UNIVERSITAT ROVIRA I VIRGILI
NANOMATERIALS IN CATALYSIS: STUDY OF MODEL REACTIONS.
Ricardo José Chimentao
ISBN: 978-84-690-7618-7 / DL: T.1326-2007

Chapter II.1

Different morphologies of silver nanoparticles catalysts for the selective oxidation of styrene in gas phase

UNIVERSITAT ROVIRA I VIRGILI
NANOMATERIALS IN CATALYSIS: STUDY OF MODEL REACTIONS.
Ricardo José Chimentao
ISBN: 978-84-690-7618-7 / DL: T.1326-2007

II.1.1. Literature Review

Direct gas phase partial oxidation of olefins by molecular oxygen to epoxides is long considered one of the most important reactions in commercial catalysis [1, 2]. The styrene is a useful alkene model to study the mechanism reaction of terminal alkene epoxidation [3]. Silver is considered almost the unique effective catalyst for the heterogeneous epoxidation reaction [4]. In 1931, Lefort first reported success using silver as catalyst [5]. The ethylene epoxidation is the most studied partial oxidation reaction in industrial process and silver catalyst is the uniquely used under practical conditions [6].

It is well accepted that the selective oxidation reactions on supported noble metals catalyst proceed via Mars-van Krevelen mechanism. The redox property of the catalyst is therefore expected to play an important role in these reactions. Alkaline metals are observed to enhance the redox activities of a number supported metal catalysts [7]. Commercial catalysts for the epoxidation of ethylene consist of silver supported on low surface area materials such as α-Al_2O_3. Alkali metals and their salts have been proposed as promoters in these catalysts. Cesium is usually added to the catalyst to improve the selectivity toward the epoxide [8-13].

To understand the reaction mechanism, the adsorption of oxygen on silver catalysts has been thoroughly performed. This technique gives information about which type of adsorbed oxygen species are responsible in the epoxidation reaction. It has been observed that the oxygen shows different adsorption states. The studies devoted to oxygen-silver system suggests that mainly two different type of oxygen are the active species: electrophilic oxygen leading to selective

UNIVERSITAT ROVIRA I VIRGILI
NANOMATERIALS IN CATALYSIS: STUDY OF MODEL REACTIONS.
Ricardo José Chimentao
ISBN: 978-84-690-7618-7 / DL: T.1326-2007

oxidation products and nucleophilic oxygen producing combustion products [14]. These oxygen species exist on silver catalysts under ethylene epoxidation conditions (160 - 300 ^{0}C) through reversibly and irreversibly adsorption process. However, the study of oxygen adsorption on practical silver catalysts is especially complex since silver surfaces are polycrystalline and contains a significant proportion of defect [15]. Some results indicate that the (111) orientation is an important crystal face for real silver catalyst presumably due to the fact that it has the lowest surface energy [16]. There is a growing interest to obtain advanced materials using nanoscale building blocks, in order to control the sizes and shapes of inorganic nanocrystals [17]. Therefore the synthesis of well-controlled shapes of metal nanoparticles represents a new avenue in the study of selective oxidation reactions over silver catalysts.

In present work, an important objective of this work is to study how the size and morphology of silver nanoparticles affect the catalytic behavior of silver catalysts supported on α-Al_2O_3 in the selective oxidation of styrene in gas phase. Herewith we also investigated the performance of cesium promoted silver nanoparticles catalysts supported α-Al_2O_3 in the epoxidation of styrene. Styrene ($C_6H_5CH=CH_2$) is a good choice because the phenyl group π-electrons activate the olefinic bound towards electrophilic attack by oxygen [19]. In this work, silver nanowires were synthesized by polyol process [18] and then supported on α-Al_2O_3. Besides, the effect of the addition of cesium and the O_2: styrene molar ratios in the catalytic behavior were also studied. For comparison it was also studied a catalyst prepared by wetness impregnation with an aqueous solution of $AgNO_3$. Temperature programmed reduction (TPR) and X-ray photoelectron

UNIVERSITAT ROVIRA I VIRGILI
NANOMATERIALS IN CATALYSIS: STUDY OF MODEL REACTIONS.
Ricardo José Chimentao
ISBN: 978-84-690-7618-7 / DL: T.1326-2007

spectroscopy (XPS) were performed to characterize the oxygen species formed on the silver nanowires after exposure to O_2. The samples were also structurally characterized using X-ray diffraction (XRD) and scanning electron microscopy (SEM), in order to correlate the morphological dependence of metal particles with its catalytic activity.

II.1.2 Experimental

II.1.2.1 Preparation of the catalysts

Silver nanowires catalysts were prepared by polyol process. In a typical synthesis of silver nanoparticles, 30 ml ethylene glycol solution of $AgNO_3$ (0.25 M, Aldrich) and 30 ml ethylene glycol solution of polyvinyl-pyrrolidone (PVP) (0.375 M in repeating unit weight-average molecular weight ≈ 40,000, Aldrich) were simultaneously added in 50 ml ethylene glycol at 433 K under vigorous magnetic stirring. The reaction mixture was then refluxed for 45 min at this temperature. The obtained nanoparticles were diluted with acetone and separated from ethylene glycol by centrifugation at 4000 rpm for 20 min. Then, silver nanowires (11 wt. %) were dispersed by impregnation on α-Al_2O_3 with an acetone solution. The α-Al_2O_3 support, that shows a surface area of around 0.4 m^2/g, was calcined at 673 K for 4 h before its use. For comparison, a silver catalyst obtained by support impregnation with an aqueous solution of silver nitrate with the same metal content (11 wt. %) was also prepared.

The procedure for catalyst activation, before the characterization and the activity tests, involved heating up to a temperature of 623 K in O_2 flow (heating rate 2 K/min), and then reduced in H_2 flow up to a temperature of 623 K (heating rate 5 K/min) at atmospheric pressure,

UNIVERSITAT ROVIRA I VIRGILI
NANOMATERIALS IN CATALYSIS: STUDY OF MODEL REACTIONS.
Ricardo José Chimentao
ISBN: 978-84-690-7618-7 / DL: T.1326-2007

followed by isothermal reduction at this temperature for 3 h. To investigate the promotion effect by cesium the catalysts were impregnated by an aqueous solution containing appropriate amounts of CsOH. After that the promoted catalyst was activated using the same protocol.

II.1.2.2 Catalyst Characterization

II.1.2.2.1 X-ray diffraction (XRD)

XRD measurements were made using a Siemens D5000 diffractometer (Bragg-Bentano parafocusing geometry and vertical θ-θ goniometer) fitted with a curved graphite diffracted-beam monochromator, incident and diffracted –beam Soller slits, a 0.06º receiving slit and scintillation counter as detector. The angular 2θ diffraction range was between 30^0 and 120^0. The data were collected with an angular step of 0.05º at 3s per step and sample rotation. $Cu_{K\alpha}$ radiation was obtained from copper X-ray tube operated at 40 kV and 30 mA.

II.1.2.2.2 Scanning electron microscopy (SEM)

The morphologies of the catalysts were observed by SEM with a JEOL JSM-35C scanning microscope operated at an acceleration voltage of 15 kV. A small portion of each sample powder was coated on a metallic disk holder and covered with a thin gold layer before the SEM analysis.

II.1.2.2.3 Temperature-programmed reduction (TPR)

TPR experiments were performed in a TPDRO 1100 (Thermo

UNIVERSITAT ROVIRA I VIRGILI
NANOMATERIALS IN CATALYSIS: STUDY OF MODEL REACTIONS.
Ricardo José Chimentao
ISBN: 978-84-690-7618-7 / DL: T.1326-2007

Finnigan), equipped with a thermal conductivity detector (TCD) and coupled to a mass spectrometer QMS 422 Omnistar. The catalysts were treated in O_2 for 1 h at 623 K before TPR analysis. Then, the samples were purged with argon flow before the TPR analysis. The TPR of silver catalysts was carried out using 5% H_2 in Ar flow as reducing agent, the gas flow rate was 20 ml/min and the weight of sample was 1.0 g. The gases evolved during the TPR experiment was monitored by TCD and mass spectrometer detector. The temperature was raised from 323 K up to 1073 K at a rate of β = 20 K/min. Water produced during TPR was trapped in CaO + Na_2O (Soda lime).

II.1.2.2.4 X-ray photoelectron spectroscopy (XPS)

The XPS analyses were acquired in a VG Escalab 200R electron spectrometer equipped with a hemispherical electron analyzer operating in a constant pass energy mode and a non-monochromatic Mg-Kα (hv = 1253.6 eV, 1 eV = 1.603×10^{-19} J). X-ray source operated at 10 mA and 12 kV. Kinetic energies of photoelectrons were measured using a hemispherical electron analyzer working in the constant pass energy mode. The background pressure in the analysis chamber was kept below 7 x 10^{-9} mbar during data acquisition. The powder samples were pressed into copper holders and then mounted on a support rod placed in the pretreatment chamber. All the spectra were signal-averaged for at least 80 scans and were taken in increments of 0.1 eV with dwell times of 50 ms. The sample cleaning was performed by cycles of Ar^+ etching (1.5 keV, 5 min), oxygen treatments at 573 K with subsequent annealing in vacuum. After three cycles of cleaning carbon contamination was very low and the remaining C 1s signal was used to calibrate the binding

UNIVERSITAT ROVIRA I VIRGILI
NANOMATERIALS IN CATALYSIS: STUDY OF MODEL REACTIONS.
Ricardo José Chimentao
ISBN: 978-84-690-7618-7 / DL: T.1326-2007

energies (BE C1s = 284.9 eV). High resolution spectral envelopes were obtained by curve fitting synthetic peak components using the software XPS Peak. Symmetric Gaussian-Lorentzian product functions were used to approximate the line shapes of the fitting components.

II.1.2.2.5 Catalytic activity

The catalytic epoxidation of styrene was performed in a stainless steel tubular down flow reactor. The size of the fix-bed reactor was Ø10 mm x 20 cm long provided with a temperature control system. Reaction temperature was measured in the middle of the catalyst bed by means of a K-type thermocouple. The reactor was filled with the catalyst (1.0 g), which had been previously ground and sieved in the range of 75-100 mesh. The reactor was placed in an electric furnace with a temperature control system. A pressure indicator was used to measure the pressure drop in the catalyst bed. Catalytic activity was measured at steady state conditions (after 5 hours of time on stream). The feedstock gas, consisted of a mixture of O_2-Ar, was fed to the reactor by independent mass flow controllers, using a total flow rate between 100-300 ml/min. The styrene was introduced into the reactor by a high-pressure metering pump, which worked in a flow-rate range of 0.1-1.0 ml/h. The reaction temperatures were in the range of 503-623 K working at atmospheric pressure. The effluent gas was rapidly cooled and analyzed off-line using a Shimadzu GC 2010 gas-chromatograph equipped with an Ultra 2 capillary column and flame ionization detector (FID). The presence of combustion products was determined by on-line TCD and mass spectrometer.

UNIVERSITAT ROVIRA I VIRGILI
NANOMATERIALS IN CATALYSIS: STUDY OF MODEL REACTIONS.
Ricardo José Chimentao
ISBN: 978-84-690-7618-7 / DL: T.1326-2007

II.1.3 Results and Discussion

Figure II.1.1 shows the morphologies of the silver nanoparticles catalysts observed by SEM with a JEOL JSM-35C scanning microscope operated at acceleration voltage of 15 kV. The morphologies obtained for the silver nanoparticles prepared by the polyol process were found to be strongly dependent on the experimental conditions such as temperature and the molar ratio between PVP and $AgNO_3$. Previous studies have suggested that the degree of polymerization of PVP (the average number of repeating units in one PVP molecule) was also found to play an important role in determining the morphology of the silver nanoparticles [9].

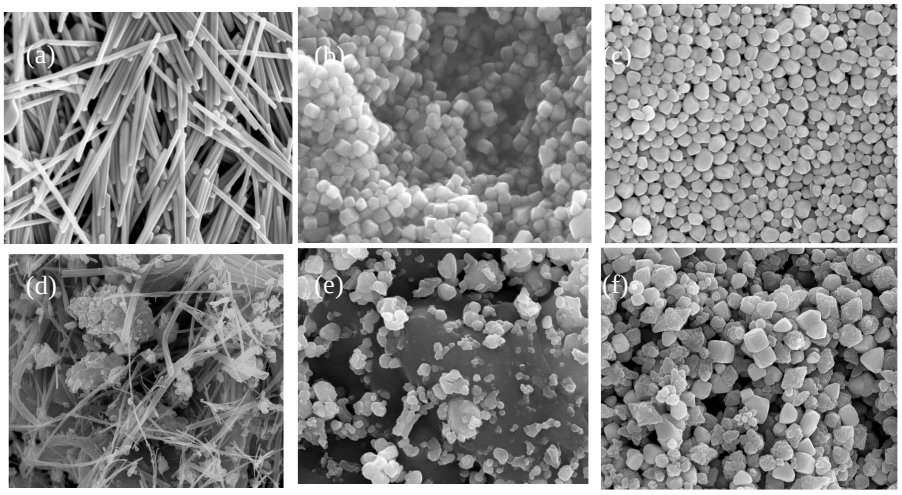

Figure II.1.1 SEM images of the different silver nanoparticles catalysts. (a-c) Silver nanowires, nanocubes and nanopolyhedra supported on α-Al_2O_3, respectively (11%$Ag^{(NW)}$/α-Al_2O_3; 11%$Ag^{(NW)}$/ α-Al_2O_3 and 11%$Ag^{(NW)}$/ α-Al_2O_3). (d) 40%Ag/MgO, (e) 15%Ag/α-Al_2O_3 and (f) Silver nanocubes supported on $CaCO_3$ (11%$Ag^{(NC)}$/$CaCO_3$). (── :

UNIVERSITAT ROVIRA I VIRGILI
NANOMATERIALS IN CATALYSIS: STUDY OF MODEL REACTIONS.
Ricardo José Chimentao
ISBN: 978-84-690-7618-7 / DL: T.1326-2007

Scale bar of 500 nm for all the samples)

We have obtained silver nanowires (Figure II.1.1a) when the molar ratio of PVP and $AgNO_3$ was 1.5. These nanowires had a mean diameter of 150 nm. No silver nanowires were formed at temperature lower than 413 K. When the molar ratio was increased from 1.5 to 3 nanocubes became the major product (Figure II.1.1b). Silver nanopolyhedra (Figure II.1.1c) were also obtained when the silver nanocubes were maintained for longer period of time in the reaction mixture. SEM image of the 40% Ag/MgO catalyst (Figure II.1.1d) prepared by impregnation shows the presence of silver nanowires and other silver particles dominated by irregular shapes with diameters between 100 nm and 500 nm. Irregular shape particles with diameter between 200- 1000 nm (Figure II.1.1e) were also observed for the 15% $Ag/\alpha\text{-}Al_2O_3$ catalyst prepared by wetness impregnation using a silver nitrate solution. Figure II.1.1f shows the image of the silver nanocubes catalyst support on $CaCO_3$. As already presented in section I.4 the X-ray diffraction of these silver nanoparticles synthesised using the polyol process suggested that silver existed purely in the face centered cubic structure. The X-ray powder diffraction (XRD) patterns were recorded using a Siemens D5000 diffractometer using nickel filtered Cu Kα radiation (λ = 1.54056 Å) in 2θ ranging from 300 to 800. The diffraction did not suggest the presence of possible impurities such as Ag_2O and $AgNO_3$. The three peaks detected for the silver nanoparticles were assigned to diffraction from the (111), (200) and (220) planes of fcc silver, respectively. The lattices constants calculated by XRD for the nanowires and nanopolygons were 4.0839 and 4.0872 Å respectively, which are very closed to the report data (a = 4.0862 Å, Joint Comittee on Powder Diffraction Standards file 04-0783). The

UNIVERSITAT ROVIRA I VIRGILI
NANOMATERIALS IN CATALYSIS: STUDY OF MODEL REACTIONS.
Ricardo José Chimentao
ISBN: 978-84-690-7618-7 / DL: T.1326-2007

ratio of intensity between (111) and (200) peaks exhibits value of 4.5 and 2.5 for nanowires and nanopolygons respectively. For the nanowires this ratio is higher than standard file (JCPDS) (4.5 versus 2.5) indicating that the nanowires were abundant in (111) facets probably due to its external morphology. Nanowires and nanopolygons tend to grow as bicrystals twinned along the (111) planes, showing (111) crystal faces at their surface [10]. The UV-Vis spectrum of the nanowires solution showed a broad peak at ca. 380 nm that could arise from surface plasmon excitation of the silver nanostructures similar to previously reported [11].

TPR profiles, after treatment in O_2 for 1 h at 623 K, of the 11% of silver nanowire supported on α-Al_2O_3 and 15% Ag/α-Al_2O_3 (prepared by wetness impregnation) catalysts are in Figure II.1.2 a,b respectively.

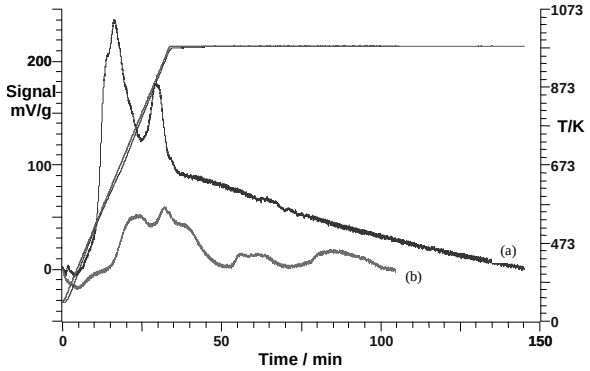

Figure II.1.2 TPR profiles obtained from fresh catalysts (a) 11% silver nanowires supported on α-Al_2O_3, (b) 15%Ag/α-Al_2O_3.

The Figure II.1.2 revealed two broad peaks for nanowires catalyst at around 633 K (most intense peak) and at around 873 K. The 40% Ag/MgO and nanopolygons catalysts show similar behaviour. These peaks have been attributed to different oxygen species (O_β, O_γ) [12].

UNIVERSITAT ROVIRA I VIRGILI
NANOMATERIALS IN CATALYSIS: STUDY OF MODEL REACTIONS.
Ricardo José Chimentao
ISBN: 978-84-690-7618-7 / DL: T.1326-2007

However for 15%Ag/α-Al_2O_3 catalyst these peaks are shifted to higher temperatures (753 and 933K, respectively), with the most intense peak for this catalyst is the second one. Besides, the intensity of these peaks are lower than the obtained from nanowires.

The selective oxidation of styrene (Table II.1.1) over Ag catalysts shows phenylacetaldehyde (Phe) and styrene oxide (SO) as main products. A blank test run with the α-Al_2O_3, MgO and $CaCO_3$ support showed no conversion of styrene at the reaction temperature (523 K). The direct combustion route of styrene was negligible for silver nanowires nanocubes and nanopolyhedra even at near total conversion condition. This fact was not observed for 15%Ag/α-Al_2O_3 catalyst which shows combustion products even at lower conversion (around 5%). The pure silver nanowires catalyst (11% $Ag^{(NW)}$/α-Al_2O_3) showed a styrene conversion of 57.6% and a selectivity to styrene oxide of 42.5%. Silver nanopolyhedra and nanocubes supported on α-Al_2O_3 showed similar catalytic performance compared to the silver nanowires. The basic properties of the catalyst, addition of $CaCO_3$ as support, improved the catalytic activity. When $CaCO_3$ was used as support for the silver nanocubes the styrene conversion increased from 42.5 to 93.1% and the selectivity toward phenylacetaldehyde increased (74.4%). It was also observed production of substancial quantities of phenylacetaldehyde when styrene oxide was heated under the reaction temperature studied. It is highly possible that the phenylacetaldehyde obtained in the reaction is formed from the thermolisis of the styrene oxide [13]. Comparing the reaction activity and selectivity with the result of TPR profiles we could suggest that the first peak is the responsible for the different performance and it is prbably related with oxygen species that preferentially lead to high activity and selectivity.

UNIVERSITAT ROVIRA I VIRGILI
NANOMATERIALS IN CATALYSIS: STUDY OF MODEL REACTIONS.
Ricardo José Chimentao
ISBN: 978-84-690-7618-7 / DL: T.1326-2007

Table II.1.1 Results of the catalytic activity tests for the silver nanoparticles in the epoxidation of styrene at 573 K

Catalyst[a]	Catalytic Activity		
	X(%)[b]	Phe(%)[c]	SO(%)[d]
15%Ag/α-Al_2O_3	4.9	53.2	15.6
11%$Ag^{(NW)}$/α-Al_2O_3	57.6	57.5	42.5
11%$Ag^{(NC)}$/α-Al_2O_3	56.9	68.6	31.4
11%$Ag^{(NP)}$/α-Al_2O_3	57.5	69.2	30.8
11%$Ag^{(NW)}$/$CaCO_3$	93.1	74.4	24.6
40%$Ag^{(NW)}$/MgO	77.1	82.9	17.1

[a] NW: silver nanowires, NC: silver nanocubes, NP: silver nanopolyhedra. [b] conversion (X) of styrene,
[c] selectivity to phenylacetaldehyde (Phe%), [d] selectivity to styrene oxide (SO%). O_2: C_8H_8 molar ratio of 50.

II.1.4 Conclusion

In summary, we report the synthesis of Ag nanoparticles using of poly(vinyl pyrrolidone) (PVP) as template. Three silver nanoparticles were obtained: silver nanowires, nanocubes and nanopolyedra. The top crystal face of these nanoparticles was the (111) and is possible that this face shows beneficial effect in the selective oxidation of styrene. The morphology and the chemical composition of silver catalyst were determinant in the activity and selectivity for the styrene oxidation reaction. These differences can be explained taking into account the presence of different oxygen species in the silver catalyst confirmed by TPR. It was found that the catalytic performance of the Ag nanoparticles for the selective oxidation of styrene can be improved increasing the basic character of the catalysts. Synthesis of silver nanoparticles with shape controller shows potential applications for selective oxidation of olefins.

ISBN: 978-84-690-7618-7 / DL: T.1326-2007

II.1.5 References

[1] F. W. Zemicael, A. Palermo, M.S. Tikhov, R. M. Lambert, *Catal. Lett.* 2002, **80**, 93

[2] L. N. Lewis, *Chem. Rev.* 1993, **93**, 2693

[3] Y Sun, B Gates , B. Mayers , Y. Xia, *Nano Lett*. 2002, **2**, 165.

[4] Y. Sun and Y. Xia, *Science* 2002, **298**, 2176.

[5] F. Fivet, J. P. Lagier, M. Figlarz, *Mater. Res. Soc. Bull*. 1989, **14**, 29.

[6] A. T. Bell , *Science* 2003, **299**, 1688

[7] M. Haruta, *J. Nanoparticle Res.* 2003, 5, 3-4.

[8] Z. M Hu, H. Nakai, H. Nakatsuji, *Surf. Sci*. 1998, **401**, 371.

[9] Y. Sun and Y. Xia, *Adv. Mater*. 2002, **14**, 833

[10] B. D. Cullity, S. R. Stock, *Elements of X-Ray Diffraction* (Prentice-Hall, Upper Saddle River, N. J, ed. 3, 2001), pp. 402-404.

[11] X. C. Jiang, Y. Xie, J. Lu, L. Y., Zhu, W. He, Y. T. Qian, *J. Mater. Chem.* 2001, **11**, 1775

[12] A. J. Nagy, G. Mestl, *Appl. Cat.* 1999, **188**, 337

[13] J. M. Watson, *US Patent* 1975, 3,860,614

UNIVERSITAT ROVIRA I VIRGILI
NANOMATERIALS IN CATALYSIS: STUDY OF MODEL REACTIONS.
Ricardo José Chimentao
ISBN: 978-84-690-7618-7 / DL: T.1326-2007

Chapter II.2

Styrene epoxidation over Cs promoted silver nanowires catalysts

UNIVERSITAT ROVIRA I VIRGILI
NANOMATERIALS IN CATALYSIS: STUDY OF MODEL REACTIONS.
Ricardo José Chimentao
ISBN: 978-84-690-7618-7 / DL: T.1326-2007

II.2.1 Silver nanowires catalysts characterization

X-ray diffraction (XRD) pattern of the nanowires synthesized by the polyol process suggested that silver existed purely in the face-centered cubic (fcc) structure (Figure II.2.1 A(a)). The diffraction pattern of the silver nanowires did not suggest the presence of possible impurities such as Ag_2O and $AgNO_3$. The peaks detected for the silver nanoparticles were assigned to diffraction from the (111), (200) and (220) planes. The lattice constant calculated by XRD for the silver nanowires was 4.0839 Å, which is very close to the report data (a = 4.0862 Å, Joint Committee on Powder Diffraction Standards file 04-0783). The ratio of intensity between (111) and (200) diffraction lines for silver nanowires was higher than for the file JCPDS (4.5 versus 2.5) for the standard silver (Figure II.2.1A, B) indicating that the nanowires show preferred orientation in (111) facets. This fact indicates that silver nanowires tend to grow as bicrystals twinned along the (111) planes, showing (111) crystal faces at their surface [20]. Twinning is the mechanism for forming these particles and it is the result of two subgrains sharing a common crystallographic plane [21]. Figure II.1.2.1B shows the XRD patterns of the $11\%Ag^{(0.25\%Cs-\ NW)}/\alpha\text{-}Al_2O_3$ fresh and after 30 days of reaction catalysts. XRD only revealed the presence of metallic Ag not detecting the presence of silver oxide peaks. Besides, the presence of Cs was not detected probably due to the low amount. It is important to mention that the XRD pattern for both catalysts is quite similar. This indicates that after a period of reaction of 30 days the particle size and the morphological structure of the catalyst were preserved.

Figure II.2.2a shows the SEM image of the silver catalyst obtained by

UNIVERSITAT ROVIRA I VIRGILI
NANOMATERIALS IN CATALYSIS: STUDY OF MODEL REACTIONS.
Ricardo José Chimentao
ISBN: 978-84-690-7618-7 / DL: T.1326-2007

impregnation with an aqueous solution of silver nitrate. SEM image shows the presence of irregular Ag particles distributed on the α-Al_2O_3 support. However, the SEM image observed in Figure II.2.2b shows a well dispersion of silver nanowires on the support. The diameters of these nanowires were reasonable uniform, with an average value of 150 nm. Together with the silver nanowires (but in low amount) the presence of nanocubes and nanopolyhedra were also observed. The cross section of the Ag nanowires (Inset Figure II.2.2b) clearly presents a pentagonal shape according to previous studies [22].

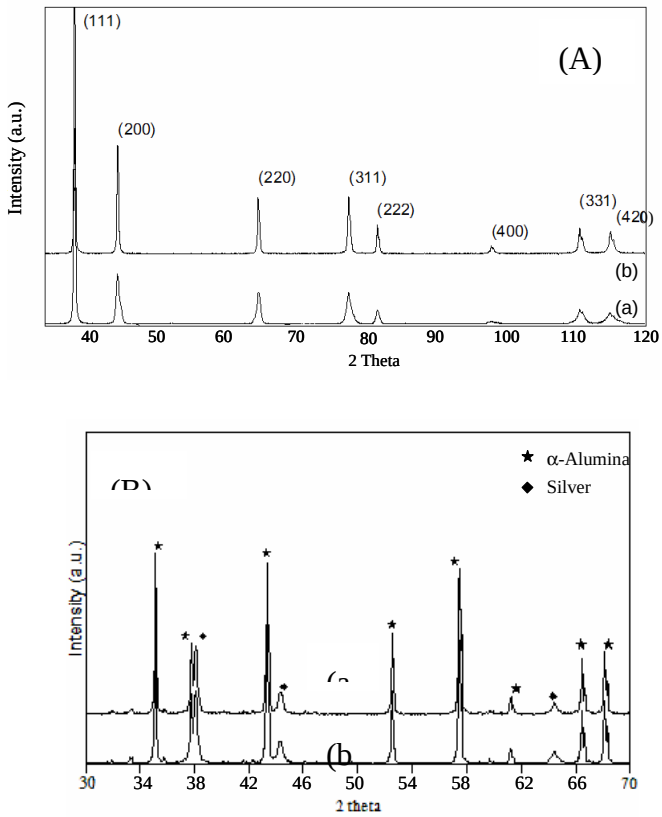

Figure II.2.1 (A) XRD of the silver nanowires (a) and standard silver sample (b). (B) Pattern obtained for the 11%$Ag^{(NW\text{-}0.25\%Cs)}$/$\alpha$-$Al_2O_3$ catalyst (a) fresh, (b) after 30 days on stream.

UNIVERSITAT ROVIRA I VIRGILI
NANOMATERIALS IN CATALYSIS: STUDY OF MODEL REACTIONS.
Ricardo José Chimentao
ISBN: 978-84-690-7618-7 / DL: T.1326-2007

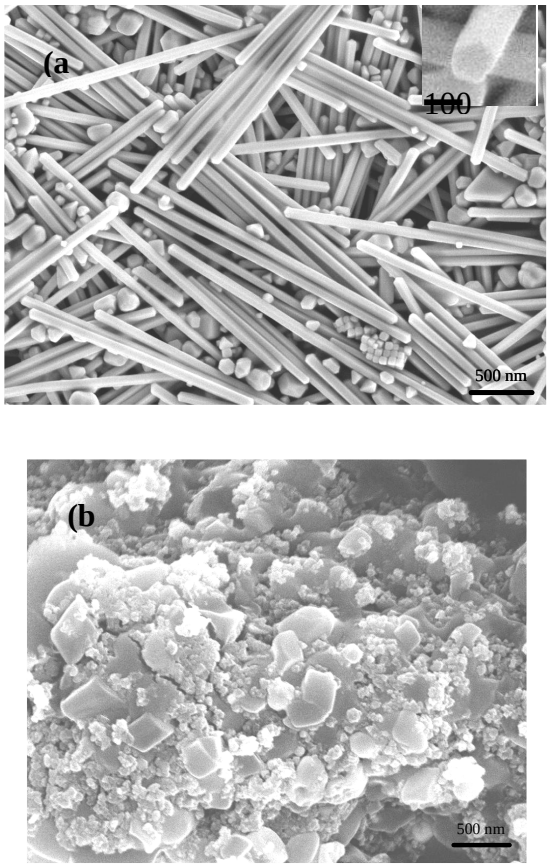

Figure II.2.2 (a) SEM image of silver silver nanowires catalyst and (b) impregnated catalyst

TPR analysis was used to characterize the oxygen species formed by exposure of silver catalyst under O_2 flow. Prior to the TPR experiments, catalyst samples were treated in oxygen at 623 K. Figure II.2.3 (1-5) shows the TPR profiles of the silver nanowires with different loading of cesium. The unpromoted silver nanowires catalyst (11% $Ag^{(NW)}/\alpha$-Al_2O_3) and the silver impregnated catalyst (11% Ag/α-Al_2O_3) are also shown in the inset of Figure II.2.3.The peaks observed in TPR can be assigned based on the temperature at which they appear. Previous studies have shown that the peak around 600 K is attributed to

UNIVERSITAT ROVIRA I VIRGILI
NANOMATERIALS IN CATALYSIS: STUDY OF MODEL REACTIONS.
Ricardo José Chimentao
ISBN: 978-84-690-7618-7 / DL: T.1326-2007

the presence of subsurface oxygen (O_β) [24-30]. Furthermore, the presence of reduction peaks at higher temperatures can be attributed to the presence of oxygen species that are strongly chemisorbed on the surface of silver and are labeled as (O_γ) [27, 31-33].

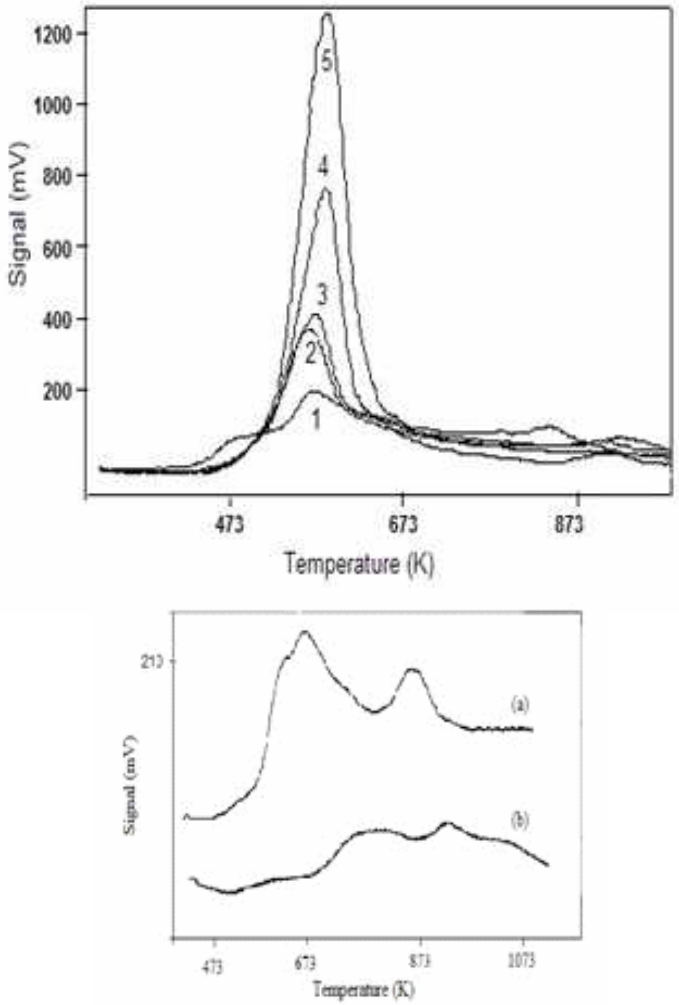

Figure II.2.3 Temperature programmed reduction profiles of silver catalysts with different loading of cesium (referred to the silver content); (1) 0.0625%, (2) 0.125%, (3) 0.25%, (4) 0.5%, (5) 1.0%. Inset: (a) unpromoted silver nanowires, (b) silver impregnated catalyst.

UNIVERSITAT ROVIRA I VIRGILI
NANOMATERIALS IN CATALYSIS: STUDY OF MODEL REACTIONS.
Ricardo José Chimentao
ISBN: 978-84-690-7618-7 / DL: T.1326-2007

TPR results show that the impregnated catalyst has the lowest intense reduction peaks when compare with silver nanowires ones. Besides, the reduction peaks appear at higher temperatures (753 K and 933 K) (see the inset b of Figure II.2.3). The most intense peak for this catalyst is the second one. However, more intense reduction peaks are observed for silver nanowires catalyst. The unpromoted silver nanowires catalyst (inset a of Figure Figure II.2.3) shows two broad peaks at around 623 K (the most intense peak) and 873 K. So, the main oxygen species for this catalyst is the O_β. When silver nanowires were promoted by Cs a strong increase in the signal of the first peak of TPR was observed. It is noteworthy to observe that T_{max} value first decreased when the pure silver nanowires were promoted with 0.0625 wt.% of cesium content and then shifted toward higher values when the cesium content continues increasing. However, the reduction peaks (T_{max}) for cesium promoted catalysts are always shifted to lower temperatures in comparison with unpromoted silver ones. Table II.2.1 shows the temperature of peak maxima and the hydrogen consumption of this first peak at different cesium amount. The signal increased with cesium loading. Furthermore, for Cs promoted catalysts a broad peak at higher reduction temperature (between 700 and 950 K) with very low intensity was also observed. This indicates the presence of O_γ on the surface of the silver particles even at these higher reduction temperatures.

The analysis of the near surface of the silver nanowires was performed by XPS technique. The study of the electronic state by XPS was carried out on non supported silver nanowires in order to avoid the overshadowed of the oxygen component arising from the α-Al_2O_3 support. However the presence of oxygen component arising from the promoter (cesium oxide) is expected. The XPS profiles of the

UNIVERSITAT ROVIRA I VIRGILI
NANOMATERIALS IN CATALYSIS: STUDY OF MODEL REACTIONS.
Ricardo José Chimentao
ISBN: 978-84-690-7618-7 / DL: T.1326-2007

unpromoted and cesium promoted silver nanowires are depicted in Figure II.2.4A and II.2.4B respectively. Table II.2.1 shows the binding energies values for unpromoted silver nanowires and 0.25 wt. % cesium promoted silver nanowires samples oxidized at 623 K and reduced in situ in the XPS equipment between 573 and 773 K. Figure II.2.4A shows the XPS spectra of the oxidized silver nanowires (a) and then reduced at 573, 673 and 773 K (b, c and d, respectively). The XPS profile of the unpromoted silver nanowires (Figure II.2.4A) showed only one peak for the binding energy of Ag $3d_{5/2}$ centered between 367.5 and 367.7 eV as is shown in Table II.2.1 that can be ascribed to Ag_2O [34]. This is also confirmed by the value of O/Ag of around 0.48 obtained by XPS for the unpromoted oxidized sample. Besides, the binding energy values are around of 367.5 eV for samples reduced at 773 K. This indicates that under reduction conditions, in the XPS equipment, the first atomic layers of the surface of silver nanowires (that have the main contribution to the XPS signal) are in oxidized state. This fact indicates the presence of oxygen species with a strong interaction with the silver surface (O_γ), which are difficult to reduce even at 773 K, in agreement with TPR results. From Table II.2.1, the O1s peak signal observed for the unpromoted silver nanowires was around 529.7 eV for both reduced and oxidized samples. However, when cesium was added (Figure II.2.4B), the O 1s peak showed two components, the major one at around 531.5 eV and a less intense one at around 529.8 eV. These O-species have been ascribed to O_β and O_γ species respectively [25, 31]. The distinction between different types of oxygen detected by XPS was recognized on the basis of the way in which of the oxygen specie was embedded into the surface lattice of the silver nanowires.

UNIVERSITAT ROVIRA I VIRGILI
NANOMATERIALS IN CATALYSIS: STUDY OF MODEL REACTIONS.
Ricardo José Chimentao
ISBN: 978-84-690-7618-7 / DL: T.1326-2007

From the XPS spectra of the unpromoted silver nanowires the O_γ was the unique specie detected on the surface of the nanowires. When 0.25 wt. % of cesium was introduced on the silver nanowires the O_β was the major oxygen species detected by XPS as shown in Table II.2.1. It seems that the addition of Cs promotes the formation of the O_β species. Figure II.2.4B also shows the XPS spectra of the oxidized sample (a) and reduced at 573, 673 and 773 K (b, c and d, respectively). The deconvoluted peak of the O1s component with a binding energy value of around 531.5 eV represents around 90% for the cesium promoted silver nanowires oxidized at 623 K. Further information about the nature of oxygen species on the cesium promoted silver nanowires surface was obtained by monitoring the reduction of the nanowires under hydrogen during XPS analysis.

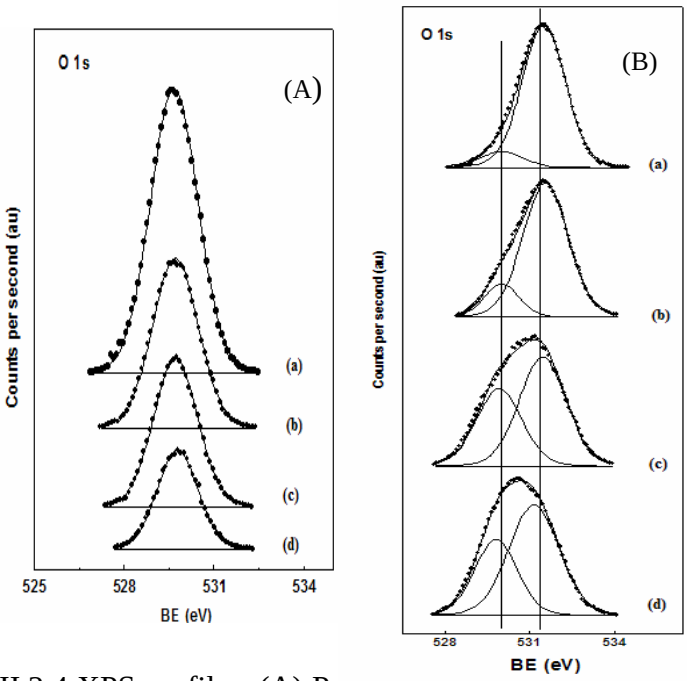

Figure II.2.4 XPS profiles. (A) Pure silver nanowires and (B) promoted Ag nanowire by 0.25% of Cs after oxidation at 623 K (a), and then reduced at different temperatures (b-d)573, 673 and 773 K respectively.

UNIVERSITAT ROVIRA I VIRGILI
NANOMATERIALS IN CATALYSIS: STUDY OF MODEL REACTIONS.
Ricardo José Chimentao
ISBN: 978-84-690-7618-7 / DL: T.1326-2007

From Figure II.2.4B, the O 1s component at around 531.5 eV of the Cs promoted silver nanowires sample decreases its relative intensity from 90 to 60 % as the reduction temperature increases. In parallel, The O 1s component at around 529.8 eV increases its relative intensity from 10 to 40%. The increase in the relative signal of this O1s component can be attributed to the decrease in the signal of the peak around 531.5 eV due to the reduction process, as well as the formation of new O_γ species probably by interstitial diffusion of the subsurface oxygen (O_β) to the catalyst surface [31]. The presence of the peak around 531.5 eV at higher reduction temperature (773 K) could be also attributed to the contribution of the oxygen of cesium oxide species [35], which is overlapping the peak of the O_β species.

Table II.2.1 Binding energies (eV) and surface atomic ratios of silver nanowires

Treatment	Binding Energy, eV Ag nanowires		Binding Energy, eV 0.25% Cs promoted Ag nanowires		
	$Ag3d_{5/2}$	O1s	$Ag3d_{5/2}$	O1s	$Cs3d_{5/2}$
Oxidation at 623 K	367.6	529.7	367.7	529.9 (10) 531.5 (90)	724.0
Reduction at 573 K	367.7	529.7	367.7	529.9 (16) 531.6 (84)	723.9
Reduction at 673 K	367.6	529.7	367.4	529.8 (39) 531.4 (61)	723.9
Reduction at 773 K	367.5	529.8	367.5	529.8 (40) 531.2 (60)	724.1

UNIVERSITAT ROVIRA I VIRGILI
NANOMATERIALS IN CATALYSIS: STUDY OF MODEL REACTIONS.
Ricardo José Chimentao
ISBN: 978-84-690-7618-7 / DL: T.1326-2007

II.2.2 Catalytic Activity

The selective oxidation of styrene, at steady state, over silver catalysts shows phenylacetaldehyde (Phe) and styrene oxide (SO) as the main products. Table II.2.2 shows the catalytic performance of the silver catalysts for the epoxidation of styrene with molecular oxygen as oxidant at a reaction temperature of 523 K. A blank test run with the α-Al_2O_3 support showed no conversion of styrene at the reaction temperatures studied. Silver impregnated catalyst showed a styrene conversion of 1.0 % at 523 K. However, a conversion of 10 % and selectivity to styrene oxide of 42.5 % was observed at the same reaction conditions for silver nanowires catalyst. It is important to mention that the deactivation of the catalyst during an operation time of 30 days was negligible.

Table II.2.2 Results of TPR and catalytic activity at 523 K

Catalyst	TPR analysis		Catalytic Activity Tests		
	T_{max} (K)	H_2 consumption (μmol/g)[a]	X(%)[b]	Phe(%)[c]	SO(%)[d]
	753	0.5	1.0	51.4	48.6
$11\%Ag^{(NW)}/\alpha\text{-}Al_2O_3$	623	1.3	10.0	57.5	42.5
$11\%Ag^{(NW\text{-}0.0625\%Cs)}/\alpha\text{-}Al_2O_3$	568	2.6	50.9	48.6	51.4
$11\%Ag^{(NW\text{-}0.125\%Cs)}/\alpha\text{-}Al_2O_3$	570	2.7	60.1	46.8	53.2
$11\%Ag^{(NW\text{-}0.25\%Cs)}/\alpha\text{-}Al_2O_3$	572	2.8	94.6	44.4	55.6
$11\%Ag^{(NW\text{-}0.30\%Cs)}/\alpha\text{-}Al_2O_3$	575	3.8	90.5	26.7	73.3
$11\%Ag^{(NW\text{-}0.5\%Cs)}/\alpha\text{-}Al_2O_3$	583	4.9	72.4	25.1	74.9
$11\%Ag^{(NW\text{-}1.0\%Cs)}/\alpha\text{-}Al_2O_3$	587	8.1	42.3	24.1	75.9

[a] peak signal from the first peak detected by temperature programmed reduction (TPR), [b] conversion (X), [c] selectivity to phenylacetaldehyde (Phe%), [d] selectivity to styrene oxide (SO%), O_2: C_8H_8 molar ratio of 50.

The promotion of silver nanowires catalysts with cesium increased the catalytic activity up to 94.6 % for a cesium loading of 0.25 wt. %. Besides, the selectivity to styrene oxide increased from 42.5 % up to 75.9 % when silver nanowires catalyst was promoted with 1 wt. % of

UNIVERSITAT ROVIRA I VIRGILI
NANOMATERIALS IN CATALYSIS: STUDY OF MODEL REACTIONS.
Ricardo José Chimentao
ISBN: 978-84-690-7618-7 / DL: T.1326-2007

cesium.

In the case of catalytic oxidation reactions it is well accepted that the redox properties of the catalyst play a fundamental role on the activity [7, 36]. Alkali metals are electropositive promoters, which act to enhance the chemisorption of electron acceptor adsorbates and weaken chemisorption of electron donor adsorbates, as they themselves are electron donors. Besides, the incorporation of an alkaline metal may result in a decrease in surface acidity, since acid sites are neutralized [37]. The enhancement in epoxide selectivity observed in the presence of CsOH was probably due to suppression of acid centers in the α-Al_2O_3 support and hence the isomerization route of styrene oxide to phenylacetaldehyde was decreased. Consequently, the addition of cesium increased both the catalytic activity and the selectivity to the epoxide. So, the cesium modified the Ag surface particularly toward the epoxidation direction. Previous experimental studies have show that some alkenes without allylic hydrogen atoms, such as ethylene, can be directly epoxidize with high selectivity with molecular oxygen in the gas phase over Ag catalysts [38]. In line with these studies, the catalytic results observed for our silver nanowires catalysts indicates that these materials are indeed very active for epoxidation since styrene has no allylic hydrogens. Thus it is really expected that the styrene behave as ethylene in epoxidation over the silver catalysts. Moreover previous studies [39] have also shown that this reaction is sensitive to particle size and more selective on large particles. This fact can also reinforce the high catalytic performance on the silver nanowires since these materials are dominated by dense crystal planes.

The silver nanowires catalyst promoted by 0.25 wt. % of Cs showed the highest conversion of 94.6% for the styrene. The fact that both activity

UNIVERSITAT ROVIRA I VIRGILI
NANOMATERIALS IN CATALYSIS: STUDY OF MODEL REACTIONS.
Ricardo José Chimentao
ISBN: 978-84-690-7618-7 / DL: T.1326-2007

and selectivity change with the amount of Cs on Ag catalysts strongly suggests that the promotion effect is electronic in origin [40]. However, the activity increases up to a cesium loading of 0.25 wt. % and beyond this amount the conversion of styrene decreases progressively. The decrease of conversion at higher Cs loadings (Cs > 0.25 wt. %) can be probably attributed to the effect of cesium dispersion. The excess of cesium can block the active surface and thus decrease the catalytic activity. This change in the catalytic activity is also intimately correlated with results obtained by XPS depicted in Table II.2.3. On the basis of the XPS results in Table II.2.3 the sample with a cesium loading of 0.125 wt. % shows a Cs/Ag atomic ratio of 0.119. When the cesium increased up to 0.25 wt. % the Cs/Ag ratio increased up to 0.24. This proportion between Cs/Ag ratio and the amount of Cs in the sample indicates that cesium is well dispersed on the surface of silver nanowires. However for samples with higher cesium content the Cs/Ag atomic ratios decreased. For instance, the $11\%Ag^{(NW\text{-}0.5\%Cs)}/\alpha\text{-}Al_2O_3$ sample, which has two times of cesium amount than for $11\%Ag^{(NW\text{-}0.25\%Cs)}/\alpha\text{-}Al_2O_3$, the Cs/Ag molar ratio detected by XPS analysis is lower (0.119). Similar behaviour is observed for the catalysts with a cesium amount of 1.0 wt% that shows a Cs/Ag ratio quite similar than for the catalyst with a cesium amount of 0.125 wt.%. This indicates that agglomeration of cesium species on the silver surface is produced at higher cesium loading that covers the silver surface producing the poisoning of the active sites. Thus, the increase in the cesium content may cover progressively the silver surface decreasing the active sites. Furthermore, correlating the epoxidation performance with the XPS results, it was also found that there is a direct relationship between the epoxidation performance of catalyst and O1s signal associated with O_β

UNIVERSITAT ROVIRA I VIRGILI
NANOMATERIALS IN CATALYSIS: STUDY OF MODEL REACTIONS.
Ricardo José Chimentao
ISBN: 978-84-690-7618-7 / DL: T.1326-2007

specie. The O_β species seems to be critical for the activation of the silver for this reaction.

Table II.2.3 ICP-AES and XPS surface analysis of silver nanowires catalyst.

Catalyst	ICP-AES analysis (Atomic ratio)		XPS analysis (Atomic ratio)	
	Cs/Al	Cs/Ag	Cs/Al	Cs/Ag
$11\%Ag^{(NW\text{-}0.125\%Cs)}/\alpha\text{-}Al_2O_3$	0.00005	0.0009	0.005	0.119
$11\%Ag^{(NW\text{-}0.25\%Cs)}/\alpha\text{-}Al_2O_3$	0.0001	0.0018	0.009	0.240
$11\%Ag^{(NW\text{-}0.5\%Cs)}/\alpha\text{-}Al_2O_3$	0.0002	0.0036	0.020	0.119
$11\%Ag^{(NW\text{-}1.0\%Cs)}/\alpha\text{-}Al_2O_3$	0.0004	0.0072	0.023	0.220

This can also explain both the low activity and selectivity observed for the 11% $Ag/\alpha\text{-}Al_2O_3$ impregnated catalyst since the main oxygen species detected is O_γ that is more strongly bound and harder to react. There is a strong correlation between the peak signal of the O_β specie with the catalytic activity toward the epoxidation of the styrene. This specie seems to be responsible for the high activity and selectivity while the strongly adsorbed surface atomic oxygen (O_γ) showed lower activity.

In line with these observations, the shift of peak maxima (T_{max}) in the TPR analysis (Table II.2.2) to lower temperatures for the cesium promoted silver nanowires samples may clearly indicate the formation of more reducible silver species compared with the unpromoted samples. All the cesium promoted samples presented higher catalytic activity compared to the unpromoted silver samples (pure silver nanowires (11% $Ag^{(NW)}/\alpha\text{-}Al_2O_3$) and impregnated sample (11% Ag/α-

ISBN: 978-84-690-7618-7 / DL: T.1326-2007

Al_2O_3)) which could be a consequence of electronic effects of the cesium on the properties of the silver since alkaline metals may act as electron donator [37] increasing the electron density of Ag and hence affecting their reducibility. When the silver nanowires were promoted by 0.25 wt. % of cesium the conversion of styrene and the selectivity to styrene oxide increased.

However, with higher cesium content (Cs > 0.25 wt. %) the styrene conversion decreased. This fact is also reinforced by the XPS results depicted in Table II.2.3. At higher Cs content (> 0.25 wt.%) the active silver surface are been probably disengaged from the catalytic cycle by Cs, however those still active do not suffer from any modification by cesium and this maybe the reason that the selectivity remains unaffected.

In fact since repetitive redox cycles occur during the selective oxidation of styrene it also can be suggested that the low catalytic activity observed for the unpromoted silver samples may be due to the fact that the oxidation-reduction cycle is more difficult than for the cesium promoted silver nanowires samples. So, cesium promotion may play an important role increasing the catalytic activity as well as preventing the isomerization route to phenylacetaldehyde.

Table II.2.4 lists the conversion and selectivity to styrene oxide on $11\%Ag^{(NW\text{-}0.25\%Cs)}/\alpha\text{-}Al_2O_3$ catalyst at 503 K with different C_8H_8: O_2 molar ratios. The increase in the O_2: C_8H_8 molar ratio improved the conversion and selectivity to styrene oxide.

UNIVERSITAT ROVIRA I VIRGILI
NANOMATERIALS IN CATALYSIS: STUDY OF MODEL REACTIONS.
Ricardo José Chimentao
ISBN: 978-84-690-7618-7 / DL: T.1326-2007

Table II.2.4 Conversion and selectivity at different O_2:C_8H_8 molar ratios for styrene epoxidation reaction on 11%$Ag^{(NW\text{-}0.25\%Cs)}$/$\alpha$-$Al_2O_3$ catalyst[a]

Molar ratio O_2:C_8H_8	Conversion (%)	Selectivity to SO (%)
25	59.3	55.3
50	76.5	68.4
100	79.7	70.5
150	84.2	73.5

[a] Reaction temperature: 503 K

When the O_2: C_8H_8 molar ratio was 25, the conversion was 59.3% and the selectivity reaches 55.3%, while for O_2: C_8H_8 molar ratio of 150 the conversion was 84.2% and the selectivity to styrene oxide was 73.5%. These results are in agreement with previous results [38]. It seems that an oxygen rich atmosphere is also beneficial for both activity and selectivity in the epoxidation reaction of styrene. This fact indicates a strong competition between styrene and oxygen on the active sites of the catalyst.

Figure II.2.5 shows the catalytic behaviour of cesium promoted silver nanowires catalysts at different reaction temperatures, such as 503, 513 and 523 K. The results show that the amount of cesium in the catalyst plays an important role in the conversion in the range of the temperatures studied. Catalyst containing 0.25 wt. % of cesium showed the highest activity in all the range of temperatures reaction tested the styrene conversion over silver nanowires catalysts changes with the cesium loading. Higher reaction temperature improves the catalytic activity but reduces the selectivity to SO. At 503 K, the selectivity to SO was 68.4% and the styrene conversion was 76.5%. At

UNIVERSITAT ROVIRA I VIRGILI
NANOMATERIALS IN CATALYSIS: STUDY OF MODEL REACTIONS.
Ricardo José Chimentao
ISBN: 978-84-690-7618-7 / DL: T.1326-2007

523 K the selectivity to SO decreased to 55.6% while the conversion of styrene increased to 94.6%.

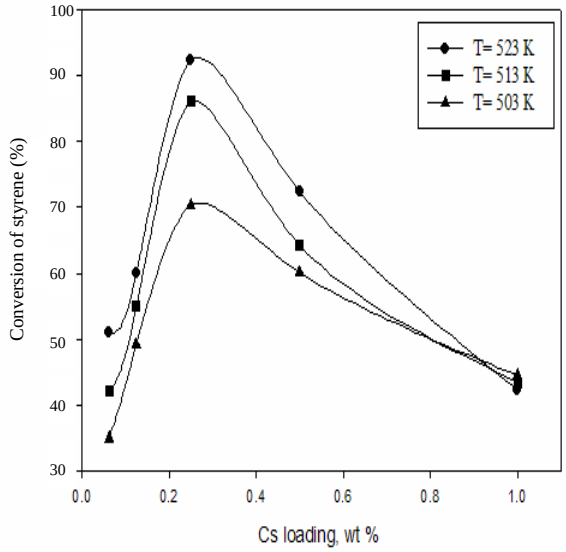

Figure II.2.5 Catalytic Activity of cesium promoted silver nanowires at different reaction temperatures.

In order to study the stability of the catalysts, a reaction test during a period of 30 days was performed using the silver nanowires catalyst containing 0.25 wt% of cesium. The activity and selectivity at different reaction temperatures (503, 513, 523 K), and an O_2: C_8H_8 molar ratio of 100, are shown in Figure II.2.6 as a function of time on stream. As the reactor temperature was increased the selectivity to the epoxide decreased. A styrene conversion of around 79 % and selectivity to styrene oxide of around 70% was achieved during the first five days of reaction at 503 K. Then, the reaction was carried out at 513 K on the following five days and the conversion of styrene increased up to 86.2% while the selectivity to SO decreased to 66.6%. After 10 days of reaction the temperature was increase from 513 to 523 K and the

UNIVERSITAT ROVIRA I VIRGILI
NANOMATERIALS IN CATALYSIS: STUDY OF MODEL REACTIONS.
Ricardo José Chimentao
ISBN: 978-84-690-7618-7 / DL: T.1326-2007

conversion of styrene increased up to 94.6% while the selectivity to SO decreased to 55%. This cycle was repeated again obtaining similar catalytic behaviour. This indicates that this catalyst was stable during this reaction test.

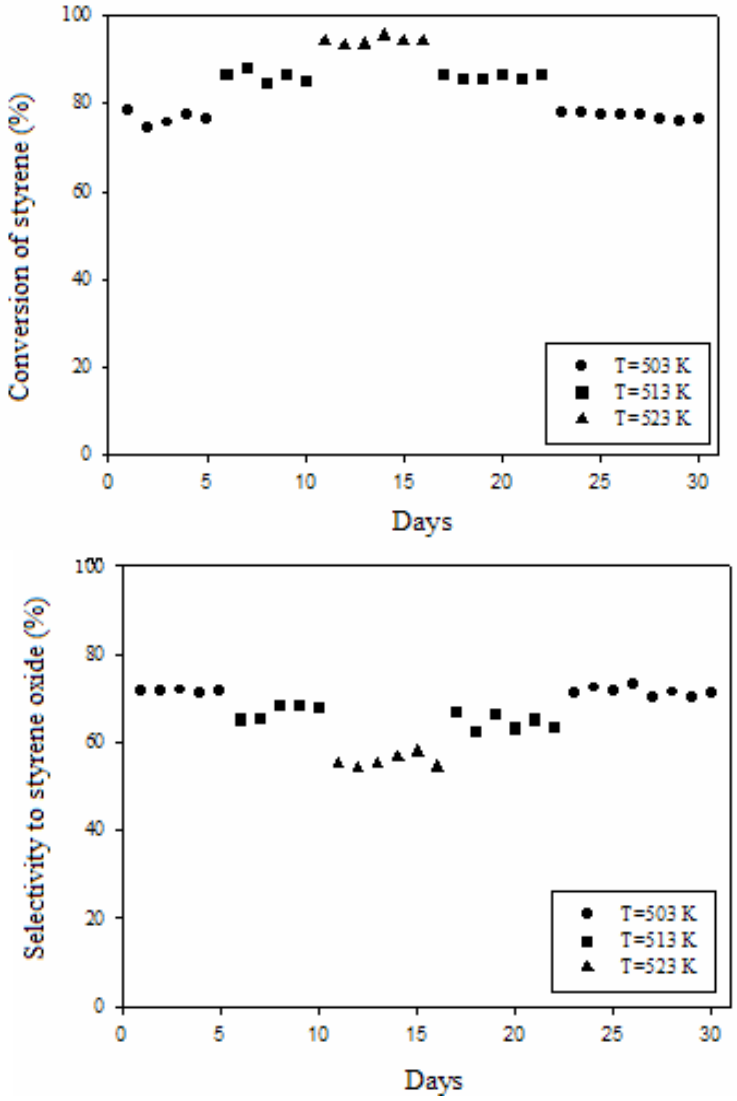

Figure II.2.6 Catalytic activity of 11%$Ag^{(NW-\ 0.25\%Cs)}$/α-Al_2O_3 catalyst in the epoxidation of styrene as a function of time on stream and reaction temperature.

UNIVERSITAT ROVIRA I VIRGILI
NANOMATERIALS IN CATALYSIS: STUDY OF MODEL REACTIONS.
Ricardo José Chimentao
ISBN: 978-84-690-7618-7 / DL: T.1326-2007

II.2.3 Conclusion

Styrene epoxidation by oxygen was carried out on silver nanowires promoted with different contents of cesium. Addition of CsOH significantly improves conversion of styrene and the selectivity to SO. The maximum activity was obtained when the silver nanowires were promoted by 0.25 % of Cs. A higher reaction temperature can improve the activity of the catalyst, but reduces the selectivity to SO. TPR experiments indicated that the cesium affected the reducibility of the silver. Besides, the selectivity to styrene oxide was enhanced by cesium promotion. The selectivity to styrene oxide was also enhanced in oxygen rich atmosphere. Furthermore, correlating the epoxidation performance with the XPS results, can be stated that there is a direct relationship between the epoxidation performance of catalyst and O1s signal associated with O_{β} specie. The O□ species seems to be critical for the activity of the silver catalysts. Besides, negligible deactivation of the silver nanowires catalyst promoted with 0.25% of cesium was observed over 30 days of reaction. These results indicate the feasibility of shape controlled silver nanoparticles as catalysts for styrene epoxidation and how the activity and selectivity of the catalyst can be changed by Cs promotion.

Acknowledgements

This work was supported by the Ministerio de Ciencia y Tecnologia (Spain) under Projects REN2002-04464-CO2-01 and PETRI 95-0801.OP. Thanks are also due to Destilaciones Bordas S.A.

II.2.4 References

[1] A. K. Santra, J. J. Cowell, R. M Lambert, *Catal. Lett.,*. **67**

UNIVERSITAT ROVIRA I VIRGILI
NANOMATERIALS IN CATALYSIS: STUDY OF MODEL REACTIONS.
Ricardo José Chimentao
ISBN: 978-84-690-7618-7 / DL: T.1326-2007

(2000) 87.

[2] T. S. Ahmadi, Z. L. Wang, T. C. Green, A. Henglein, M. A. El-Sayed, *Science*, **272** (1996) 1924.

[3] R. B. Grant, R. M. Lambert, *J. Catal.* **93** (1985) 92.

[4] C. T. Campbell, *J. Phys. Chem.* **89** (1985) 5789.

[5] Lefort, T. E. (to Societe Francaise de Catalyse Generalise), Fr. Pat. 729, 952, March 27, 1931, and subsequent additions.

[6] W.M.H. Sachtler, C. Backx, R. A. Van Santen, *Cat. Rev.- Sci. Eng.* **23**(1&2) (1981) 127.

[7] J. Haber in: G. Ertl, H. Knozinger, J. Weitkamp (Eds.), *Handbook of Heterogeneous Catalysis*, vol. 5, VCH, Weinheim, 1997, p. 2253.

[8] W. S. Epling, G. B. Hoflund, D. M. Minahan, *J. Catal.* **171** (1997) 490.

[9] N. Macleod, J. M. Keel, R. M. Lambert, *Cat. Lett.* **86** (2003) 51.

[10] E. A. Podgornov, I. P. Prosvirin, V. I: Bukhtiyarov, *J. Mol. Catal. A: Chem.* **158** (2000) 337.

[11] J. R. Monnier, J. L. Stavinoha Jr, R. L. Minga, *J. Catal.* **226** (2004) 401.

[12] C. T. Campbell, B. E. Koel, *J. Catal.* **92** (1985) 272.

[13] Cowell, J. J., Santra, A. K., Lindsay R., Lambert, R. M., Baraldi, A., Goldini, A., *Surf. Sci.* **437** (1999) 1.

[14] Carter, E. A., Goddard III, W. A., *Surf. Sci.* **209** (1989) 243.

[15] G. I. N. Waterhouse, G. A. Bowmaker, J. B. Metson, *Appl. Surf. Sci.* **214** (2003) 36.

[16] Bao, X., Muhler, M., Pettinger, B., Schlögl, Ertl, G., *Catal. Lett.* **22** (1993) 215.

UNIVERSITAT ROVIRA I VIRGILI
NANOMATERIALS IN CATALYSIS: STUDY OF MODEL REACTIONS.
Ricardo José Chimentao
ISBN: 978-84-690-7618-7 / DL: T.1326-2007

[17] V. F. Puntes, K. M. Krishnan, A. P. Alivisatos, *Science* **291** (2001) 2117.

[18] Y. Sun and Y. Xia, *Science* **298** (2002) 2176.

[19] F. J. Williams, D. P. C. Bird, E. C. H. Sykes, A. K. Santra, R. M: Lambert, *J. Phys. Chem. B* **107** (2003) 3824.

[20] B. D. Cullity, S. R. Stock, *Elements of X-Ray Diffraction*, (Prentice-Hall, Upper Saddle River, N.J., ed. 3, 2001), pp. 402-404.

[21] Z. L. Wang, *J. Phys. Chem. B.* **104** (2000) 1153.

[22] Y. Gao, P. Jiang, D. F. Liu, H. J. Yuan, X. Q. Yan, Z. P. Zhou, J. X. Wang, L. Song, L. F. Liu, W. Y. Zhou, G. Wang, C. Y. Wang, S. S. Xie, *Chem. Phys. Lett.* **380** (2003) 146.

[22] J. R. Monnier, J. L. Stavinoha Jr, R. L. Minga, *J. Catal.* **226** (2004) 401.

[23] M. R. Salazar, J. D. Kress, A. Redondo, *Surf. Sci.* **469** (2000) 80.

[24] A. J. Nagy, G. Mestl, D. Herein, G. Weinberg, E. Kiltzelmann, R. Schlögl, *J. Catal.* **182** *(* 1999) 417.

[25] A. J. Nagy, G. Mestl, *Appl. Catal.* **188** (1999) 337.

[26] A. J. Nagy, G. Mestl R. Schlögl, *J. Catal.* **188** (1998) 58.

[27] D. Herein, A. Nagy, H. Schubert, G. Weinberg, E. Kitzelmann, R. Schlögl, *Z. Phys. Chem.* **197** (1996) 67.

[28] A. J. Nagy, G. Mestl, D. Herein, G. Weinberg, E. Kiltzelmann, R. Schlögl, *J. Catal.* **182** (1999) 417.

[29] G. A. Somorjai, *Introduction to Surface Chemistry and Catalysis*. Wiley, New York, 1994.

[30] W. X. Li, C. S. Stampfl, M. Scheffler, *Phys. Rev. B* **67***(* 2003) 045408.

UNIVERSITAT ROVIRA I VIRGILI
NANOMATERIALS IN CATALYSIS: STUDY OF MODEL REACTIONS.
Ricardo José Chimentao
ISBN: 978-84-690-7618-7 / DL: T.1326-2007

[31] X. Bao, M. Muhler, T. Scedel-Niedrig, R. Schlögl, *Phys. Rev. B* **54** (1996) 2249.

[32] A. Nagy, G. Mestl, T. Rüle, G. Weinberg, R. Schlögl, *J. Catal.* **179** (1998) 548.

[33] G. I. N. Waterhouse, G. A. Bowmaker, J. B. Metson, *Appl. Catal.* **214** (2003) 36.

[34] XPS International fundamental XPS data tables, www. xpsdata.com.

[35] C. Stegelmann, N. C. Schiodt, C. T. Cambell, P. Stolze, *J. Catal.* **221** (2004) 630.

[36] M. D, Argyle, K. Chen, A. T. Bell, E. Iglesia, *J. Catal.* **208** (2002) 39.

[37] J. P. Dum, H. G. Stanger Jr., I. E. Wachs, Wachs, *Catal. Today.* **301** (1999) 51.

[38] J. C. Wu, P. Harriot, *J. Catal.* **39** (1975) 395.

[39] M. Jarjoui, B. Moravec, P. C. Gravelle, S. J. Teichner, J. Chim. Phys. 75 (1978) 1061.

[40] E. A. Podgornov, I. P. Prosvirin, V. I. Bukhtiyarov, *J. Mol. Catal. A: Chem*. **158** (2000) 337.

UNIVERSITAT ROVIRA I VIRGILI
NANOMATERIALS IN CATALYSIS: STUDY OF MODEL REACTIONS.
Ricardo José Chimentao
ISBN: 978-84-690-7618-7 / DL: T.1326-2007

Chapter II.3

Propylene epoxidation by nitrous oxide over Au-Cu/TiO_2 alloy catalysts

UNIVERSITAT ROVIRA I VIRGILI
NANOMATERIALS IN CATALYSIS: STUDY OF MODEL REACTIONS.
Ricardo José Chimentao
ISBN: 978-84-690-7618-7 / DL: T.1326-2007

II.3.1 Abstract

Gold-copper alloy catalysts were prepared by impregnation of TiO_2 (anatase) support with mixed chloride precursors and tested in the gas-phase epoxidation of propene. The bimetallic systems contained different Au-Cu molar ratios and a total metal content of 4 wt. %. The corresponding monometallic Au/TiO_2 and Cu/TiO_2 catalysts were also prepared for comparison. X-ray diffraction, XPS and transmission electron microscopy studies indicated that alloying was achieved. The copper content in the catalyst seemed to have a strong influence on the dispersion of the metal particles and in their catalytic properties. In particular, the greater the Cu content in the alloy, the smaller the metal particle size achieved. These changes also contributed to an increase in the activity and in the selectivity to propene oxide. The sample with a Cu/Au ratio of 3/1 showed the best catalytic behavior. Besides, the catalytic activity of the samples can be correlated with the results obtained by TPR.

Keywords: alloy, gold, copper, propene, epoxidation, catalysts, nitrous oxide, HRTEM, XPS

UNIVERSITAT ROVIRA I VIRGILI
NANOMATERIALS IN CATALYSIS: STUDY OF MODEL REACTIONS.
Ricardo José Chimentao
ISBN: 978-84-690-7618-7 / DL: T.1326-2007

II.3.2. Introduction

Propene oxide (PO) is one of the most important chemical feedstocks for producing resins such as polyurethane [1-3]. Major conventional manufacturing methods require two-stage process, using chlorohydrin or Halcon (hydroperoxides) as an oxidant. In the chlorohydrin method, large amounts of Cl_2 are consumed, which gives rise to serious problems of equipment corrosion and environmental pollution. The Halcon method is capital intensive and its economics depends on the economic fortunes of the byproducts, namely styrene or tert-butyl-alcohol. In analogy to ethylene epoxidation, much attention has been paid to the direct oxidation of propene using air or oxygen as the oxidant directly [4]. Epoxidation of ethylene with gaseous oxygen over Ag catalysts was developed many years ago, but the same reaction with propene has not been successful. Propene is different from ethylene by an existence of a methyl group. It is generally believed that this low efficiency of propene epoxidation is associated with the presence of allylic hydrogen atoms in the alkene, which readily undergo abstraction on oxygenated silver, yielding a stable adsorbed allyl species precluding selective oxidation and leading to combustion. Haruta and co-workers [5] have reported that certain Au/TiO_2 catalysts exhibit selectivity greater than 90% for the production of propene oxide (PO) using a combination of H_2 and O_2 as oxidation mixture, although the reactant conversion was very low (1.1%). When formed as particles of less than 10 nm and supported on metal oxides, Au is an active catalyst with unusual size-dependent activity and selectivity for propene epoxidation [6, 7]. For active supports such as TiO_2, the oxygen activation occurred on the support surface and the oxidation reaction

UNIVERSITAT ROVIRA I VIRGILI
NANOMATERIALS IN CATALYSIS: STUDY OF MODEL REACTIONS.
Ricardo José Chimentao
ISBN: 978-84-690-7618-7 / DL: T.1326-2007

occurred at the periphery between the support and the gold nanoparticles. Thus, the requirement for very small metal nanoparticles may arise mainly from larger contact peripherals. The preparation route of gold catalysts has been also determined to be particularly important for propene epoxidation. Among single metal oxides, TiO_2 makes Au selective for propene epoxidation only in the anatase form [8]. Another constraint is the deactivation of gold catalysts with time on stream [9]. Accumulation of PO and other successively oxidized products on the catalyst surfaces was considered to be a major reason for this phenomenon and for the limited propene conversion. Recently Lambert et al. have shown that copper is also extremely effective in the epoxidation of propene [10]. Therefore it is interesting to examine whether how copper and gold alloy catalysts behave in the propene epoxidation. The structure of bulk Au-Cu alloy is well known and this alloy is known to form solid solution very easily. The main objective of the present work was to explore the performance of Au-Cu alloy in the epoxidation of propene by nitrous oxide (N_2O). The decomposition of N_2O can be expected to generate oxygen species with an electrophilic characteristic on an appropriate catalyst, which may account for the highly selective epoxidation of propene [11,12]. The only byproduct is N_2 and the process using N_2O as oxidant is thus environmentally benign. In this work several Au-Cu bimetallic catalysts, as well as monometallic Cu and Au ones, were prepared. The materials were characterized by N_2-adsorption, TPR, XRD, HRTEM, EELS and XPS. The role of copper on Au dispersion and the catalytic properties were assessed, which leads to relevant structure-function relationships for the investigated reaction over a novel catalytic system.

UNIVERSITAT ROVIRA I VIRGILI
NANOMATERIALS IN CATALYSIS: STUDY OF MODEL REACTIONS.
Ricardo José Chimentao
ISBN: 978-84-690-7618-7 / DL: T.1326-2007

II.3.3 Experimental

II.3.3.1 Catalyst Preparation

Gold-copper alloy catalysts supported on titanium oxide were prepared covering the entire composition since gold is miscible with copper at any composition range. The Au-Cu/TiO_2 catalysts were prepared by impregnation the support (TiO_2, anatase) with an acidic aqueous solution of $HAuCl_4 \cdot 3H_2O$ and $CuCl_2 \cdot H_2O$ in adequate amounts. The samples were dried in vacuum for 2 h. Then, the resulting samples were dried at 373 K for 12 h and finally reduced in hydrogen flow (50 mL min^{-1}) at 673 K for 6 h. The total metal loading of all samples (monometallic and bimetallic samples) was fixed at 4 wt. %. The Au/Cu molar ratios in bimetallic samples were 3/1, 1/1 and 1/3. Besides, a monometallic gold sample with 0.5 wt % of gold was prepared in order to study the effect of the amount of gold and metal particle size in the catalytic behaviour.

The sample code of the bimetallic catalysts refers to the molar ratios (e.g. Au_3Cu_1).

II.3.3.2 Catalyst Characterization

N_2 physisorption. N_2 adsorption-desorption isotherms at 77 K were measured in a Micromeritics ASAP 2000 instrument. Samples were previously evacuated at 623 K for 16 h. The BET method was used to calculate the total surface area of the samples [13]. The BET surface area of the samples were around 28-31 $m^2 \cdot g^{-1}$, that is quite similar than for the support (31 $m^2 \cdot g^{-1}$).

UNIVERSITAT ROVIRA I VIRGILI
NANOMATERIALS IN CATALYSIS: STUDY OF MODEL REACTIONS.
Ricardo José Chimentao
ISBN: 978-84-690-7618-7 / DL: T.1326-2007

Temperature-Programmed Reduction (TPR). TPR experiments were performed in a TPDRO 1100 (Thermo Finnigan) instrument equipped with a thermal conductivity detector (TCD) and coupled to a mass spectrometer QMS 422 Omnistar. The catalysts were treated in O_2 for 1 h at 623 K before TPR analysis. Then, the samples were purged with argon flow before the TPR analysis. The TPR of the catalysts was carried out using 5% H_2 in Ar flow as reducing agent, the gas flow rate was 20 mL min^{-1} and the weight of sample was around 30 mg. The temperature was raised from 323 K up to 1073 K at a rate of 20 K min^{-1}. Water produced during TPR was trapped in CaO + Na_2O (Soda lime).

X-ray diffraction. X-ray diffraction (XRD) measurements were made using a Siemens D5000 diffractometer (Bragg-Bentano parafocusing geometry and vertical θ-θ goniometer) fitted with a grazing incident (ω: 0.52^0) attachment for thin film analysis and scintillation counter as a detector. The samples were dispersed on Si (510) sample holder. The angular 2θ diffraction range was between 10^0 and 120^0. The data were collected with an angular step of 0.03^0 at 12 s per step and sample rotation. $Cu_{K\alpha}$ radiation (λ = 1.54056 Å) was obtained from a copper X-ray tube operated at 40 kV and 30 mA. The crystalline phases were identified using the JCPDS files.

Transmission electron microscopy (TEM). Transmission electron microscopy studies were performed at 200 kV with a JEOL JEM 2010F instrument equipped with a field emission source and an electron energy-loss spectroscopy (EELS) detector. The microscope was

UNIVERSITAT ROVIRA I VIRGILI
NANOMATERIALS IN CATALYSIS: STUDY OF MODEL REACTIONS.
Ricardo José Chimentao
ISBN: 978-84-690-7618-7 / DL: T.1326-2007

operated in high-resolution (HRTEM) and scanning (STEM) modes, both in bright-field and dark-field configurations. Samples were dispersed in alcohol in an ultrasonic bath and a drop of supernatant suspension was poured onto a holey carbon coated grid and dried completely before measurements.

X-ray photoelectron spectroscopy (XPS). X-ray photoelectron spectra (XPS) were acquired with a VG Escalab 200R spectrometer equipped with a hemispherical electron analyzer and an Mg-Kα (hv = 1253.6 eV, 1 eV = 1.603×10^{-19} J). X-ray source operated at 10 mA and 12 kV. The peaks were fitted by a non-linear least square fitting program using a properly weighted sum of Lorentzian and Gaussian component curves after background subtraction according to Shirley and Sherwood [14]. The constant charging of the samples was corrected by referencing all energies to the Al 2p peak at 74.5 eV.

Catalytic activity. The catalytic reactions were carried out using a fixed-bed reactor operated at atmospheric pressure. The experiments were carried out with typically 0.14 g of catalyst and a gas flow of 50 NmL min^{-1} (GHSV 9000 h^{-1}). The gas mixture consisted of 10% of N_2O and 10% propene in argon. Before reaction, catalysts were pretreated with gas flow containing Ar (100 mL min^{-1}) and H_2 (10 mL min^{-1}) at 673 K for 2 h. After the temperature was decreased to the desired reaction temperature, the reactant gas mixture of Ar, C_3H_6 and N_2O was introduced to start the reaction. The products were analyzed by two on-line gas chromatographs equipped with Porapak T and molecular sieves columns using FID and TCD detectors. All lines and valves between the exit of the reactor and the gas chromatographs were

UNIVERSITAT ROVIRA I VIRGILI
NANOMATERIALS IN CATALYSIS: STUDY OF MODEL REACTIONS.
Ricardo José Chimentao
ISBN: 978-84-690-7618-7 / DL: T.1326-2007

heated at 373K to prevent the condensation of the products.

II.3.4 Results and Discussion

XRD. X-ray diffraction of all samples was conducted to ensure that alloying has been obtained in the bimetallic formulations with the preparation procedure adopted in this study. The XRD patterns in Figure II.3.1 show broad peaks due to the anatase support (JCPDS 211272). For 4%Au/TiO_2 and 0.5% Au/TiO_2 samples, diffraction lines of gold were identified at 38.2°, 44.3°, 64.5° and 77.6°, which have been assigned to the (111), (200), (220), (311) planes of the fcc structure of gold, respectively (JPCDS 04-0784). Typical XRD of the Cu sample (Cu/TiO_2) showed 2θ values at 43.4, 50.6 and 74.2° that are indexed as (111), (200) and (220) planes of the fcc structure of copper (JCPDS file, 4-386). Other phases such as CuO and Cu_2O were not detected. This means that if part of the copper exists in the form of copper oxide clusters, these are under the detection capabilities of XRD [15]. In the bimetallic samples, broad diffraction lines corresponding to (111) planes of Au-Cu alloys were identified, whereas (200) and (220) Bragg reflections became hardly visible due to peak broadening. This effect is more pronounced as copper content increases in sample formulation. The mean particle diameter calculated from the (111) reflection by the Scherrer formula for the samples 4%Au/TiO_2, 0.5%Au/TiO_2, 4%Au_3Cu_1/TiO_2, 4%Au_1Cu_1/TiO_2 and 4%Au_1Cu_3/TiO_2 are respectively Au=27.1 nm, Au=8.6 nm; Au_3Cu_1=13.5 nm, Au_1Cu_1=9.3 nm, Au_1Cu_3=7.3 nm and Cu =5.5 nm. For pure gold samples, when the amount of gold decreased from 4% to 0.5 % the gold particle size decreased from 27.1 nm to 8.6 nm. On the other hand, for bimetallic catalysts, when the copper content increased the bimetallic

UNIVERSITAT ROVIRA I VIRGILI
NANOMATERIALS IN CATALYSIS: STUDY OF MODEL REACTIONS.
Ricardo José Chimentao
ISBN: 978-84-690-7618-7 / DL: T.1326-2007

particles size decreased. Pure monometallic copper catalyst showed the lowest metal particle size (5.5 nm). When gold and copper are brought together to form a solid, there is a compression of the electronic charge density [16]. This may contribute to the stability of the as-synthesized bimetallic particles against agglomeration compared to the pure elements. The formation of alloys in the bimetallic samples is demonstrated by the d_{111} values, which progressively decreased with Cu content with respect to pure Au. The lattice parameters of the metal crystallites in our samples as function of bulk composition are depicted in Figure II.3.2. When the copper content increased from a Cu/Au molar ratio of 1/3 to 3/1, the lattice parameter gradually decreased. So, a linear evolution of the lattice parameter of the Au-Cu crystallites clearly indicates the formation of alloys in the bimetallic samples.

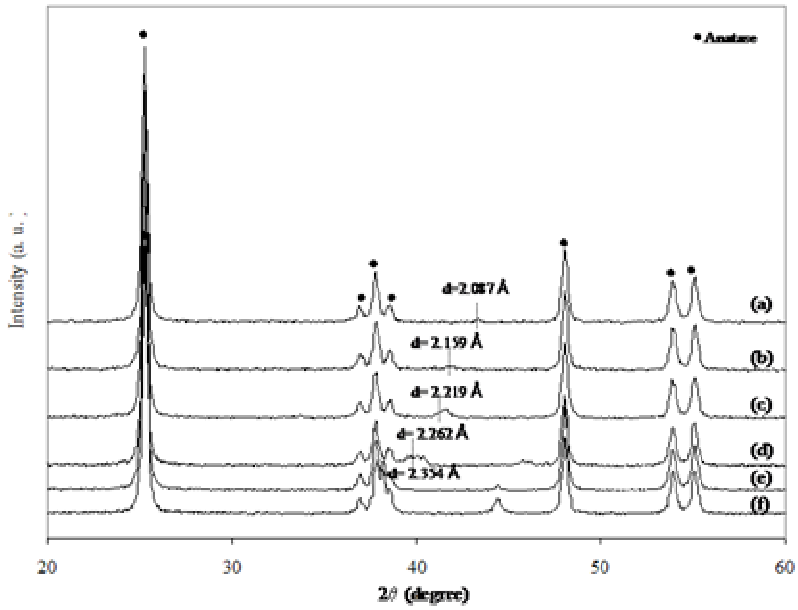

Figure II.3.1 XRD patterns of Au, Cu and Au-Cu alloys supported on TiO_2. (a) 4%Cu/TiO_2, (b) 4%Au_1Cu_3/TiO_2, (c) 4%Au_1Cu_1/TiO_2, (d) 4%Au_3Cu_1/TiO_2, (e) 0.5%Au/TiO_2 and (f) 4%Au/TiO_2.

UNIVERSITAT ROVIRA I VIRGILI
NANOMATERIALS IN CATALYSIS: STUDY OF MODEL REACTIONS.
Ricardo José Chimentao
ISBN: 978-84-690-7618-7 / DL: T.1326-2007

However, the lattice parameters of our bimetallic samples exhibit some small deviations of the Vegard's law in agreement with previous works [17].

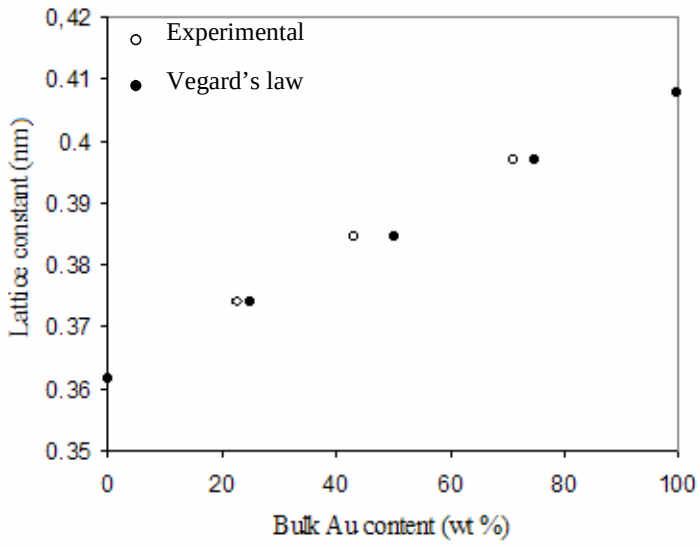

Figure II.3.2 Effect of Au-Cu composition on the lattice parameter, a_0, of fcc alloy crystallites calculated from the (111) crystallographic plane by XRD.

TEM. In order to get a more insight about the nature of the metal and alloy particles identified by XRD, we carried out a detailed TEM-EELS study over all the catalysts. 4%Au/TiO_2 catalyst is constituted by small metal particles ranging from 8 to 15 nm in diameter as well as by large agglomerates up to 100-250 nm. This is shown in Figure II.3.3, where the location of gold particles and agglomerates are seen in the same area taken in bright-field (BF) and dark-field (DF) modes. This indicates that the size distribution of Au particles in this sample is quite heterogeneous, and that agglomeration of Au easily occurs. In contrast, monometallic catalyst 4%Cu/TiO_2 is mainly constituted by copper

UNIVERSITAT ROVIRA I VIRGILI
NANOMATERIALS IN CATALYSIS: STUDY OF MODEL REACTIONS.
Ricardo José Chimentao
ISBN: 978-84-690-7618-7 / DL: T.1326-2007

metal particles between 10 and 20 nm in diameter. Similarly, all the bimetallic samples and 0.5%Au/TiO_2 sample, are constituted only by well-dispersed metallic particles at the nanometer scale. Figure II.3.4 shows a representative image of a metallic particle in catalyst 4%Au_3Cu_1/TiO_2 obtained under Z-contrast, BF and DF STEM modes.

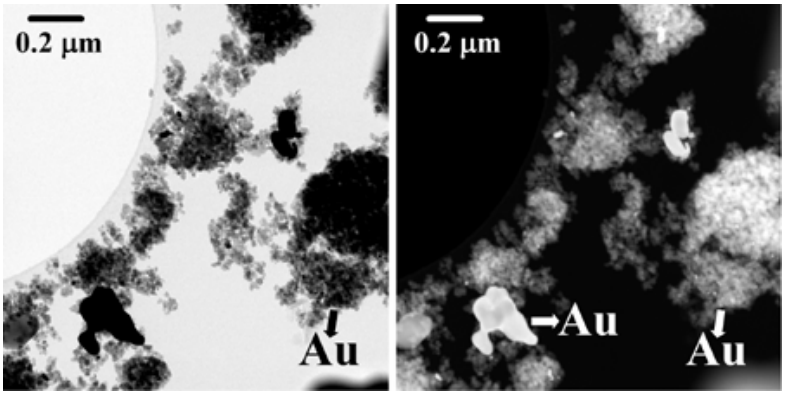

Figure II.3.3. Bright-field (left) and dark-field (right) TEM images of catalyst Au/TiO_2 at low magnification. In the DF image, individual gold particles as well as gold agglomerates appear bright.

All particles imaged in this catalyst exhibited diameters of about 15-25 nm. High-resolution TEM (HRTEM) and electron energy-loss spectroscopy (EELS) were performed over individual particles. In all cases, EELS data revealed the simultaneous presence of gold and copper for each individual metallic particle analyzed, and HRTEM revealed the presence of the Au_3Cu_1 alloy (Figure II.3.4). Particles in catalyst 4%Au_1Cu_1/TiO_2 exhibited a narrow size distribution of about 5-10 nm. Figure II.3.5 shows STEM images for this catalyst as well as EEL spectra recorded over different areas. Area labeled “a” in the figure, with low Z-contrast, correspond to the TiO_2 support according to EELS (characteristic pattern with peaks at about 5, 11, 23, 38 and 46 eV), whereas area labeled “b” in the figure depicts a particle with high

UNIVERSITAT ROVIRA I VIRGILI
NANOMATERIALS IN CATALYSIS: STUDY OF MODEL REACTIONS.
Ricardo José Chimentao
ISBN: 978-84-690-7618-7 / DL: T.1326-2007

Z-contrast and with an EEL spectrum that indicates a bimetallic Cu-Au composition (a single signal at ca. 25 eV).

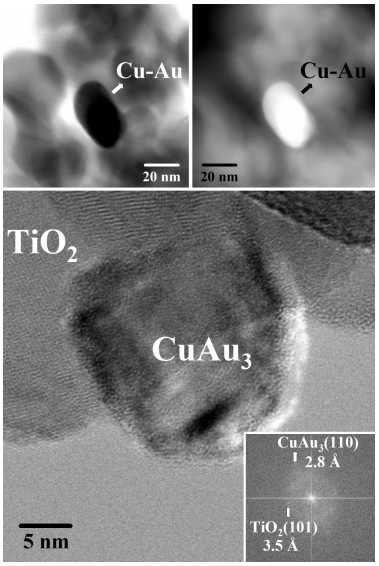

Figure II.3.4 Z-contrast STEM, HRTEM, and FT images of individual metal particles in catalyst 4%Au_3Cu_1/TiO_2. EELS analysis reveal that particles are bimetallic, and lattice-fringe and FT analysis show $CuAu_3$ particles supported on TiO_2.

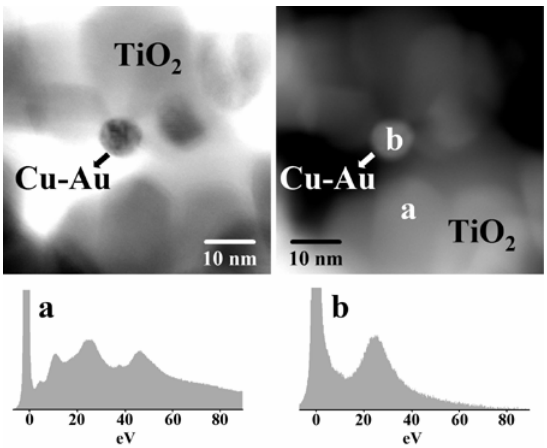

Figure II.3.5. Z-contrast STEM images of catalyst 4%Au_1Cu_1/TiO_2 and EEL spectra recorded over areas marked as “a” (corresponding to TiO_2) and “b” (bimetallic Cu-Au particle).

UNIVERSITAT ROVIRA I VIRGILI
NANOMATERIALS IN CATALYSIS: STUDY OF MODEL REACTIONS.
Ricardo José Chimentao
ISBN: 978-84-690-7618-7 / DL: T.1326-2007

Another individual particle in catalyst Au_1Cu_1/TiO_2 is shown in Figure II.3.6 in BF and DF STEM modes as well as under HRTEM conditions. The atomic-scale image along with FT indicates that the particle corresponds to the CuAu alloy. All the lattice-fringe images recorded over metallic particles in catalyst $4\%Au_1Cu_1/TiO_2$ corresponded to the AuCu alloy and no other alloys in the Au-Cu system were identified. Figure 7 corresponds to STEM images of a representative particle in catalyst Au_1Cu_3/TiO_2. In this catalyst, particles exhibit sizes in the range 10-15 nm. Again, EELS data demonstrated the bimetallic composition of particles and, in this case, HRTEM analysis identified Au_1Cu_3 crystallites located on top TiO_2 crystals of the support (Figure II.3.7).

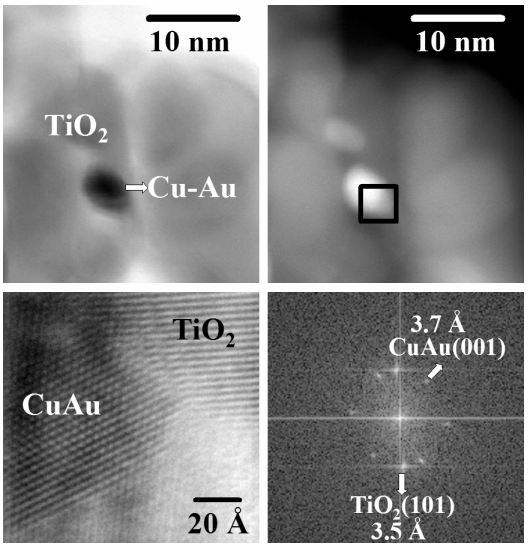

Figure II.3.6. Z-contrast STEM images of an individual metal particle in catalyst Au_1Cu_1/TiO_2 and HRTEM and FT images corresponding to the area enclosed by the square. The lattice-fringe analysis indicates that the particle is CuAu alloy.

UNIVERSITAT ROVIRA I VIRGILI
NANOMATERIALS IN CATALYSIS: STUDY OF MODEL REACTIONS.
Ricardo José Chimentao
ISBN: 978-84-690-7618-7 / DL: T.1326-2007

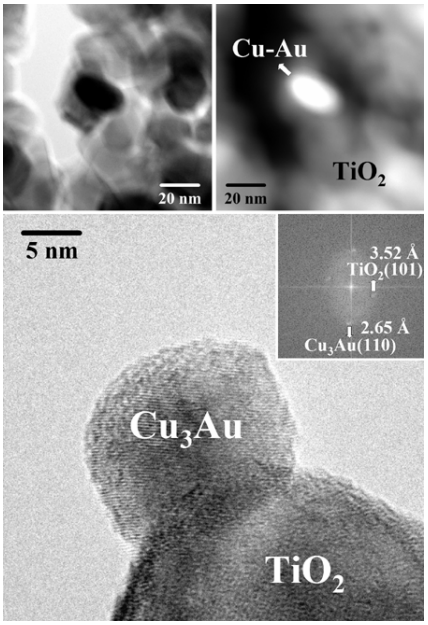

Figure II.3.7. Z-contrast STEM, HRTEM, and FT images of individual metal particles in catalyst 4%Au_1Cu_3/TiO_2. EELS analysis indicate that particles are bimetallic, and lattice-fringe and FT analysis correspond to 4%Cu_3Au particles supported on TiO_2.

TPR. TPR profiles recorded over 4%Au-Cu alloy catalysts with various compositions as well as over 4%Au/TiO_2 and 4%Cu/TiO_2 samples are shown in Figure 8a. The TPR profile for Cu/TiO_2 sample presented two reduction peaks centered at 460 and 630 K, which can be ascribed as highly dispersed Cu(II)O clusters and the isolated Cu(II) ions, respectively [18-20]. Similarly, two TPR peaks were recorded over all catalysts with Au-Cu alloys, as depicted in Figure II.3.8a, but their position and absolute intensity depended on the composition of the alloy particles. Both the low-temperature and high-temperature TPR peaks of the bimetallic samples shift to lower values with increasing Cu

UNIVERSITAT ROVIRA I VIRGILI
NANOMATERIALS IN CATALYSIS: STUDY OF MODEL REACTIONS.
Ricardo José Chimentao
ISBN: 978-84-690-7618-7 / DL: T.1326-2007

content. The maximum of the low temperature peak was found to vary from ca. 470 K for the 4%Au_3Cu_1/TiO_2 catalyst to around 440 K for 4%Au_1Cu_1/TiO_2 and 4%Au_1Cu_3/TiO_2 catalysts. The high temperature peak shifted from 650 K for 4%Au_1Cu_1/TiO_2 to 630 K for 4%Cu/TiO_2. This may be explained taking into account that copper atoms can affect the electronic structure of gold by near-neighbor interactions [21].

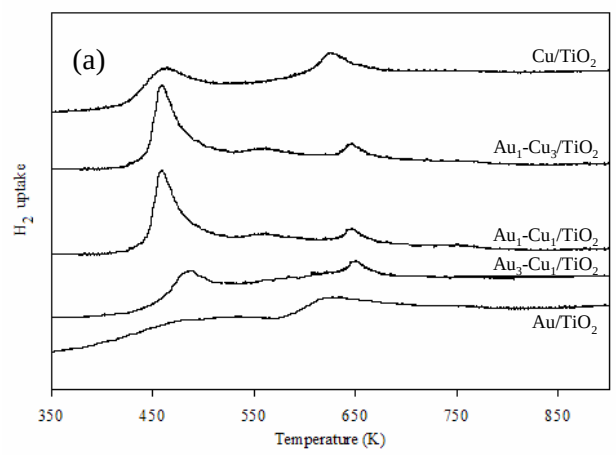

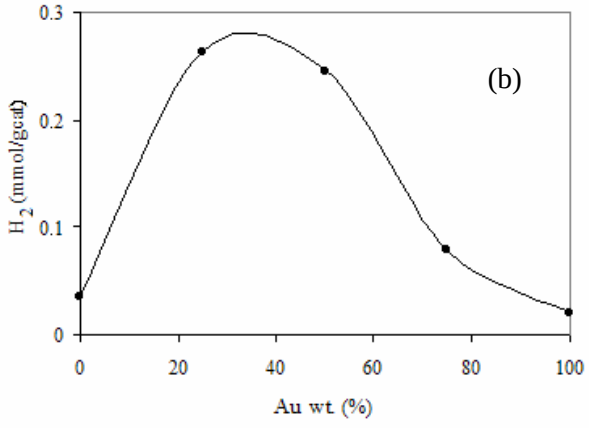

UNIVERSITAT ROVIRA I VIRGILI
NANOMATERIALS IN CATALYSIS: STUDY OF MODEL REACTIONS.
Ricardo José Chimentao
ISBN: 978-84-690-7618-7 / DL: T.1326-2007

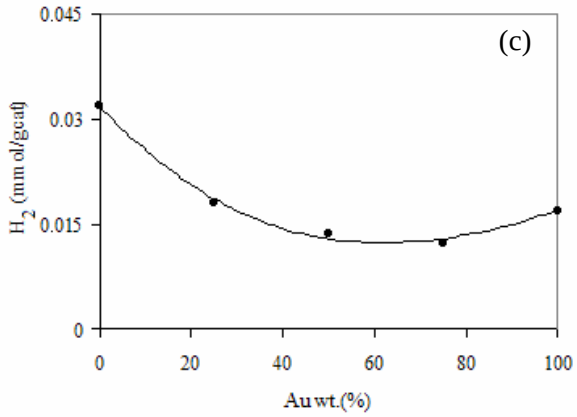

Figure II.3.8. (a) TPR profiles of Cu/TiO_2, Au/TiO_2 and $Au\text{-}Cu/TiO_2$ catalysts. Amount of hydrogen uptake: (b) Low temperature and (c) High temperature peak.

The work function of Cu is reported to be 4.65 eV while that of gold is 5.1 eV. Since the work function of copper is lower than that of gold, electronic interactions between Au and Cu atoms are expected to result in electron transfer from copper to gold, which in turn results in a lower reduction temperature. Additionally, as the size of the bimetallic particle decreased with the copper content, such as confirmed by XRD and HRTEM results, obviously the fraction of the surface atoms also increases. At the same time, because the overlap of electron orbitals decreases as the average number of bonds between atoms becomes less, the band structure is weakened, and surface atoms in particular start to behave more as individuals than as members of the cluster [22]. This fact could also explain the shift to lower temperatures values observed in the TPR when the Cu content increased. Besides, there is another important fact that must be considered. For the bimetallic samples, and particularly for $4\%Au_1Cu_1/TiO_2$ and $4\%Au_1Cu_3/TiO_2$ samples, the low temperature peak increased in intensity while the high temperature

UNIVERSITAT ROVIRA I VIRGILI
NANOMATERIALS IN CATALYSIS: STUDY OF MODEL REACTIONS.
Ricardo José Chimentao
ISBN: 978-84-690-7618-7 / DL: T.1326-2007

peaks decreased (see Figures 8b and 8c, respectively). From Figure 8b it is clear that the low-temperature TPR peaks in catalysts 4%Au_1Cu_1/TiO_2 and 4%Au_1Cu_3/TiO_2 are significantly more intense than those of the other samples. The H_2 consumption observed for our bimetallic samples was higher than the theoretically expected. The discrepancy between theoretical and experimental values can be tentatively explained by the reduction of the support surface upon hydrogen spillover. Copper may act as a dispersant agent for gold decreasing the bimetallic particle size of clusters, as confirmed by our XRD and HRTEM analysis. This fact increases the dissociative adsorption of hydrogen on such metal sites to the adjacent support sites. Previous work regarding on the activation of hydrogen in Au/TiO_2 catalysts showed that H_2 dissociates on nanosized gold producing the reduction of the support by spillover [23]. This can also explain the small H_2 uptake value observed for the monometallic Au/TiO_2, since such larger gold particles does not adsorb H_2 at any appreciable extent. This fact is an important distinct behavior among catalysts and may have an important influence on catalytic performance. The higher reducibility of catalysts 4%Au_1Cu_1/TiO_2 and 4%Au_1Cu_3/TiO_2 may be related to the decrease of particle size with respect to the other samples (as evidenced by XRD and TEM results) as well as to geometric effects in the alloy particles [24]. This also suggests a dependence of hydrogen adsorption on the particle size. Finally, an additional evidence for a strong alloying-derived effect in these samples is the appearance of a low-intense, intermediate TPR peak at ca. 555 K.

XPS. XPS is a powerful technique to obtain valuable information of chemical compositions of nanoparticles [25, 26]. For this reason

UNIVERSITAT ROVIRA I VIRGILI
NANOMATERIALS IN CATALYSIS: STUDY OF MODEL REACTIONS.
Ricardo José Chimentao
ISBN: 978-84-690-7618-7 / DL: T.1326-2007

surface analysis by XPS was performed. Table II.3.1 summarizes the elemental XPS positions together with the atomic ratios of Cu/Ti and Au/Ti. The binding energy of the Ti $2p_{3/2}$ peak at 458.7 eV was unchanged for all samples. The corresponding XPS core-level spectra acquired for the Au-4f and Cu-2p regions are shown in Figure II.3.9. For the 4%Au/TiO_2 sample the Au 4f spectra, characterized by the spin-orbit splitting (Au $4f_{7/2}$ and Au $4f_{5/2}$ components), shows values of 84.0 eV and 87.7 eV, respectively. Both peaks originating from the Au indicate that these binding energies are consistent with the Au^0 oxidation state. The Au $4f_{7/2}$ binding energies obtained from the bimetallic samples were in the range 83.7- 83.8 eV. As the copper content in the bimetallic catalysts increases, the binding energy of the Au $4f_{7/2}$ shifted towards lower binding energies with respect to the monometallic gold sample. According to Pauling´s eletronegativity table, the electronegativity of Au is higher than Cu. We should therefore expect some electron transfer from copper to gold atoms by shifting the Au core levels towards lower binding energies [27]. The shift of the Au $4f_{7/2}$ to the lower energies observed for our samples containing alloy particles is consistent with this general rule. No evidence for Au bonded to oxygen was encountered because the oxide shows binding energies around 85.8 and 89.5 eV for Au $4f_{7/2}$ and Au $4f_{5/2}$, respectively [28-30].

Concerning copper, as the Au content in the bimetallic samples increased, the binding energies of Cu $2p_{3/2}$ slightly shifted to higher energy values than those of the monometallic copper sample. The higher electron affinity of gold with respect to that of copper led to an electron transfer from the Cu to Au, thus decreasing the electron density of the Cu atoms. The Cu $2p_{3/2}$ values were found in all cases to

UNIVERSITAT ROVIRA I VIRGILI
NANOMATERIALS IN CATALYSIS: STUDY OF MODEL REACTIONS.
Ricardo José Chimentao
ISBN: 978-84-690-7618-7 / DL: T.1326-2007

be between 932.2 and 932.5 eV, about 1.5 eV lower than for CuO, thus precluding the form of CuO. It is interesting to consider, from the relative surface atomic ratios (Au/Ti and Cu/Ti) presented in Table II.3.1, how the state of dispersion of the bimetallic samples was affected by the addition of copper.

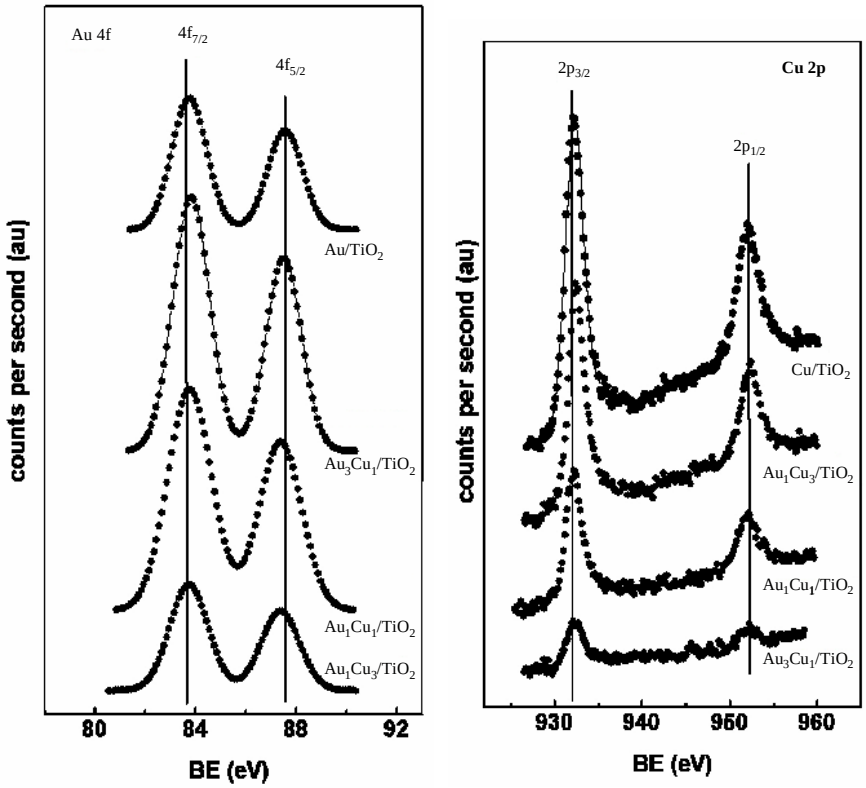

Figure II.3.9. X-ray photoelectron spectra recorded over 4%Cu/TiO_2, Au/TiO_2 and Au-Cu/TiO_2 catalysts.

For example 4%Au_1Cu_1/TiO_2 shows an Au/ Ti ratio of 0.0083 while for monometallic gold catalysts the Au/ Ti ratio is 0.0068. So, taking into account the amount of gold in these samples we can conclude that the addition of copper produce a significant increase in the dispersion of

UNIVERSITAT ROVIRA I VIRGILI
NANOMATERIALS IN CATALYSIS: STUDY OF MODEL REACTIONS.
Ricardo José Chimentao
ISBN: 978-84-690-7618-7 / DL: T.1326-2007

the bimetallic samples. However this effect was not observed for copper suggesting that the particle size of our pure copper catalysts is quite similar with the bimetallic samples as has been confirmed by XRD and HRTEM.

Table II.3.1. Binding energies and surface atomic ratios of TiO_2 supported Au-Cu catalysts

Catalyst	Ti $2p_{3/2}$	Cu $2p_{3/2}$	Au $4f_{7/2}$	Au/Ti at	Cu/Ti at
Cu/TiO_2	458.7	932.3	-	-	0.064
Au_3Cu_1/TiO_2	458.7	932.2	83.8	0.0089	0.012
Au_1Cu_1/TiO_2	458.7	932.2	83.7	0.0083	0.022
Au_1Cu_3/TiO_2	458.7	932.5	83.7	0.0030	0.040
Au/TiO_2	458.7	-	84.0	0.0068	-

Catalytic activity. The direct propene epoxidation reaction with N_2O was tested at different reaction temperatures (between 530 and 653 K). The main products obtained were acrolein, acetone, propanal, propene oxide and total combustion products (H_2O and CO_x). In a blank experiment it was determined that TiO_2 alone had no activity for the epoxidation of propene with N_2O in the range of temperatures tested. The values of propene conversion and selectivity to different products obtained over the different catalysts are compiled in Table II.3.2. Among all samples tested, $4\%Au/TiO_2$ showed the lowest activity. In contrast, bimetallic catalysts were more active and propene conversion and selectivity towards propene oxide progressively increased with copper content. The $4\%Cu/TiO_2$ sample was also active in propene

UNIVERSITAT ROVIRA I VIRGILI
NANOMATERIALS IN CATALYSIS: STUDY OF MODEL REACTIONS.
Ricardo José Chimentao
ISBN: 978-84-690-7618-7 / DL: T.1326-2007

epoxidation as has been reported previously by Lambert et al. [31], but the catalytic performance of $4\%Au_1Cu_1/TiO_2$ and $4\%Au_1Cu_3/TiO_2$ catalysts was superior than for the monometallic $4\%Cu/TiO_2$ sample.

Table II.3.2 Summary of the catalytic performance of $Au\text{-}Cu/TiO_2$ catalysts for propylene epoxidation at 573 K

Catalyst	C_3H_6 (X%)	Selectivity (%)[a] PO	PA	AC	ACR	CO_x	Rate ($mmol.g_{cat}^{-1}.h^{-1}$)
Au/TiO_2	0.8	7.4	6.4	10.4	31.2	44.6	0.36
Au_3Cu_1/TiO_2	1.9	12.4	12.2	11.3	21.4	42.7	0.86
Au_1Cu_1/TiO_2	3.9	23.6	10.1	11.5	18.5	36.3	1.78
Au_1Cu_3/TiO_2	4.3	24.3	12.7	13.2	15.6	34.2	1.96
Cu/TiO_2	2.4	12.6	10.3	11.1	24.0	42.0	1.09

[a] PO- propylene oxide, PA- propanal, AC- acetone, ACR- acrolein, CO_x (CO_2 and CO). Pressure: 1atm, GHSV 9000 h^{-1}.

At a reaction temperature of 573K, as shown in Table II.3.2, the $4\%Cu/TiO_2$ catalyst exhibit 2.4% of propene conversion while the $4\%Au/TiO_2$, $4\%Au_1Cu_1/TiO_2$ and $4\%Au_1Cu_3/TiO_2$ the propene conversion was 0.8, 3.9, and 4.3% respectively. In order to compare the catalytic behaviour of monometallic gold catalysts ($4\%Au/TiO_2$ and $0.5\%Au/TiO_2$), an experiment loading 1.12 g of $0.5\%Au/TiO_2$ catalyst instead of 0.140 g of $4\%Au/TiO_2$ catalyst was performed (8 times higher in order to have the same amount of gold). The propene conversion was 1.4% for $0.5\%Au/TiO_2$. This conversion was higher than for the $4\%Au/TiO_2$ catalyst (0.89%) but lower with respect to the monometallic copper catalyst and bimetallic ones. Besides, the bimetallic catalyst with the lowest Cu content, $4\%Au_3Cu_1/TiO_2$, exhibited the lowest activity when compare the bimetallic samples.

UNIVERSITAT ROVIRA I VIRGILI
NANOMATERIALS IN CATALYSIS: STUDY OF MODEL REACTIONS.
Ricardo José Chimentao
ISBN: 978-84-690-7618-7 / DL: T.1326-2007

Therefore, the relative content of Au and Cu appeared to play a determinant role in the catalytic behavior. There was evidence for alloy formation in the bimetallic samples. Furthermore, we have shown by TPR experiments that $4\%Au_1Cu_1/TiO_2$ and $4\%Au_1Cu_3/TiO_2$ catalysts that have the highest conversion also have an enhanced low-temperature reduction peak with respect to the other catalysts. Taking into account the metal particle sizes of our samples, the particular behavior observed for bimetallic catalysts could result from alloying effects [32]. It has been suggested that upon alloying copper with gold, a net transfer of electrons from copper to gold is expected, rendering copper deficient in electrons [33, 34]. This fact has been confirmed by XPS analysis. Presumably, electron transfer also takes place from the reduced support to the metal clusters during the reaction. By electron transfer due to the interaction of nanosized clusters, the metal particles may become enriched in valence electron density, thereby altering the interaction of the active sites with the functional group and facilitating a partial transfer of electron density to the π^* orbital of unsaturated bond of the olefin. This may also favor the adsorption at cationic sites, and consequently the electrophilic oxygen species are enhanced increasing the catalytic activity toward selective oxidation [35]. Additionally, the resulting weaker copper-gold bonds may favor the desorption of the reaction products, which may also explain the increase in the catalytic activity observed for our bimetallic catalysts. Indeed intimate metal-titania contacting appears to be essential for the production of partial oxidation capability. As the copper content increased the metal particle size, determined by XRD, decreased down from 27.1 nm for $4\%Au/TiO_2$ catalyst to ca. 7.3 nm for $4\%Au_1Cu_3/TiO_2$ catalyst, increasing the catalytic performance for the

UNIVERSITAT ROVIRA I VIRGILI
NANOMATERIALS IN CATALYSIS: STUDY OF MODEL REACTIONS.
Ricardo José Chimentao
ISBN: 978-84-690-7618-7 / DL: T.1326-2007

bimetallic samples. Surely this size effect can also induce changes in the electronic properties of the metal nanoparticles [7].

Figure II.3.10 shows the temperature dependence on the catalytic performance of 4%Au_1Cu_3/TiO_2 catalyst for the selective oxidation of propene by N_2O at 10 minutes of reaction. Propene conversion and selectivity to propene oxide were sensitive to the change of reaction temperature. Propene conversion of 4.3% and a selectivity of 26.3% in propene oxide were obtained for the 4%Au_1Cu_3/TiO_2 catalyst at 573 K (Figure II.3.10). At a reaction temperature of 533 K the conversion was 1.9% and a selectivity to propene oxide of 40.5%, while at higher reaction temperature (653 K) the conversion was 13.6% and a selectivity to propene oxide of 10.9%.

It is of interest that in the range of reaction temperatures studied the propene oxide (PO) selectivity decreased while in general acrolein and CO_x selectivities increased as the reaction temperature increased. However, bimetallic catalysts always show higher conversion and lower selectivity to CO_x than the monometallic ones. These data provide another evidence of the different catalytic behavior of alloy samples. So, copper played a marked effect on the catalytic properties of the Au.

It should be stressed that during the catalytic tests some deactivation process was observed. According to previous studies, the deactivation may occur mainly due to an irreversible adsorption of propene oxide on the catalyst surface which undergoes further oligomerization, re-arrangment, cracking, coupling, etc. on acid sites [9]. The deactivation, however, was completely reversible and the activity was completely restored after a regeneration procedure at 573 K under an oxygen/helium atmosphere.

UNIVERSITAT ROVIRA I VIRGILI
NANOMATERIALS IN CATALYSIS: STUDY OF MODEL REACTIONS.
Ricardo José Chimentao
ISBN: 978-84-690-7618-7 / DL: T.1326-2007

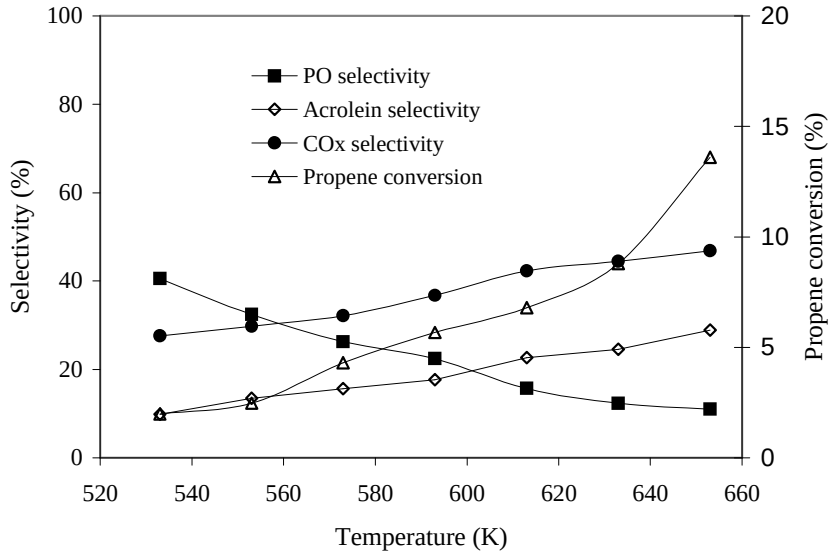

Figure II.3.10. Effect of temperature on the selectivity of the main products (left axis) and propylene conversion (right axis) for the epoxidation of propylene on 4% Au_1Cu_1/TiO_2. Pressure: 1atm, GHSV 9000 h^{-1}.

II.3.5 Conclusions

Bimetallic Au-Cu particles supported over TiO_2 have been characterized and tested in the epoxidation of propene by N_2O. Structural studies carried out by X-ray diffraction, XPS and transmission electron microscopy techniques demonstrated the existence of Au-Cu alloy particles. In addition, the alloy particle size decreased as the amount of copper content increased in the catalysts. It is possible to use Cu to modify the reactivity of Au with respect to the epoxidation of propene. Copper-gold bimetallic catalysts constituted by alloy particles of about 5-15 nm in size proved to be much active and selective towards propene oxide than monometallic Au or Cu samples

supported over TiO_2. The most active catalysts consumed the largest amount of hydrogen at low temperature in TPR experiments, suggesting that some spill over effect occurs in the bimetallic catalysts. Both effects, particle size and alloying, are considered to play a determinant role in the catalytic performance.

Acknowledgments. This research was sponsored by the Ministerio de Ciencia y Tecnología (Spain) under Projects REN2002-04464-CO2-01, PETRI 95-0801.OP and by the Ministerio de Educación y Ciencia (Spain) under Project CTQ2006-08196/PPQ. A portion of this work was performed at Institut de Tècniques Energètiques (Universitat Politècnica de Catalunya) which was supported by the Ministerio de Educación y Ciencia (Spain) under Project ENE2006-06925/ALT.

References

[1] B. Hammer, J. K. Norskov, *Nature* **376** (1995) 238.

[2] M. Haruta, N. Yamada, T. Kobayashi, S. Iijima, *J. Catal*. **115** (1989) 301.

[3] M. Haruta, S. Tsubota, T. Kobayashi, H. Kageyama, M. J. Genet, B. Delmon, *J. Catal.* **144** (1993) 175

[4] S. J. Ainsworth, *Chem. Eng. News* (1992) 9.

[5] T. Hayashi, K. Tanaka, M. Haruta, *J. Catal.* **178** (1998) 566.

[6] A. K. Sinha, S. Seelan, S. Tsubota, M. Haruta, *Angew. Chem. Int. Ed.* **43** (2004) 1546.

[7] M. Haruta and M. Daté, *Appl. Catal., A* **222** (2001) 427.

[8] T. A. Nijhuis, B. J. Huizinga, M. Makkee, J. A. Moulijn, *Ind. Eng. Chem. Res.* **38** (1999) 884.

[9] T. A. Nijhuis, T. Visser, B. M. Weckhuysen, *J. Phys. Chem.* B **109**

UNIVERSITAT ROVIRA I VIRGILI
NANOMATERIALS IN CATALYSIS: STUDY OF MODEL REACTIONS.
Ricardo José Chimentao
ISBN: 978-84-690-7618-7 / DL: T.1326-2007

(2005) 19309.

[10] O. P. H. Vaughan, G. Kyriakou, N. Macleod, M. Yikhov, R. M. Lambert, *J. Catal.* **236** (2005) 401.

[11] G. Ramis, G. Busca, F. Bregani, *Gazz. Chim. Ital.* **122** (1992) 79.

[12] V. Duma, D. Hönicke, *J. Catal.* **191** (2000) 93.

[13] S. J. Greg and K. S. W. Sing. *Adsorption, Surface Area and Porosity*. Academic Press. Londres.2ed. 1982.

[14] D. Briggs, M. P. Seah, *Practical surface analysis: by Auger and X-ray photoelectron spectroscopy*, John Wiley & Sons, New York 1987.

[15] B. Coq, D. Tachon, F. Figuéras, G. Mabilon, M. Prigent, *Appl. Catal. B* **6** (1995) 271.

[16] D. Gelatt, H. Enrenreich, *Phys Rev. B* **10** (1974) 398.

[17] G. De, C. N. R. Rao, *J. Phys Chem. B* **107** (2003) 1397.

[18] H. Chu, L. Yang, Q. Zhang, Y. Wang, *J. Catal.* **241** (2006) 225.

[19] S. Velu, K. Susuki, M. Okasaki, M. P. Kapoor, T. Osaki, F. Ohashi, *J. Catal.* **194** (2000) 373.

[20] L. J. Kundakovic, M. F. Stephanopoulos, *Appl. Catal. A*, **171** (1998) 13.

[21] V. Ponec, *Catal. Rev. Sci. Eng.* **11** (1975) 41.

[22] G. C. Bond, *Catal. Today* **72** (2002) 5.

[23] S. Schimpf, M. Lucas, C. Mohr, U. Rodemerck, A. Brückenr, J. Radnik, H. Hofmeister, P. Claus, *Catal. Today* **72** (2005) 63.

[24] R. E. Kramer and H. Zuegg, *J. Catal.* **80** (1983) 446.

[25] F. Delannay, *Characterization of Heterogeneous Catalysts*, Decker, New York, 1984.

[26] D. Briggs and M.P. Seah: Practical Surface Analysis. Auger and X-ray Photoelectron Spectroscopy. (John Wiley and Sons, Chichester, 1990).

[27] J. K. A. Clark, *Chem. Rev.* **75** (1975) 29.

[28] A. Q. Wang, J. H. Liu, S. D. Lin, T. S. Lin and C. Y. *J. Catal.* **233** (2005)186.

[29] J. J. Pireau, M. Liehr, P. A. Thirty, J. P. Delrue and R. Caudano. *Surf. Sci*. **141** (1984) 221.

[30] B. Koslowski, H. G. Boyen, C. Wilderotter, G. Kästle, P. Ziemann, R. Wahrenberg and P. Oelhafen, *Surf. Sci*. **475** (2001) 1.

[31] O. P. H. Vaughan, G. Kryakou, N. Macleod, Mintcho Tikhov, R. M. Lambert, *J. Catal.* **236** (2005) 401.

[32] T. Akita, K. Tanaka, S. Tsuota, M. Haruta, *J. Elec. Microsc.* **49** (2000) 657.

[33] D. Gelatt, H. Ehrenreich, *Phys Rev. B* **10** (1974) 398

[34] H. Over, G. Gilarowski, H. Niehus, *Surf. Sci. Lett.* **381** (1997) L619.

[35] M. Haruta, B.S. Uphade, S. Tsubota, A. Myamoto, *Res. Chem. Intermed.* **24** (1998) 329.

UNIVERSITAT ROVIRA I VIRGILI
NANOMATERIALS IN CATALYSIS: STUDY OF MODEL REACTIONS.
Ricardo José Chimentao
ISBN: 978-84-690-7618-7 / DL: T.1326-2007

Chapter II.4

Oxidation of Ethanol to Acetaldehyde over Na-promoted vanadium oxide catalysts

UNIVERSITAT ROVIRA I VIRGILI
NANOMATERIALS IN CATALYSIS: STUDY OF MODEL REACTIONS.
Ricardo José Chimentao
ISBN: 978-84-690-7618-7 / DL: T.1326-2007

II.4.1 Abstract

Sodium-promoted vanadium oxide catalysts supported on MCM-41 and TiO_2 (anatase) were investigated for the partial oxidation of ethanol to acetaldehyde. The catalysts were prepared by incipient wetness impregnation with a vanadium oxide content of 6 wt. %. The experimental characterization was performed by X-ray diffraction (XRD), N_2 adsorption, temperature programmed reduction (TPR), temperature programmed oxidation (TPO) of carbon deposits after reaction and diffuse reflectance UV-Vis. The presence of sodium plays a strong role in the dispersion and reducibility of the vanadium species as detected by temperature programmed reduction analysis and optical absorption spectroscopy. Additionally, temperature programmed oxidation of the spent catalysts revealed an increase in the Na loading decreases the carbon deposition during reaction. In the case of the catalysts supported on MCM-41 these modifications were mirrored by an increase on the activity and selectivity to acetaldehyde. In contrast, in the VO_2/TiO_2 catalysts the catalytic activity decreased as the sodium content in the catalyst augmented. A model in which sodium plays a strong role on the morphology of the vanadia species has been proposed to explain all these observations.

Keywords: Vanadium oxide; oxidation; ethanol; MCM-41; TiO_2; Na; DRS-UV-Vis, XRD, TPO.

UNIVERSITAT ROVIRA I VIRGILI
NANOMATERIALS IN CATALYSIS: STUDY OF MODEL REACTIONS.
Ricardo José Chimentao
ISBN: 978-84-690-7618-7 / DL: T.1326-2007

II.4.2 Introduction

Catalysts based on supported vanadium oxides are known to be active and selective for a number of industrially important reactions, including the selective oxidation reactions of *o*-xylene [1-4], ammoxidation of hydrocarbons [5], and selective reduction of NO_x with NH_3 in the presence of O_2 [6- 9]. In these catalysts Al_2O_3, SiO_2, TiO_2, MgO and ZrO_2 are commonly used as the supports [10- 12]. In fact, it well known that the support plays an important role in both activity and selectivity of vanadium oxide catalyst affecting the morphology of the dispersed surface metal oxide phase. For instance, vanadium oxide supported on titanium oxide (anatase) is one of the best catalytic systems for the selective oxidations. The spreading of vanadia over the TiO_2 support leads to a modification of the chemical physical properties of the former and to an enhancement of its catalytic properties [13, 14]. It has been proposed that the essential role of the anatase is to favor the formation of a stable VO_x monolayer [15]. By contrast to TiO_2 the interaction of vanadia species with SiO_2 is weak and, therefore the properties of VO_x species over SiO_2 are different, showing higher tendency for thermally induced aggregation and a low dispersion of the active phase [16, 17]. Indeed, in silica, isolated vanadium sites are formed just at low vanadium content (below 1- 5 wt.%), while at higher loading polymeric species and even crystalline V_2O_5 species containing a large number of V-O-V entities are observed [18]. The presence of polymerized vanadium species may have not only a detrimental influence on the selectivity but may also exert a negative effect on the catalyst activity, due to the presence of vanadyl centers which are no accessible to the reactant molecules. It is clear that in order to obtain a more active and selective vanadium based catalysts high dispersion of

UNIVERSITAT ROVIRA I VIRGILI
NANOMATERIALS IN CATALYSIS: STUDY OF MODEL REACTIONS.
Ricardo José Chimentao
ISBN: 978-84-690-7618-7 / DL: T.1326-2007

vanadium oxide species even at high vanadium loadings should be achieved. Therefore, great efforts have been dedicated toward the potential applications of high surface area materials as supports for dispersing vanadium oxide [19, 20].

Among these high surface area supports the discovery of the family of siliceous mesostructured materials have attracted much attention as catalyst supports since they posses high surface areas (> 800 m^2 g^{-1}) and good thermal stability as well as hexagonal channels (2-8 nm) with tunable pore sizes [21, 22]. In spite of these advantages there are very few references in the literature about the use of mesoporous silicates as supports for vanadium oxide species. For instance, Kondratenko and coworkers have reported relatively high dispersions of vanadia species on MCM-41 at up to 5.3 wt % loadings [23]. And recent studies of suported vanadium oxides on mesoporous silicas have revealed that such materials show unusual activity and selective for oxidative dehydrogenation reactions [24, 25].

In the case of oxidation reactions it is well accepted that the redox properties of the catalyst play a fundamental role on activity [26, 27], and for the particular case of metal oxide catalysts alkaline metals are observed to enhance the redox activitiy [28]. Indeed, the promotion of vanadium oxide with alkali compounds or basic oxides and their effect for catalytic performance in different reactions has been subject of several studies [29]. For instance, the addition of potassium to vanadia catalysts influences the activity of surface vanadia species by retarding its redox potential and simultaneously increasing its selectivity in oxidation reactions [30]. An explanation has been proposed attributing electropositive properties to the alkaline ions which will weaken chemisorption of electron donor adsorbates, as they themselves are

UNIVERSITAT ROVIRA I VIRGILI
NANOMATERIALS IN CATALYSIS: STUDY OF MODEL REACTIONS.
Ricardo José Chimentao
ISBN: 978-84-690-7618-7 / DL: T.1326-2007

electron donors [31]. More recent, studies of the partial oxidation of toluene to their corresponding aldehydes on alkali metal-containing vanadia catalysts have shown that toluene conversion and aldehyde selectivity is a function of the alkali cation size [32, 33]; which seems to be in line with the electronic effect hypothesis

In the present communication we investigate the effect of sodium on the catalytic behavior of vanadia catalysts supported on mesoporous silica (MCM-41) and TiO_2 (anatase) using the partial oxidation of ethanol to acetaldehyde. The materials were characterized XRD, N_2 adsorption, diffuse reflectance UV visible, temperature-programmed reduction (TPR) and temperature-programmed oxidation (TPO). The role of the effect of the Na on the vanadium dispersion and the catalytic activity of the catalyst were evaluated, leading to relevant structure-function relationships for the investigated reaction over this catalytic system.

II.4.3 Experimental

II.4.3.1 Preparation of Catalysts

Catalysts were prepared by depositing vanadium on the supports by incipient wetness impregnation. The supports used were TiO_2 and MCM-41. The TiO_2 support was in the anatase crystalline form (Alpha Aesar) with a surface area (S_{BET}) of 60 $m^2\ g^{-1}$. The mesoporous MCM-41 support was obtained from Mobil. The Na promoted catalysts were prepared by incipient wetness impregnation of the supports with aqueous solution of $NaNO_3$ prior to the impregnation of the vanadium oxide preocursor. The resultant solids were by dried and then calcined in a muffle at 773 K overnight. Catalysts were prepared with different

UNIVERSITAT ROVIRA I VIRGILI
NANOMATERIALS IN CATALYSIS: STUDY OF MODEL REACTIONS.
Ricardo José Chimentao
ISBN: 978-84-690-7618-7 / DL: T.1326-2007

Na/V molar ratios in the range 0 – 2, and the amount of $NaNO_3$ added to the MCM-41 was varied accordingly. Vanadium was introduced in the Na-doped supports by incipient wetness using a vanadyl oxalate aqueous solution. The amount of vanadium in the aqueous solution corresponds to the one needed to get a loading of 6 wt. % V_2O_5. The resultant solids were finally dried at 383 K for 12 h and calcined in dry air at 673K for 3h.

II.4.3.2 Catalyst Characterization

N_2 adsorption. N_2 adsorption-desorption isotherms at 77 K were measured using a Micromeritics TriStar 3000 equipment. Before the analysis the samples were degassed (1.33×10^{-2} Pa) at 473 K. The specific area was calculated following the method of Brunauer, Emmet, and Teller (BET). The BJH method was used to determine the pore size distribution (PSD).

X-ray diffraction. X-ray diffraction (XRD) measurements were made using a Siemens D5000 diffractometer (Bragg-Bentano parafocusing geometry and vertical θ-θ goniometer) fitted with a grazing incident (ω: 0.52^0) attachment for thin film analysis and a scintillation counter as a detector. The V-MCM-41 and V-TiO_2 catalysts were dispersed on Si (510) sample holder. The angular 2θ diffraction range was between 1^0 to 10^0 and 10^0 to 120^0. The data were collected with an angular step of 0.03^0 at 12 s per step and sample rotation. $Cu_{K\alpha}$ radiation (λ = 1.54056 Å) was obtained from a copper X-ray tube operated at 40 kV and 30 mA. The crystalline phases were identified using the JCPDS files.

UNIVERSITAT ROVIRA I VIRGILI
NANOMATERIALS IN CATALYSIS: STUDY OF MODEL REACTIONS.
Ricardo José Chimentao
ISBN: 978-84-690-7618-7 / DL: T.1326-2007

H_2-TPR. Temperature programmed reduction was performed using a Thermo Finnigan instrument TPD/R/O/1100, equipped with a thermal conductivity detector (TCD) and coupled to a mass spectrometer QMS 422 Omnistar. Typically the sample (40 mg) was first pretreated in a quartz reactor with a gas flow containing O_2 and N_2 at 673 K for 1 h followed by purging in UHP argon. After the sample was cooled to 323 K, an H_2-Ar (5 vol% H_2) mixture was introduced into the reactor and the temperature was raised to 1073 K at a rate of 10 K min^{-1} at a flow of 20 ml/min. The amount of hydrogen consumed (in mmol/g) was calculated by integrating the TCD signal intensities under the corresponding TPR peaks, using CuO as a reference.

Diffuse reflectance UV-visible spectra. The UV-Vis spectra were recorded on a Varian Cary-5000 spectrometer equipped with a diffuse reflectance accessory. The spectra were collected at 200- 800 nm with MgO as a reference. The sample cell was equipped with a heater unit, a thermocouple, and a gas flow system for in situ measurements. The samples were dehydrated in situ in air at 673 K for 30 minutes. The spectra were recorded upon cooling down to room temperature, with dry air flowing through the sample to avoid rehydration. The absorption edge energies for dehydrated spectra were determined by finding the intercept of the straight line in the low-energy rise of a plot of $[F(R\infty)h\upsilon]^{1/2}$ against $h\upsilon$ where $F(R\infty)$ is the Kubelka-Munk function and $h\upsilon$ is the energy of the incident photon [34, 35].

Temperature programmed oxidation (TPO) of the spent catalysts. TPO measurements of spent catalysts were performed to analyze the amount

UNIVERSITAT ROVIRA I VIRGILI
NANOMATERIALS IN CATALYSIS: STUDY OF MODEL REACTIONS.
Ricardo José Chimentao
ISBN: 978-84-690-7618-7 / DL: T.1326-2007

of carbon deposited on the catalysts after the reaction. The TPO experiments were carried out by passing a continuous flow of 2% O_2/He (Airgas, 99.99%) over a range of temperature between 323 and 1073 K with a heating rate of 0.2 $K.s^{-1}$. CO_2 and CO formed were quantitatively converted to methane in a methanator using 15%Ni/Al_2O_3 as catalyst and working at 673 K. Methane formation was measured by a flame ionization detector (FID) calibrated with 100 µl pulses of CO_2, and by combustion of known amounts of graphite.

II.4.3.3 Catalytic activity

The experiments were carried out at atmospheric pressure in a fixed bed microcatalytic reactor connected to an on-line Agilent 3000 micro GC, equipped with a temperature conductivity detector and a Plot Q column. Typically around 40 mg of catalyst were dispersed on a quartz frit and held in the middle of a quartz flow reactor (0.7 cm i.d.). All samples were treated in flowing dry air (0.8 $cm^3\ s^{-1}$) at 673K for 1 h before catalytic measurements. After reducing the temperature to 400 K , ethanol was introduced into the reactor by vaporizing it into a flowing mixture (80 sccm) of 5% O_2/He (Airgas) at 100.1 kPa and 370 K by controlled injection with a syringe pump to give a constant ethanol pressure (0.85 kPa). The outlet of the reactor to the micro GC was heated to avoid condensation of the products. The catalytic runs were performed in the temperature range 400-700 K. Conversion and selectivity to products were calculated on a carbon atom basis, expressed as a mol % ratio of ethanol transformed to ethanol fed, and a ratio of ethanol transformed to each product to the total ethanol transformed, respectively. The rate of partial oxidation of ethanol was calculated according to Eq (1) :

UNIVERSITAT ROVIRA I VIRGILI
NANOMATERIALS IN CATALYSIS: STUDY OF MODEL REACTIONS.
Ricardo José Chimentao
ISBN: 978-84-690-7618-7 / DL: T.1326-2007

$$r_{C_2H_6O} = \frac{F_t.\rho}{3600.M_w} C(C_2H_6O) \qquad (1)$$

where F_t is the total volumetric flow (cm^3_{STP}/min), ρ refers to the density of ethanol (g/cm^3), M_w molecular weigth of ethanol (g/mol) and $C(C_3H_6O)$ is the ethanol conversion. These rates were normalized by the molar amount of vanadium present in the catalyst.

II.4.4 Results

II.4.4.1 N_2 adsorption

The BET surface areas of V_2O_5/TiO_2 (V-TiO_2) and V_2O_5/MCM-41 (V-MCM-41) catalysts with different Na contents are shown in Table II.4.1. The addition of 6 wt. % of vanadium in MCM-41 produces a decrease in the BET surface area from 700 to 645 m^2/g. The pore volume of the sample also decreases when vanadium was introduced on the MCM-41 support (from 1.25cm^3/g to 0.95 cm^3/g). Table II.4.1 also shows the average pore diameter of the samples.

Pure MCM-41 shows the highest average pore diameter (around 6.1 nm). When vanadium was introduced the average pore diameter decreases up to 5.8 nm. The low decreases in both BET area and pore volume observed when the vanadium was introduced on the MCM-41 support indicates that the vanadium species are probably located inside the channels, coating the w alls of the mesoporous matrix of the MCM-41. Further decrease was also observed in BET surface areas, pore volume and average pore diameter when Na was present in the V_2O_5/MCM-41 sample.

UNIVERSITAT ROVIRA I VIRGILI
NANOMATERIALS IN CATALYSIS: STUDY OF MODEL REACTIONS.
Ricardo José Chimentao
ISBN: 978-84-690-7618-7 / DL: T.1326-2007

Table II.4.1 BET surface area and average pore diameter of the vanadium catalysts

Na/V Molar ratio	V_2O_5/MCM-41				V_2O_5/TiO_2		
	S_{BET} (m^2/g)	Vp (cm^3g^{-1})	D_{BJH} [a] (nm)	$d_{100} \rightarrow a_{100}$ [b] (Å)	S_{BET} (m^2/g)	Vp (cm^3g^{-1})	D_{BJH} [a] (nm)
Support	700	1.25	3.4	44.8→ 51.8	60	0.12	10
0	645	0.95	3.3	44.9→ 51.2	42	0.13	12
0.5	638	0.92	3.2	44.8→ 51.7	29	0.14	15
1.0	567	0.84	3.2	43.1→ 49.7	28	0.14	19
1.5	561	0.84	3.1	43.8→ 50.5	23	0.14	27
2.0	537	0.93	3.0	42.5→ 49.1	26	0.15	25

[a] The pore-size distribution (PSD) based on the BJH method

[b] Unit cell parameter values calculated using $a_0=2d_{100}/\sqrt{3}$

A slight decrease of BET area is observed for Na/V molar ratios lower than 1.0. Higher Na/V molar ratios (between 1.0 and 2.0) produce a sensible decrease in the surface area (from 645 m^2/g to 537 m^2/g). Besides, the addition of Na also causes a reduction of the average pore diameter and pore volume of the samples. Surprisingly, the sample with the highest amount of Na and the lowest BET area (537 m^2/g) shows an unexpected high average pore diameter (around 5.4 nm) and pore volume (0.93 cm^3/g). This could suggest that some pores of the sample are blocked due to the presence of Na.

Figure II.4.1 shows the N_2 adsorption-desorption isotherm and the corresponding pore size distribution curves of V_2O_5/MCM-41 catalysts with different Na loadings. These isotherms are characteristic of mesoporous solids with uniformly sized mesopores (type IV IUPAC classification) and exhibit an H1 hysteresis loop, which are typical to mesoporous materials.

UNIVERSITAT ROVIRA I VIRGILI
NANOMATERIALS IN CATALYSIS: STUDY OF MODEL REACTIONS.
Ricardo José Chimentao
ISBN: 978-84-690-7618-7 / DL: T.1326-2007

As the partial pressure increases ($P/P_0 > 0.25$), the isotherm exhibits an inflection characteristic of capillary condensation within the mesopores [36]. The addition of sodium did not significantly modify the textural properties of the MCM-41 catalysts. The pore size distribution of the V_2O_5/MCM-41 catalysts shows that the mesoporous structure of the support has been preserved after the Na addition. On the other hand, when the vanadium species were added in the TiO_2, the BET surface area decreased from 60 to 42 m^2/g. The surface area also shows a significant decrease upon increasing the sodium loading (see Table II.4.1).

II.4.4.2 X-ray diffraction

Figure II.4.2a shows the XRD patterns for the V_2O_5/MCM-41 catalysts at low diffraction angles. X-ray diffractograms of V-MCM-41 catalysts is characterized by three distinct Bragg reflections at low angles, indexed to (100), (110), (200) which are representative of MCM-41-type ordered materials with hexagonal arrangements of mesopores. This suggests that the mesoporous structure of MCM-41 was maintained after the introduction of sodium and vanadium species. Moreover it seems that the intensity of the d_{100} peak remains almost constant (inset of Figure II.4.2a) when vanadium and sodium species were loaded in the MCM-41. This indicates the absence
of the degradation of the hexagonal arrangement of the MCM-41 pores. This fact corroborates that the ordered hexagonal arrangement of the MCM-41 frameworks upon sodium introduction was maintained as observed by N_2 adsorption. However, compared to the pure MCM-41 the d_{100} and a_0 values for Na promoted V-MCM-41 materials show slight decrease as depicted in Table II.4.1. The decrease in a_0 values

UNIVERSITAT ROVIRA I VIRGILI
NANOMATERIALS IN CATALYSIS: STUDY OF MODEL REACTIONS.
Ricardo José Chimentao
ISBN: 978-84-690-7618-7 / DL: T.1326-2007

may be attributed to the coating of the pore wall of the silica mesoporous material by the vanadium and Na species [37].

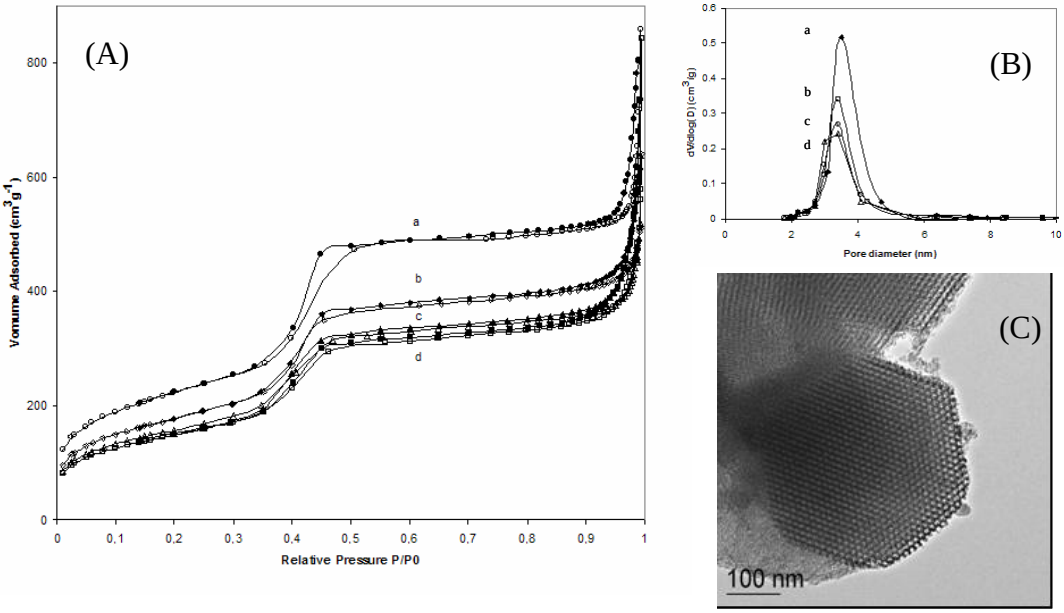

Figure II.4.1 (A) Nitrogen adsorption-desorption isotherms (a) V/MCM-41 (Na/V=0, ●: adsorption, o: desorption); (b) V/MCM-41 (Na/V=0.5, ♦:adsorption, ◊: desorption); (c) V/MCM-41 (Na/V=1.0, ▲: adsorption, Δ: desorption); (d) V/MCM-41 (Na/V=2.0, ■: adsorption, □: desorption). (B) Pore size distribution (PSD) profiles of the corresponding samples. (C) TEM image of the MCM-41 support.

All of the MCM-41 samples showed the same characteristics, demonstrating that the mesoporous structure of the MCM-41 support was preserved after the catalyst preparation process. More important, diffraction peaks are not observed at higher angles (Figure II.4.2b). These results indicate that the vanadia phases are highly dispersed on the surface of the silica support. For V_2O_5/TiO_2 catalyst, the crystallographic phases identified by X-ray diffraction were anatase

UNIVERSITAT ROVIRA I VIRGILI
NANOMATERIALS IN CATALYSIS: STUDY OF MODEL REACTIONS.
Ricardo José Chimentao
ISBN: 978-84-690-7618-7 / DL: T.1326-2007

(JCPDS File N0, 21-1272) and rutile phases (JCPDS File N0, 21-1276) of titania, respectively as shown Figure II.4.3. The presence of sodium vanadate phase was not detected. Again, diffraction peaks indicating the presence of crystalline vanadium oxides were not observed.

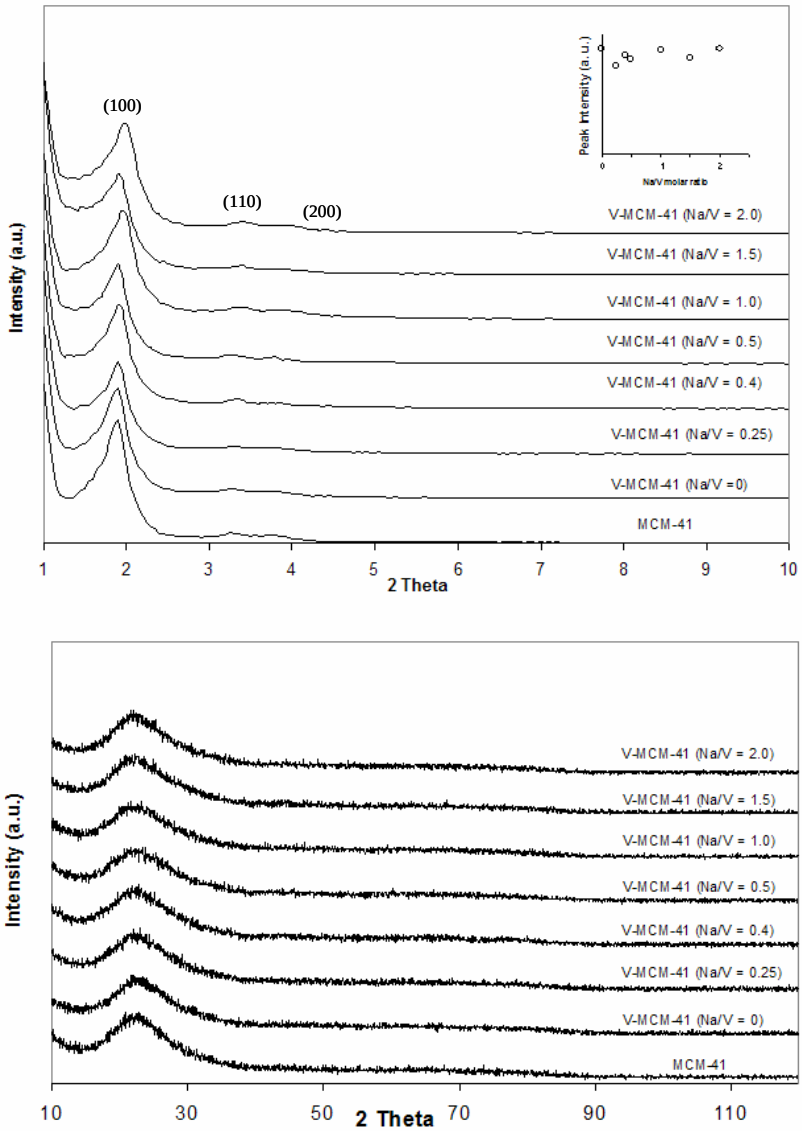

Figure II.4.2 X-ray diffraction patterns obtained for V_2O_5/MCM-41. (a) Low diffraction angles (1-10^0) and (b) High diffraction angles (10-120^0).

UNIVERSITAT ROVIRA I VIRGILI
NANOMATERIALS IN CATALYSIS: STUDY OF MODEL REACTIONS.
Ricardo José Chimentao
ISBN: 978-84-690-7618-7 / DL: T.1326-2007

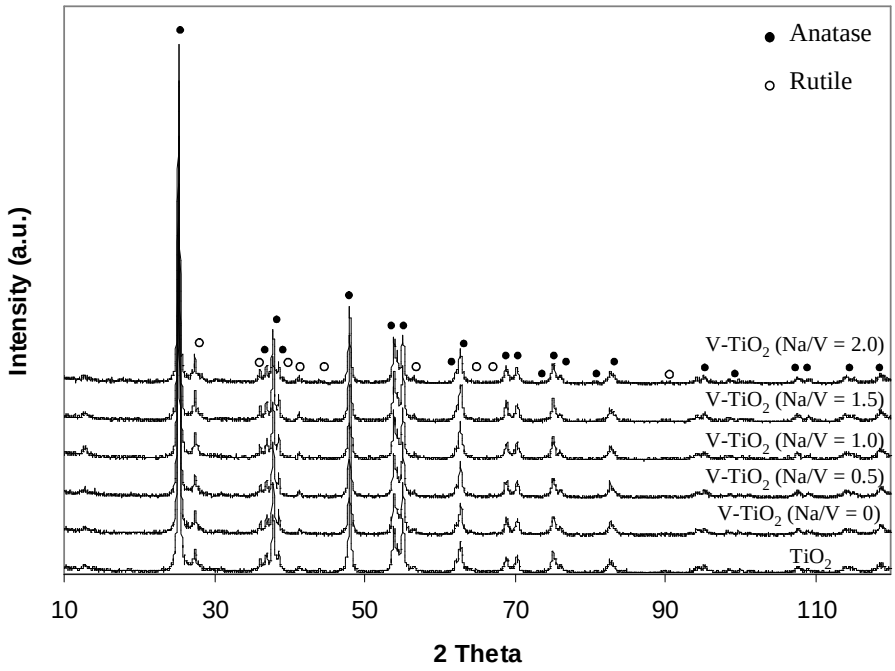

Figureure II.4.3. X-ray diffraction patterns obtained for the V_2O_5/TiO_2 catalysts.

II.4.4.3 Temperature programmed reduction (TPR)

The TPR experiments were carried out to determine the effect of Na on the redox properties of the vanadium species. No TPR studies were performed above 973K to avoid damage to the MCM-41 structure. TPR of the V_2O_5/MCM-41 and V_2O_5/TiO_2 catalyst with different Na loadings are shown in Figures II.4.4a and II.4.4b respectively. The single T_{max} obtained for all the V-MCM-41 samples may suggest a single step of reduction. Indeed, the TPR profile of the undoped V_2O_5/MCM-41 sample shows a single peak with a maximum around 820 K. Wachs and co-workers [38] have reported that the reduction peak of surface vanadium oxide highly dispersed on silica appears at

UNIVERSITAT ROVIRA I VIRGILI
NANOMATERIALS IN CATALYSIS: STUDY OF MODEL REACTIONS.
Ricardo José Chimentao
ISBN: 978-84-690-7618-7 / DL: T.1326-2007

around 800 K. This temperature is almost the same as that observed here for V_2O_5/MCM-41. Figure II.4.4a, also shows a shift to higher temperatures in the T_{max} as the Na/V molar ratio in the MCM-41 supported catalysts increases. This behavior is in agreement with the results obtained by Fierro et al. on K-promoted vanadia catalysts [30].

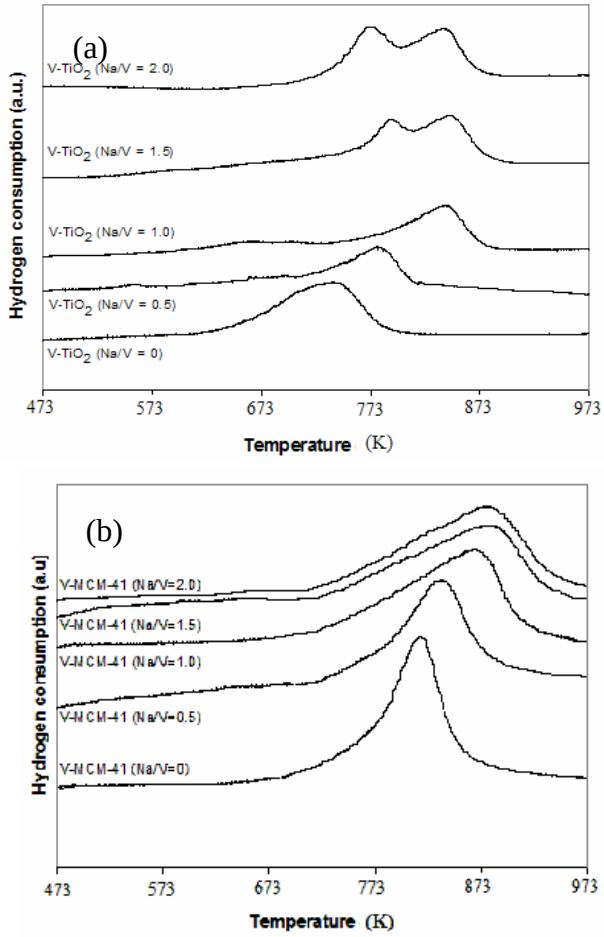

Figure II.4.4 TPR profiles for (a) V_2O_5/MCM-41 and (b) V_2O_5/TiO_2 catalysts.

The increase in the T_{max} value qualitatively reflects a decrease on the overall reducibility of the vanadium species supported on MCM-41.

UNIVERSITAT ROVIRA I VIRGILI
NANOMATERIALS IN CATALYSIS: STUDY OF MODEL REACTIONS.
Ricardo José Chimentao
ISBN: 978-84-690-7618-7 / DL: T.1326-2007

The single T_{max} obtained for the samples may suggest a single step of reduction of the V^{+5} to V^{+3}. However, it cannot be excluded that a fraction of V^{+4} is also present. Indeed, quantification of the hydrogen uptake (Table II.4.2) indicated a lower hydrogen consumption than the one necessary for a complete reduction of V^{+5} to V^{+3}. The progressive shift of peak maxima of H_2 consumption to higher temperatures with the Na loading may suggest a formation of less reducible vanadia species.

Table II.4.2 Position of the peak maxima and hydrogen comsuption (expressed as the V/H molar ratio) obtained from TPR analysis

Na:V Molar ratio	V_2O_5/MCM-41		V_2O_5/TiO_2	
	T_{max} (K)	V/H[a]	T_{max} (K)	V/H[a]
0	821	0.55	742	0.80
0.5	838	0.83	793	1.29
1.0	872	0.50	845	1.19
1.5	888	0.49	775, 856	1.23
2.0	885	0.59	795, 844	1.62

[a] mmol vanadium per mmol of hydrogen consumed

TPR of V_2O_5/TiO_2 catalysts are shown in Figure II.4.4b. Non-doped sodium sample shows a main reduction peak at around 740 K. This reduction temperature is lower than the obtained for non-doped V_2O_5/MCM-41 catalyst. This indicates that vanadium species are easier to reduce in titanium oxide than in MCM-41 support. This main peak also shows a shoulder at 725 K, that probably suggests the presence of more dispersed vanadium species [30]. At Na/V molar ratios of 1.5 and 2.0 two peaks in the TPR profiles were detected. The assignment of the two peaks in the V_2O_5/TiO_2 TPR profile can be ascribed to polymeric

UNIVERSITAT ROVIRA I VIRGILI
NANOMATERIALS IN CATALYSIS: STUDY OF MODEL REACTIONS.
Ricardo José Chimentao
ISBN: 978-84-690-7618-7 / DL: T.1326-2007

vanadium and isolated vanadium species, respectively [39- 41]. It is well known that the redox properties of the vanadia species species depend on their interaction with the support as well as on their domain size [29]. Hence, the progressive shift of peak maxima of H_2 consumption to higher temperatures for the V-MCM-41 and V-TiO_2 samples with the Na loading may clearly indicate the formation of less reducible vanadium species which could be consequence of a modification of either their interaction with the support or their domain size by sodium. Another possible explanation might be sodium acting as electron donor [31] increasing the electron density of vanadia and hence affecting its reducibility.

II.4.4.4 UV-visible spectroscopy

The information obtained on the band gap energy is particularly useful to evaluate the dispersion and local structure of supported VO_x species [42, 43]. Several methods have been proposed to estimate the band gap energy of vanadium oxide compounds by using optical absorption spectroscopy. A general power law form has been suggested by Davis and Mott [44] which relates the absorption coefficient with the photon energy. The order of this power function is determined by the type of transition involved. However, in the case of vanadium oxide species it seems that this choice is based mostly on the best linear fit of the energy gap curve [45, 46] Barton, *et al.* [47] have recommended using the square root of the Kubelka-Munk function multiplied by the photon energy. By plotting this new function versus the photon energy, the position of the absorption edge can then be determined by extrapolating the linear part of the rising curve to zero. The values thus obtained

UNIVERSITAT ROVIRA I VIRGILI
NANOMATERIALS IN CATALYSIS: STUDY OF MODEL REACTIONS.
Ricardo José Chimentao
ISBN: 978-84-690-7618-7 / DL: T.1326-2007

carry information about the average domain size of the oxide nanoparticles since, as for the case of a particle in a box, the band gap energy decreases as the domain size increases [48].

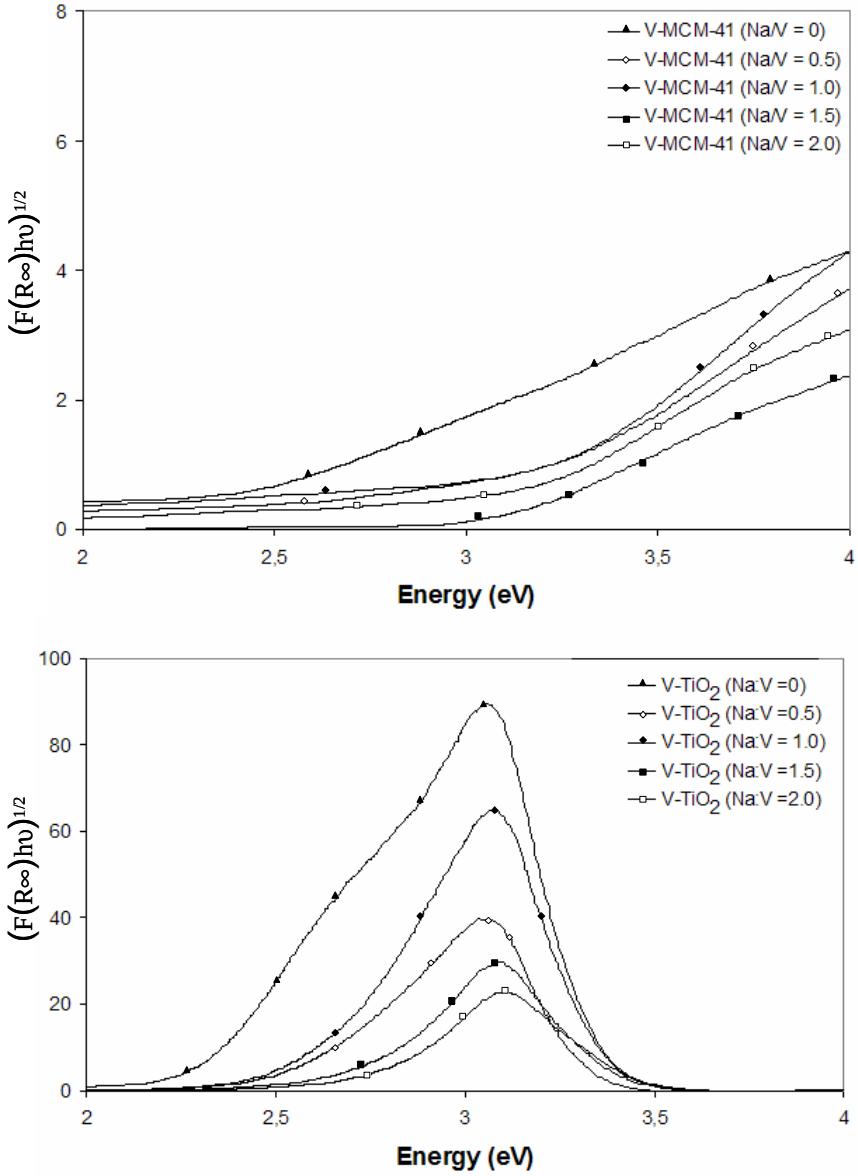

Figure II.4.5 Optical absorption spectra expressed as function of the photon energy for (a) V_2O_5/MCM-41 and (b) V_2O_5/TiO_2 catalysts.

UNIVERSITAT ROVIRA I VIRGILI
NANOMATERIALS IN CATALYSIS: STUDY OF MODEL REACTIONS.
Ricardo José Chimentao
ISBN: 978-84-690-7618-7 / DL: T.1326-2007

Typical diffuse reflectance UV-Vis. spectra obtained for the samples of the present study are shown in Figure II.4.5. The absorption band reflects a ligand to metal charge transfer band (LCT) transition [49]. The results obtained for the band gap energy are reported in Figure 6 as a function of the Na/V molar ratio in the catalysts. The V_2O_5/MCM-41 samples (Figure II.4.5a) exhibit band gap energy values between 2.3 and 3.1 eV. The addition of sodium up to a Na/V molar ratio of 0.5 produces and increase in the edge energy. Further sodium loading did not produced ulterior edge energy increase.

For the case of the undoped V_2O_5/TiO_2 (Figure II.4.5b) samples an edge energy value around 2.3 eV was observed. This indicate the formation of highly agglomerated vanadyl species; this apparently surprising result might be rationalized taking into account the high vanadium loadings in the catalyst and the high surface area of the mesopours (700 m^2/g) with respect to the TiO_2 support (60 m^2/g).

As mentioned above, for both supports an increase in the gap energy values is observed when the amount of Na in the catalysts increases, as depicted in the Figure 6. While for the undoped catalyst the energy gap lies close to the values corresponding to highly polymerized vanadium oxide [46]; for doped catalysts the energy gap shifts to higher values, indicating a decrease in the number of next nearest neighbors of the VO_x species of the vanadia domains [50]. These band energy values (E_g ~ 3.1 eV) indicate the formation of isolated surface VO_4 species, perhaps in the form of a non-stoichometric surface sodium vanadate [51]; it is clear then that the dispersion of oxidic vanadium species is deeply influenced by the presence of sodium.

UNIVERSITAT ROVIRA I VIRGILI
NANOMATERIALS IN CATALYSIS: STUDY OF MODEL REACTIONS.
Ricardo José Chimentao
ISBN: 978-84-690-7618-7 / DL: T.1326-2007

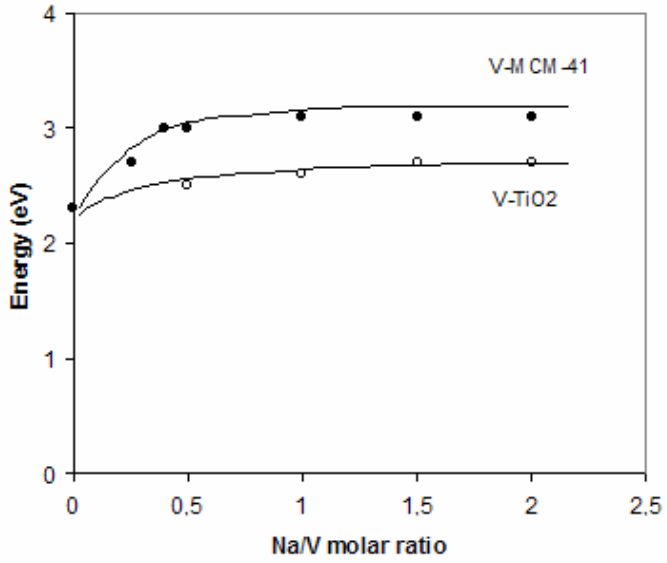

Figure II.4.6 Band gap energy values obtained from the optical absorption spectra for V_2O_5/MCM-41 and V_2O_5/TiO_2 catalysts as a function of the Na/V molar ratio on the catalysts.

II.4.4.5 Catalytic Activity for partial oxidation of ethanol

The partial oxidation of ethanol to acetaldehyde was used to evaluate the catalytic activity of the vanadium SiO_2 and TiO_2 catalysts. A blank test run with the MCM-41 and TiO_2 supports showed no conversion of ethanol at the reaction temperature (523 K). When running the vanadium catalysts the only products observed were acetaldehyde and ethylene. Combustion products (CO and CO_2) were not observed. Figure II.4.7 shows steady-state ethanol oxidation rates per V atom and the selectivity to acetaldehyde as a function of time on stream using different space velocities (SV) for V_2O_5/MCM-41 samples These data show that the ethanol partial oxidation rates are strongly influenced by the amount of sodium dopant. Moreover, the presence for sodium seems to affect the selectivity to acetaldehyde as well. Figure II.4.7a

UNIVERSITAT ROVIRA I VIRGILI
NANOMATERIALS IN CATALYSIS: STUDY OF MODEL REACTIONS.
Ricardo José Chimentao
ISBN: 978-84-690-7618-7 / DL: T.1326-2007

also show that, with increasing of SV the conversion of ethanol decreases although as Figure II.4.7b indicates the selectivity was not affected by the space velocity.

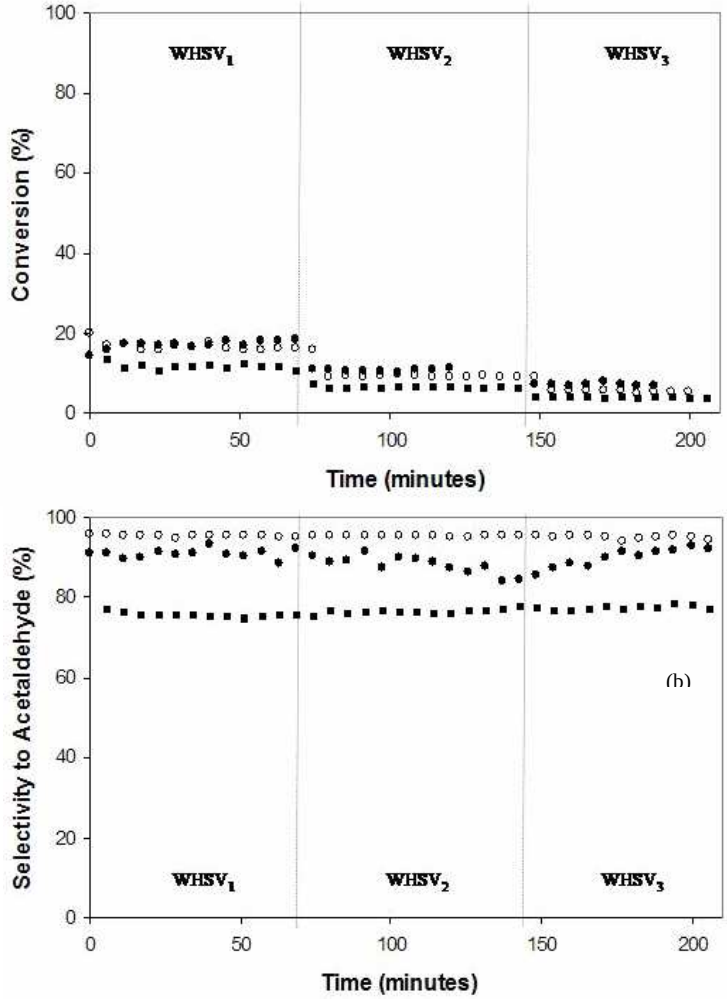

Figure II.4.7 Catalytic activity data of the V-MCM-41 sample with different Na/V molar ratios (■ Na/V =0; o Na/V=0.5 and • Na/V= 1.0). (a) Conversion of ethanol and (b) selectivity to acetaldehyde as a function of time on stream using different weight hourly space velocities (WHSV); $WHSV_1$= 96.84 (mol ethanol/mol V.h); $WHSV_2$=193.68 (mol ethanol/mol V.h); $WHSV_3$=338.94 (mol ethanol/molV.h).

UNIVERSITAT ROVIRA I VIRGILI
NANOMATERIALS IN CATALYSIS: STUDY OF MODEL REACTIONS.
Ricardo José Chimentao
ISBN: 978-84-690-7618-7 / DL: T.1326-2007

A more rigorous comparison of intrinsic reactivity requires that we extrapolate measured rates to zero reactant conversion; these rates are shown in Figure II.4.8 as a function of the Na loading in the catalyst, for both MCM-41 and TiO_2 supports. For the case the MCM-41 (Figure II.4.8a) catalyst partial oxidation rates increased as the amount of Na increases in the catalyst until they reached a maximum at Na/V molar ratios close to 0.5, then they begin to drop again as the amount of Na dopant keeps increasing. A contrasting behavior was observed in the case of the TiO_2 supported materials (Figure II.4.8b). In this case a monotonically decrease on activity was observed as the amount of Na increases on the catalyst. Figure II.4.9 depicted the initial selectivities (extrapolated at zero conversion) to aceltadehyde and ethylene for the V-MCM-41 and V-TiO_2 catalysts. For the case of the TiO_2 catalyst almost total selectivity of aceltadehyde was observed under our reaction conditions and this was not affected by the presence of sodium. However for the case of the MCM-41 supported catalyst a gradual enhancement in the selectivity to aceltadehyde was observed as the amount of Na increased in the catalyst. After a value of 1 is obtained for the Na/V molar ratio the selectivity to aceltadehyde reaches its maximum and then continuous addition of Na to the catalyst did not improve the selectivity but, as Figure II.4.8 shows takes a toll on the activity for partial oxidation. Moreover this increase in selectivity observed in the MCM-41 supported materials is at the expense of the generation of ethylene. Indeed as FigureII.4.9 clearly shows, the increase on the selectivity to acetaldehyde is followed by a simultaneous decrease in the selectivity to ethylene.

UNIVERSITAT ROVIRA I VIRGILI
NANOMATERIALS IN CATALYSIS: STUDY OF MODEL REACTIONS.
Ricardo José Chimentao
ISBN: 978-84-690-7618-7 / DL: T.1326-2007

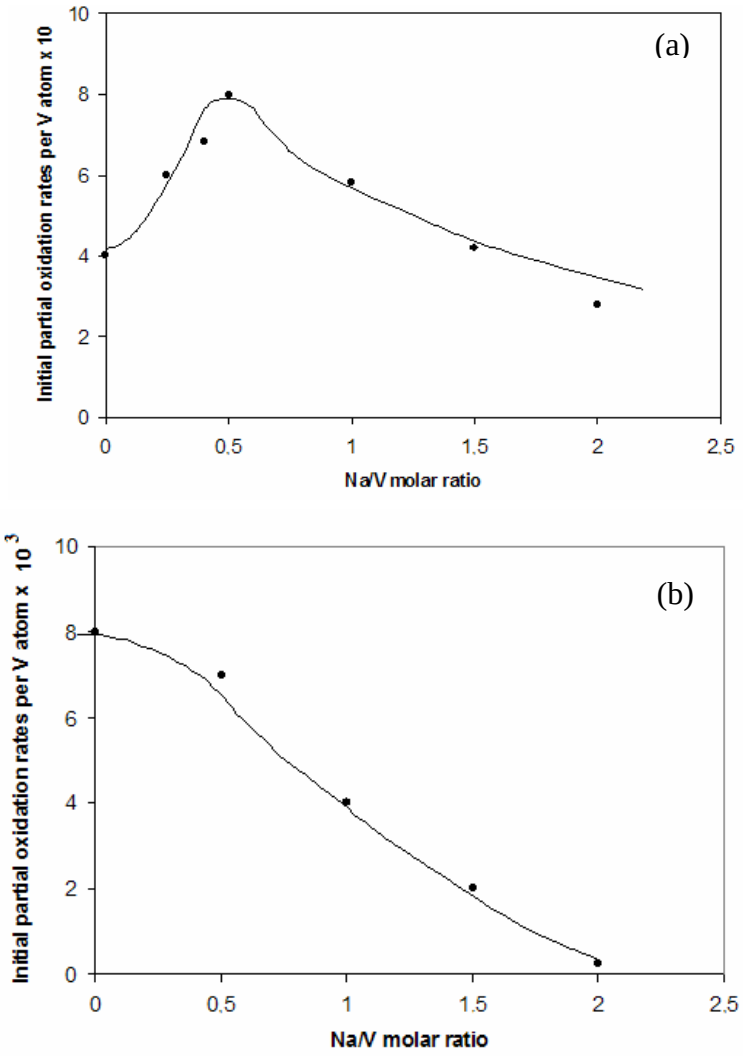

Figure II.4.8 Initial partial oxidation rates normalized by the amount of vanadium present in the catalyst as a function of the Na content for the (a) V_2O_5/MCM-41 and (b) V_2O_5/TiO_2 catalyst series.

UNIVERSITAT ROVIRA I VIRGILI
NANOMATERIALS IN CATALYSIS: STUDY OF MODEL REACTIONS.
Ricardo José Chimentao
ISBN: 978-84-690-7618-7 / DL: T.1326-2007

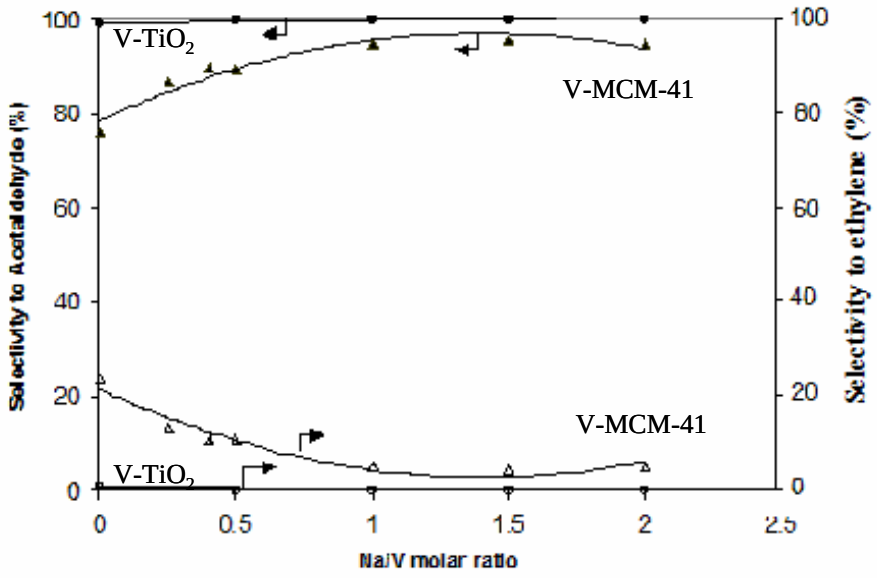

Figure II.4.9 Initial selectivities to acetaldehyde and ethylene observed for the V_2O_5/MCM-41 and V_2O_5/TiO_2 catalysts as a function of the Na content.

II.4.4.6 Temperature Programmed Oxidation (TPO)

TPO can be used to probe carbonaceous deposits on catalyst surfaces. The analysis of the CO_2/CO evolved allows both qualitative and quantitative assessments of the type and reactivity of these deposits [52]. TPO measurements detected significant amounts of carbon deposited in the catalyst after partial oxidation of ethanol. Figure II.4.10 shows the amount of carbon in the V-MCM-41 and V-TiO_2 samples determined by TPO as a function of the Na/V ratio on the catalyst. For all samples the addition of Na decreased the amount of carbon deposited after reaction. However a plateau in the amount of carbon deposits is apparent for molar Na/V ratios in the 0.5-1.5 range.

UNIVERSITAT ROVIRA I VIRGILI
NANOMATERIALS IN CATALYSIS: STUDY OF MODEL REACTIONS.
Ricardo José Chimentao
ISBN: 978-84-690-7618-7 / DL: T.1326-2007

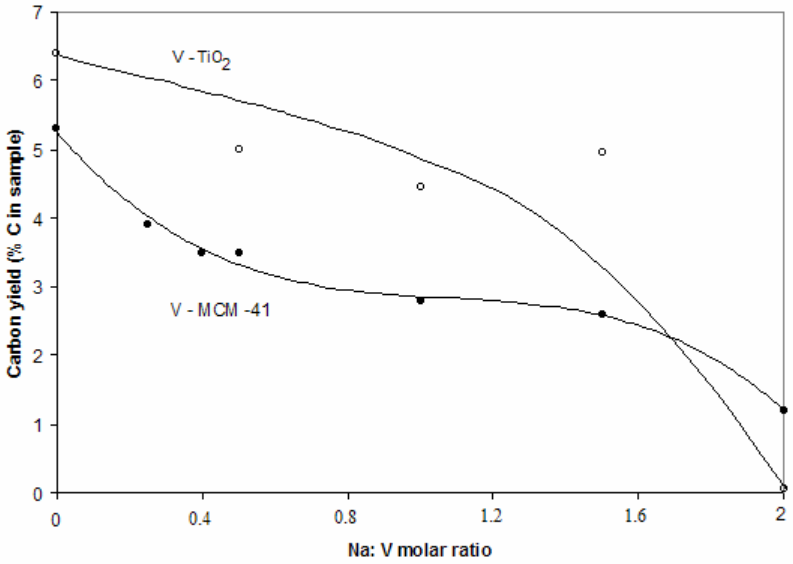

Figure II.4.10 Amount of carbon deposits (weight % of C in the sample) as determined by TPO analysis of the spent V_2O_5/MCM-41 and V_2O_5/TiO_2 catalysts.

II.4.5 Discussion

From the results described above it is clear that the presence of sodium influences the catalytic activity on both MCM-41 and TiO_2 supported materials, however the extent of the modification of the catalytic materials seems to depend on both the Na loading and the support itself. First, from the XRD results it is clear that in both supports highly dispersed surface VO_x species are present. On the basis of our XRD results for the V-MCM-41 samples it was suggested that the MCM-41 mesoporous structure was preserved in all samples after introduction of vanadium and sodium species. BET of the V-MCM-41 material also showed that in the presence of vanadium and sodium species, the mesoporous channels remain accessible. However, the main pore

UNIVERSITAT ROVIRA I VIRGILI
NANOMATERIALS IN CATALYSIS: STUDY OF MODEL REACTIONS.
Ricardo José Chimentao
ISBN: 978-84-690-7618-7 / DL: T.1326-2007

diameter decreased significantly (Table II.4.1, the main pore size decreased of ≈ 11 %). This last observation suggests that vanadium and sodium species are probably locate inside the channels, coating the walls of the mesoporous matrix. Indeed, these results are backed up by the optical absorption experiments which indicated the presence of relatively high dispersed vanadia species on the catalyst. The catalytic activity results showed that the performance of V-MCM-41 and V-TiO_2 catalysts in the oxidative dehydrogenation of ethanol was also dependent on the dispersion of VO_x species on the catalyst surface. In our experimental conditions a small amount ethylene was formed on V-MCM-41 catalysts. Previous reports indicate that ethylene is usually formed through a parallel route in which catalytic sites of acidic nature present on the VO_x domains play a significant role. The presence of these very active acidic catalytic sites, responsible for ethylene formation, are usually linked to vanadium oxide domains which are not interacting strongly with the support [53]. Accordingly, Bond and Flamerz [54] have reported that when vanadia strongly interacts with the support faster rates for dehydrogenation than for dehydration are observed. The exact nature of the proposed acidic sites is still under discussion in the literature; although G. Fierro [55] using XPS has proposed that these sites can be identified as V^{+5} cations coordinating to hydroxyl groups. In line with these studies, the formation of ethylene observed in our V-MCM-41 catalysts indicates the presence of acidic sites in these materials, which indeed are very active for dehydration. These acidic sites seem not to be present on the TiO_2 supported materials since ethylene was not observed. The evaluation of catalytic properties of the Na-doped catalyst reported on this work provides strong evidence of role of the sodium on the V-TiO_2 catalysts;

UNIVERSITAT ROVIRA I VIRGILI
NANOMATERIALS IN CATALYSIS: STUDY OF MODEL REACTIONS.
Ricardo José Chimentao
ISBN: 978-84-690-7618-7 / DL: T.1326-2007

particularly at higher Na contents. Indeed the initial catalytic rates observed for the V-TiO_2 samples decreased with the Na content (Figure II.4.8b); while the UV-DRS and TPR results clearly indicated that when the sodium loading increased the vanadium species formed highly dispersed but very refractory sodium vanadate (Fig. II.4.5a and Table II.4.2 respectively). Figure II.4.11 illustrates this dependence on the dispersion (expressed as the UV-visible absorption edge energy) for the V-MCM-41 and V-TiO_2 samples respectively. For the V-TiO_2 catalysts (Figure II.4.11b) the initial rates decreased with the increase in the edge energy, i.e. decrease in dispersion. This decrease on the number of active vanadium species may be the reason for the decline on the catalytic activity and also for the lack of change on the selectivity toward acetaldehyde; i.e vanadium oxides species are been disengaged from the catalytic cycle by sodium however those still active do not suffer from any modification by sodium and the selectivity remains unaffected. On the other hand, the differences in the amount of carbonaceous deposits observed for the TiO_2-supported series seem to be related to an increase on the resistance to carbon deposition during acetaldehyde formation as depicted in the Figure II.4.10. Indeed, it is well known that a number of alkali metal oxides can promote carbon gasification, these processes usually involving oxygen transfer steps in which the catalyst participates in a redox cycle between stoichiometric and substoichiometric oxide species [56]. However this increase on the resistance to carbon deposition does not seem to play an important role on the overall catalytic performance of the TiO_2 supported catalyst. A contrasting behaviour is displayed by the V-MCM-41 catalysts. In this case a steady increase on the catalytic activity is observed when the sodium

UNIVERSITAT ROVIRA I VIRGILI
NANOMATERIALS IN CATALYSIS: STUDY OF MODEL REACTIONS.
Ricardo José Chimentao
ISBN: 978-84-690-7618-7 / DL: T.1326-2007

content increases up to Na/V = 0.5 molar ratio; beyond this limit the activity decreased progressively as the amount of Na present on the catalyst increases (Figure II.4.8a). These changes in activity were also intimately correlated to the changes in the edge energies values and reducibility observed in the DRS-UV Vis and TPR experiments respectively (Figs. II.4.11a and II.4.4a respectively). Indeed when the amount of sodium increases in the catalyst the edge energy values shifted to larger values, indicating a dispersion of the vanadium oxides species as showed in Figure II.4.11a., Moreover, in contrast to the case of the TiO_2 support, in this case the amount of reducible vanadium oxide species (obtained form the quantification of the H_2 uptake) does not present a monotonic decrease, but a minimum at Na loading values (Table II.4.2 V/H values) that correlate well with the maximum observed in activity as depicted in Figure II.4.8a. At high Na loadings (Na/V > 0.5), a fraction of the vanadium species may become refractory surface sodium vanadates and thereof unreducible and in a similar way as the case of the TiO_2 catalyst the activity decreases. In fact, since repetitive redox cycles occur during the oxidative dehydrogenation of ethanol it also can be suggested that the decrease on the reducibility observed for the doped VO_x/TiO_2 catalysts indicates that for these samples the re-reduction is more difficult than for the undoped ones. This may be another reason for the lower activity of the doped vanadium catalysts particularly at highest Na/V molar ratios. It becomes clear then that the reducibility of the vanadium species is dependent on the amount of sodium present on the catalyst but also on their domain size. However these observations do not explain the decrease in the amount of carbon deposits or changes on selectivity observed on the catalysts when Na is added. These observations have to

UNIVERSITAT ROVIRA I VIRGILI
NANOMATERIALS IN CATALYSIS: STUDY OF MODEL REACTIONS.
Ricardo José Chimentao
ISBN: 978-84-690-7618-7 / DL: T.1326-2007

be explained proposing a decrease in the surface acidity of the catalyst generated by Na titration [57]. In other words, the selectivity of ethanol to acetaldehyde was enhanced by basic promotion. The decrease in the acidity can be due to elimination of Bronsted acidic centers via replacing surface protons with the alkaline cations [29]. The sodium promotion may play the following pivotal roles in the increasing of the catalytic performance of the MCM-41 catalysts: increasing the activity by raising the dispersion of vanadium species and eliminating the surface acidity thereby preventing the dehydration route. Furthermore, the decrease in the dehydration route as already mentioned can also explain the decrease in the carbon deposition observed for the vanadium catalysts supported on MCM-41 and TiO_2 materials with the increase of the sodium content since it is expected that dehydrogenated species may suffer polymerization forming carbon deposits on the catalyst surface. The lower amounts of carbon deposits observed in our TPO results confirms that an increase in the sodium content decreased the activity for dehydrogenation and clearly decreased the amount of acid sites.

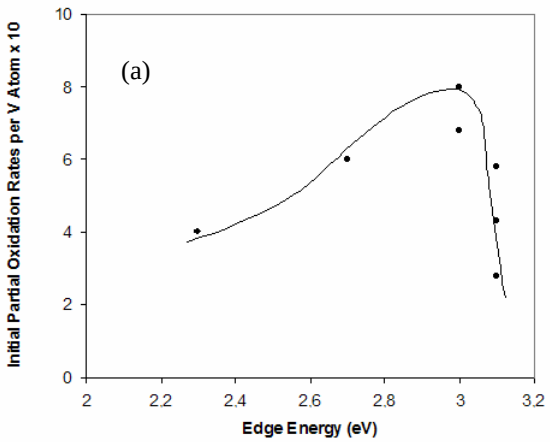

UNIVERSITAT ROVIRA I VIRGILI
NANOMATERIALS IN CATALYSIS: STUDY OF MODEL REACTIONS.
Ricardo José Chimentao
ISBN: 978-84-690-7618-7 / DL: T.1326-2007

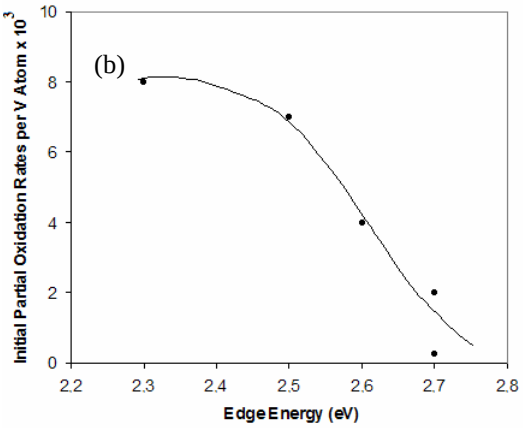

Figure II.4.11 Initial partial oxidation rates normalized by the amount of vanadium present in the catalyst as a function of the edge energies obtained for the (a) V_2O_5/MCM-41 and (b) V_2O_5/TiO_2 catalysts.

II.4.6 Conclusion

Vanadium (V) oxide supported on mesoporous silica (MCM-41) and TiO_2 (anatase) promoted by sodium were investigated in the partial oxidation of ethanol to acetaldehyde. These results were correlated with the nature of the vanadia species formed, particularly at intermediate sodium contents. The optical absorption and TPR experiments indicated that as the sodium content increased the dispersion of the vanadium species is further enhanced, affecting their reducibility as well. Moreover, for the case of the silica support the acid/bases properties of the catalyst are also affected as the TPO results and the variation on selectivity indicated. These results indicate the feasibility of mesoporous materials for catalyst support and how the selectivity of the catalyst can be changed by Na doping.

Acknowledgement. This work was supported by U. S. Department of energy (DOE), Office of Basic energy Sciences, Division of Chemical Sciences. The research was performed in the Environmental Molecular

Sciences Laboratory, a national scientific user facility sponsored by the DOE. Office of Biological and Environmental Research and located at the Pacific Northwest National Laboratory. The TPR and XRD experiments were carried out at the Universitat Rovira y Virgili (URV) at Tarragona (Spain). The URV experiments were funded by a grant from the the Ministerio de Ciencia y Tecnologia (Spain) under Projects REN2002-04464-CO2-01 and PETRI 95-0801.OP.

II.4.7 References

[1] B. Grzybowska-Swierkosz, Appl. Catal. A 157 (1997) 263.

[2] K. V. Narayana, A. Venugopal, K. S. Rama Rao, S. Khaja Mastahn, V. Venkat Rao, Appl. Catal. A 167 (1998) 11.

[3] C. R. Dias, M. F. Portela, G. C. Bond, J. Catal. 157 (1995) 344.

[4] T. Mongkhonsi, L. Kerhenbaun, Appl. Catal. A 170 (1998) 33.

[5] G. Centi, Appl. Catal. A 147 (1996) 267.

[6] M.D. Amiridis, I. E. Wachs, G. Deo, J.-M. Jejng. D. S. Kim, J. Catal. 161 (1996) 247.

[7] L. Casagrand, L. Lietti, I. Nova, P. Forzatti, A. Baiber, Appl. Catal. B 22 (1999) 63.

[8] O. Zegaoui, C. Hoang-Van, M. Karroua, Appl Catal. B 9 (1996) 211.

[9] M.A. Reiche, E. Ortelli, A. Baiker, Appl Catal. B 23 (1999) 187.

[10] Y. Murakami, M. Inomata, K. Mori, T. Ui, K. Susuki, A. Miyamoto, T. Hattori, in: Preparation of Catalysts III. (G. Poncelet, P. Grange, and P. A. Jacobs, Eds), p. 531, elsevier Amsterdam, 1983.

UNIVERSITAT ROVIRA I VIRGILI
NANOMATERIALS IN CATALYSIS: STUDY OF MODEL REACTIONS.
Ricardo José Chimentao
ISBN: 978-84-690-7618-7 / DL: T.1326-2007

[11] J. Kijenski, A. Baiker, M. Glinski, P. Dollenmeier, A. Wokaun, J. Catal. 101 (1986) 1.

[12] I. E. Wachs, F. D. Hardcastle in, Proceedings of the 9th International Congress on Catalysis, Calgary, 1988, (M. J. Philips and M. Ternan, eds) Vol. 3, p1449, Chem. Inst. Canada Ottawa, 1988.

[13] X. Wang, I. E. Wachs, Catal. Today 96 (2004) 211.

[14] I.E. Wachs , B. M. Weckhuysen, Appl. Catal. A 157 (1997) 67.

[15] G. C. Bond, Appl. Catal. A 157 (1997) 91.

[16] M. Takagi, M. Soma, T. Onishi, K. Tamaru, Can. J. Chem. 58 2132 (1980).

[17] F. Roozeboom, M. C. Mittelmeijer-Hazeleger, J. A. Moulijin, J. Medena, V. H. J. De Beer, P. J. Gellings, J. Phys. Chem. 84 (1980) 2783.

[18] Y. M.Liu, Y. Cao, N. Yi, W. L. Feng, W. L. Dai, S. R. Yan, H. Y. He, K. N. Fan, J. Catal. 224 (2004) 417.

[19] C. Pack, A. T. Bell, T. D. Tilley, J. Catal. 206 (2002) 49.

[20] R. Zhou, Y. Cao, S. R. Yan, J. F. Deng, Y. Y. Liao, B. F. Hong, Catal. Lett. 75 (2001) 107.

[21] J. S. Beck, J. C. Vartuli, W. J. Roth, M. E. Leonowicz, C. T. Kresge, K. D. Schmitt, C. T. W. Chu, D. H. Olsen, e. W. Sheppard, S. B. McCullen, J. B. Higgins, J. L. Schlenker, J. Am. Chem. Soc. 114 (1992) 10834.

[22] A. Corma, Chem. Rev. 97 (1997) 2373.

[23] E. V. Kondratenko, M. Cherian, M. Baerns, D. Su, R. Schlögl, X. Wang, I. E. Wachs, J. Cat. 234 (2005) 131.

[24] G. Guruebert, J. Rathouský, G. S. Ekloff, M. Wark, A. Zukal, Microporous and mesoporous materials 22 (1998) 225.

UNIVERSITAT ROVIRA I VIRGILI
NANOMATERIALS IN CATALYSIS: STUDY OF MODEL REACTIONS.
Ricardo José Chimentao
ISBN: 978-84-690-7618-7 / DL: T.1326-2007

[25] H. Berndt, A. Martin, A. Bruckner, E. Schreier, D. Muller, H. Muller, H. Kosslick, G. U. Wolf, B. Lucke, J. Cat. 191 (2000) 384.

[26] J. Haber in: G. Ertl, H. Knozinger, J. Weitkamp (Eds,), Handbook of Heterogeneous Catalysis, vol. 5, VCH, Weinheim, 1997, p. 2253.

[27] M. D, Argyle, K. Chen, A. T. Bell, E. Iglesia, J. Catal. 208 (2002) 139.

[28] G. Deo, I. E. Wachs, J. Catal. 146 (1994) 335.

[29] L. Lietti, P. Forzatti, G. Ramis, G. Busca, F. Bregani, Appl. Catal. 3 (1993) 13.

[30] G. Garcia Cortes, J. L. G. Fierro, M. A. Bañares, Catal. Today 78 (2003) 219.

[31] J. P. Dum, H. G. Stanger Jr., I. E. Wachs, Wachs, Catal. Today. 301 (1999) 51.

[32] A. Martin, U. Bentrup, G.U. Wolf, Appl. Catal. A 227 (2002) 131

[33] I.E. Wachs, B. M. Weckhuysen, Appl. Catal. 157 (1997) 67

[34] R. S. Weber, J. Catal. 151 (1995) 470.

[35] D. G. Barton, M. Shtein, r. D. Wilson, S. L. Soled, E. Iglesia, J. Phys Chem. B 103 (1999) 630.

[36] J. George, S. Shylesh, A. P. Singh, Appl. Catal. 290 (2005) 148.

[37] N N Greenwood and A Earnshaw, Chemistry of the Elements, 2nd Edition, Butterworth/Heinemann, Oxford, 1997, pp. 1341

[38] C. B. Wang, G. Deo, I. E. Wachs, J. Catal. 178 (1998) 640.

[39] M. M. Koranne, J. G. Goodwin Jr, . Marcelin, J. Catal. 148 (1994) 369, 388.

[40] F. Arena, N. Giordano, A. Parmaliana, J. Catal. 167, (1997) 66.

UNIVERSITAT ROVIRA I VIRGILI
NANOMATERIALS IN CATALYSIS: STUDY OF MODEL REACTIONS.
Ricardo José Chimentao
ISBN: 978-84-690-7618-7 / DL: T.1326-2007

[41] U. Scharf, M. Scharami-Marth, A. Wokaun, A. Baiker, J. Am. Chem. Soc. Faraday Trans. 87 (19) (1991) 3299.

[42] D. Wei, G. L. Haller, Proc. 2nd Memorial G. K. Boreskov Intern. Conference, Novosibirsk, July 1997 p. 110.A.

[43] Khodakov, J. Yang, S. Su, E. Iglesia, A. T. Bell, J. Catal. 177 (1998) 343.

[44] E. A. Davis, N. F. Mott, Philos. Mag. 22 (1970) 903.

[45] A. A. Hossein, C. A. Hogarth, J. Beynon, J. Mater. Sci. Lett. 13 (1994) 1144.

[46] X. Gao, I. E. Wachs, J. Phys. Chem. B 104 (2000) 1261.

[47] D. G. Barton, M. Shtein, R. D. Wilson, S. L. Soled, E. Iglesia, J. Phys. Chem. B 103 (1999) 630

[48] X. Gao, M. A. Bañares, I. E. Wachs, J. Catal. 188 (1999) 325.

[49] M. Iwamoto, H. Furukawa, K. Matsukami, T. Takenaka, S. Kagawa, J. Am. Chem. Soc. 105 (1983) 3719.

[50] A. Khodakov, B. Olthof, A. T. Bell, E. Iglesia, J. Catal. 181 (1999), 205.

[51] M. Baltes, K. Cassiers, P. Van der Voort, B. M. Weckhuysen, R.A. Schoonheydt, F. Vansant. J. Catal. 197 (2001) 160.

[52] S. T. Oyama, G. A. Somorjai, Catal. Sci. Tech. 1 (1991) 219.

[53] B. M. Weckhuysen, D. E. Keller, Catal. Today 78 (2003) 1.

[54] G. C. Bond and S. Flamerz, Appl. Catal. 33 (1987) 219.

[55] N. E. Quaranta, J. Soria, V. Cortes Corberan, J. L. G. Fierro, J. Catal. 171 (1997)1.

[56] D. E. Resasco, B.K. Marcus, C.S. Huang, V.A. Durante, J. Catal. 146 (1994) 40.

[57] D.W. McKee, Carbon 25 (1987) 587.

UNIVERSITAT ROVIRA I VIRGILI
NANOMATERIALS IN CATALYSIS: STUDY OF MODEL REACTIONS.
Ricardo José Chimentao
ISBN: 978-84-690-7618-7 / DL: T.1326-2007

CHAPTER II.5

Effect of a sonicated reconstruction on the accessibility of active sites in hydrotalcite-like compounds

UNIVERSITAT ROVIRA I VIRGILI
NANOMATERIALS IN CATALYSIS: STUDY OF MODEL REACTIONS.
Ricardo José Chimentao
ISBN: 978-84-690-7618-7 / DL: T.1326-2007

II.5.1 Abstract

Mg-Al hydrotalcite-like materials with atomic ratio of 4 were tested as heterogeneous catalyst in the styrene epoxidation reaction. The effect on the catalytic activity by using different rehydration procedures such as mechanical stirring or ultrasounds was related to the structure and basicity of the resulting materials. An enhancement in the catalytic activity was observed when both the stirring and ultrasound time was increased during the rehydration procedure. This was correlated with the increase in BET surface area of the obtained materials and the accessibility of the basic sites of the catalysts. High resolution transmission electron microscopy showed that sonication produced a high amount of defects in the lamellar structure of small hydrotalcite nanoplatelets, causing the presence of stronger and more active basic sites for epoxidation reaction as determined by CO_2-TPD and benzoic acid titration.

Keywords: hydrotalcite; rehydration; exfoliation; nanoplatelets; ultrasounds, styrene epoxidation.

UNIVERSITAT ROVIRA I VIRGILI
NANOMATERIALS IN CATALYSIS: STUDY OF MODEL REACTIONS.
Ricardo José Chimentao
ISBN: 978-84-690-7618-7 / DL: T.1326-2007

II.5.2 Introduction

In this chapter, the formation of defect sites in the agglomeration of layers has been deliberately attempted by the use of ultrasounds or high mechanical stirring during reconstruction of mixed oxides derived from hydrotalcites and accurately observed by HRTEM. The materials were also characterized by N_2 adsorption, and TGA. The catalytic role of the basic sites has been envisaged through the base-catalyzed epoxidation of styrene. Determination of the effective basic sites on the reconstructed catalysts has been validly assessed by poisoning with benzoic acid as a probe molecule. A linear correlation between reaction rates and number of active sites has been found for the rehydrated hydrotalcites by mechanical stirring whereas two intersecting linear segments were observed for the sonicated materials.

It is well known that some clay minerals undergo spontaneous exfoliation in water. Similar exfoliation has been artificially achieved for several classes of layered materials such as some hydrotalcites by ultrasounds or mechanical stirring. Exfoliation is regarded as an effective way of maximizing the accessibility and utility of the LDH host layer as well as introducing unusual physicochemical properties or quantum effects [1,2]. In the presence of an applied acoustic field, (cavitation) bubbles that are within a certain range are forced to oscillate and grow in size. Gas bubbles are inherently present in liquids. However, a free gas bubble in a liquid does not remain stable [3]. It either dissolves or floats to the surface of the liquid, depending on the size of the bubble. Acoustic cavitation is the ultrasound-driven formation, growth, and collapse of the microbubbles. So, the use of ultrasounds should stimulate the exfoliation of the hydrotalcites particles during the rehydration. Nanoplatelet-based reconstructed

UNIVERSITAT ROVIRA I VIRGILI
NANOMATERIALS IN CATALYSIS: STUDY OF MODEL REACTIONS.
Ricardo José Chimentao
ISBN: 978-84-690-7618-7 / DL: T.1326-2007

hydrotalcites are originated. The number of external OH^- groups near the edges of the layers of the resulted materials increased, obviously due to the most accessibility. The chemical properties of nanomaterials are dominated by surface effects. The nanoplatelet based reconstructed hydrotalcites exhibit preference face-to face orientations due to the increase in surface atoms relative to the bulk material. Atoms on the surface and edges are not fully coordinated. As the particles become smaller, the chemistry is dominated by the surface atoms, as they represent a greater percentage of the total structure. Based on this, reconstructed hydrotalcite platelets produced by exfoliation which possess small crystallites that are beneficial for the activity compared to larger crystals.

II.5.3 Experimental

The Mg-Al hydrotalcite (Mg/Al molar ratio = 4) was prepared by coprecipitation at constant pH of an aqueous solution of $Mg(NO_3)_2.6H_2O$ (1 M) and $Al(NO_3)_3.9H_2O$ (1 M) and a second solution of NaOH (2 M). Both solutions were mixed dropwise under stirring at 298 K, and after addition of the reactants, the slurry was aged for 18 h at room temperature. The resultant slurry was filtered and thoroughly washed with deionized water and finally dried at 383 K to yield the as-synthesized hydrotalcite (HT-as). This sample was calcined at 723 K in air for 48 h to obtain the corresponding Mg(Al)O mixed oxide (HT-ca). This material was reconstructed in decarbonated water (0.05 g in 5 ml of water) by means of high mechanical stirring (500 rpm) for different times (25 min, 4 h and 24 h) or by sonication (25 and 50 min). The reconstructed samples, denoted hereafter as HT-rm(25min), HT-rm(4h) and HT-rm(24h) or HT-rus(25min) and HT-

UNIVERSITAT ROVIRA I VIRGILI
NANOMATERIALS IN CATALYSIS: STUDY OF MODEL REACTIONS.
Ricardo José Chimentao
ISBN: 978-84-690-7618-7 / DL: T.1326-2007

rus(50min) (according to the reconstruction by mechanical stirring or by ultrasonication, respectively), were kept under inert atmosphere for further use.

The chemical composition of the samples was determined by ICP-OES in a Perkin-Elmer Plasma 400. X-ray diffraction (XRD) measurements were made using a Siemens D5000 diffractometer (Bragg-Bentano parafocusing geometry and vertical θ-θ goniometer) fitted with a grazing incident (ω: 0.52º) attachment for thin film analysis and scintillation counter as a detector. The samples were dispersed on Si (510) sample holder. The angular 2θ diffraction range was between 5º and 70º. The data were collected with an angular step of 0.03º at 12 s per step and sample rotation. CuK_α radiation (λ = 1.54056 Å) was obtained from a copper X-ray tube operated at 40 kV and 30 mA. The crystalline phases were identified using the JCPDS files. For high-resolution transmission electron microscopy studies (HRTEM), a JEOL JEM 2010F electron microscope equipped with a field emission gun was used working at an accelerating voltage of 200 kV. Samples were dispersed in ethanol in an ultrasonic bath and a drop of supernatant suspension was poured onto a holey carbon coated grid and dried completely before measurements. N_2 adsorption and desorption isotherms at 77 K were measured on a Micromeritics ASAP 2000 surface analyzer. Before analysis, the samples were degassed in vacuum at 393 K for 16 h. Temperature programmed desorption (TPD) of CO_2 from hydrotalcites samples was studied using a TPD/R/O 1100 (Thermo-Finnigan) equipped with a TCD detector and coupled to a mass spectrometer QMS 422 Omnistar. Before the TPD, the samples (200 mg) were treated at 80ºC with 3% CO_2/He flow (20 cm^3/min) for 1 h. After that, the desorption process was carried out from 80 to 900º

UNIVERSITAT ROVIRA I VIRGILI
NANOMATERIALS IN CATALYSIS: STUDY OF MODEL REACTIONS.
Ricardo José Chimentao
ISBN: 978-84-690-7618-7 / DL: T.1326-2007

at 10ºC min^{-1} in He flow. Determination of the base amount of the HT catalysts was also estimated by titration using benzoic acid. Thermal analysis was performed in a Perkin-Elmer TGA 7 thermobalance, equipped with a programmable temperature furnace. The sample (50 mg) was heated from room temperature up to 1073 K in argon (80 $cm^3(STP)min^{-1}$) at 5 K min^{-1}. The epoxidation of styrene was performed in a batch reactor at 313 K and atmospheric pressure. Typically, styrene (4 mmol), acetone 8.0 ml (0.136 mol), acetonitrile 6.3 ml (0.153 mol), water (5 ml), H_2O_2 (3 ml at 33% in water) and 50 mg of hydrotalcite sample (calcined or rehydrated). H_2O_2 efficiency was determined by $KMnO_4$ titration. Samples were taken at regular time periods for both reactions and were analyzed off-line by a SHIMADZU GC-17 gas chromatograph using an ULTRA 2 capillary column (15 m x 0.32 mm x 0.25 μm) and equipped with a FID detector. All the reactants were purchased from Aldrich and used without further purification.

II.5.4 Results and discussion

II.5.4.1 X-ray diffraction

The layered structured of the as-synthesized, calcined and rehydrated hydrotalcites was confirmed by XRD as show in Figure II.5.1. The XRD pattern of the as-synthesized (HT-asy) sample exhibited sharp and symmetric reflections for the (003), (006), (110) planes and broad symmetric peaks for the (113), (102), (105) and (108) planes, which are characteristics of hydrotalcite-like materials (JCPDS 22-700). The reflections correspond to an hexagonal lattice with *R3m* rhombohedral symmetry.

UNIVERSITAT ROVIRA I VIRGILI
NANOMATERIALS IN CATALYSIS: STUDY OF MODEL REACTIONS.
Ricardo José Chimentao
ISBN: 978-84-690-7618-7 / DL: T.1326-2007

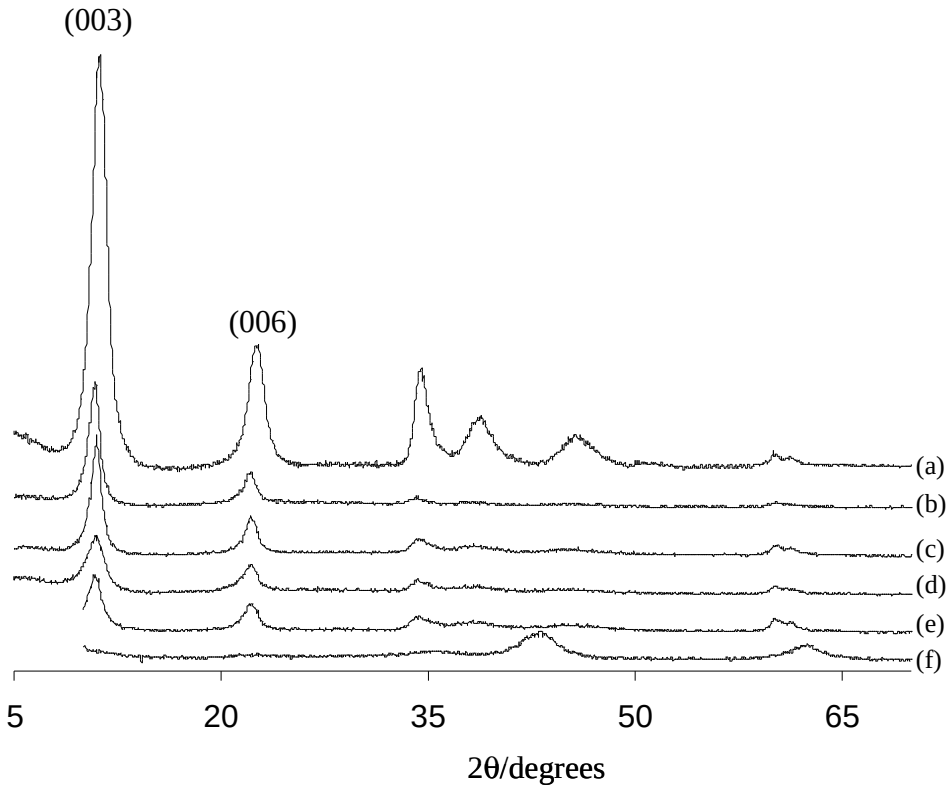

Figure II.5.1 X-ray diffraction of the LDHs materials. (a) HTasy; (b) HT-rm(25min) (c) HT-rm(4h), (d)HT-rus(25min); (e) HT-rus(50min); and (f) HT-cc.

The (003) and (006) reflections at 11.6°and 23.4°, respectively, were used to calculate the basal spacing between the layers, *d*. The (110) reflection (at 61.1°) was used to calculate the unit cell dimension, a, where $a = 2d_{110}$ [13]. The results of these calculations are shown in Table II.5.1. The lack of the (003) reflection in the XRD pattern of the calcined product at 723 K (HT-cc sample in Figure 1f) indicates that the layered structure of the HT has been destroyed by calcination. For the HT-cc, the characteristic reflections observed at $2\theta \approx 43$ and 63° correspond to a Mg-Al-O (periclase-like structure, JCPDS 87-0653).

ISBN: 978-84-690-7618-7 / DL: T.1326-2007

This observation was also confirmed by HRTEM.

Reconstruction of the calcined samples resulted in the recovery of the layered structure back to meixnerite (JCPDS 35-0965), as a result of the well-known “memory effect” [14]. In that, the presence of water restores the interlayer hydrogen bonding network and gallery spacing while the original carbonate anions in the as-synthesized hydrotalcite have been replaced by Brønsted OH-sites [15-17]. The X-ray patterns of the rehydrated samples are depicted in Figure 1(b-e). One of the most striking features for the platelet-like sample is the loss of intensity of sharp basal peaks, particularly for the sonicated samples (HT-rus(25min) and HT-rus(50min)), which appear as broad reflections. This could indicate that the exfoliation treatment leads to a more amorphous structure with smaller crystals, in which the hydrotalcite layers are no longer in parallel.

The (110) reflection is discerned at 60.5˚, indicating that the two dimensional crystalline order of LDH was still preserved. The new term *nanosheets* [18] has been widely accepted to represent this two-dimensional anisotropy, typically micrometer in lateral size while nanometer in thickness, of the individual host layers. It is noteworthy that similar broad profiles have been taken as compiling evidence of exfoliated layered materials [19].

UNIVERSITAT ROVIRA I VIRGILI
NANOMATERIALS IN CATALYSIS: STUDY OF MODEL REACTIONS.
Ricardo José Chimentao
ISBN: 978-84-690-7618-7 / DL: T.1326-2007

Table II.5.1 Surface area of the hydrotalcite samples and calculation of lattice parameter and basal plane spacing as a function of the exfoliation process

Sample code	Mg:Al Atom ratio[a]	Surface area (m^2g^{-1})	d_{003} (Å)	d_{110} (Å)	a Å)
HT-ca	3.90	196	-	-	-
HT-rm(25min)	3.88	215	8.113	1.516	3.032
HT-rm(4h)	3.91	286	8.045	1.512	3.024
HT-rus(25min)	3.90	437	8.135	1.511	3.022
HT-rus(50min)	3.87	466	8.106	1.514	3.028

[a] ICP-AES

II.5.4.2 HRTEM

To investigate the morphology and microstructure at atomic level of the hydrotalcite samples obtained after rehydration under mechanical stirring or ultrasounds, as well as of the calcined sample, an accurate HRTEM study was performed. Low-resolution transmission electron microscopy images of these materials are shown in Figure II.5.2.

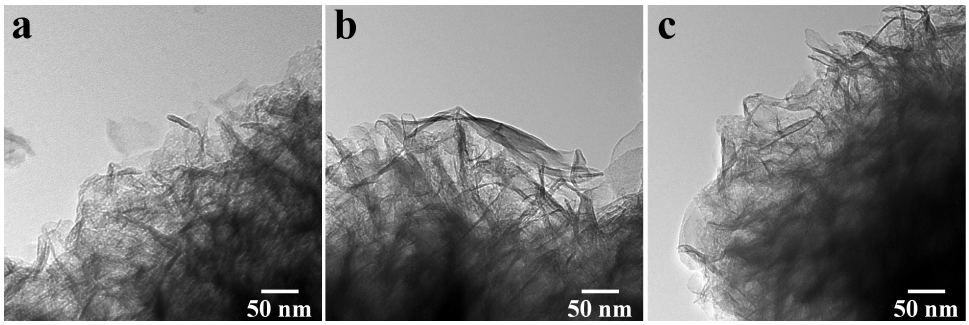

Figure II.5.2 Low-magnification, bright-field transmission electron microscopy images of the calcined sample (a), and rehydrated samples obtained under mechanical stirring (b) and ultrasounds (c) treatments.

In all cases, a platelet morphology characteristic of hydrotalcite-type

UNIVERSITAT ROVIRA I VIRGILI
NANOMATERIALS IN CATALYSIS: STUDY OF MODEL REACTIONS.
Ricardo José Chimentao
ISBN: 978-84-690-7618-7 / DL: T.1326-2007

materials is observed. However, platelets in the sample obtained after rehydration under mechanical stirring (Figure II.5.2b) are generally larger than those present in the sample obtained by rehydration under ultrasounds (Figure II.5.2c), which in turn are similar to those present in the calcined sample (Figure II.5.2a). Although no noticeable change in the morphology of the samples was detected at low-magnification, important differences were observed in the lattice-fringe images obtained at higher magnification under high-resolution TEM conditions. Figure II.5.3 corresponds to a HRTEM image of the calcined sample. The inset corresponds to the Fourier transform image (FT) of the crystallographically oriented crystallite in the center of the HRTEM image. Spots at 2.4 and 2.1 Å correspond to the (111) and (200) planes, respectively, of the *bcc* periclase structure. The relative position of the spots in the FT image indicate that the crystallite is oriented along the [011]-type crystallographic direction. Selected-area electron diffraction patterns (SAED) recorded over several areas show that the calcined sample is mainly constituted by the periclase structure (rings at 2.4, 2.1 and 1.5 Å), although minor amounts of the original hydrotalcite phase are still recognizable (at 3.8 and 2.6 Å).

Figure II.5.4 corresponds to a representative HRTEM picture of the sample rehydrated under mechanical stirring. The sample is constituted by crystallites showing a well-developed platelet morphology. The platelet at the center of the image in Figure II.5.4 is crystallographically oriented and a portion of its lattice-fringe image (inside the marked square) is enlarged and showed apart, along with the corresponding Fourier transform image.

UNIVERSITAT ROVIRA I VIRGILI
NANOMATERIALS IN CATALYSIS: STUDY OF MODEL REACTIONS.
Ricardo José Chimentao
ISBN: 978-84-690-7618-7 / DL: T.1326-2007

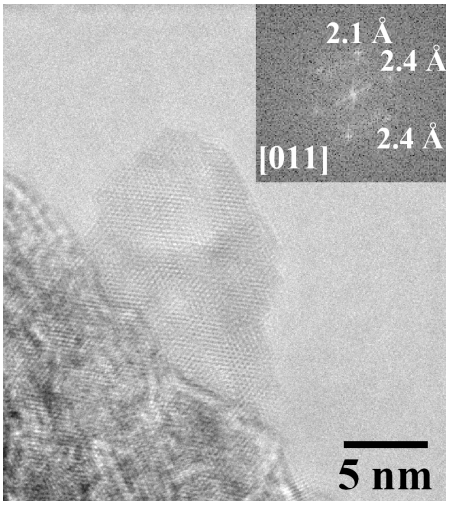

Figure II.5.3. HRTEM image corresponding to the calcined sample and FT image of the oriented crystallite at the center of the image.

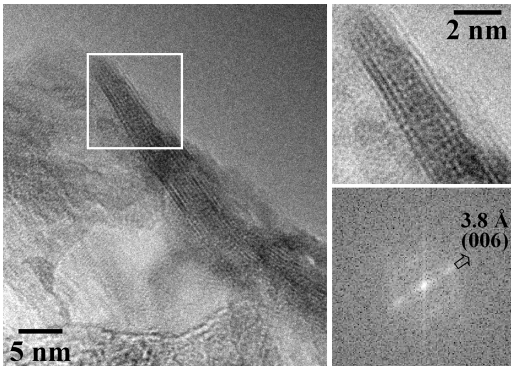

Figure II.5.4 HRTEM image corresponding to the rehydrate sample under mechanical stirring. The inset show an enlarge of the area enclosed by the square and its corresponding FT image.

Spots at 3.8 Å correspond to (006) planes of the hydrotalcite phase, thus indicating that the platelet is oriented perpendicular to the *c* crystallographic axis, or in other words, that the basal plane of the platelets coincides with the *ab* crystallographic plane of the hydrotalcite structure. The enlarged image has atomic resolution and shows a

UNIVERSITAT ROVIRA I VIRGILI
NANOMATERIALS IN CATALYSIS: STUDY OF MODEL REACTIONS.
Ricardo José Chimentao
ISBN: 978-84-690-7618-7 / DL: T.1326-2007

general well-ordered array of atomic rows, with little structural defects. Figure II.5.5 corresponds to a similar analysis performed over the sample rehydrated under ultrasounds (exactly the same magnification and data analysis). In this case, however, there are important differences with respect to the sample rehydrated under mechanical stirring.

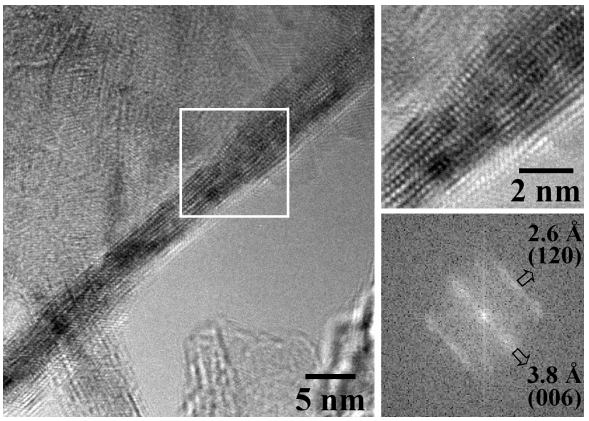

Figure II.5.5 HRTEM image corresponding to the rehydrated sample under ultrasounds. The insets show an enlarged view of the area enclosed by the square and its corresponding FT image.

The Fourier transform image corresponding to the enlarged area of the platelet enclosed in the square in Figure II.5.5 does not show single spots at 3.8 Å corresponding to (006) planes of the hydrotalcite phase, as it is observed in the sample rehydrated under mechanical stirring (Figure II.5.4). Instead of this, in the FT image of the sample rehydrated under ultrasounds there are parallel strings of spots which are indicative of short-range atomic ordering. Within the main string, spots around 3.8 Å are brighter, which correspond to (006) planes, whereas the strings are separated at exactly 2.6 Å, which corresponds to (120) planes in the basal plane of the platelet. The lack of single spots

UNIVERSITAT ROVIRA I VIRGILI
NANOMATERIALS IN CATALYSIS: STUDY OF MODEL REACTIONS.
Ricardo José Chimentao
ISBN: 978-84-690-7618-7 / DL: T.1326-2007

and the presence of the strings in the FT image is interpreted in terms of a highly disordered structure for the hydrotalcite phase obtained by rehydration under ultrasounds. This is seen clearly at the atomic scale in the enlarged, direct-space HRTEM inset of Figure II.5.5 where high density of structural defects is easily identified. The hydrotalcite platelets maintain the same crystallographic habit as in the sample rehydrated under mechanical stirring, that is, with the basal plane perpendicular to the *c* crystallographic axis, but in the sample rehydrated under ultrasounds the extent of well-ordered arrays of atomic rows within the hydrotalcite platelets is limited due to the existence of numerous structural defects. The highly defective structure of platelets in the sample rehydrated under ultrasounds is also depicted in Figure II.5.6, where extensive structural defects are indicated by arrows.

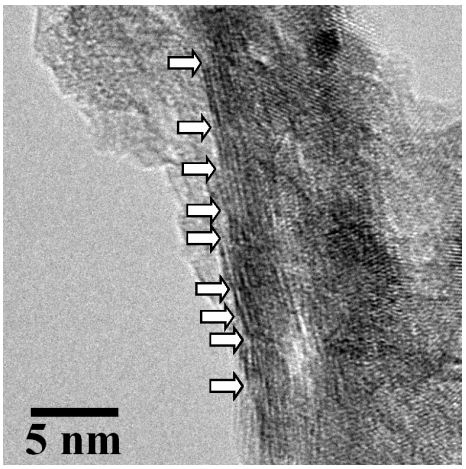

Figure II.5.6. HRTEM image corresponding to the rehydrated sample under ultrasounds. Several structural defects are marked by arrows.

Another representative HRTEM image of the rehydrated sample under ultrasounds is shown in Figure II.5.7. In this case several platelets are

UNIVERSITAT ROVIRA I VIRGILI
NANOMATERIALS IN CATALYSIS: STUDY OF MODEL REACTIONS.
Ricardo José Chimentao
ISBN: 978-84-690-7618-7 / DL: T.1326-2007

stacked and curved together. The Fourier transform image (inset of Figure II.5.7) shows three different strings of spots that correspond to the different orientation of platelets following three different directions (labeled “a”, “b”, and “c”). Within the strings, spots due to (006) planes of the hydrotalcite structure at 3.8 Å are recognizable but, again, the presence of the strings is indicative for the existence of abundant structural defects in the platelets. Spots at 2.6 Å correspond to (120) planes of the hydrotalcite structure and are located in the FT image perpendicular to the string labeled as “b”, thus indicating that they belong to the basal plane of platelets “b”. SAED patterns recorded for rehydrated samples both under mechanical stirring and ultrasounds exhibit rings corresponding to the hydrotalcite phase, but also some minor amount of the periclase structure, which constitutes the bulk of the calcined sample. This indicates that the rehydration of the periclase structure into hydrotalcite is almost complete in both cases.

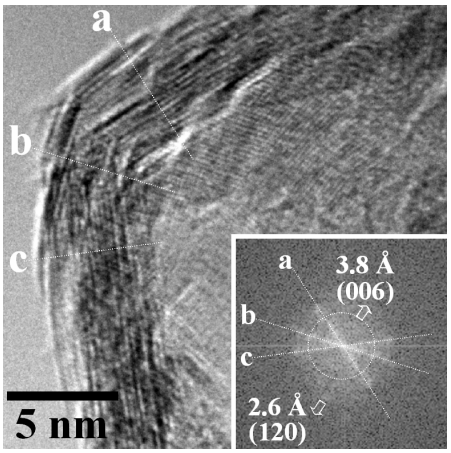

Figure II.5.7 HRTEM image corresponding to the rehydrated sample under ultrasounds and its associated FT image.

UNIVERSITAT ROVIRA I VIRGILI
NANOMATERIALS IN CATALYSIS: STUDY OF MODEL REACTIONS.
Ricardo José Chimentao
ISBN: 978-84-690-7618-7 / DL: T.1326-2007

II.5.4.3 TGA

The thermogravimetric analysis of the reconstructed samples, as well as that of the calcined sample, is shown in Figure II.5.8. A low weight loss was observed during the TGA experiment for the HT-cc sample (Figure 8a). This fact indicates that during the calcination process, practically all the hydrotalcite was transformed into the periclase-like phase. All the rehydrated solids display the two characteristic stages of weight loss in the temperature range of 343 to 1073 K of hydrotalcite-like materials [20,21]. The first weight loss is noticed between 343 and 553 K for all the samples, which is attributed to the loss of adsorbed and interlayer water. The second step of weight loss in the temperature range of 553 to 1073 K is ascribed to dehydroxylation of the brucite-like sheets [13], resulting from the collapse of the meixnerite structure. The TGA results and the corresponding degrees of reconstruction of the solids are summarized in Table II.5.2. The HT-rus(25min) and HT-rus(50min) hydrotalcites showed a reconstruction of 94% and 100%, respectively. In contrast, the samples prepared by mechanical stirring (HT-rm(25min), HT-rm(4h) and HT-rm(24h)) showed a lower degree of reconstruction, with values at 48.0, 80.2 and 84.1% respectively. Accordingly, the materials reconstructed under ultrasounds presented higher weight losses in both decomposition steps, as compared to the samples prepared by mechanical stirring. This clearly indicates that a great number of OH groups is present in the sonicated samples.

This is reasonable taking into account that the sonication produces higher surface materials and small crystallites by exfoliation and consequently the diffusion of the water in the interlayer space to form the meixnerite-like phase is enhanced. This fact derives in the presence of larger number of exposed OH- materials, and particularly those

UNIVERSITAT ROVIRA I VIRGILI
NANOMATERIALS IN CATALYSIS: STUDY OF MODEL REACTIONS.
Ricardo José Chimentao
ISBN: 978-84-690-7618-7 / DL: T.1326-2007

located at the edges of the platelets [2,23]. Moreover, this sonication effect is dramatically pronounced when larger contact times are used (HT-rm(50 min) vs HT-rm(25 min)).

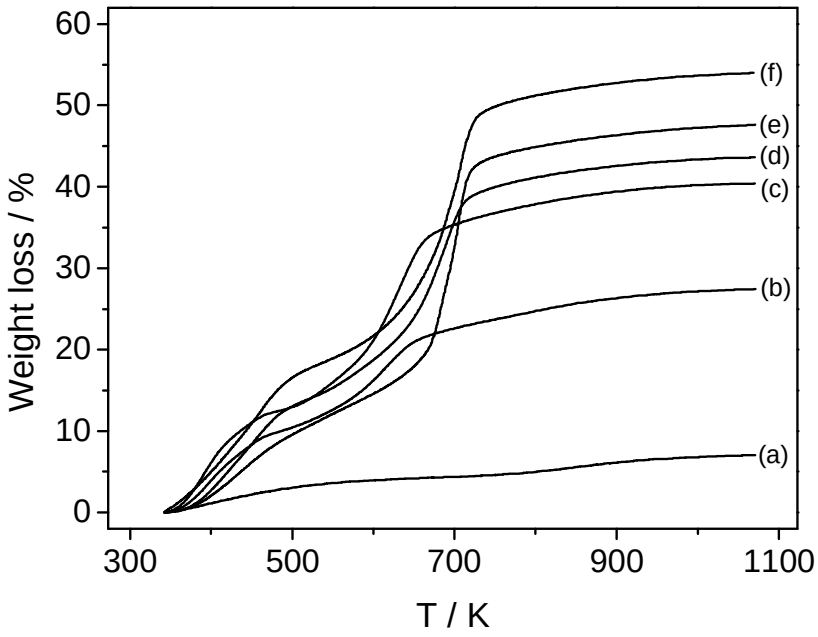

Figure II.5.8 Thermogravimetric analysis of the hydrotalcite samples. (a) HT-cc; (b) HT-rm(25min), (c) HT-rm(4h) and (d) HT-rm(24h) (e) HT-rus(25min) and (f) HT-rus(50min).

II.54.4 Temperature programmed desorption of CO_2

The measure of the base site density was obtained by TPD of CO_2. The peaks observed can be assigned based on the temperature at which they appear. Previous studies have shown that the first peak which decomposes at temperatures about 693 K can be attributed to the contribution of mainly bidendate carbonates species, together with bicarbonate species, on the catalyst surface. The presence of a small peak at higher temperature (813 K) can be attributed to the presence of monodentate species [22]. Figure II.5.9 shows the CO_2 uptake during

UNIVERSITAT ROVIRA I VIRGILI
NANOMATERIALS IN CATALYSIS: STUDY OF MODEL REACTIONS.
Ricardo José Chimentao
ISBN: 978-84-690-7618-7 / DL: T.1326-2007

temperature-programmed desorption experiments over two representative samples, prepared under mechanical stirring or ultrasounds, respectively. The low temperature peak (613 K) was detected for all the samples whatever the reconstruction treatment employed, whereas the peak at higher temperature was only observed for the sonicated materials.

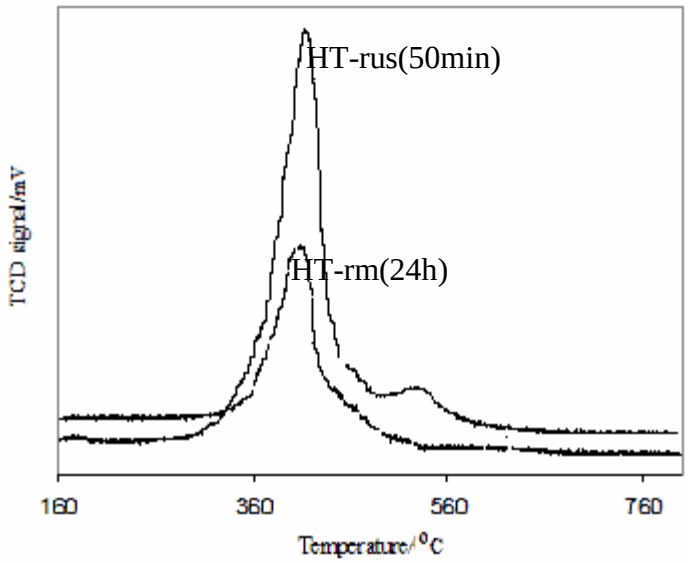

Figure II.5.9 CO_2 uptake during temperature-programmed desorption experiments over HT-rm(24h) and HT-rus(50min) samples.

Since the calcination treatment was sufficiently long to avoid the presence of residual carbonates in all the samples, the peak observed at higher temperature could be ascribed to the presence of strong basic sites in the sonicated samples. Integration of the corresponding profiles, calculated as the amount of CO_2 evolved, is reported in Table II.5.3. The total number of basic sites for the HT-rus(25min) and HT-rus(50min) samples was 1200 and 1820 μmol g_{cat}^{-1}, respectively. As determined by ICP analysis, the total number of basic sites can be

UNIVERSITAT ROVIRA I VIRGILI
NANOMATERIALS IN CATALYSIS: STUDY OF MODEL REACTIONS.
Ricardo José Chimentao
ISBN: 978-84-690-7618-7 / DL: T.1326-2007

calculated from the number of Al^{+3} ions present in the hydrotalcite, which is proportional to that of the compensating anions (OH^-). From the quantification in Table II.5.3, the amount of CO_2 evolved with respect to the bulk Al content indicated that approximately 38 and 57% of the OH^- sites were detected for HT-rus(25min) and HT-rus(50min), respectively. In contrast, only 16 and 26% of the OH^- sites were detected in the HT-rm(4h) and HT-rm(24h) samples, indicating that the amount of basic sites seems to be dependent on the reconstruction procedure. In particular, these results not only evidence that not all of the total OH^- sites are evaluated by CO_2-TPD experiments, but also that the OH^- groups in the sonicated samples are actually more accessible. Moreover, the presence of the two peaks suggests the existence of basic sites of different nature.

Table II.5.3 Quantification of the basicity by CO_2-TPD profiles and benzoic acid titration for rehydrated hydrotalcites

Sample	Peak at 693 K (%)	Peak at 813 K (%)	Total CO_2 [$\mu molg_{cat}^{-1}$]	CO_2/Al ratio[a]	Benzoic Acid [$\mu molg_{cat}^{-1}$][d]
HT-rm(4h)	100	-	520	0.16	310
HT-rm(24h)	100	-	850	0.26	420
HT-rus(25min)	90.5	9.5	1200 (114)[b]	0.38 (0.0 36)[c]	700 (120)[e]
HT-rus(50min)	85.2	12.8	1820 (232)[b]	0.57 (0.073)[c]	1100 (190)[e]

[a] Mol of total adsorbed CO_2 per mol of Al in the HT. [b, c] Between brackets, contribution of the peak at 813 K. [d, e] Mol of total benzoic acid consumed during the titration of the HT obtained from the plot of initial reaction rate versus benzoic acid amount in Figure II.5.11 (between brackets, contribution from the first linear segment).

The differences in basicity observed along the reconstructed materials are likely due to the existence of abundant structural defects in the

UNIVERSITAT ROVIRA I VIRGILI
NANOMATERIALS IN CATALYSIS: STUDY OF MODEL REACTIONS.
Ricardo José Chimentao
ISBN: 978-84-690-7618-7 / DL: T.1326-2007

platelets in the sonicated samples, as revealed by HRTEM analysis. Furthermore, the smaller crystallites and corresponding high surface area of the sonicated samples automatically derives in a larger number of exposed OH^-, which are not only located at the edges of the platelets [2, 23], but also at defect sites generated after exfoliation.

II.5.5 Catalytic Activity

The epoxidation of styrene was carried out to find structure-sensitive correlations between the rehydration methods and the presence of defect sites on the catalytic activity. A representative reaction profile for the epoxidation is presented in Figure II.5.10.

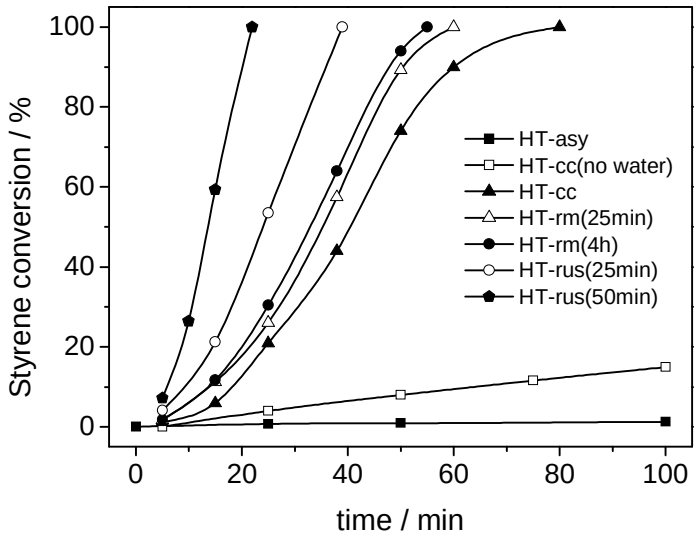

Figure II.5.10 Conversion vs time for the styrene epoxidation at 313 K for the different hydrotalcite samples. (a) HT-asy; (b) HT-cc (reaction without water) (c) HT-cc (d) HT-rm(25min) and (e) HT-rm(4h) (f) HT-rus(25min) and (g) HT-rus(50min).

In all cases, the selectivity to styrene oxide was higher than 95%. The as-synthesized sample (HT-asy) displayed an extremely low activity of

UNIVERSITAT ROVIRA I VIRGILI
NANOMATERIALS IN CATALYSIS: STUDY OF MODEL REACTIONS.
Ricardo José Chimentao
ISBN: 978-84-690-7618-7 / DL: T.1326-2007

around 1.2 % of styrene conversion after 100 minutes of reaction. The activity of the calcined sample, without water in the reaction medium, as depicted in Figure 10, was slightly higher than that obtained for the HT-asy. However, a very significant enhancement of the styrene conversion up to 90% was achieved after 60 min of reaction with the HT-cc sample, when water was introduced in the reaction medium. The latter leads to the reconstruction of the mixed oxide during reaction [24], and further suggests that the presence of Brønsted basic sites in the catalyst is a key parameter governing the catalytic activity of this reaction. Accordingly, the catalytic activity was impressively increased when the reconstructed materials were employed in the reaction. A total styrene conversion was achieved in 60 min using the catalysts reconstructed under mechanical stirring (HT-rm(25min) or HT-rm(4h)), while more pronounced is the increase in catalytic activity for the samples previously treated under ultrasounds (HT-rus(25min) and HT-rus(50min)). In the latter case, only 30 min were necessary to reach the total conversion. From these results, it can be concluded that vigorous stirring and the use of ultrasounds produce the exfoliation of the mixed oxides during reconstruction, leading to materials with an enhanced catalytic activity. However, the initial rate of the sonicated hydrotalcite (HT-rus(50min) was ca. 6-fold higher than that of the catalyst obtained under mechanical stirring. Therefore, the formation of defect sites (as previously observed by HRTEM) in the sonicated samples is likely accounting for the increase in the number of accessible OH^- groups. In order to elucidate the origin of the remarkable activity of the sonicated catalysts, and correlate it with the enhanced basicity observed during CO_2-TPD experiments, an additional determination of the effective base amount was carried out by titration with benzoic acid. In order to

UNIVERSITAT ROVIRA I VIRGILI
NANOMATERIALS IN CATALYSIS: STUDY OF MODEL REACTIONS.
Ricardo José Chimentao
ISBN: 978-84-690-7618-7 / DL: T.1326-2007

accomplish this, different amounts of benzoic acid previously dissolved in acetone, were added during reconstruction of the mixed oxide, either by mechanical stirring or by ultrasounds. The catalysts were subsequently used in the styrene epoxidation reaction, and the results are presented in Figure II.5.11.

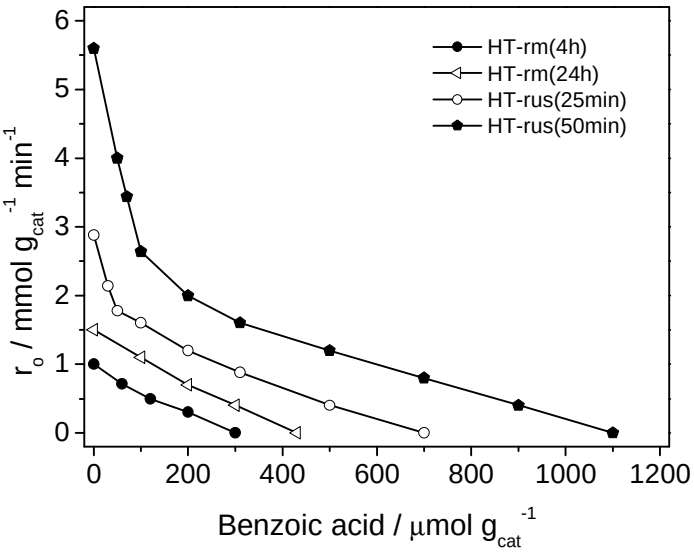

Figure II.5.11 Titration by benzoic acid for the determination of the base amount of the HT catalysts. Reaction rate versus amount of benzoic acid added. (a) HT-rm(4h) and (e) HT-rm(24h) (f) HT-rus(25min) and (g) HT-rus(50min).

The catalytic activity can be extremely reduced by annihilation of the active sites if the latter are neutralized with benzoic acid. This implies that the addition of benzoic acid is able to reduce the amount of basic sites, and consequently decrease the styrene conversion at a certain extent. Accordingly, a linear correlation between the amount of benzoic acid and the initial rate was found for the hydrotalcites reconstructed under mechanical stirring (HT-rm(4h) and HT-rm(24h)). As the amount

UNIVERSITAT ROVIRA I VIRGILI
NANOMATERIALS IN CATALYSIS: STUDY OF MODEL REACTIONS.
Ricardo José Chimentao
ISBN: 978-84-690-7618-7 / DL: T.1326-2007

of benzoic acid was increased, the corresponding initial reaction rate decreased until no activity was detected. Extrapolation of the linear segment at $y = 0$ leads to the amount of benzoic acid that is able to eliminate the catalytic activity of that catalyst. The amount of benzoic acid was 310 and 420 μmol g_{cat}^{-1} (see Table 3), respectively. The samples treated under ultrasounds exhibited a different behavior upon reconstruction with different amounts of benzoic acid. From Figure 11, two intersecting linear segments can be easily observed in HT-rus(25min) and HT-rus(50min) hydrotalcites, suggesting the existence of at least two kinetically distinguishable active OH^- sites. A very fast decrease of the initial reaction rate (first linear segment) was observed for the HT-rus(25min) sample, followed by a gradual decrease down to 700 μmol g_{cat}^{-1} (second linear segment).

More pronounced was the decrease in initial reaction rate for the HT-rus(50min) sample when small amounts of benzoic acid were added, but finally reaching a total number of evaluated OH^- sites of 1100 μmol g_{cat}^{-1} until no activity. Strikingly, the existence of the two segments in the sonicated samples suggests the presence of two types of basic sites in the reconstructed hydrotalcites. The latter would be in agreement with the presence of two different desorption peaks in the CO_2-TPD analysis, assigned to basic sites of different strength. In fact, the values derived from the extrapolation of the first segment to zero leads to a corresponding number of basic sites of 120 and 190 μmol g_{cat}^{-1}, for HT-rus(25min) and HT-rus(50min), respectively, rather similar to the values obtained by CO_2-TPD (Table II.5.3). These stronger basic sites, which are primary titrated, can be ascribed to those located at defect sites in the sonicated samples. From titration experiments, it seems that not all of the basic OH^- sites in the sonicated

UNIVERSITAT ROVIRA I VIRGILI
NANOMATERIALS IN CATALYSIS: STUDY OF MODEL REACTIONS.
Ricardo José Chimentao
ISBN: 978-84-690-7618-7 / DL: T.1326-2007

samples are equally accessible as compared to the samples treated under mechanical stirring. This implies that a relatively small amount of benzoic acid is sufficient to inhibit the catalytic performance to a significant extent, particularly in the sonicated samples. For example, adding only 190 μmol g_{cat}^{-1} of benzoic acid leads to a 2-fold decreased initial rate, while an important number of basic sites still remain in the catalyst until final annihilation of the catalytic performance. Therefore, the catalysts prepared under ultrasounds display a certain amount of strong basic sites and a higher amount of basic sites with medium strength. This is confirmed in the samples reconstructed under mechanical stirring, displaying lower values in the total number of basic sites. The basic sites related to the defects produced by sonication have around 6 times more activity than the basic sites obtained by exfoliation. Basicity results are in good agreement with the thermogravimetric analysis (Figure II.5.8), in which the higher weight loss of the samples reconstructed under ultrasounds leads to a higher degree of reconstruction. This derives into an additional amount of OH^- groups, which in fact, are able to be detected by TPD or titration.

As previous works demonstrated [9,10], a properly activation of hydrotalcites is clearly a critical factor. The exfoliation during reconstruction leads to a more irregular structure, favoring the accessibility of the OH^- groups near the edges of the platelets. This specific feature occurred upon reconstruction under ultrasounds has been confirmed with our HRTEM analysis (Figure II.5.5), leading to the conclusion that the dramatic disorder produced in the solid is responsible for the increase in the basic strength. This fact is also confirmed by our TPD experiments, which revealed an increase of the amount of CO_2 evolved in the sonicated samples as compared to those

exfoliated by mechanical stirring.

The activation of the mixed oxides via reconstruction combined with ultrasounds most likely causes the generation of edge defects, thus increasing the accessibility to the interlayer galleries and facilitating the exposure of a major number of OH^- groups. Indeed, it appears that the OH^- groups located at these defects are much more effective for the epoxidation reaction. Moreover, the catalytic activity increases with the increasing surface area (from 215 m^2g^{-1} (HT-rm25min) up to 446 m^2g^{-1} (HT-rus(50min.)), further indicating not only that a great number of exposed OH^- are easily accessible, but also that smaller hydrotalcite crystals (see HRTEM) are present in the sonicated samples.

The use of ultrasounds not only changes the total number of basic sites but also reinforces the fraction of stronger ones. Solids with lower crystal size possess a higher concentration of sites with low coordination number. Those OH^- species located in corners of the crystals likely present a stronger basicity than those located on crystal faces, thus favoring the performance towards the epoxidation reaction. These results support the fact that the epoxidation of styrene reaction effectively proceed at Brønsted basic sites located either at the edges of the nanoplatelets, or/and at defect sites of the reconstructed hydrotalcite.

II.5.6 Conclusion

Exfoliation is regarded as an effective way of maximizing the accessibility and utility of the OH^- groups in reconstructed hydrotalcites for epoxidation reactions. This was achieved by formation of small hydrotalcite nanoplatelets. The exfoliation method (sonication or mechanical stirring) applied during reconstruction of the mixed oxides

derived from hydrotalcite clearly influences the catalytic activity in styrene epoxidation. The formation of defect sites in the hydrotalcite nanoplatelets upon ultrasounds treatment is a more effective method to create stronger and more active basic sites, since higher surface areas and an increased number of exposed basic sites finally lead to an improved catalytic activity in the styrene epoxidation. This aspect can be further generalized to other base-catalyzed reactions.

Acknowledgements. Ministerio de Educación y Ciencia of Spain for financial support (CTQ2006-08196/PPQ; ENE2006-06925)

References

[1] F. Cavani, F. Trifirò, A. Vaccari, *Catal. Today* **11** (1991) 173.

[2] S. Abelló, F. Medina, D. Tichit, J. Pérez-Ramírez, J.C. Groen, J.E. Sueiras, P. Salagre, Y. Cesteros, *Chem. Eur. J.* **11** (2005) 728.

[3] D. Tichit, B. Coq, CATTECH 7 (2003) 206.

[4] F. Figueras, J. Lopez, J. Sánchez-Valente, T.T.H. Vu, J.M. Clacens, and J. Palomeque, J. Catal. **211** (2002) 144.

[5] Y. Ono, J. Catal. **216** (2003) 406.

[6] M.L. Kantam, B.M. Choudary, C.V. Reddy, K.K. Rao, F. Figueras, Chem. Commun. **9** (1998) 1033.

[7] M. Adachi-Pagano, C. Forano, J.-P. Besse, *Chem. Commun*. (2000) 91.

[8] J.C.A.A. Roelofs, A.J. van Dillen, K.P. de Jong, *Catal. Today* **60** (2000) 297.

[9] S. Abelló, F. Medina, D. Tichit, J. Pérez-Ramírez, Y. Cesteros, P. Salagre, J.E. Sueiras, *Chem. Commun.* (2005) 1453.

[10] F. Winter, X. Xia, B.P.C. Hereijgers, J.H. Bitter, A.J.van Dillen,

M. Muhler, K.P.de Jong, *J. Phys. Chem. B* **110** (2006) 9211.

[11] F. Winter, A.J. van Dillen, K.P. de Jong, *Chem. Commun*. (2005) 3977.

[12] M.B.J. Roeffaers, B.F. Sels, H. Uji-i, F.C. De Schryver, P.A. Jacobs, D.E. De Vos, J. Hofkens, *Nature* **439** (2006) 572.

[13] F. Cavani, F. Trifirò, A. Vaccari, *Catal. Today* **11** (1991) 173.

[14] K. Rao, M. Gravelle, J. Valente, F. Figueras, *J. Catal.* **173** (1998) 115.

[15] A. J. Jacobson, *Mater. Sci. Forum*, 1994, 152-152, 1

[16] N. Miyamoto, H. Yamamoto, R. Kaito, K. Kuroda, *Chem. Commun.* (2002), 2378.

[17] A. Takagi, M. Sugisawa, D. Lu, J. N. Kondo, M. Hara, K. Domen, S. Hayashi, *J. Am. Chem. Soc.*, **125** (2003) 5479.

[18] R. Ma, Z. Liu, L. Li, N. Iyi, T. Sasaki, *J. Mater. Chem.* **16** (2006) 3809.

[19] L. Li, R. Ma, Y. Ebina, Y. N. Iyi, T. Sasaki, *Chem. Mater.* **17** (2005) 4386.

[20] E. Kanezaki, *Inorg. Chem.* **73** (1998) 2588.

[21] W. T. Reichle, *J. Catal.* **94** (1985) 547.

[22] V.K. Díez, C. R. Apesteguía, J. I. Di Cosimo, *J. Catal.* **215** (2003) 220.

[23] J. C. A. A. Roelofs, A. J. van Dillen, K. P. de Jong, *Catal. Today* **60** (2000) 297.

[24] I. Kirm, F. Medina, X. Rodríguez, Y. Cesteros, P. Salagre, J. Sueiras, Appl. Catal. A: General **272** (2004)175.

UNIVERSITAT ROVIRA I VIRGILI
NANOMATERIALS IN CATALYSIS: STUDY OF MODEL REACTIONS.
Ricardo José Chimentao
ISBN: 978-84-690-7618-7 / DL: T.1326-2007

Chapter II.6

Hydrogenolysis of methylcyclopentane over bimetallic Ir-Au/γ-Al_2O_3 catalysts

UNIVERSITAT ROVIRA I VIRGILI
NANOMATERIALS IN CATALYSIS: STUDY OF MODEL REACTIONS.
Ricardo José Chimentao
ISBN: 978-84-690-7618-7 / DL: T.1326-2007

II.6.1 Abstract

The gas-phase hydrogenolysis of methylcyclopentane (MCP) was investigated over bimetallic Ir-Au/γ-Al_2O_3 catalysts. The bimetallic systems, which contained atomic Au/Ir ratios in the range of 0.125-8 and a fixed total metal content of 8 wt. %, were prepared by sequential impregnation and co-impregnation methods. The corresponding monometallic Ir/γ-Al_2O_3 and Au/γ-Al_2O_3 catalysts were also prepared. The materials were characterized by ICP, XRD, N_2 adsorption, TEM, and H_2 chemisorption. Highly dispersed iridium nanoparticles (<10 nm) were obtained in all cases, while the size of gold nanoparticles increased (up to 50 nm) upon increasing the gold content in the catalyst. The monometallic gold catalyst did not adsorbed H_2. The incorporation of gold increased the amount of irreversible adsorbed hydrogen in the Ir-Au/γ-Al_2O_3 catalysts with respect to the monometallic ones. The products obtained in the MCP hydrogenolysis were 2-methylpentane (2-MP), 3-methylpentane (3-MP) and n-hexane (n-H). The initial rate (molecules of MCP reacted s^{-1} g_{Ir}^{-1}) increased with the gold content. Moreover, the deactivation of the catalysts was lower for bimetallic catalysts, particularly for the co impregnated ones. Consequently, the addition of gold played a marked effect on the chemisorption and catalytic properties of the Ir.

Keywords: bimetallic; catalysts; chemisorption; MCP; hydrogen; hydrogenolysis; Ir; Au.

UNIVERSITAT ROVIRA I VIRGILI
NANOMATERIALS IN CATALYSIS: STUDY OF MODEL REACTIONS.
Ricardo José Chimentao
ISBN: 978-84-690-7618-7 / DL: T.1326-2007

II.6.2. Introduction

Methylcyclopentane (MCP) is a recognized probe molecule in the investigation of the structure sensitivity of several hydrocarbon conversions catalyzed usually by noble metal-based catalysts [1-5]. These include reactions involving skeletal rearrangement of hydrocarbons with an accompanying hydrogenation step. The isomerization of pentanes has been usually taken as a test reaction to study particle size and alloying effects on the catalytic performance. The classical work by Gault et al. investigated the arrangement of methylcyclopentane (MCP) on alumina supported Pt catalysts by ^{13}C tracer technique, which made it possible to distinguish elementary steps involved in the reactions [6]. Two mechanisms were proposed: cyclic and bond shift mechanisms, denoted as CM and BS respectively. The CM involves adsorbed methylcyclopentane (MCP) as the intermediate transition state. From this intermediate, three products were obtained (n-hexane (n-H), 2-methylpentane (2-MP) and 3- methylpentane (3-MP)), whose distribution changed with the Pt content and dispersion. Gault et al. showed that, for high dispersion of Pt/Al_2O_3 catalysts, the mechanism of the hydrogenolysis is non-selective and the product distribution is 40% n-H, 40% of 2-MP and 20% of 3-MP. For low dispersion catalysts, the mechanism is selective, resulting in 67% of 2-MP and 33% of 3-MP [7]. The partial H_2 pressure plays a prominent role in the skeletal rearrangement of hydrocarbons [8-10]. In the absence or low hydrogen amounts, the noble metal sites are covered by hydrogen-deficient hydrocarbon residues. As a result, the catalyst dehydrogenation activity largely determines the overall reaction rate. Due to the low hydrogenation activity, formation of strongly adsorbed olefinic species is favored. Upon increasing the hydrogen partial

UNIVERSITAT ROVIRA I VIRGILI
NANOMATERIALS IN CATALYSIS: STUDY OF MODEL REACTIONS.
Ricardo José Chimentao
ISBN: 978-84-690-7618-7 / DL: T.1326-2007

pressures, the hydrocarbon hydrogenation is accelerated and the catalytic process is controlled by isomerization of the olefinic intermediates on the acid centers of the support [11, 12]. Suitable catalysts for hydrocarbon rearrangement are bifunctional in nature. The metal component is responsible for hydrogenation-dehydrogenation activities, while the isomerization function is related with the acidic properties of the support (typically alumina) [13, 14]. Pt/γ-Al_2O_3 was applied industrially for hydrocarbon rearrangement during the 1950s and 1960s, however it is largely changed over to bimetallic systems such as Pt-Re [15], Pt-Au [16], Pt-Ir [17], Pt-Sn [18] and Pd-Au [19]. In all these catalytic systems, the two metal components are miscible. However, catalytic systems of interest for reactions involving hydrocarbon rearrangement are not only limited to combinations of metals that form bulk alloys. Herewith we investigated bimetallic catalysts with very limited miscibility in the bulk [20] such as Ir-Au/γ-Al_2O_3 in methylcyclopentane (MCP) hydrogenolysis. Monometallic Ir supported on oxides has been usually included in systematic studies dealing with hydrogenolysis, dehydrogenation, and isomerization of aliphatic hydrocarbons [21, 22]. The presence of Au in Ir-based catalysts might modulate the catalytic performance of Ir for MCP hydrogenolysis, since Au is virtually inactive for dissociatively adsorption of H_2. Furthermore gold may also induce a different morphology, dispersion, and cluster composition of the resulting Ir species in the material [23-25]. The catalysts were prepared by sequential impregnation and co-impregnation methods. The atomic ratio Au/Ir was systematically varied in the range 0.125-8, including also the corresponding monometallic catalysts. The materials were characterized by ICP, H_2 chemisorption, N_2 adsorption, XRD, and

UNIVERSITAT ROVIRA I VIRGILI
NANOMATERIALS IN CATALYSIS: STUDY OF MODEL REACTIONS.
Ricardo José Chimentao
ISBN: 978-84-690-7618-7 / DL: T.1326-2007

TEM. The role of Au on the Ir dispersion and the H_2 adsorption properties of the catalyst were assessed, which leads to relevant structure-function relationships for the investigated reaction.

II.6.3. Experimental

II.6.3.1 Catalyst Preparation

The support used was γ-Al_2O_3 (Degussa, Type 221) with a grain size of 45-175 μm and a specific surface area (S_{BET}) of 220 m^2 g^{-1}. The as-received support was calcined in static air at 800 K for 4 h before metal incorporation. The Ir-Au/γ-Al_2O_3 catalysts were prepared by impregnation using equimolar acidic aqueous solutions $H_2IrCl_6 \cdot 6H_2O$ and $HAuCl_4 \cdot 3H_2O$ (0.6 M). Two series of Ir-Au/γ-Al_2O_3 catalysts were investigated. The first series was prepared by co-impregnation of alumina with the metal precursor solutions. The samples were dried in vacuum for 2 h. Finally, the resulting samples were dried at 373 K for 12 h and reduced in flowing of hydrogen (50 cm^3 min^{-1}) at 750 K for 4 h. The second series was prepared by sequential impregnation with Ir first, followed by Au. Impregnation of each metal was followed by the removal of solvent under vacuum for 2 h and drying at 373 K for 12 h. The catalysts were reduced at 750 K (4 h) after impregnation with iridium and at 600 K (4 h) after the impregnation with gold. The total metal loading of all samples was fixed at 8 wt. %. The catalysts were prepared with different Au/Ir atomic ratios (0.125, 0.25, 0.5, 1, 2, 4, and 8). Reference monometallic Ir/γ-Al_2O_3 and Au/γ-Al_2O_3 catalysts were also prepared. Ir/γ-Al_2O_3 catalysts were prepared with the same iridium content as in the corresponding bimetallic samples. The monometallic gold catalyst was prepared with 8 wt. %. The

UNIVERSITAT ROVIRA I VIRGILI
NANOMATERIALS IN CATALYSIS: STUDY OF MODEL REACTIONS.
Ricardo José Chimentao
ISBN: 978-84-690-7618-7 / DL: T.1326-2007

monometallic iridium and gold catalysts were reduced at 750 K and 600 K for 4 h respectively. Table 1 summarizes the catalysts prepared in this study and their chemical composition as determined by ICP-AES. The sample code of the bimetallic catalysts refers to the atomic metal ratio (e.g. Au_8- Ir_1) and the preparation method (CI: co-impregnation and SI: sequential impregnation).

Table II.6.1 Chemical composition of the bimetallic and monometallic catalysts

Sample	Au/Ir atomic ratio (at./at.)	Metal content Nominal (wt.%) (wt.%)		In solid	
		Au	Ir	Au	Ir
Ir_8-Au_1 (CI)	0.125	0.91	7.09	0.96	7.00
Ir_4-Au_1 (CI)	0.25	1.63	6.37	1.60	6.44
Ir_2-Au_1 (CI)	0.5	2.71	5.29	2.68	5.32
Ir_1-Au_1 (CI)	1	4.05	3.95	4.12	3.83
Ir_1-Au_2 (CI)	2	5.38	2.62	5.68	2.84
Ir_1-Au_4 (CI)	4	6.43	1.57	6.58	1.52
Ir_1-Au_8 (CI)	8	7.13	0.87	7.34	0.92
Ir_8-Au_1 (SI)	0.125	0.91	7.09	0.90	7.05
Ir_4-Au_1 (SI)	0.25	1.63	6.37	1.65	6.42
Ir_2-Au_1 (SI)	0.5	2.71	5.29	2.75	5.21
Ir_1-Au_1 (SI)	1	4.05	3.95	4.10	3.90
Ir_1-Au_2 (SI)	2	5 .38	2.62	5.25	2.58
Ir_1-Au_4 (SI)	4	6.43	1.57	6.53	1.50
Ir_1-Au_8 (SI)	8	7.13	0.87	7.01	0.85
Ir_8	-	-	7.09	-	7.03
Ir_4	-	-	6.37	-	6.44
Ir_2	-	-	5.29	-	5.25
Ir_1	-	-	3.95	-	3.94
$Ir_{0.5}$	-	-	2.62	-	2.52
$Ir_{0.25}$	-	-	1.57	-	1.53
$Ir_{0.125}$	-	-	0.87	-	0.82
Au_8	-	8.0	-	7.94	-

UNIVERSITAT ROVIRA I VIRGILI
NANOMATERIALS IN CATALYSIS: STUDY OF MODEL REACTIONS.
Ricardo José Chimentao
ISBN: 978-84-690-7618-7 / DL: T.1326-2007

The Ir monometallic catalysts were denoted by Ir_x where x is in the range 0.125- 8. The monometallic iridium catalysts have the same Ir content as the corresponding bimetallic samples. For example, Ir_8 contains 7.09 wt. % Ir, as Ir_8-Au_1, see Table II.6.1). The monometallic gold catalyst (Au_8) contains 8 wt. % Au.

II.6.3.2 Catalyst Characterization

II.6.3.2.1 Chemical composition

The Ir and Au content in the samples were determined by ICP-AES (Philips Scientific PU 7000 spectrometer).

II.6.3.2.2 N_2 adsorption

N_2 adsorption-desorption isotherms at 77 K were measured in a Micromeritics ASAP 2000. Samples were previously evacuated at 623 K for 16 h. The BET method was used to calculate the total surface area of the samples [26].

II.6.3.2.3 X-ray diffraction

X-ray diffraction were measured in a Philips Analytical X' Pert PW 3050 diffractometer using nickel-filtered Cu kα radiation (λ = 1.54056 Å). Spectra were obtained in the 2θ range of 10- 85º, using a scan rate of 4º min^{-1} and a 0.02º data interval. The crystalline phases were identified using the JCPDS files. The average metal particle size (d) was determined by the Scherrer equation, $d = 0.9\lambda/B\cos\theta$, where λ is the wavelength of the radiation (1.5418 Å), □ is the Bragg diffraction angle, and B is the full width at half maximum (fwhm) taking into account the instrumental line broadening using the Warren's correction

UNIVERSITAT ROVIRA I VIRGILI
NANOMATERIALS IN CATALYSIS: STUDY OF MODEL REACTIONS.
Ricardo José Chimentao
ISBN: 978-84-690-7618-7 / DL: T.1326-2007

($B = \sqrt{B_M^2 - B_I^2}$), where BM is the experimental fwhm and BI is the instrumental fwhm.

II.6.3.2.4 Transmission electron microscopy

The morphology and size distribution of the metal particles was investigated by TEM in a JEOL JEM-2000EX II microscope operated at 80 kV. The solid sample, which was homogeneously dispersed in pure ethanol by means of an ultrasonic bath, was deposited in the copper grid and then the solvent was allowed to evaporate under vacuum before analysis.

II.6.3.2.5 H_2 chemisorption

Hydrogen chemisorption was conducted in a Micromeritics ASAP 2010 apparatus. Prior to the measurement, the samples were evacuated at 400 K for 1 h, treated in flow of pure hydrogen (30 cm^3 min^{-1}) at the 600 K for 1 h, evacuated at 600 K for 2 h, and finally cooled down to 310 K for chemisorption. The amount of irreversibly adsorbed H_2 was measured using the double isotherm method [27]. From the first isotherm, measured in the 0-68 kPa pressure range, the total volume of hydrogen adsorbed was obtained. Then, the catalyst was evacuated (about 10^{-6} Torr) again at the chemisorption temperature for 10 min for back sorption measurements in order to obtain the volume of hydrogen reversibly adsorbed. The linear portion of each isotherm was extrapolated to zero pressure in order to estimate the total adsorbed volume and the reversibly adsorbed volume of hydrogen. The difference between two hydrogen uptakes provides the volume of irreversibly adsorbed hydrogen. The fraction of exposed iridium was calculated by the ratio of the irreversible uptake to the total metal

UNIVERSITAT ROVIRA I VIRGILI
NANOMATERIALS IN CATALYSIS: STUDY OF MODEL REACTIONS.
Ricardo José Chimentao
ISBN: 978-84-690-7618-7 / DL: T.1326-2007

content assuming an adsorption stoichiometry of H:Ir = 1:1 [28, 29].

II.6.3.2.6 Catalytic activity

The gas-phase hydrogenolysis of methylcyclopentane (MCP) was studied in a fixed-bed tubular quartz reactor (10 mm i.d.) at 457 K using 50 mg of catalyst. The reaction temperature was controlled by a thermocouple located inside the catalytic bed. A feed of hydrogen saturated with MCP vapor was generated by bubbling H_2 (5 cm^3min^{-1}) through a saturator, which was inserted in a water thermostat at 273 K. Based on this, the partial pressures of H_2 and MCP at the reactor inlet were 94 mbar and 5 mbar, respectively (molar H_2/MCP ratio = 18.8). The reaction products were analyzed on-line using a gas chromatograph (HP6890) equipped with FID and TCD detectors and a Chromosorb WAW 100/120 mesh column.

II.6.4 Results and Discussion

II.6.4.1 Chemical composition and N_2 adsorption

Table II.6.1 shows the iridium and gold loading in the samples as determined by ICP-AES. The nominal metal contents and the values analyzed in the solids were very similar, indicating the efficiency of the preparations. Consequently, we have referred to nominal Au/Ir ratios to describe the experimental results and discussion along the manuscript. Characterization by N_2 adsorption has shown a decrease of the surface area of the catalyst upon impregnation with the metals. The BET area of the calcined γ-Al_2O_3 support (220 m^2 g^{-1}) decreased upon increasing the metal loading (down to 180 m^2 g^{-1} in the bimetallic catalysts).

UNIVERSITAT ROVIRA I VIRGILI
NANOMATERIALS IN CATALYSIS: STUDY OF MODEL REACTIONS.
Ricardo José Chimentao
ISBN: 978-84-690-7618-7 / DL: T.1326-2007

II.6.4.2 X-ray diffraction

The XRD patterns of the reduced Ir-Au/γ-Al_2O_3 catalysts prepared by co-impregnation and sequential impregnation as well as the support are shown in Figure II.6.1. The catalysts were always analyzed in reduced state. The diffraction lines of γ-Al_2O_3 are relatively broad and weak, indicating its low crystallinity. Diffraction lines of Au were identified (JPCDS 04-0784), which have been assigned to the (111), (200), (220), (311), (222) planes of the face centered cubic (fcc) structure of the metal. Contrarily, reflections associated with iridium were not detected in none of the samples, indicating a high dispersion of this metal on the alumina support (Figures II.6.1A-C). The lattice parameter of Au in the catalysts was determined from the (111) reflection using the Bragg equation, resulting in a value around of 4.0781 Å. This is very close to the reported value of a = 4.0786 Å in the JCPDS card. This fact suggests that alloying did not occur in any composition in our samples since Ir and Au are, in bulk, of very limited miscibility [30]. The size of the gold particles, that were estimated from the line width of the (111) reflection using the Scherrer equation, increased upon increasing the gold content in the catalyst (see Figure II.6.1d). The error in this determination is equivalent to the diameter of the symbols used in the figure. However, the particle size of gold for CI catalysts is always lower than for the SI ones. Besides, it can be observed a sharp increase in particle size when going from Au/Ir = 0 to 2, followed by a slight increase at higher gold contents. The increase of the Au cluster size can be rationalized considering that mass transport of gold is significant at temperatures above 1/4 from its melting point [31], resulting in sintering.

UNIVERSITAT ROVIRA I VIRGILI
NANOMATERIALS IN CATALYSIS: STUDY OF MODEL REACTIONS.
Ricardo José Chimentao
ISBN: 978-84-690-7618-7 / DL: T.1326-2007

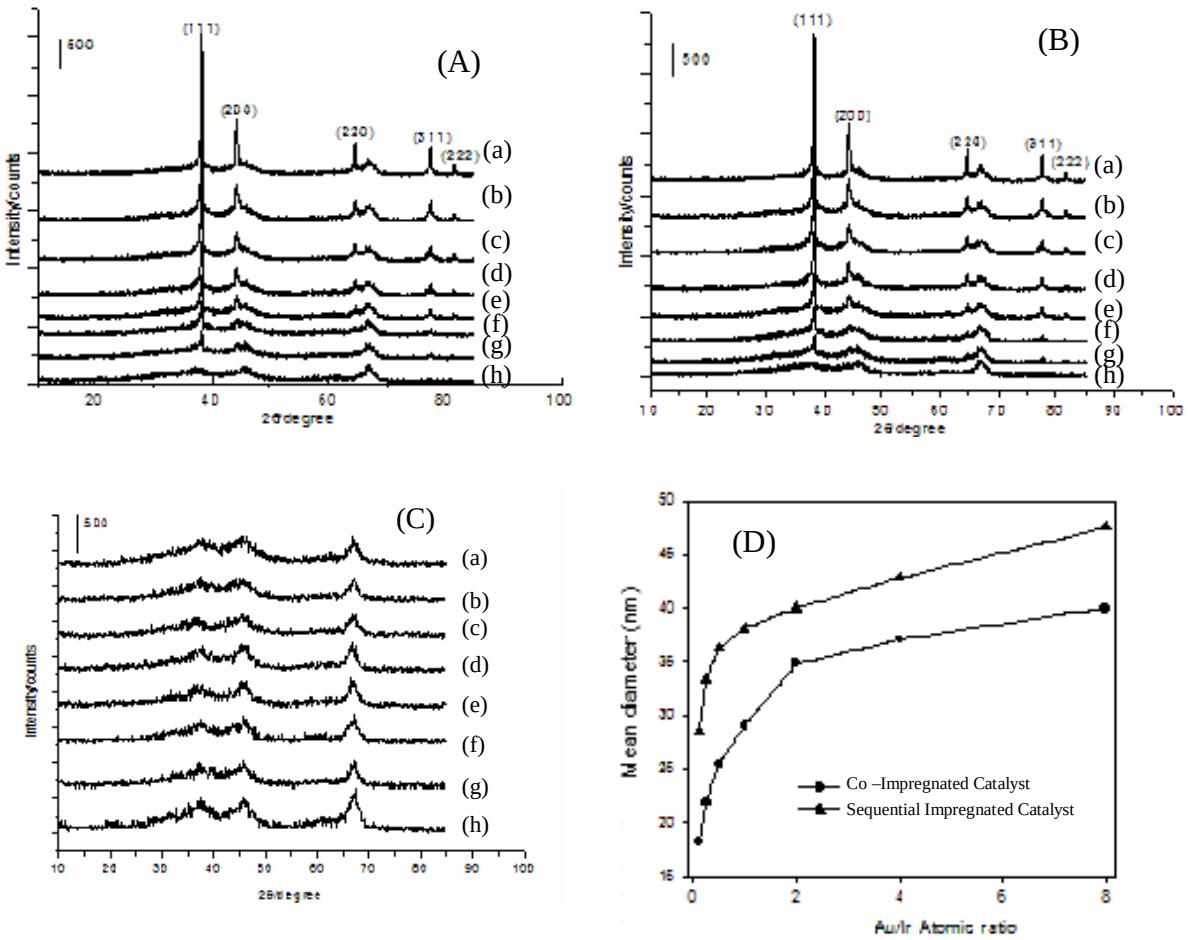

Figure II.6.1 X-ray diffraction of the samples investigated in this study. (A) Co-impregnated (CI) catalysts (a: Ir_1-Au_8; b: Ir_1-Au_4; c: Ir_1-Au_2; d: Ir_1-Au_1; e: Ir_2-Au_1; f: Ir_4-Au_1; g: Ir_8-Au_1; h: γ-Al_2O_3), (B) Sequential Impregnated (SI) catalysts a: Ir_1-Au_8; b: Ir_1-Au_4; c: Ir_1-Au_2; d: Ir_1-Au_1; e: Ir_2-Au_1; f: Ir_4-Au_1; g: Ir_8-Au_1; h: γ-Al_2O_3), (C) Monometallic Ir catalysts (a: $Ir_{0.125}$; b: $Ir_{0.25}$; c: $Ir_{0.5}$; d: Ir_1; e: Ir_2; f: Ir_4; g: Ir_8; h: γ-Al_2O_3). (D) Mean gold particle size as a function of the Au loading in the bimetallic Ir-Au/γ-Al_2O_3 catalysts.

It can be tentatively put forward that the low particle size of gold

UNIVERSITAT ROVIRA I VIRGILI
NANOMATERIALS IN CATALYSIS: STUDY OF MODEL REACTIONS.
Ricardo José Chimentao
ISBN: 978-84-690-7618-7 / DL: T.1326-2007

observed for CI catalysts with respect to SI ones, is probably due to a high interaction between gold atoms and the catalyst support or due to the presence of iridium during the co- impregnation. Taking into consideration these facts, there are several possibilities for the structure of the Ir-Au system in the catalyst. In such case, when two metals have very limited miscibility in bulk, separate clusters of the pure components can be expected to form on the support. Besides, it is also possible that gold atoms cover progressively the iridium surface because metals from the IB group possess lower surface free energy than metals from the VIII group (1410 erg cm^{-2} for Au and 3000 erg cm^{-2} for Ir) [32]. Based on this, enrichment of the iridium surface by gold could be expected. Consequently, the Au and Ir particle size as well as the enrichment of the Ir surface by gold depends on the preparation method of the catalysts.

II.6.4.3 TEM

Figure II.6.2a,b,c shows the TEM images for the representative reduced Ir_2-Au_1 (CI), Ir_2-Au_1 (SI), and Ir_2 catalysts, respectively, which have the same iridium content (~5.3 wt. % Ir, Table 1). Well-defined γ-Al_2O_3 crystallites were observed in all the samples, where the metal particles are stabilized. The monometallic Ir_2 catalyst (Figure 3c) exhibits iridium clusters of uniform size (3-4 nm), which were not identified by XRD. The SI bimetallic catalysts (Figure II.6.2b) show a broader size distribution (3-40 nm) compared with the monometallic iridium sample. Metal iridium particles with similar size than for monometallic iridium samples are observed. Besides, together with metal iridium particles, larger metal gold particles (between 10-40 nm) were also observed.

UNIVERSITAT ROVIRA I VIRGILI
NANOMATERIALS IN CATALYSIS: STUDY OF MODEL REACTIONS.
Ricardo José Chimentao
ISBN: 978-84-690-7618-7 / DL: T.1326-2007

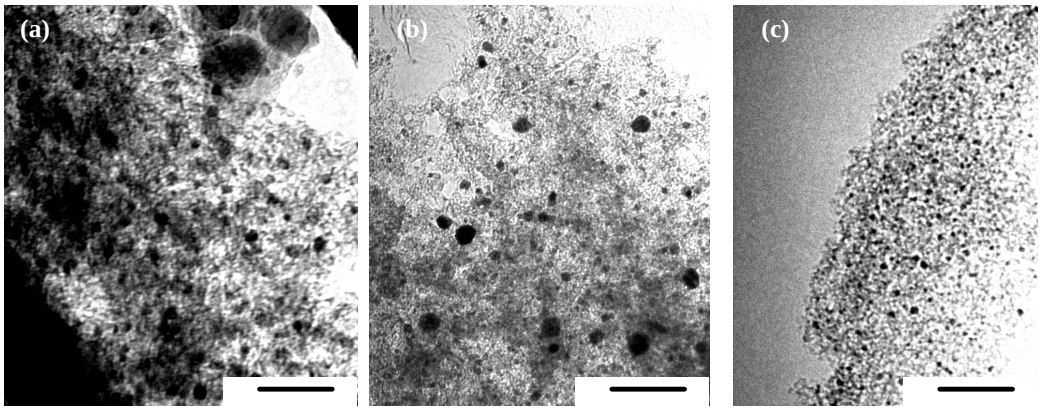

Figure II.6.2 TEM images of Ir_2-Au_1 (CI) (a), Ir_2-Au_1 (SI) (b) and Ir_2 catalysts (c). The bars correspond to 100 nm.

The gold metal particles of the SI catalyst seem to be larger than the gold particles for CI sample (see Figures II.6.3a and 3b), that is in agreement with the crystall sizes determined by XRD. Besides, under magnification values in this work (below 100.000 x) the metal iridium particles for CI sample are not detected.

II.6.4.4 H_2 chemisorption

The results of H_2 chemisorption at 310 K on the reduced catalysts are summarized in Table II.6.2. As expected, the irreversible H_2 uptake diminishes with decreasing the iridium loading (see Table II.6.2 and Figure II.6.3). Comparing catalysts with similar iridium content the irreversible H_2 uptake was in the following order CI>SI> monometallic catalysts. This fact is more evident for low iridium loading. For example, the Ir_1-Au_8 (CI) catalyst has five times more irreversible hydrogen than the corresponding monometallic sample ($Ir_{0.125}$).The monometallic gold-containing catalyst did not show hydrogen

UNIVERSITAT ROVIRA I VIRGILI
NANOMATERIALS IN CATALYSIS: STUDY OF MODEL REACTIONS.
Ricardo José Chimentao
ISBN: 978-84-690-7618-7 / DL: T.1326-2007

adsorption, in agreement with previous works [23, 24]. Typical isotherms for Ir-Au catalysts are shown in Figure II.6.3A-C. The lines represent strongly adsorbed hydrogen, that is, the difference between the total hydrogen adsorption and the weakly adsorbed hydrogen. Metallic dispersions were expressed in terms of the quantity H/Ir, which represents the ratio between the number of irreversibly adsorbed hydrogen atoms and the total number of iridium atoms (see also Table II.6.2). For high Ir loading all the samples showed quite similar H_2 uptake (between 2.41 and 2.67 μmol. g^{-1} cat) as well as H/Ir (between 0.58 and 0.65). However a strong difference was observed in the samples with low iridium contents. For the co impregnated catalysts (CI) the H/Ir remained practically unaffected by the amount of iridium or gold in the sample (the H/Ir values are around 0.6). Contrarily, for SI catalysts the H/Ir value decreased when the iridium amount decreased. This effect is more evident for monometallic iridium samples. For example, Ir_1-Au_8 (CI), Ir_1-Au_8 (SI) and $Ir_{0.125}$ samples which have the same iridium amount show an H/Ir value of 0.59, 0.21, and 0.12, respectively. These facts are also illustrated in Figure II.6.3d. The highest H/Ir decrease observed for monometallic Ir catalysts, mainly at lower iridium contents, could be attributed to a strong interaction between the Ir and the support. Probably, due to the acid character of the iridium precursor ($H_2IrCl_6 \cdot 6H_2O$) some part of the surface of the support (γ-Al_2O_3) can be dissolved covering the surface of the iridium particle and consequently decreasing the H_2 chemisorption. The highest H/Ir values observed for SI catalysts with respect to the monometallic iridium catalysts could be explained taking into account that gold apparently spreads over the iridium surface. This suggestion is reasonable because Au has lower surface free energy than Ir. In this

UNIVERSITAT ROVIRA I VIRGILI
NANOMATERIALS IN CATALYSIS: STUDY OF MODEL REACTIONS.
Ricardo José Chimentao
ISBN: 978-84-690-7618-7 / DL: T.1326-2007

sense, the higher H_2 uptake in the bimetallic catalysts as compared to the monometallic Ir catalysts can be tentatively associated with the spillover of atomic hydrogen from iridium sites to adjacent gold sites [33]. This fact is more evident for the bimetallic catalysts obtained by co-impregnation method (CI catalysts). Alternatively, this result can be also explained by a change in the adsorption stoichiometry of hydrogen on iridium induced by an electronic effect due to adjacent gold ions [35].

Besides, considering the TEM results, particularly for the CI samples, it seems that the incorporation of gold changes the Ir dispersion and as consequence the hydrogen adsorption properties of iridium was improved. This local bimetallic domain, where Au and Ir may have a direct interaction, induces an electronic effect. The presence of gold clearly has a marked effect on surface processes occurring on iridium. This effect is more evident in the co-impregnated catalysts. Probably in these sites, iridium atoms dissociatively adsorb H_2, which is subsequently spillover to the surrounding Au atoms, explaining the overall enhanced H_2 uptake.

UNIVERSITAT ROVIRA I VIRGILI
NANOMATERIALS IN CATALYSIS: STUDY OF MODEL REACTIONS.
Ricardo José Chimentao
ISBN: 978-84-690-7618-7 / DL: T.1326-2007

Table II.6.2 H_2 chemisorption at 310 K data of Ir-Au catalysts by chemisorption

Samples	Irreversible H_2 uptake ($\mu mol\ g^{-1}cat$)	H/Ir (-)
Ir_8-Au_1 (CI)	2.60	0.63
Ir_4-Au_1 (CI)	2.22	0.60
Ir_2-Au_1 (CI)	1.92	0.62
Ir_1-Au_1 (CI)	1.47	0.64
Ir_1-Au_2 (CI)	1.03	0.67
Ir_1-Au_4 (CI)	0.61	0.66
Ir_1-Au_8 (CI)	0.30	0.59
Ir_8-Au_1 (SI)	2.67	0.65
Ir_4-Au_1 (SI)	2.16	0.58
Ir_2-Au_1 (SI)	1.57	0.50
Ir_1-Au_1 (SI)	1.07	0.46
Ir_1-Au_2 (SI)	0.50	0.32
Ir_1-Au_4 (SI)	0.22	0.24
Ir_1-Au_8 (SI)	0.11	0.21
Ir_8	2.41	0.58
Ir_4	2.06	0.55
Ir_2	1.50	0.48
Ir_1	0.86	0.37
$Ir_{0.5}$	0.31	0.20
$Ir_{0.25}$	0.14	0.15
$Ir_{0.125}$	0.06	0.12
Au_8	-	-

UNIVERSITAT ROVIRA I VIRGILI
NANOMATERIALS IN CATALYSIS: STUDY OF MODEL REACTIONS.
Ricardo José Chimentao
ISBN: 978-84-690-7618-7 / DL: T.1326-2007

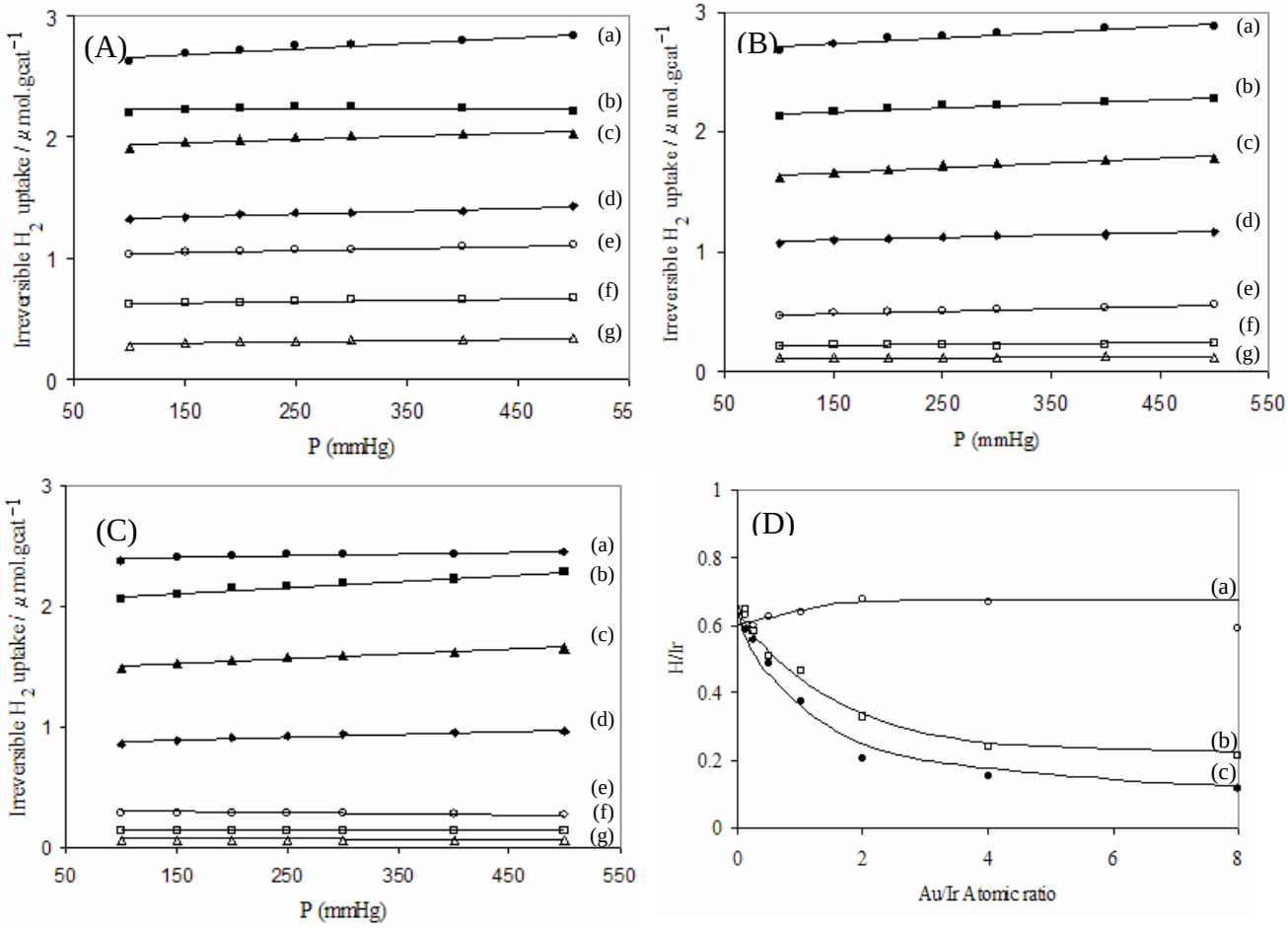

Figure II.6.3 Irreversible hydrogen adsorption isotherms of the CI, SI and Ir monometallic samples at 310 K. (A) CI samples: (a) Ir_8-Au_1; (b) Ir_4-Au_1; (c): Ir_2-Au_1; (d) Ir_1-Au_1; (e) Ir_1-Au_2; (f) Ir_1-Au_4; (g) Ir_1-Au_8. (B) SI samples: (a) Ir_8-Au_1; (b) Ir_4-Au_1; (c): Ir_2-Au_1; (d) Ir_1-Au_1; (e) Ir_1-Au_2; (f) Ir_1-Au_4; (g) Ir_1-Au_8. (C) Monometallic Ir samples: (a) Ir_8; (b) Ir_4; (c) Ir_2; (d) Ir_1; (e) $Ir_{0.5}$; (f) $Ir_{0.25}$; (g) $Ir_{0.125}$. (D) Dispersion (H/Ir) values versus atomic Au/Ir ratio for (a) CI catalysts, (b) SI catalysts, (c) monometallic Ir catalysts.

II.6.4.5 Catalytic Activity

Table II.6.3 summarizes the catalytic activity values obtained in the

UNIVERSITAT ROVIRA I VIRGILI
NANOMATERIALS IN CATALYSIS: STUDY OF MODEL REACTIONS.
Ricardo José Chimentao
ISBN: 978-84-690-7618-7 / DL: T.1326-2007

methylcyclopentane hydrogenolysis reaction. The initial rate expressed as MCP molecules reacted per second and per gram of Ir is depicted in the Table II.6.3. The catalytic activity strongly decreased in 60 minutes of reaction for all the catalysts. Previous works [35, 36] also mentioned the deactivation of MCP hydrogenolysis reaction over noble metal-based catalysts.

Table II.6.3 Catalytic activity in the MCP hydrogenolysis at 457 K

Catalyst	Initial rate (10^{19} MCP molecules s^{-1} g_{Ir}^{-1})	2-MP/3-MP[a]
Ir_8-Au_1 (CI)	3.03	2.4
Ir_4-Au_1 (CI)	3.34	2.4
Ir_2-Au_1 (CI)	3.85	2.3
Ir_1-Au_1 (CI)	5.21	2.1
Ir_1-Au_2 (CI)	5.83	2.0
Ir_1-Au_4 (CI)	6.28	2.1
Ir_1-Au_8 (CI)	6.14	2.0
Ir_8-Au_1 (SI)	2.92	2.4
Ir_4-Au_1 (SI)	2.92	2.3
Ir_2-Au_1 (SI)	3.13	2.2
Ir_1-Au_1 (SI)	3.82	2.1
Ir_1-Au_2 (SI)	3.86	2.0
Ir_1-Au_4 (SI)	3.88	2.1
Ir_1-Au_8 (SI)	3.87	2.1
Ir_8	2.77	2.4
Ir_4	2.74	2.3
Ir_2	2.53	2.2.
Ir_1	2.78	2.1
$Ir_{0.5}$	1.67	1.9
$Ir_{0.25}$	2.03	2.0
$Ir_{0.125}$	2.06	2.1
Au_8	-	-

[a] Ratio between the selectivity to 2-MP and 3-MP.

The deactivation was probably originated from the extensive

UNIVERSITAT ROVIRA I VIRGILI
NANOMATERIALS IN CATALYSIS: STUDY OF MODEL REACTIONS.
Ricardo José Chimentao
ISBN: 978-84-690-7618-7 / DL: T.1326-2007

dehydrogenation of chemisorbed hydrocarbon to highly unsaturated specie which in turn follows a sequence of dehydrogenation steps leading to the formation of carbon surface fragments deactivating the catalyst [37].

On the other hand, a blank test run with the alumina support showed no conversion of methylcyclopentane at the same reaction conditions. The monometallic gold catalyst (Au_8) also did not show activity for the MCP hydrogenolysis. The distribution of the products did not change significantly using different catalysts as is shown in Table 3. The main products obtained were 2-methylpentane (2-MP), 3-methylpanetane (3-MP) and n-hexane (n-H) with selectivity closed to 40%, 20% and 40%, respectively. The presence of the gold did not affect the ratio 2-MP/3-MP. The selectivity distribution was close to the statistical distribution of products with the ratio between the selectivity to 2-methylcyclopentane (2-MP) and the selectivity to 3-methylcyclopentane (3-MP) near to 2. The ratio 2-MP/3-MP is related to the rate in the cleavage of C-C bonds located under β position to those located in the γ position relative to the tertiary carbon atom. Based solely on statistical considerations this ratio should be 2 [38]. We did not observed cyclopentane or products of ring enlargement, such as cyclohexane and benzene. From our results it is possible to conclude that non-selective product distribution was observed for all the catalysts. The MCP hydrogenolysis results offered interesting fingerprints in probing the structure of the Ir-Au catalysts. The data in the Table II.6.3 provide a piece of evidence of interaction between gold and iridium particularly at higher gold contents in the bimetallic catalysts. For co impregnated catalysts (CI), the initial rate (MCP molecules reacted s^{-1} g_{Ir}^{-1}) increased with the gold content in the

UNIVERSITAT ROVIRA I VIRGILI
NANOMATERIALS IN CATALYSIS: STUDY OF MODEL REACTIONS.
Ricardo José Chimentao
ISBN: 978-84-690-7618-7 / DL: T.1326-2007

catalyst. For example, the Ir_1-Au_8(CI) catalyst has an initial rate of around two times higher than for Ir_8-Au_1(CI) catalyst. For SI samples a similar trend was observed. However, the initial rate was always lower than the correspondent CI samples. The monometallic samples showed the lowest initial rate values. Besides, the initial rate for monometallic catalysts slightly decreased when the iridium content decreased. Consequently, the addition of gold in the bimetallic catalysts increased the initial reaction rate compared with the corresponding monometallic Ir catalysts as depicted in Figure II.6.4. Taking in consideration that similar hydrogen amount with respect to iridium content and H/Ir values were obtained for all the CI catalysts, while for the SI and monometallic Ir samples the H/Ir values decreased when the Ir content decreased, these data provide further strong indication of interaction between the Ir and Au. However an increase in the initial rate was observed for CI and SI bimetallic catalysts when the Au content increased compared to the correspondent monometallic ones. If the catalysts consisted of merely separated gold clusters and iridium clusters, it would be reasonable to expect that the initial rate must be not affected when gold was incorporated in the catalysts.

This expectation would be based on the fact that the gold did not present activity for the MCP hydrogenolysis, so the incorporation of gold would presumably behave as an inert diluent. However, the addition of gold in the bimetallic catalysts increased the initial rate compared with the corresponding monometallic Ir catalysts. These data provide another evidence of interaction between the Ir and Au in the bimetallic catalysts, particularly for the CI samples.

This fact may favor the hydrogenolysis reaction instead of the dehydrogenation reaction that produces the strong adsorption of

UNIVERSITAT ROVIRA I VIRGILI
NANOMATERIALS IN CATALYSIS: STUDY OF MODEL REACTIONS.
Ricardo José Chimentao
ISBN: 978-84-690-7618-7 / DL: T.1326-2007

dehydrogenated organic molecules on the surface of the catalysts leading the deactivation. In this sense, the deactivation process has been studied. The results are shown in Figure II.6.5.

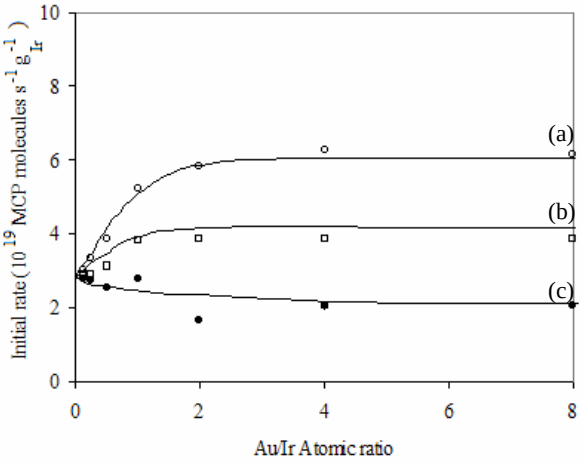

Figure II.6.4 Evolution of initial rate (MCP molecules reacted s^{-1} g_{Ir}^{-1}) versus Au/Ir atomic ratios. (a) CI catalysts, (b) SI catalysts, (c) monometallic Ir catalysts.

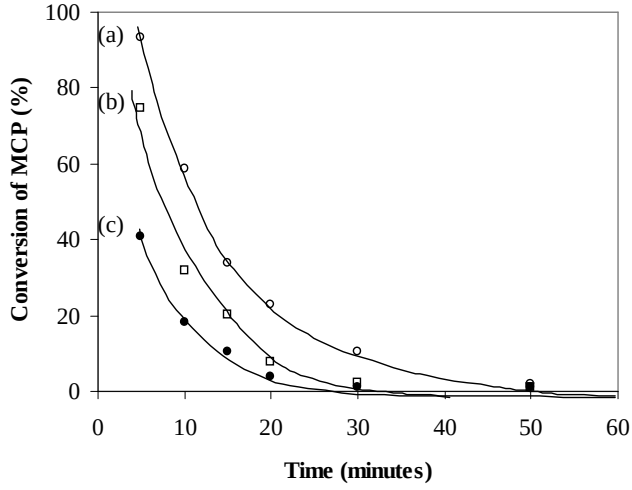

Figure II.6.5 Conversion vs. time curves in the methylcyclopentane reaction at 457K: (a) CI catalysts, (b) SI catalysts, (c) monometallic Ir

UNIVERSITAT ROVIRA I VIRGILI
NANOMATERIALS IN CATALYSIS: STUDY OF MODEL REACTIONS.
Ricardo José Chimentao
ISBN: 978-84-690-7618-7 / DL: T.1326-2007

catalysts.

Nevertheless all the catalysts suffered deactivation under the experimental conditions, the order of stability of the catalysts is as follows: CI > SI > monometallic catalysts. The bimetallic catalysts showed less severe deactivation compared with the monometallic ones, particularly the CI catalysts. The addition of gold seemed to play an important role in the stability of the catalysts that could be related with the presence of Au atoms on the surface of the iridium that increases the capability for the adsorption of hydrogen in the surface of the catalyst improving the catalytic behavior.

II.6.5 Conclusion

Several Ir-Au/γ-Al_2O_3 catalysts were prepared by co-impregnation and sequential impregnation methods. Iridium and gold monometallic catalysts were also prepared as references. XRD analysis indicated a broader particle size distribution of the gold (10-40 nm). The iridium particles distributed on the support originating high-dispersed particles. Monometallic gold catalyst was inactive for the adsorption of hydrogen. The chemisorption results showed higher hydrogen adsorption of Ir-Au system compared with the pure Ir. This fact indicated that the adsorption properties were determined by the localized properties of the metal surface sites suggesting interaction between the metals. The main products obtained in the MCP hydrogenolysis were 2-methylpentane (2-MP), 3-methylpentane (3-MP) and n-hexane (n-H). The catalysts tested in this work showed non-selective product distribution. In applying MCP hydrogenolysis as a probe to establish interaction between iridium and gold, it was found that the incorporation of gold increased the initial rate (MCP molecules

reacted s^{-1} g_{Ir}^{-1}) compared to the monometallic Ir catalysts. Besides, a low deactivation rate was observed for bimetallic catalysts. To explain this different catalytic behaviour one could consider that some type of interaction between Ir and Au in the bimetallic catalysts occurs.

Acknowledgement. This work was supported by the Fundação de Amparo à Pesquisa do Estado de São Paulo, Brazil (FAPESP- Project 99/12371-4) and Projects REN2002-04464-CO2-01 and PETRI 95-0801.OP, from Ministerio de Ciencia y Tecnologia (Spain).

II.6.6 References

[1] M. Boudart, *Adv. Catal.* **20** (1969) 153.

[2] G. Leclercq, L. Leclercq and R. Maurel, *J. Catal.* **50** (1977) 87.

[3] J. M. Dartigues, A. Chambellan, F. G. Gault, *J. Am. Chem. Soc.* **98** (1976) 856.

[4] J. H. Sinfelt, *Bimetallic catalysts: Discoveries, concepts and Applications*, John Wiley & Sons, New York, 1983.

[5] Z. Paál and P. Tétényi, *Nature* **267** (1977) 234.

[6] F. G. Gault, *Adv. Catal.* **30** (1980) 1.

[7] F. G. Gault, V. A. Ebrahimi, F. Garin, P. Parayre and F. Weisang, *Bull. Soc. Chim. Belg.* **88** (1979) 475.

[8] Z. Paál, P. Tétényi and M. Dobrovoliszky, *React. Kinet. Catal. Lett.* **163** (1988) 37.

[9] F. G. Ciapetta and D. N. Wallace, *Catal. Rev.* **5** (1) (1971) 67.

[10] G.A Mills, H. Heinemann and T. H. Milliken, *Ind. Eng. Chem.* **45** (1953) 134.

[11] J. B. F. Anderson, R. Burch and J. A. Cairns, *J. Catal.* **107** (1987) 351.

UNIVERSITAT ROVIRA I VIRGILI
NANOMATERIALS IN CATALYSIS: STUDY OF MODEL REACTIONS.
Ricardo José Chimentao
ISBN: 978-84-690-7618-7 / DL: T.1326-2007

[12] J. B. F. Anderson, R. Burch and J. A. Cairns, J. Catal. 107 (1987) 364.

[13] C. Corolleur, S. R. Corolleur and F. G. Gault, *J. Catal.* **24** (1972) 385.

[14] C. Corolleur, D. Tomanova and F. G. Gault, *J Catal.* **24** (1972) 401.

[15] W. Juszczyk and Z. Karpinski, *Appl. Catal.* **206** (2001) 67.

[16] J. K. A. Clarke, A. F. Kane and T. Baird, *J. Catal.* **64** (1980) 200.

[17] Y. J. Huang, S. C. Fung, W. E. Gates and G. B. Mcvicker, *J. Catal.* **118** (1998) 192.

[18] K. Balakkrishnan and J. Schwank, *J. Catal.* **132** (1979) 458.

[19] Y. L. Lam and M. Boudart, *J. Catal.* **50** (1977) 530.

[20] K. E. Foger and J. R. Anderson, *J. Catal.* **64** (1980) 448.

[21] Y. Barron, G. Maire, J. M. Muller and F. G. Gault, *J. Catal.* **5** (1966) 428.

[22] K. E. Foger and J. R. Anderson, *J. Catal.* **59** (1979) 325.

[23] M Okada, M. Nakamura, K. Moritani and T. Kasai, *Surf. Sci.* **523** (2003) 218.

[24] B. Hammer and J. K. Nøbskov, *Nature* **376** (1995) 238.

[25] G. A. Somorjai, *Adv. Catal.* **26** (1977) 1.

[26] S. J. Greg and K. S. W. Sing. *Adsorption, Surface Area and Porosity*. Academic Press. Londres.2ed. 1982.

[27] J. H. Sinfelt, Y. L. Lam, J. A. Cusumano and A. E. Barnett, *J. Catal.* **42** (1976) 227.

[28] G. B. McVicker, R. T. K. Baker, R. L. Garten and E. L. Kugler, *J. Catal.* **65** (1980) 207.

[29] J. M. Guil, A. P. Masía, R. A Panigo and J. M. T. Menayo,

UNIVERSITAT ROVIRA I VIRGILI
NANOMATERIALS IN CATALYSIS: STUDY OF MODEL REACTIONS.
Ricardo José Chimentao
ISBN: 978-84-690-7618-7 / DL: T.1326-2007

Thermochimica Acta, **312**, 1998, 115-124

[30] Elliott R. P. *Constitution of Binary Alloys*. McGraw Hill, New York, 1965.

[31] M. Hansen. *Constitution of Binary Alloys*. McGraw-Hill, New York, 1958.

[32] G. Somorjai in *Chemistry in two dimensions*. Cornell University Press, Cornell, 1980.

[33] W. C. Conner and J. L. Falcone, *Chem. Rev.* **95** (1995) 759.

[34] M. Okada, S. Ogura, W. A. Diño, M. Wilde, K. Fukutani and T. Kasai, *Appl. Surf. Sci.* **246** (2005) 68.

[35] R. E. Kramer and H. Zuegg, *J. Catal.* **80** (1983) 446.

[36] R. E. Kramer and H. Zuegg, *J. Catal.* **85** (1984) 530.

[37] J. H. Sinfelt, *Prog. Solid State Chemistry*, **10** (1975) 55.

[38] Z. Karpiński, *Adv. Catal.* **37** (1990) 45.

UNIVERSITAT ROVIRA I VIRGILI
NANOMATERIALS IN CATALYSIS: STUDY OF MODEL REACTIONS.
Ricardo José Chimentao
ISBN: 978-84-690-7618-7 / DL: T.1326-2007

Final Considerations

- Because the high symmetry of the *fcc* system, forcing noble-metal colloidal particles to acquire a non-spherical shape is not an easy matter, and involves a competition against the desire of the systems to minimize the surface area energy through the formation of spherical particles. Therefore, the most common morphologies are isotropic particles, ranging from quasi-spherical to highly faceted particles, typically being octahedral or cubic in shape as well as nanowires/rods, nanopolyhedra and nanocubes. The production of this thermodynamically unfavorable reaction environment was attributed to the preferential absorption of the capping agent, such as the case of the silver nanowires produced by the polyol method in the presence of poly(vinyl pyrrolidone) (PVP). Different shapes of Ag nanoparticles have been prepared by polyol process using PVP as a structure-directing agent. The morphologies of the silver nanoparticles prepared by the polyol process were found to depend heavily on the experimental conditions such as temperature and the molar ratio between PVP and $AgNO_3$. Three silver nanoparticles were obtained: silver nanowires, nanocubes and nanopolyhedra with preferred orientation in (111) facets. It is highly possible that the PVP, under specific reaction conditions, is truly helping to increase the yield of a particular structure, but the growth mechanism should also consider nucleation and kinetics, and not only thermodynamics or physical constrictions imposed y the modifying agent. This suggestion relies on the formation of twin planes that probably

ISBN: 978-84-690-7618-7 / DL: T.1326-2007

promote the creation of favorable sites for further growth, leading to the anisotropic growth as observed for our silver particles.

- We chose noble metals (such as Ag-Au system) as an example to demonstrate the effectiveness of the phase transfer system in yielding high quality of nanocrystals. Silver and gold form random solid solutions over the entire composition range. As a result, alloy samples with a large variation in surface composition can be formulated and studied. Uniform nobel metal quantum dots, or nanocrystals, were obtained through the reduction by $NaBH_4$ of the nobel metal ions inside the micells. Our transmission electron microscopy analysis revealed good uniformity and that the particules were usually in round shapes with smooth surface. The diameters of the nanocrystals can be reasonably tuned from about 4 to 15 nm. X-ray diffraction measurement have proven the successful synthesis of face centered cubic structure Ag (JCPDS 4-183), Au (JCPDS 4-184). Uniform Au-Ag alloy were obtained. Our XPS analysis were consistent with the EDX results. All the nanocrystals was easily dispersed in an nonpolar solvent such as toluene to form homogeneous colloidal solutions which were stable for months. By dropping the solution on the surface of a substrate monolayer film of functional nanocrystals which will greatly increase their application in nanoscience and technology.

- Styrene epoxidation by oxygen was carried out on silver nanowires promoted with different contents of cesium. Two

UNIVERSITAT ROVIRA I VIRGILI
NANOMATERIALS IN CATALYSIS: STUDY OF MODEL REACTIONS.
Ricardo José Chimentao
ISBN: 978-84-690-7618-7 / DL: T.1326-2007

species of oxygen was detected: (i) subsurface oxygen (O_β) and strongly chemisorbed oxygen (O_γ). Addition of CsOH significantly improves conversion of styrene and the selectivity to SO. The cesium may affect the acid-base properties by changing the electron density around the metal. TPR experiments indicated that the cesium affected the reducibility of the silver. The presence of cesium may also influence the type of oxygen present on the silver surface in equilibrium with gaseous oxygen and the reaction conditions in the reoxidation step. Indeed the alkaline metals in metal-based catalysts are known to facilitate the dissociation of an oxygen molecule. This can explain the positive effect of the alkaline metal promoter observed on the rate of the partial oxidation of styrene. The O_β species seemed to be critical for the activity of the silver catalysts. There is a strong correlation between the peak signal of the O_β specie with the catalytic activity toward the epoxidation of the styrene. This specie was responsible for the high activity and selectivity while the strongly adsorbed surface atomic oxygen (O_γ) showed lower activity. If the O_β specie does not participate in the epoxidation directly at least serve as like an oxygen reservoir that supplies oxygen for the reaction playing a key role for the epoxidation.

- The greater the Cu content in the alloy, the smaller the clusters size achieved. Highly dispersed copper species are required for the partial oxidation of propylene by N_2O. The spectroscopy and microscopy findings suggest that the active species for

UNIVERSITAT ROVIRA I VIRGILI
NANOMATERIALS IN CATALYSIS: STUDY OF MODEL REACTIONS.
Ricardo José Chimentao
ISBN: 978-84-690-7618-7 / DL: T.1326-2007

propylene epoxidation consists of a highly dispersed nanoscopic copper metallic phase. The active phase of copper appears to be a highly dispersed form of metallic Cu. Higher metal particles favor the formation of total combustion products.

- Vanadium (V) oxide supported on mesoporous silica (MCM-41) and TiO_2 (anatase) promoted by sodium were investigated in the partial oxidation of ethanol to acetaldehyde. These results were correlated with the nature of the vanadia species formed, particularly at intermediate sodium contents. The introduction of sodium may modify properties essential for activity and selectivity of the vanadium catalyst, such as acid-base properties, reducibility (T_{max}) and rate of electron transfer in the catalyst and between the catalyst and adsorbed ethanol. The optical absorption and TPR experiments indicated that as the sodium content increased the dispersion of the vanadium species is further enhanced. This work has elucidated that Na plays a strong role on the dispersion of the vanadium species mainly for supports with high surface area such as MCM-41. As the sodium content increased the dispersion of the vanadium species is further enhanced. The positive effect of Na addition on the selectivity to acetaldehyde is mainly due to the decrease in acidity and increase in basicity. The role of the Na it is also related with the depression of the carbonaceous deposits on the surface of the catalyst. UV-vis spectra and TPR analysis also reinforced that sodium governs the dispersion and the reducibility of the vanadium species. By TPO analysis revealed that as the Na content increased a less yield in the carbon

UNIVERSITAT ROVIRA I VIRGILI
NANOMATERIALS IN CATALYSIS: STUDY OF MODEL REACTIONS.
Ricardo José Chimentao
ISBN: 978-84-690-7618-7 / DL: T.1326-2007

deposition was found. The Na seems to have a strong role in the adsorption and catalytic properties of the vanadium catalysts.

- Exfoliation is regarded as an effective way of maximizing the accessibility and utility of the LDH host layers as well as introducing physicochemical properties effects. The materials obtained through exfoliation were composed of very small crystallites, usually several tens of nanometers in lateral size, and often in aggregate form of heavily buckled fine crystallites. The method of exfoliation onto hydrotalcites clearly influenced the catalytic activity in the styrene epoxidation, since difference in textural properties were obtained. Higher surface area was generated by exfoliation in the hydrotalcite materials. Exfoliated materials by ultrasound presented the higher surface area. This fact leaded to an increase number exposed basic sites, and thus to an improved catalytic activity.

- Although the iridium-gold system can hardly be considered on which form alloys, bimetallic Ir-Au aggregates showed improved adsorption and catalytic properties compared with the monometallic iridium sample in the MCP hydrogenolysis reaction. Several Ir-Au/γ-Al_2O_3 catalysts were prepared by co-impregnation and sequential impregnation methods. Iridium and gold monometallic catalysts were also prepared as references. XRD analysis indicated a broader particle size distribution of the gold (10-40 nm). The iridium particles distributed on the support originating high-dispersed particles. The chemisorption

UNIVERSITAT ROVIRA I VIRGILI
NANOMATERIALS IN CATALYSIS: STUDY OF MODEL REACTIONS.
Ricardo José Chimentao
ISBN: 978-84-690-7618-7 / DL: T.1326-2007

results showed higher hydrogen adsorption of Ir-Au system compared with the pure Ir. H_2 adsorbs on Ir while it does not adsorb, at any appreciable extent, on gold. This fact indicated that the adsorption properties were determined by the localized properties of the metal surface sites suggesting interaction between the metals. The amount H_2 adsorbed was expressed in terms of the quantity H/Ir which represents the ratio of the number of hydrogen atoms adsorbed to the number of the iridium atoms in the catalyst. The stoichiometry of the strongly chemisorbed fraction was considered to correspondent closely to one hydrogen atom per surface of iridium atom. Values of H/Ir were higher for bimetallic samples than for monometallic iridium sample, indication some interaction between iridium and gold. These results were interpreted primarily in terms of near-neighbor electronic interactions between gold and iridium atoms. The gold may affect the electron structure of surface of the iridium atoms and in terms of geometric alterations of surface. The main products obtained in the MCP hydrogenolysis were 2-methylpentane (2-MP), 3-methylpentane (3-MP) and n-hexane (n-H). The catalysts tested in this work showed non-selective product distribution. In applying MCP hydrogenolysis as a probe to establish interaction between iridium and gold, it was found that the incorporation of gold increased the initial rate (MCP molecules reacted s^{-1} g_{Ir}^{-1}) compared to the monometallic Ir catalysts. Besides, a low deactivation rate was observed for bimetallic catalysts. To explain this different catalytic behaviour one could consider that some type of

UNIVERSITAT ROVIRA I VIRGILI
NANOMATERIALS IN CATALYSIS: STUDY OF MODEL REACTIONS.
Ricardo José Chimentao
ISBN: 978-84-690-7618-7 / DL: T.1326-2007

interaction between Ir and Au in the bimetallic catalysts occurred.

UNIVERSITAT ROVIRA I VIRGILI
NANOMATERIALS IN CATALYSIS: STUDY OF MODEL REACTIONS.
Ricardo José Chimentao
ISBN: 978-84-690-7618-7 / DL: T.1326-2007

Congress Participation

1. Reunión de la Sociedad Española de Catálisis (SECAT) Málaga, España. Junio 22 – 25 de 2003.Chimentao, R.J; Medina, F.; Rodríguez, X.; Cesteros, Y.; Salagre, P.; Sueiras, J.E. *Nuevas Rutas Sintéticas de Materiales Mesoporosos Mediante Copolimeros No Iónicos.*

2. SECAT 2005 (Reunión de la Sociedad Española de Catálisis), Móstoles, 27- 29 junio 2005. Catálisis R.J. Chimentão, F. Medina, J.L.G. Fierro, J.E. Sueiras, Y. Cesteros y P. Salagre. *Catalizadrores de nanofilamentos de plata promocionados con cesio en la epoxidacion del estireno*

3. 13th International Congress on Catalysis in. Paris 2004. R.J Chimentao, I. Kirm,; F. Medina, X. Rodríguez, Y. Cesteros, P. Salagre, J.E. Sueiras, J.L.G. Fierro. *Study of Different Morphologies of Silver Nanoparticles Catalysts for the Selective Oxidation of Styrene*

4. International Symposium Effects of Surface Heterogeneity in Adsorption and catalysis on Solids (ISSHAC-V, Gdanski, Poland (2004)). R.J Chimentao, I. Kirm,; F. Medina, X. Rodríguez, Y. Cesteros, P. Salagre, J.E. Sueiras, J.L.G. Fierro, *Sensitivity of Styrene Oxidation Reaction to the Catalyst Structure of Silver Nanoparticles*

5. International Symposium Effects of Surface Heterogeneity in

Adsorption and catalysis on Solids (ISSHAC-VI, Zakopane, Poland (2006)). R.J. Chimentão, G. P. Valença, F. Medina, J. Pérez-Ramírez, *Hydrogenolysis of methylcyclopentane over bimetallic Ir-Au/γ-Al_2O_3 catalysts*

6. 4th EFCATS School on Catalysis CATALYST DESIGN – FROM MOLECULAR TO INDUSTRIALLEVEL, Tsar Village (St. Petersburg), Russia September 20-24, 2006. R. J. Chimentão, Jose E. Herrera, Ja Hun Kwak, Yong Wang, F. Medina, Charles. H. F. Peden. *Oxidation of Ethanol to Acetaldehyde over Na-promoted vanadium oxide catalysts.*

7. Workshop on Size Dependent Effects in Materials for environmental Protection and Energy Application May 25 - 27, 2006, Varna, BulgariaChimentao, R.J; ; Medina, F.; Cesteros, Y.; Salagre, P.; Sueiras, J.E.; Fierro, J.L.G. *Effects of morphology and cesium promotion over silver nanoparticles catalysts in the styrene epoxidation*

UNIVERSITAT ROVIRA I VIRGILI
NANOMATERIALS IN CATALYSIS: STUDY OF MODEL REACTIONS.
Ricardo José Chimentao
ISBN: 978-84-690-7618-7 / DL: T.1326-2007

Published Articles

COMMUNICATION

ChemComm
www.rsc.org/chemcomm

Different morphologies of silver nanoparticles as catalysts for the selective oxidation of styrene in the gas phase

R. J. Chimentão,[a] I. Kirm,[a] F. Medina,*[a] X. Rodriguez,[a] Y. Cesteros,[b] P. Salagre[b] and J. E. Sueiras[a]

[a] *Departament d'Enginyeria Química, Universitat Rovira i Virgili, 43007 Tarragona, Spain. E-mail: fmedina@etse.urv.es; Fax: (+34) 977559667; Tel: (+34) 977559787*

[b] *Departament de Química Inorgánica, Universitat Rovira i Virgili, 43005 Tarragona, Spain*

Received (in Cambridge, UK) 16th January 2004, Accepted 11th February 2004
First published as an Advance Article on the web 26th February 2004

Silver nanoparticles of different morphologies were prepared using the polyol process and then dispersed on α-alumina. Catalysts were tested for the selective oxidation of styrene in the gas phase. Activity and selectivity were strongly dependent on the morphology of the silver nanoparticles.

Silver catalysts have become increasingly important in the selective oxidation of olefins for the synthesis of industrially interesting products such as epoxides and aldehydes.[1] Metal nanoparticles have attracted considerable attention because of their novel physical properties and their potential applications in areas such as catalysis.[2] Recently, silver nanoparticles have been synthesised by reducing silver nitrate with ethylene glycol in the presence of poly(vinylpyrrolidone) (PVP) *via* a polyol process.[3–5] It is well known that the activity and selectivity of catalyst nanoparticles are strongly dependent on their size, shape and surface structure, as well as on their bulk and surface composition.[6] The shape-controlled synthesis of metal nanoparticles can open up a new world of heterogeneous catalysis. This approach may help to understand the effect of crystal planes on chemical reactivity.[7] Oriented nanoparticles could also be extended to industrial applications to obtain many useful chemicals. In these regards, catalysts obtained from silver nanoparticles seem to be particularly interesting for studying the selective oxidation of olefins with oxygen as oxidant because it has been demonstrated that silver is a selective catalyst for olefin epoxidation.[8]

This study investigates how different morphologies of silver nanoparticles supported on α-Al_2O_3 and MgO affect the selective oxidation of styrene in the gas phase using oxygen as oxidant. The promotion effect of potassium hydroxide on the catalytic activity has also been investigated.

The catalysts were prepared by two procedures. In the first, the wetness impregnation method was used to impregnate α-Al_2O_3 and MgO supports with an appropriate amount of an aqueous solution of silver nitrate to obtain 15 and 40 wt% of silver, respectively. In the second, silver nanoparticles (11 wt%) were dispersed on α-Al_2O_3 with an acetone solution. The silver nanoparticles were synthesized *via* a polyol process. In a typical synthesis of silver nanoparticles, 30 ml ethylene glycol solution of $AgNO_3$ (0.25 M, Aldrich) and 30 ml ethylene glycol solution of PVP (0.375 M in repeating unit weight-average molecular weight ≈ 40 000, Aldrich) were simultaneously added in 50 ml ethylene glycol at 433 K under vigorous stirring. The reaction mixture was then refluxed for 45 minutes at this temperature. The nanoparticles obtained were diluted with acetone (about 10 times by volume) and separated from ethylene glycol by centrifugation at 4000 rpm for 20 minutes. Silver nanoparticles were also prepared with a PVP/$AgNO_3$ molar ratio of 3. The catalysts were dried in an oven at 393 K for 24 hours and reduced in H_2 at 623 K for 3 hours before the characterization and the activity tests.

The samples were structurally characterized using X-ray diffraction (XRD), temperature programmed reduction (TPR), scanning electron microscopy (SEM), transmission electron microscopy (TEM) and UV–vis absorption spectroscopy. The selective oxidation of styrene in gas phase at 573 K was carried out in a continuous fixed-bed reactor over 1.0 g catalyst at atmospheric pressure. The catalytic tests were operated at different styrene : O_2 : Ar molar ratios. The feed gas mixture (O_2, Ar) was delivered by means of mass flow controllers and the styrene was introduced into the reactor by a pump. The products were analysed by a Shimadzu GC 2010 gas chromatograph equipped with a capillary column and FID detector.

Fig. 1 shows the morphologies of the catalysts observed by SEM with a JEOL JSM-35C scanning microscope operated at an acceleration voltage of 15 kV.

The morphologies of the silver nanoparticles prepared by the polyol process were found to depend heavily on the experimental conditions such as temperature and the molar ratio between PVP and $AgNO_3$. Previous studies have suggested that the degree of polymerization of PVP (the average number of repeating units in one PVP molecule) also plays an important role in determining the morphology of the silver nanoparticles.[9] We obtained silver nanowires (Fig. 1a) when the molar ratio of PVP and $AgNO_3$ was 1.5. These nanowires had a mean diameter of 150 nm. This was consistent with TEM results. When the molar ratio was increased from 1.5 to 3, nanopolyhedra were the major product (Fig. 1b). The SEM image of the 40% Ag/MgO catalyst (Fig. 1c) prepared by impregnation shows the presence of silver nanowires and other silver particles dominated by irregular shapes with diameters between 100 nm and 500 nm. Irregularly shaped particles with diameters between 200 nm and 1000 nm (Fig. 1d) were also observed for the 15% Ag/α-Al_2O_3 catalyst prepared by wetness impregnation using a silver nitrate solution.

The X-ray diffraction of the nanowires and nanopolyhedra synthesized using the polyol process suggested that silver existed purely in a face-centered cubic structure (Fig. 2). The X-ray powder diffraction (XRD) patterns were recorded using a Siemens D5000 diffractometer using nickel filtered Cu Kα radiation (λ = 1.54056 Å) in 2θ ranging from 30° to 80°.

The diffraction did not suggest the presence of possible impurities such as Ag_2O and $AgNO_3$. The three peaks detected for the silver nanoparticles were assigned to diffraction from the (111), (200) and (220) planes of fcc silver, respectively. The lattice constants calculated by XRD for the nanowires and nanopolyhedra were 4.0839 and 4.0872 Å, respectively, which are very close to the report data (a = 4.0862 Å, Joint Committee on Powder Diffraction Standards file 04–0783). The ratio of intensity between the (111)

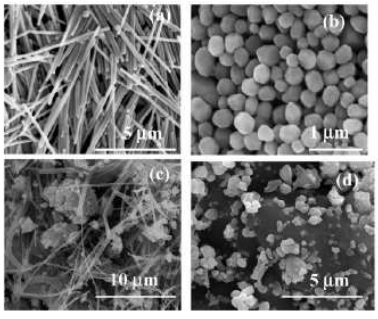

Fig. 1 SEM images of silver catalysts.

DOI: 10.1039/b400762j

UNIVERSITAT ROVIRA I VIRGILI
NANOMATERIALS IN CATALYSIS: STUDY OF MODEL REACTIONS.
Ricardo José Chimentao
ISBN: 978-84-690-7618-7 / DL: T.1326-2007

Available online at www.sciencedirect.com
SCIENCE DIRECT®

Applied Surface Science 252 (2005) 793–800

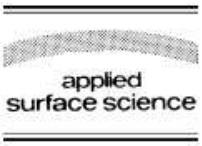

www.elsevier.com/locate/apsusc

Sensitivity of styrene oxidation reaction to the catalyst structure of silver nanoparticles

R.J. Chimentão [a], I. Kirm [a], F. Medina [a,*], X. Rodríguez [a], Y. Cesteros [b], P. Salagre [b], J.E. Sueiras [a], J.L.G. Fierro [c]

[a] Departament d'Enginyeria Química, Universitat Rovira i Virgili, 43007 Tarragona, Spain
[b] Departament de Química Inorgánica, Universitat Rovira i Virgili, 43005 Tarragona, Spain
[c] Instituto de Catalisis y Petroleoquimica, CSIC, Cantoblanco, 28049 Madrid, Spain

Available online 16 March 2005

Abstract

This study shows how different morphologies of silver nanoparticles affect the selective oxidation of styrene in the gas phase using oxygen as oxidant. Silver nanoparticles (nanowires and nanopolyhedra), prepared using the polyol process, were supported on α-Al_2O_3. For comparison, a conventional catalyst obtained by wet impregnation was also prepared. Phenylacetaldehyde (Phe) and styrene oxide (SO) were the main products for nanoparticles catalysts. The promotion effect on the catalytic activity of potassium and cesium on the silver nanowires catalysts was also studied. At 573 K, the styrene conversion and selectivity to styrene oxide with the silver nanowires catalyst were 57.6 and 42.5%, respectively. Silver nanopolyhedra catalyst showed 57.5% conversion and 30.8% selectivity to styrene oxide. The promotion by cesium played an important role in improving the epoxidation of styrene. The samples were structurally characterized using X-ray diffraction (XRD), ultraviolet–visible spectroscopy (UV–vis), scanning electron microscopy (SEM) and transmission electron microscopy (TEM). X-ray photoelectron spectroscopy (XPS) and temperature programmed reduction (TPR) were applied to characterize the oxygen species detected (O_β, O_γ) on the silver surface.

Keywords: Silver nanoparticles; Nanowires; Nanopolyhedra; Styrene; Selective oxidation

1. Introduction

Metal nanoparticles have attracted considerable attention because of their novel physical properties and their potential applications in areas, such as catalysis [1]. Metal nanoparticles with shape control can have structures and properties significantly different from those conventional materials [2]. Recently, silver nanoparticles have been synthesized by reducing silver nitrate with ethylene glycol in the presence of poly(vinyl pyrrolidone) (PVP) via a polyol process [3–7]. It is well known that the activity and

* Corresponding author. Tel.: +34 9775 59787; fax: +34 9775 59667.
E-mail address: fmedina@etse.urv.es (F. Medina).

0169-4332/$ – see front matter © 2005 Elsevier B.V. All rights reserved.
doi:10.1016/j.apsusc.2005.02.064

UNIVERSITAT ROVIRA I VIRGILI
NANOMATERIALS IN CATALYSIS: STUDY OF MODEL REACTIONS.
Ricardo José Chimentao
ISBN: 978-84-690-7618-7 / DL: T.1326-2007

Available online at www.sciencedirect.com
ScienceDirect
Journal of Molecular Catalysis A: Chemical 258 (2006) 346–354
JOURNAL OF MOLECULAR CATALYSIS A: CHEMICAL
www.elsevier.com/locate/molcata

Styrene epoxidation over cesium promoted silver nanowires catalysts

R.J. Chimentão [a], F. Medina [a,*], J.L.G. Fierro [b], J.E. Sueiras [a], Y. Cesteros [c], P. Salagre [c]

[a] Dept. d'Enginyeria Química, Universitat Rovira i Virgili, 43007 Tarragona, Spain
[b] Instituto de Catalisis y Petroleoquimica, CSIC, Cantoblanco, 28049 Madrid, Spain
[c] Dept. de Química Inorgánica, Universitat Rovira i Virgili, 43005 Tarragona, Spain

Received 28 June 2006; received in revised form 10 July 2006; accepted 11 July 2006
Available online 24 August 2006

Abstract

Epoxidation of styrene to styrene oxide (SO) by molecular oxygen was studied over cesium promoted silver nanowires catalysts. Styrene oxide (SO) and phenylacetaldehyde (Phe) were the main products. The results showed that Cs plays an important role improving the efficiency of the catalyst. The effect of the reaction temperature and the O_2:C_8H_8 molar ratio on the catalytic epoxidation was also investigated. Low reaction temperatures or high O_2:C_8H_8 ratios increase the selectivity to SO. The catalytic activity shows a maximum for silver nanowires promoted with 0.25 wt.% of Cs, achieving 94.6% of conversion and total selectivity to desired oxidation products (styrene oxide and phenylacetaldehyde). Besides, negligible deactivation of the catalyst was observed over 30 days of reaction. The experimental characterization was performed by X-ray diffraction (XRD), scanning electron microscopy (SEM), temperature-programmed reduction (TPR) and X-ray photoelectron spectroscopy (XPS). The presence of cesium plays a strong role in reducibility of the silver as detected by temperature-programmed reduction analysis affecting the catalytic activity. The results also suggested the presence of two different species of oxygen formed on the silver nanowires surface after oxygen exposure.

Keywords: Silver nanoparticles; Nanowires; Styrene; Cs; Epoxidation; XPS; SEM

1. Introduction

Direct gas phase partial oxidation of olefins by molecular oxygen to epoxides is long considered one of the most important reactions in commercial catalysis [1,2]. The styrene is a useful alkene model to study the mechanism reaction of terminal alkene epoxidation [3]. Silver is considered almost the unique effective catalyst for the heterogeneous epoxidation reaction [4]. In 1931, Lefort first reported success using silver as catalyst [5]. The ethylene epoxidation is the most studied partial oxidation reaction in industrial process and silver catalyst is the uniquely used under practical conditions [6].

It is well accepted that the selective oxidation reactions on supported noble metals catalyst proceed via Mars–van Krevelen mechanism. The redox property of the catalyst is therefore expected to play an important role in these reactions. Alkaline metals are observed to enhance the redox activities of a number supported metal catalysts [7]. Commercial catalysts for the epoxidation of ethylene consist of silver supported on low surface area materials such as α-Al_2O_3. Alkali metals and their salts have been proposed as promoters in these catalysts. Cesium is usually added to the catalyst to improve the selectivity toward the epoxide [8–13].

To understand the reaction mechanism, the adsorption of oxygen on silver catalysts has been thoroughly performed. This technique gives information about which type of adsorbed oxygen species are responsible in the epoxidation reaction. It has been observed that the oxygen shows different adsorption states. The studies devoted to oxygen-silver system suggests that mainly two different type of oxygen are the active species: electrophilic oxygen leading to selective oxidation products and nucleophilic oxygen producing combustion products [14]. These oxygen species exist on silver catalysts under ethylene epoxidation conditions (160–300 °C) through reversibly and irreversibly adsorption process. However, the study of oxygen adsorption on practical silver catalysts is especially complex since silver surfaces are polycrystalline and contains a significant proportion of defect [15]. Some results indicate that the (1 1 1) orientation is

* Corresponding author. Tel.: +34 977559787; fax: +34 977559667.
E-mail address: francesc.medina@urv.cat (F. Medina).

1381-1169/$ – see front matter © 2006 Elsevier B.V. All rights reserved.
doi:10.1016/j.molcata.2006.07.028

+ Models
APSUSC 14896 1–6
ARTICLE IN PRESS

Available online at www.sciencedirect.com
ScienceDirect

ELSEVIER

Applied Surface Science xxx (2007) xxx–xxx

applied surface science

www.elsevier.com/locate/apsusc

Hydrogenolysis of methylcyclopentane over the bimetallic Ir–Au/γ-Al_2O_3 catalysts

R.J. Chimentão [a,*], G.P. Valença [b], F. Medina [a], J. Pérez-Ramírez [c]

[a] Department of Chemical Engineering, University of Rovira i Virgili (URV), 43007 Tarragona, Spain
[b] Department of Chemical Processes, State University of Campinas (UNICAMP), 13081-970 Campinas (SP), Brazil
[c] Laboratory of Heterogeneous Catalysis, Institute of Chemical Research of Catalonia (ICIQ), 43007 Tarragona, Spain

Abstract

The gas-phase hydrogenolysis of methylcyclopentane (MCP) was investigated over the bimetallic Ir–Au/γ-Al_2O_3 catalysts. The bimetallic systems containing the atomic Au/Ir ratios in the range of 0.125–8 and a fixed total metal content of 8 wt.%, were prepared by the sequential impregnation (SI) and co-impregnation (CI) methods. The corresponding monometallic Ir/γ-Al_2O_3 and Au/γ-Al_2O_3 catalysts were also prepared. The materials were characterized by ICP, XRD, N_2 adsorption, TEM, and H_2 chemisorption. Highly dispersed Ir nanoparticles were obtained in all cases, while the size of Au nanoparticles increased (up to 50 nm) upon the increasing Au content in the catalyst. The monometallic gold catalyst did not adsorb H_2. The incorporation of Au increased the amount of irreversible adsorbed H_2 in the Ir–Au/γ-Al_2O_3 catalysts with respect to the monometallic ones. The products obtained in the MCP hydrogenolysis were 2-methylpentane (2-MP), 3-methylpentane (3-MP) and *n*-hexane (*n*-H). The initial rate (molecules of MCP reacted s^{-1} g_{Ir}^{-1}) increased with the Au content. The deactivation was lower for bimetallic catalysts, particularly for the CI ones. The addition of Au played a significant effect on chemisorption and catalytic properties of Ir.

Keywords: Bimetallic; Catalysts; Chemisorption; MCP; Hydrogen; Hydrogenolysis; Ir; Au

1. Introduction

Methylcyclopentane (MCP) is a recognized probe molecule in the investigation of the structure sensitivity of several hydrocarbon conversions catalyzed by noble metal-based catalysts [1–5]. The classical work by Gault et al. investigated [6] the arrangement of methylcyclopentane (MCP) on alumina supported Pt catalysts by ^{13}C tracer technique. Two mechanisms were distinguished: cyclic and bond shift, denoted as CM and BS, respectively. The CM involves adsorbed methylcyclopentane (MCP) as the intermediate transition state. From this intermediate, three products were obtained (*n*-hexane (*n*-H), 2-methylpentane (2-MP) and 3-methylpentane (3-MP)), whose distribution changed with the Pt content and dispersion. The partial H_2 pressure plays a prominent role in the skeletal rearrangement of hydrocarbons [7,8]. In the absence or low hydrogen amounts, the noble metal sites are covered by hydrogen-deficient hydrocarbon residues. Upon increasing the H_2 partial pressures, the hydrocarbon hydrogenation is accelerated and the catalytic process is controlled by isomerization of the olefinic intermediates on the acid centers of the support [9]. Suitable catalysts for hydrocarbon rearrangement are bifunctional in nature [10]. Pt/γ-Al_2O_3 was applied industrially for hydrocarbon rearrangement during 1950s and 1960s, however, it was largely changed by miscible bimetallic systems such as Pt–Re [11], Pt–Au [12], Pt–Ir [13], Pt–Sn [14] and Pd–Au [15]. Here we investigated bimetallic catalysts with very limited miscibility in the bulk [16] such as Ir–Au/γ-Al_2O_3 in the MCP hydrogenolysis. Monometallic Ir supported on oxides has been usually included in systematic studies dealing with hydrogenolysis of aliphatic hydrocarbons [17]. The presence of Au in the Ir-based catalysts might modulate the catalytic performance of Ir for MCP hydrogenolysis since Au is virtually inactive for dissociative adsorption of H_2 [18]. The effect of Au on Ir dispersion and H_2 adsorption properties of the catalyst was determined, which leads to relevant structure–function relationships for the investigated reaction.

* Corresponding author. Tel.: +34 977 55 9787.
E-mail address: rchiment@urv.cat (R.J. Chimentão).

0169-4332/$ – see front matter © 2007 Published by Elsevier B.V.
doi:10.1016/j.apsusc.2006.12.061

Please cite this article in press as: R.J. Chimentão et al., Hydrogenolysis of methylcyclopentane over the bimetallic Ir–Au/γ-Al_2O_3 catalysts, Appl. Surf. Sci. (2007), doi:10.1016/j.apsusc.2006.12.061

UNIVERSITAT ROVIRA I VIRGILI
NANOMATERIALS IN CATALYSIS: STUDY OF MODEL REACTIONS.
Ricardo José Chimentao
ISBN: 978-84-690-7618-7 / DL: T.1326-2007

Synthesis of silver-gold alloy nanoparticles by a phase-transfer system

R.J. Chimentão, I. Cota, A. Dafinov, F. Medina,[a] and J.E. Sueiras
Departament d'Enginyeria Química, Universitat Rovira i Virgili, 43007 Tarragona, Spain

J.L. Gómez de la Fuente and J.L.G. Fierro
Instituto de Catálisis y Petroleoquímica, CSIC, Cantoblanco, 28049 Madrid, Spain

Y. Cesteros and P. Salagre
Departament de Química Inorgànica, Universitat Rovira i Virgili, 43005 Tarragona, Spain

(Received 23 June 2005; accepted 15 August 2005)

We have studied the preparation of silver-gold alloy nanoparticles based on the phase transfer of metal precursors from aqueous phase to organic solution by a fatty amine at room temperature. Silver-gold nanoparticles were synthesized with different molar ratios (2:1, 1:1, 1:2). Ultraviolet-visible absorption spectra suggested the formation of alloy phases. The elemental Ag:Au ratios in the bimetallic nanoparticles determined by energy dispersive x-ray analysis (EDX) were consistent with the Ag:Au molar ratios used in the feeding solution. Transmission electron microscopy (TEM) revealed the formation of a uniform size distribution of Ag:Au nanoparticles (around 5 nm). X-ray photoelectron spectroscopy (XPS) showed that the composition in the outer part of the Ag:Au nanoparticles was similar to that obtained by EDX analysis, which indicates the formation of homogeneous silver-gold nanoparticles. Silver-gold alloy nanoparticles on a gram scale can be obtained with this method.

I. INTRODUCTION

Metal nanoparticles are currently a very active area of research due to their potential applications in areas such as electronics and catalysis.[1] Metal nanoparticles have significantly different properties from those of bulk metals.[2] The unique chemical and physical properties of nanoparticles are determined by the large proportion of atoms in surface positions and by the shape control of the crystallographic planes on the particle surface.[3] Bimetallic nanoparticles are particularly attractive due to the improved catalytic properties and the change in the surface plasmon band energy relative to the separate metals.[4] Many alternative routes to obtaining nanometer-sized particles of metals have been developed. These include templating,[5] photochemistry,[6] microemulsion,[7] and organic encapsulation.[8] Recent publications have reported the formation of homogeneous Ag:Au alloy nanoparticles in a milligram scale.[9–14] However, these techniques do not avoid the precipitation of AgCl during the synthesis of Ag:Au nanoparticles, on a gram scale, when $HAuCl_4$ and $AgNO_3$ are used as metal precursors. A different gold salt or an adjustment in the solution concentrations is therefore required.[10,15] The Ag:Au system is a good choice because Ag and Au have face-centered cubic structures with similar parameters that lead to the formation of random solution alloys at all concentrations.[16,17] On the other hand, Ag and Au monometallic nanoparticles have a different plasmon absorption in the visible region, and the absorption spectra of Ag:Au alloy exhibit only one surface plasmon band, which is related to the alloy composition. Moreover, the high *f* density states at E_F of gold are very susceptible to modification upon alloy formation.[18]

In this study, we report a method for obtaining homogeneous Ag:Au nanoparticles on a gram scale, using $HAuCl_4$ and $AgNO_3$ salts as precursors. This method is based on extracting the metal ions from the aqueous phase to an organic phase by a fatty amine such as hexadecylamine. Different organic solutions containing silver or gold metal ions protected by the amine were prepared separately. The resultant solutions were then mixed in appropriate amounts to obtain different Ag:Au molar ratios and finally reduced with sodium borohydride.

The silver-gold nanoparticles obtained were characterized by transmission electron microscopy (TEM), ultraviolet-visible (UV-vis) absorption spectra, x-ray diffraction (XRD), energy dispersive x-ray spectroscopy

[a]Address all correspondence to this author.
e-mail: fmedina@etse.urv.es
DOI: 10.1557/JMR.2006.0014

Journal of Experimental Nanoscience,
Vol. 1, No. 4, December 2006, 399–418

Taylor & Francis
Taylor & Francis Group

Synthesis, characterization and catalytic activity of metal nanoparticles in the selective oxidation of olefins in the gas phase

R. J. CHIMENTÃO†, N BARRABÉS†, F. MEDINA*†, J. L. G. FIERRO‡, J. E. SUEIRAS†, Y. CESTEROS§ and P. SALAGRE§

†Department d'Enginyeria Química, Universitat Rovira i Virgili, 43007, Tarragona, Spain
‡Instituto de Catalisis y Petroleoquimica, CSIC, Cantoblanco, 28049, Madrid, Spain
§Department de Química Inorgánica, Universitat Rovira i Virgili, 43005, Tarragona, Spain

(*Received August 2006; in final form September 2006*)

Shape controlled metal nanoparticles were studied in the epoxidation of olefins. PVP mediated polyol processes were employed to generate silver nanowires/rods, nanocubes and nanopolyhedra. Spherical copper nanoparticles were also obtained by the polyol process. The mean diameter of the silver nanoparticles was around 150 nm. Furthermore, Cu nanoparticles were synthesized in an ethanol solution using CTAB as surfactant and as reducing agent. Additionally Au nanoparticles were synthesized by a phase-transfer system irradiated with 254 nm UV light. The mean diameter of these Au and Cu nanoparticles was around 10 nm. The catalytic activity of these nanoparticles on several supports such as α-Al_2O_3, $CaCO_3$ and spherical particles of TiO_2 obtained by the Stöber method was investigated in the epoxidation of a no-allylic olefin such as styrene, as well as for an allylic olefin, such as propene, using molecular oxygen and N_2O as oxidants. The effect of Cs promotion in the styrene epoxidation was also investigated. The type of metal, the particle size, the support and the oxidant, as well as the addition of promoters such as Cs, showed a strong influence towards the formation of selective oxidation products. The metal nanoparticles were characterized employing various techniques such as X-ray diffraction (XRD), temperature programmed reduction (TPR), UV-visible spectroscopy, transmission electron microscopy (TEM), scanning electron microscopy (SEM), X-ray photoelectron spectroscopy (XPS) and ICP-AES.

Keywords: Copper; Epoxidation; Gold; Nanocubes; Nanoparticles; Nanopolyedra; Nanowires; Olefins; SEM; Silver; TEM; UV-vis

1. Introduction

The development of uniform nanometre sized particles has been intensively pursued because of the many technological and fundamental scientific interests associated with these nanoparticles [1]. Nanoscales materials such as metal nanoparticles have received great attention due to their potential applications in the areas of nanofabrication,

*Corresponding author. Email: francesc.medina@urv.cat

Journal of Experimental Nanoscience
ISSN 1745–8080 print/ISSN 1745–8099 online © 2006 Taylor & Francis
http://www.tandf.co.uk/journals
DOI: 10.1080/17458080601024196

J Mater Sci
DOI 10.1007/s10853-006-0570-1

SIZE-DEPENDENT EFFECTS

Effects of morphology and cesium promotion over silver nanoparticles catalysts in the styrene epoxidation

Ricardo José Chimentao · Francesc Medina · Jesús Eduardo Sueiras · José Luís García Fierro · Yolanda Cesteros · Pilar Salagre

Received: 10 May 2006 / Accepted: 14 June 2006 / Published online: ■

Abstract Silver nanowires have been obtained by polyol reduction of silver nitrate in presence of polyvinyl-pyrrolidone (PVP). The as-synthesized silver nanowires were deposited on α- Al_2O_3. For comparison silver catalysts were also prepared by wetness impregnation obtaining irregularly shaped silver particles. Epoxidation of styrene to styrene oxide (SO) by molecular oxygen was studied using the silver catalysts. The main products were styrene oxide (SO) and phenylacetaldehyde (Phe). The promotion effect of the Cs on the silver nanowires catalysts was investigated. The Cs loading was in the range of 0–1 wt.% (refereed to silver). Furthermore, the effect of O_2:C_8H_8 molar ratio on the catalytic epoxidation was also investigated. Silver nanowires catalysts showed superior catalytic activity compared to those prepared by impregnation method. Besides, higher O_2:C_8H_8 ratios improved the selectivity to SO. The catalytic activity showed a maximum performance for silver nanowires promoted with 0.25 wt.% of Cs, achieving 94.6% of conversion and total selectivity to desired oxidation products (styrene oxide and phenylacetaldehyde). Moreover, the cesium promotion also contributed to the increase in the selectivity to styrene oxide. Temperature programmed reduction (TPR) and X-ray photoelectron spectroscopy (XPS) were employed to detect the presence of different species of oxygen in the catalysts indicating that subsurface oxygen was beneficial for the epoxidation. The samples were also structurally characterized using X-ray diffraction (XRD), scanning electron microscopy (SEM), transmission electron microscopy (TEM), UV-visible absorption spectra and selected area electron diffraction pattern (SAED).

R. J. Chimentao · F. Medina (✉) · J. E. Sueiras
Dept. d'Enginyeria Química, Universitat Rovira i Virgili,
43007 Tarragona, Spain
e-mail: fmedina@etse.urv.es

J. L. G. Fierro
Instituto de Catalisis y Petroleoquímica, CSIC,
28049 Cantoblanco, Madrid, Spain

Y. Cesteros · P. Salagre
Dept. de Química Inorgánica, Universitat Rovira i Virgili,
43007 Tarragona, Spain

Introduction

Materials in nanometer scale are of great interest due to their unique optical, electrical, and magnetic properties. These properties are strongly dependent on the size and the shape of the particles and therefore it is very important to be able to finely control the morphology of the nanomaterials [1, 2]. Besides, these materials have a large fraction of surface atoms per unit of volume [3]. The ratio of surface atoms to bulk depends on the particle size. So, a dramatic increase in this ratio can be expected for metal nanoparticles changing the physical and chemical properties of these materials [4]. Current research has been focused on one-dimensional nanoparticles such as nanorods and nanowires since the morphological anisotropy results in very complex physical properties and self assembly behaviors compared to those bulk materials [5]. Metal particles have been synthesized by using various methods such as templating [6, 7], photochemistry [8], seeding [9, 10], and electrochemistry [11, 12]. Reduction of the metal complexes in diluted solutions is the

Springer

Journal : 10853 | Dispatch : 17-2-2007 | Pages : 8
Article No. : 570 | ☐ LE | ☐ TYPESET
MS Code : 570 | ☑ CP | ☑ DISK

UNIVERSITAT ROVIRA I VIRGILI
NANOMATERIALS IN CATALYSIS: STUDY OF MODEL REACTIONS.
Ricardo José Chimentao
ISBN: 978-84-690-7618-7 / DL: T.1326-2007

Effect of H_2O on the Adsorption of NO_2 on γ-Al_2O_3: an in Situ FTIR/MS Study

János Szanyi,* Ja Hun Kwak, Ricardo J. Chimentao,† and Charles H. F. Peden
Institute for Interfacial Catalysis, Pacific Northwest National Laboratory, Richland, Washington 99352

Received: September 26, 2006; In Final Form: December 1, 2006

The effect of water on the adsorption of NO_2 onto a γ-Al_2O_3 catalyst support surface was investigated using Fourier transform infrared spectroscopy (FTIR) and mass spectrometry (MS). Upon room-temperature exposure of the alumina surface to small amounts of NO_2, nitrites and nitrates are formed, and at higher NO_2 doses only nitrates are observed. The surface nitrates formed were of bridging monodentate, bridging bidentate, and monodentate configuration. At elevated NO_2 pressures, the surface hydroxyls were consumed in their reaction with NO_2 giving primarily bridge-bound nitrates. A significant amount of weakly adsorbed N_2O_3 was seen as well. Exposure of the NO_2-saturated γ-Al_2O_3 surface to H_2O resulted in the desorption of some NO_2 + NO as H_2O interacted with the weakly held N_2O_3, while the bridging monodentate surface nitrates converted into monodentate nitrates. The conversion of these oxide-bound nitrates to water-solvated nitrates was observed at high water doses when the presence of liquid-like water is expected on the surface. The addition of H_2O to the NO_2-saturated γ-Al_2O_3 did not affect the amount of NO_x strongly adsorbed on the support surface. In particular, no NO_x desorption was observed when the NO_2-saturated sample was heated to 573 K prior to room-temperature H_2O exposure. The effect of water is completely reversible; i.e., during temperature-programmed desorption (TPD) experiments following NO_2 and H_2O coadsorption, the same IR spectra were observed at temperatures above that required for H_2O desorption as seen for NO_2 adsorption only experiments.

Introduction

γ-Al_2O_3 is the most frequently used oxide catalyst support material due to its superior chemical and thermal stability and high surface area. Alumina is used as a support in traditional three-way automotive catalysts, and it is proposed as the support of choice in lean NO_x trap catalysis (also known as NO_x storage reduction, NSR) as well. In this latter application, a basic oxide (most commonly BaO or K_2O) supported on high surface area γ-Al_2O_3 acts as the active NO_x storage material.[1,2] The fully formulated catalyst also contains a noble metal component (most often Pt) to convert NO to NO_2 in the lean operation cycle and to carry out traditional three-way catalysis chemistry (NO_x reduction and hydrocarbon and CO oxidations) in the rich cycle. Although it is widely accepted that most of the NO_2 is stored on the basic components of the fully formulated catalyst, it is also believed that γ-Al_2O_3 can contribute to the total NO_x storage capacity of these catalyst systems as well.

Due to its widespread use as the support of automotive exhaust control catalysts, a number of previous studies[3−6] have investigated the interaction of NO_x with γ-Al_2O_3. Using primarily FTIR spectroscopy, a variety of different types of ionic surface NO_x species have been observed when NO_x (NO and NO_2) is contacted with γ-Al_2O_3. In a comprehensive study of NO and NO + O_2 adsorption on γ-Al_2O_3 at room temperature, Venkov et al.[4] assigned the IR features observed to differently coordinated nitrite and nitrate species on alumina. When a clean alumina surface was exposed to a mixture of NO and O_2, first nitrites and then, with increasing O_2 amounts, nitrates were formed. Concomitant to the development of IR absorption features characterizing adsorbed ionic NO_x species, the intensities of the ν_{OH} features of the alumina support gradually decreased. At the same time, the accumulation of adsorbed N_2O_3 was observed as well. Westerberg and Fridell[5] studied the adsorption of NO_2 on γ-Al_2O_3 at elevated temperatures (from 373 to 673 K) and reported the formation of the same types of nitrates as just discussed. They also determined the relative abundance of these nitrate species with changing temperature. The results of those experiments allowed them to conclude that the bond strength between the alumina surface and the nitrate ions is increasing in the order of bidentate < monodentate < bridging. The thermal stabilities of NO_x species formed upon the exposure of a γ-Al_2O_3 sample to NO was studied in a combined IR and temperature-programmed desorption (TPD) investigation by Huang et al.[6] In the TPD spectra, they observed three NO desorption features at 370, 680, and 800 K: the low-temperature feature was assigned to NO desorption from adsorbed nitrosyl species, the medium temperature one to the decomposition of linear and chelated nitrites, and the high-temperature NO desorption feature (accompanied by O_2 desorption) was correlated with decomposition of surface bidentate nitrate species.

These adsorption studies were all carried out with the exclusion of H_2O that is present in most of the catalytic processes in which aluminas are used either as supports or actual catalysts. In fact, in the technology we are interested in (lean NO_x trap catalysis), there is a large amount of water present over the catalyst under practical engine operation conditions. Thus, the effect of water on the performance of BaO/Al_2O_3-based NO_x storage/reduction catalysts has been studied previously.[7,8] Epling et al.[7] found that the presence of H_2O influences primarily the NO_x uptake properties of $Pt/BaO/Al_2O_3$ NSR catalysts (shortens the time before NO_x slip occurs), and this effect was most significant under low operating temperatures.

* Corresponding author. E-mail: janos.szanyi@pnl.gov.
† Current address: Department d'Enginyeria Química, Universitat Rovira i Virgili, Tarragona, Spain.

10.1021/jp066326x CCC: $37.00
Published on Web 01/24/2007

UNIVERSITAT ROVIRA I VIRGILI
NANOMATERIALS IN CATALYSIS: STUDY OF MODEL REACTIONS.
Ricardo José Chimentao
ISBN: 978-84-690-7618-7 / DL: T.1326-2007

Water-induced morphology changes in BaO/γ-Al_2O_3 NO_x storage materials

János Szanyi,*[a] Ja Hun Kwak,[a] Do Heui Kim,[a] Xianqin Wang,[a] Jonathan Hanson,[b] Ricardo J. Chimentao[c] and Charles H. F. Peden[a]

Received (in Berkeley, CA, USA) 20th September 2006, Accepted 28th November 2006
First published as an Advance Article on the web 12th December 2006
DOI: 10.1039/b613674e

Exposure of NO_2-saturated BaO/γ-Al_2O_3 NO_x storage materials to H_2O vapour results in the conversion of surface nitrates to $Ba(NO_3)_2$ crystallites, causing dramatic morphological changes in the Ba-containing phase, demonstrating a role for water in affecting the NO_x storage/reduction properties of these materials.

The demand to develop highly fuel efficient internal combustion engines that require operational conditions of high air-to-fuel ratios (20 or higher) coincides with increasingly stringent environmental regulations on harmful exhaust gas emission levels. Under highly oxidizing (lean) conditions traditional, 3-way catalysts are unable to reduce NO_x due to their high oxidation efficiency that converts essentially all of the reducing agents present in the exhaust stream to CO_2. One of the promising technologies being considered is lean NO_x trap (LNT) systems,[1–3] that operate under cyclic fashion. NO_x is being stored on the storage component (*e.g.* BaO supported on γ-Al_2O_3) of the system primarily as nitrates in the lean cycle. Upon saturation of the NO_x storage material, a brief reducing cycle is applied in which NO_x is reduced by the precious-metal component (*e.g.* Pt) of the system, similarly to that known from 3-way automotive catalysis. Recently significant efforts have been focused on understanding the uptake of NO_x (in particular NO_2) by the Ba-containing phase. A number of spectroscopic investigations have clearly identified the presence of two different types of nitrate species present on the BaO phase upon its exposure to NO_2.[4–11] These species were identified as surface nitrates (strongly held NO_2 on the monolayer of BaO on the surface of alumina support), and bulk nitrates (nitrates that formed by the reaction of BaO particles with NO_2).[11] The thermal, chemical and spectroscopic properties of these two types of nitrate species are distinctly different. For example, surface nitrates decompose at a lower temperature than bulk nitrates and, more importantly, their desorption product is exclusively NO_2, while bulk nitrates decompose as NO + O_2 at high temperatures similarly to unsupported $Ba(NO_3)_2$ ($\sim$800 K).

Despite the extensive fundamental studies that have been conducted on these materials, key issues that strongly influence the performance of these catalytic systems still remain. One of the major concerns comes from the fact that under lean conditions the water level in the exhaust gas is very high ($\sim$10%). Previous studies have indicated a detrimental effect (although in widely varying extent) of water on the performance of these NO_x storage materials;[12–15] however no clear understanding of this effect has been developed.

Inspired by the contrasting explanations given for the effects of water on these systems, we conducted Fourier transform infrared spectroscopy (FTIR), temperature programmed desorption (TPD), and synchrotron time-resolved X-ray diffraction (TR XRD) experiments on BaO/γ-Al_2O_3 materials. The emphasis of our investigation was to follow the fate of different nitrate species formed during NO_2 adsorption (FTIR), and the corresponding changes in the morphologies of the Ba-containing phase (TR-XRD) as the samples were exposed to water.

Fig. 1 displays three FTIR spectra obtained after an 8 wt% BaO/γ-Al_2O_3 sample was first saturated with NO_2 (spectrum (a)) then exposed to H_2O at 300 K (spectrum (b)), and finally during TPD at 640 K sample temperature (spectrum (c)) . The amount of water added to the system in this experiment is very small, and the equilibrium water vapour pressure was less than 0.2 Torr after the introduction of the last H_2O dose.

Exposure of the clean BaO/γ-Al_2O_3 sample to NO_2 resulted in the development of IR features (spectrum (a)) characteristic of both surface (1294, 1582 cm^{-1}) and bulk (1325, 1434–1480 cm^{-1}) nitrate species associated with BaO,[11] while evidence was also seen for the formation of surface nitrates on the alumina support (1270, $\sim$1620 cm^{-1}). Upon the introduction of H_2O onto the NO_2-saturated sample, first a significant drop in the intensities of IR

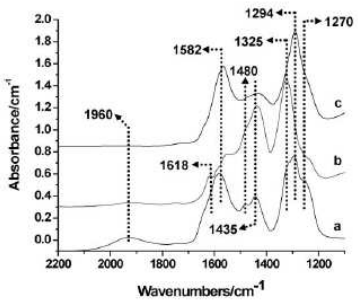

Fig. 1 FTIR spectra collected at 300 K from an 8 wt% BaO/γ-Al_2O_3 sample after NO_2 saturation (a), subsequent H_2O exposure (b), and during TPD between 640 and 670 K (c).

[a]*Institute for Interfacial Catalysis, Pacific Northwest National Laboratory, Richland, WA, 99352, USA. E-mail: janos.szanyi@pnl.gov; Fax: 509-376-5106; Tel: 509-376-6466*
[b]*Department of Chemistry, Brookhaven National Laboratory, Upton, NY, 11973, USA*
[c]*Department d'Enginyeria Química, Universitat Rovira i Virgili, Tarragona, Spain*

UNIVERSITAT ROVIRA I VIRGILI
NANOMATERIALS IN CATALYSIS: STUDY OF MODEL REACTIONS.
Ricardo José Chimentao
ISBN: 978-84-690-7618-7 / DL: T.1326-2007

Water-Induced Morphology Changes in BaO/γ-Al_2O_3 NO_x Storage Materials: an FTIR, TPD, and Time-Resolved Synchrotron XRD Study

János Szanyi,*,† Ja Hun Kwak,† Do Heui Kim,† Xianqin Wang,† Ricardo Chimentao,‡ Jonathan Hanson,§ William S. Epling,‖ and Charles H. F. Peden†

Institute for Interfacial Catalysis, Pacific Northwest National Laboratory, Richland, Washington 99352, Department d'Enginyeria Quimica, Universitat Rovira i Virgili, Tarragona, Spain, Department of Chemistry, Brookhaven National Laboratory, Upton, New York 11973, and University of Waterloo, Waterloo, ON, Canada

Received: November 29, 2006; In Final Form: January 18, 2007

The effect of water on the morphology of BaO/Al_2O_3-based NO_x storage materials was investigated using Fourier transform infrared spectroscopy, temperature programmed desorption, and time-resolved synchrotron X-ray diffraction techniques. The results of this multispectroscopy study reveal that in the presence of water surface Ba-nitrates convert to bulk nitrates and water facilitates the formation of large $Ba(NO_3)_2$ particles. The conversion of surface to bulk Ba-nitrates is completely reversible (i.e., after the removal of water from the storage material a significant fraction of the bulk nitrates reconverts to surface nitrates). NO_2 exposure of a H_2O-containing (wet) BaO/Al_2O_3 sample results in the formation of nitrites and bulk nitrates exclusively (i.e., no surface nitrates form). After further exposure to NO_2, the nitrites completely convert to bulk nitrates. The amount of NO_x taken up by the storage material, however, is essentially unaffected by the presence of water regardless of whether the water was dosed prior to or after NO_2 exposure. On the basis of the results of this study, we are now able to explain most of the observations reported in the literature on the effect of water on NO_x uptake on similar storage materials.

Introduction

Today, the drive to increase fuel efficiency in internal combustion engines is coupled with the demand to decrease hazardous exhaust gas emission. Lean engine operation (higher than stoichiometric amounts of oxygen) can lead to a significant increase in fuel efficiency; however, it prevents the use of traditional three-way catalysts (TWCs) for emission control. Under lean conditions, TWCs burn most of the reducing compounds present in the exhaust gas mixture, thus starving the system of an efficient reducing agent for reaction with NO_x. Therefore, eliminating NO_x from these highly oxidizing environments presents a great challenge. Several new technologies have been considered for lean NO_x reduction in the last two decades, although very limited practical application has been achieved. One of the more promising approaches is the NO_x storage/reduction (NSR) technology (also called lean NO_x traps, LNTs). Originally developed by Toyota in the early 1990s,[1,2] this technology requires cyclic engine operation; in the lean cycle all of the NO_x is converted to NO_2 and is stored as nitrates (mostly on alkali or alkaline earth oxides), while in a subsequent short-reducing cycle this stored NO_x is released and converted to N_2 similarly to that in the TWC technology. Despite extensive research that has contributed to an understanding of NO_x storage and reduction cycles,[3] several issues remain open and debated about the operation of these systems.

The effects of H_2O and CO_2 on the uptake of NO_x over BaO/Al_2O_3-based storage systems have been recognized and reported.[4−9] However, the extent of the effects of these compounds on the NO_x uptake and the mechanisms by which these compounds influence NO_x uptake are still widely debated. In particular, the effect of water seems poorly understood. Toops and co-workers[6,7] suggest that water primarily influences the alumina support material by preventing NO_x uptake on the alumina support itself and in this way reducing the total NO_x uptake capacity of the entire system. A completely different explanation has been given by Cant and Patterson,[5] who examined the effect of H_2O on the temperature programmed desorption (TPD) profiles of NO_2-saturated BaO/Al_2O_3 samples. They observed that in the presence of H_2O in the purge gas (1% H_2O in He) the maximum NO_x desorption rate of the low-temperature desorption feature in the TPD spectrum shifted to a higher temperature (by ∼20 K), while the total amount of NO_x desorbed in the lower-temperature desorption feature decreased at the expense of the higher-temperature one. Among a number of possible explanations that they provided, Cant and Patterson[5] preferred the one that suggested the formation of a $Ba(OH)_2$ crust on top of the $Ba(NO_3)_2$ particles that slowed down the decomposition of $Ba(NO_3)_2$. Lietti and co-workers[8] found an interesting dependence of NO_x storage in the presence of water in the gas stream during the uptake process. They found that the presence of H_2O promoted the uptake of NO_x at low temperatures (< 573 K) and inhibited it at higher temperatures. Epling et al.[4] have also shown inhibition of NO_x uptake in the presence of H_2O; in particular, in the presence of water the time required for the NO_x slip to occur was shortened in comparison as to when water was absent from the system during NO_x uptake. In general, all of the literature data available seem to suggest a detrimental effect of H_2O on NO_x uptake. However, the extent

* Corresponding author. E-mail address: janos.szanyi@pnl.gov.
† Pacific Northwest National Laboratory.
‡ Universitat Rovira i Virgili.
§ Brookhaven National Laboratory.
‖ University of Waterloo.

10.1021/jp067932v CCC: $37.00
Published on Web 03/07/2007

UNIVERSITAT ROVIRA I VIRGILI
NANOMATERIALS IN CATALYSIS: STUDY OF MODEL REACTIONS.
Ricardo José Chimentao
ISBN: 978-84-690-7618-7 / DL: T.1326-2007

(Submitted to the Applied Catalysis A)

Oxidation of Ethanol to Acetaldehyde over Na-promoted vanadium oxide catalysts

Ricardo J. Chimentão [a] , Jose E. Herrera [b], Ja Hun Kwak [b], Janos Szanyi [b], F. Medina [a], C. H. F. Peden [b,*]

[b] Institute for Interfacial Catalysis, Pacific Northwest National Laboratory, P.O. Box 999, MS k8-98, Richland, WA 99352, USA

[a] Departament d'Enginyeria Química, Universitat Rovira i Virgili, P.O. Box 43007, Tarragona, Spain

[*] Corresponding author.

E-mail addresses: chuck.peden@pnl.gov

UNIVERSITAT ROVIRA I VIRGILI
NANOMATERIALS IN CATALYSIS: STUDY OF MODEL REACTIONS.
Ricardo José Chimentao
ISBN: 978-84-690-7618-7 / DL: T.1326-2007

(Accepted to the Journal of Molecular Catalysis)

Propylene epoxidation by nitrous oxide over Au-Cu/TiO_2 alloy catalysts

R.J. Chimentão[a], F. Medina[a*], J.L.G. Fierro [b], J. Llorca[c], J.E. Sueiras[a], Y. Cesteros[d], P. Salagre[d]

*[a] *Dept. d'Enginyeria Química, Universitat Rovira i Virgili,43007 Tarragona, Spain*

[b] *Instituto de Catalisis y Petroleoquimica, CSIC, Cantoblanco, 28049 Madrid, Spain*

[c]*Barcelona, Spain*

[d] *Dept. de Química Inorgánica, Universitat Rovira i Virgili, 43005 Tarragona, Spain*

*corresponding author:

E-mail address: francesc.medina@urv.cat

UNIVERSITAT ROVIRA I VIRGILI
NANOMATERIALS IN CATALYSIS: STUDY OF MODEL REACTIONS.
Ricardo José Chimentao
ISBN: 978-84-690-7618-7 / DL: T.1326-2007

(Submitted to the Journal of Catalysis)

Delamination of layered double hydroxides by sonication: Effect of the accessibility to the interlayer space

R.J. Chimentão[a], S. Abelló[a], F. Medina[a*], J. Llorca[b], J.E. Sueiras[a], Y. Cesteros[c], P. Salagre[c]*[a] *Dept. d'Enginyeria Química, Universitat Rovira i Virgili,43007 Tarragona, Spain*

[b]*Institut de Tècniques Energètiques. Universitat Politècnica de Catalunya, Diagonal 647, ed. ETSEIB, 08028 Barcelona, Spain*

[c] *Dept. de Química Inorgánica, Universitat Rovira i Virgili, 43005 Tarragona, Spain*

Abstract

Mg-Al hydrotalcite-like materials with atomic ratio of 4 were tested as heterogeneous catalyst. In this work we study the effect on the catalytic activity by using different rehydration procedures such as mechanical stirring or ultrasounds. The obtained materials with a Mg/Al molar ratio of 4 were proved in the styrene epoxidation reaction using hydrogen peroxide as oxidant in the presence of acetonitrile, acetone and water. An enhancement in the catalytic activity was observed when both the stirring and ultrasound time was increased during the rehydration procedure that can be correlated with the increase in BET surface area of the obtained materials (>400 m^2/g) and the accessibility of the basic sites of the catalysts due to the high degree of exfoliation of the HT-platelets. The LDHs were characterized by inductively coupled plasma-emission spectrometer (ICP-AES), X-ray diffraction (XRD), thermal measurement (TG-DTG), high resolution transmission electron microscopy (TEM), N_2-adsorption and CO_2-TPD. Based on this, exfoliation of the hydrotalcites produces reconstructed materials with small crystallites which are very active in the styrene epoxidation compared to the larger crystals present in the calcined hydrotalcites.

Keywords: hydrotalcite; Mg-Al; styrene; exfoliation; nanoplatelets; HRTEM

*corresponding author

E-mail address: francesc.medina@urv.cat

UNIVERSITAT ROVIRA I VIRGILI
NANOMATERIALS IN CATALYSIS: STUDY OF MODEL REACTIONS.
Ricardo José Chimentao
ISBN: 978-84-690-7618-7 / DL: T.1326-2007